# Molecular and Cellular Mechanisms Controlling Cumulus Layer Expansion at Ovulation

By

Karen Freire Carvalho

Department of Experimental Medicine
McGill University
Montreal, QC, Canada
April 2024

A thesis submitted to McGill University in partial fulfillment of the requirements of the degree of Doctor of Philosophy

# Table of contents

## Acknowledgements

The process of developing this work has been immensely fulfilling for me, both professionally and personally. I am extremely grateful to all the people who were involved in it throughout these years.

I would like to thank my supervisor, Dr. Hugh Clarke, who welcomed me into his lab not once but twice. Thank you for your patience, constant guidance and encouragement. It has been a privilege working with you.

I would also like to thank the members of my Supervisory Committee, Dr. Sarah Kimmins, Dr. Daniel Bernard and Dr. Simon Rousseau, for their advice and kindness.

My deepest thanks to the members of the Clarke Lab. Dr. Qin Yang, your technical expertise and support were essential. Sofia, I will always cherish our deep conversations and discussions, be they sitting by the microscope or strolling around the streets of Valencia. Sibat and Herthana, my fellow “kids of the Clarke lab”, thank you for all the laughter and friendship. Ophélie, obrigada por ser a amiga francesa mais brasileira que eu tenho. Wusu, Karl, and Laleh thank you for all your company and support.

I would also like to send a huge thank you to the other friends that Montreal and the MUHC have brought me. Heather, my friend and writing buddy, thank you for all the silly moments. Marie, mon amie, merci infiniment d'être une personne si gentille et de me soutenir toujours, je t'apprécie beaucoup. Laurie, thank you for “adopting me” and sharing the ups and downs of these last steps with me.

My most wholehearted thank you to my everyday furry and loving companions, Kiki and Kiva.

My most sincere thanks to Collin. You are my person. Thank you for always being there for me and sharing this ride with me.

Eu gostaria de agradecer a minha família, em especial a minha mãe. Mãe, muito obrigada pelo apoio incondicional, pelo esforço, pela luta e por ser tão incrível.

Também gostaria de agradecer meus velhos amigos. AdS, vocês continuam sendo a parte exata e sempre necessária da minha vida. Lê, Tama, Re, Ju e Ro, vocês são parte do que eu sou e nada disso teria sido possível sem vocês. Obrigada por tudo!

## Abstract

Inside preovulatory ovarian follicles, oocytes are enclosed by several layers of tightly packed cumulus cells (CCs), forming cumulus-oocyte complexes (COCs). At ovulation, the CCs secrete a hyaluronan-rich extracellular matrix and become displaced away from the oocyte. This process, called cumulus layer expansion, is essential for ovulation and fertilization. Downstream of the ovulatory stimulus, Epidermal Growth Factor Receptor (EGFR) signalling initiates expansion, but how this signalling triggers cumulus cell displacement is poorly understood. In other cell types, particularly cells showing highly invasive behaviour, cell migration requires the activation of Non-muscle Myosin II (NMII), controlled by NMII kinases such as Rho-associated kinases (ROCK) and Myotonic dystrophy-related CDC42-binding kinases (MRCK), which are, in turn, regulated by Small Rho GTPases such as RhoA. Therefore, we investigated whether cumulus cell displacement during expansion was similarly regulated. We first showed that CCs depend on EGFR signalling to trigger cumulus matrix production but then rely on oocyte-secreted factors and cell attachment to sustain it. Moreover, CC detachment is accompanied by an extensive actin cytoskeleton rearrangement, which is underlined both by the retraction of transzonal projections and by the extension of actin-related cellular structures, such as membrane blebs. These events are hallmarks of cell migration. Next, we observed that coinciding with cytoskeletal rearrangement and membrane blebbing, NMII became activated in the CCs. Pharmacological inhibition of NMII activity blocked membrane blebs and impaired CC displacement. In contrast, inhibiting ERK activity only moderately impaired NMII activation, indicating that this crucial transducer of EGFR signalling does not regulate NMII activation. Moreover, in the absence of EGF, pharmacological stimulation of RhoA activated NMII and caused membrane blebbing. When we targeted the activity of ROCK and MRCK, we found that inhibition of either target individually partially impaired NMII activation and CC displacement, whereas inhibition of both impaired these events substantially. Functionally, blocking the activity of ROCK, MRCK, or NMII significantly reduced the number of sperm that reached the oocyte following incubation with capacitated sperm. Taken together, these findings suggest that RhoA-ROCK and MRCK cooperatively activate NMII to stimulate CC migration during expansion and that NMII-dependent migration is necessary for fertilization. The understanding of these molecular and cellular events may help diagnose and treat infertility as well as aid in the betterment of Assisted Reproductive Techniques.

## Résumé

À l’intérieur des follicules ovariens préovulatoires, les ovocytes sont entourés de plusieurs couches de cellules cumulus (CC) étroitement emballées, formant des complexes cumulus-ovocytes (COC). Lors de l'ovulation, les CC sécrètent une matrice extracellulaire riche en hyaluronane et s'éloignent de l'ovocyte. Ce processus, appelé expansion des cumulus, est essentiel à l’ovulation et à la fécondation. En aval du stimulus ovulatoire, la signalisation du récepteur de facteur de croissance épidermique (R-EGF) initie l'expansion, mais la manière dont cette signalisation déclenche le déplacement des cellules du cumulus est mal comprise. Dans d'autres types de cellules, en particulier les cellules présentant un comportement hautement invasif, la migration cellulaire nécessite l'activation de la myosine II non musculaire (NMII), contrôlée par les kinases NMII telles que les kinases associées à Rho (ROCK) et les kinases de liaison CDC42 liées à la dystrophie myotonique (MRCK), qui sont, à leur tour, régulés par les Small Rho GTPases telles que RhoA. Par conséquent, nous avons étudié si le déplacement des cellules du cumulus au cours de l’expansion était régulé de la même manière. Nous avons d’abord montré que les CC dépendent de la signalisation R-EGF pour déclencher la production de matrice cumulus, mais qu’ils s’appuient ensuite sur des facteurs sécrétés par les ovocytes et sur l’attachement cellulaire pour la maintenir. De plus, le détachement du CC s'accompagne d'un réarrangement étendu du cytosquelette d'actine, souligné à la fois par la rétraction des projections transzonales et par l'extension de structures cellulaires liées à l'actine, telles que les bulles membranaires. Ces événements sont les caractéristiques de la migration cellulaire. Ensuite, nous avons observé que, coïncidant avec le réarrangement du cytosquelette et le saignement membranaire, le NMII était activé dans les CC. L'inhibition pharmacologique de l'activité du NMII a bloqué les bulles membranaires et altéré le déplacement du CC. En revanche, l'inhibition de l'activité ERK n'a que modérément altéré l'activation du NMII, ce qui indique que ce transducteur crucial de la signalisation EGFR ne régule pas l'activation du NMII. De plus, en l’absence d’EGF, la stimulation pharmacologique de RhoA a activé le NMII et provoqué des saignements membranaires. Lorsque nous avons ciblé l'activité de ROCK et de MRCK, nous avons constaté que l'inhibition de l'une ou l'autre cible altère individuellement partiellement l'activation du NMII et le déplacement du CC, alors que l'inhibition des deux altère considérablement ces événements. Sur le plan fonctionnel, le blocage de l'activité de ROCK, MRCK ou NMII réduisait considérablement le nombre de spermatozoïdes atteignant l'ovocyte

après l'incubation avec des spermatozoïdes capacités. Pris ensemble, ces résultats suggèrent que RhoA-ROCK et MRCK activent de manière coopérative NMII pour stimuler la migration des CC pendant l'expansion et que la migration dépendante de NMII est nécessaire à la fécondation. La compréhension de ces événements moléculaires et cellulaires peut aider à diagnostiquer et à traiter l'infertilité ainsi qu'à améliorer les techniques de procréation assistée.

## Contribution to original knowledge

The ovulatory stimulus, besides triggering oocyte maturation and its release from the follicle, also triggers cumulus layer expansion. During this process, the cumulus cells produce and secrete a hyaluronan-rich extracellular matrix, the cumulus matrix, and become displaced away from the oocyte. The work presented in this thesis reveals new insights into the cellular and molecular mechanisms controlling cumulus cell displacement and its impact on fertility.

In the first part of this thesis, we show for the first time that cumulus cell displacement takes place during the second half of the process, opposing the gene expression responsible for cumulus matrix production, which is concentrated during the first few hours of expansion. We indicate that high TGFβ signalling and consequent cumulus matrix production require cell attachment. We also show that cumulus cell displacement is accompanied by intense membrane blebbing, preceded by cumulus cell detachment and underlined by an extensive actin cytoskeletal rearrangement. The actin cytoskeletal rearrangement is underlined by the retraction of Transzonal Projections that link the cumulus cells to the oocyte, a long-known process that mediates the uncoupling between the somatic and the germ compartment, freeing the oocyte for fertilization.

In the second part of the thesis, we show that cumulus cell displacement during expansion has an active cell migration component. For the first time, we described this migration as dependent on actomyosin contractility, powered by Non-muscle Myosin II activity. We further describe the molecular mechanism responsible for activating Non-muscle Myosin II that, opposing the current knowledge on the regulatory pathways controlling expansion, does not depend on Extracellular Regulated Kinases 1 and 2 activity. In functional studies, we indicate that this Non-muscle Myosin II-dependent cumulus cell migration is required before fertilization so the sperm can penetrate the cumulus layer and reach the mature oocyte. Altogether, these results further highlight the impact of cumulus layer expansion on female fertility, providing a more comprehensive basis for future infertility diagnosis and treatment.

## List of publications and Author Contributions

**1.** Abbassi L, El-Hayek S, **Carvalho KF**, Wang W, Yang Q, Granados-Aparici S, Mondadori R, Bordignon V, and Clarke HJ. Epidermal growth factor receptor signalling uncouples germ cells from the somatic follicular compartment at ovulation. Nat Commun. 2021;12(1). Available from: https://www.nature.com/articles/s41467-021-21644-z doi: 10.1038/s41467-021-21644-z.

The candidate, Carvalho KF, provided intellectual contributions in addition to designing, performing, and analyzing the data for the experiments described in Figure 1 (a, b), 6 (a, b, g, h), and Supplemental Figure 1 (a, c).

**2.** Wang W, **Carvalho KF**, Yang Q, and Clarke HJ. Cell contact drives receptor localization and SMAD signalling within the ovarian follicle. Cell Rep. (*under revision*).

The candidate, Carvalho KF, provided intellectual contributions in addition to designing, performing, and analyzing data for specific experiments (showcased in Figures 43 and 44 of this thesis).

**3. Carvalho KF** & Clarke HJ. Non-muscle Myosin II-dependent cumulus cell migration at ovulation is essential for sperm to reach the oocyte before fertilization (*in preparation*).

The candidate, Carvalho KF, provided intellectual contribution in addition to designing, performing the experiments, analyzing the data and preparing the figures for this manuscript.

## Author Contributions

This thesis contains six chapters. Please find below a detailed description of the author's contributions.

*Chapter 1: Introduction.*

The candidate, Karen Freire Carvalho, wrote this chapter and prepared all the figures, with the exception of Figure 1 and Figure 2, which were adapted from the literature (as indicated in the figure descriptions). The supervisor, Hugh Clarke, reviewed and provided guidance.

*Chapter 2: Material and Methods.*

The candidate, Karen Freire Carvalho, wrote this chapter and prepared all the figures featured in it. The supervisor, Hugh Clarke, reviewed and provided guidance.

*Chapter 3: Cumulus matrix production, cumulus cell detachment, cytoskeletal rearrangement, and displacement during cumulus layer expansion.*

The candidate, Karen Freire Carvalho, designed, performed, and analyzed the data for the experiments and prepared all the figures featured in this chapter. The supervisor, Hugh Clarke, contributed to the experimental design, provided guidance, and reviewed this chapter.

*Chapter 4: Molecular Mechanisms Controlling Cumulus Cell Displacement During Cumulus Layer Expansion*

The candidate, Karen Freire Carvalho, designed, performed, and analyzed the data for the experiments and prepared all the figures featured in this chapter. The supervisor, Hugh Clarke, contributed to the experimental design, provided guidance, and reviewed this chapter.

*Chapter 5: Discussion.*

The candidate, Karen Freire Carvalho, wrote this chapter. The supervisor, Hugh Clarke, provided guidance and reviewed it.

*Chapter 6: Conclusion.*

The candidate, Karen Freire Carvalho, wrote this chapter and prepared the figure featured in it. The supervisor, Hugh Clarke, provided guidance and reviewed this chapter.

## List of abbreviations

| | |
|---|---|
| 1D | One-dimensional |
| 2D | Two-dimensional |
| 3D | Tridimensional |
| ACTH | Adrenocorticotropic Hormone |
| ADAMTS | A disintegrin and metalloproteinase with thrombospondin-like motifs |
| AMT | Amoeboid-to-Mesenchymal Transitions |
| AREG | Amphiregulin |
| Arp | Actin-Related Protein |
| ARTs | Assisted Reproductive Technologies |
| BB | Blocking Buffer |
| BMP | Bone Morphogenetic Protein |
| BSA | Bovine Serum Albumin |
| BTC | Betacellulin |
| C1 | C-terminal kinase C conserved region |
| cAMP | Cyclic adenosine monophosphate |
| CAPA-IVM | Capacitation IVM |
| CC | Cumulus cell |
| CD168 | Cluster of Differentiation 168 |
| CD44 | Cluster of Differentiation 44 |
| CDK1 | Cyclin-dependent kinase 1 |
| cGMP | Cyclic guanosine monophosphate |
| CEBPB | CCAAT/enhancer binding protein beta |
| CH | Citron homology domain |
| CITK | Citron Kinase |
| CNP | C-type natriuretic peptide |
| COC | Cumulus-oocyte complexes |

| | |
|---|---|
| COS | Controlled ovarian stimulation |
| Co-SMAD | Common SMAD |
| CREB | cAMP response element-binding protein |
| DON | 6-diazo-5-oxo-l-norleucine |
| E | Embryonic day |
| ECM | Extracellular matrix |
| EGF | Epidermal growth factor |
| EGFR | EGF receptor |
| EI | Elongation Index |
| EMT | Epithelial-to-Mesenchymal Transition |
| EREG | Epiregulin |
| ERK1/2 | Extracellular regulated kinases 1 and 2 |
| ERM | Ezrin, Radixin and Moesin |
| F-actin | Filamentous actin |
| FH2 | Formin homology 2 domain |
| FOXO3 | Forkhead box O3 |
| FSH | Follicle Stimulating Hormone |
| FSHR | FSH receptor |
| G-actin | Globular actin |
| GAPs | GTPase-activating proteins |
| GDF9 | Growth Differentiation Factor 9 |
| GDIs | Guanine nucleotide dissociation inhibitors |
| GEFs | Guanine nucleotide exchange factors |
| GH | Growth Hormone |
| GlcA | Glucuronic acid |
| GlcNAc | N-acetylglucosamine |
| GnRH | Gonadotropin-releasing hormone |

| | |
|---|---|
| GOC | Granulosa-Oocyte Complexes |
| GV | Germinal vesicle |
| GVBD | Germinal vesicle breakdown |
| HA | Hyaluronan |
| HAS | HA synthases |
| HBP | Hexosamine biosynthetic pathway |
| hCG | Human chorionic gonadotropin |
| HCs | Heavy chains |
| HMMP | Hyaluronan-mediated motility receptor |
| HPG | Hypothalamic-pituitary-gonadal |
| HRP | Horse Radish Peroxidase |
| HYAL | Hyaluronidases |
| ICSI | Intracytoplasmic sperm injection |
| IUI | Intrauterine Insemination |
| IVF | *In Vitro* Fertilization |
| IVM | *In vitro* maturation |
| KIT | Kit receptor |
| KITL | Kit ligand |
| LGBTQIA | Lesbian, gay, bisexual, transgender, queer, intersex, and asexual |
| LPA | Lysophosphatidic acid |
| LH | Luteinizing Hormone |
| MAT | Mesenchymal-to-Amoeboid Transition |
| MET | Mesenchymal-to-Epithelial Transition |
| MHC | Myosin heavy chains |
| $MLC_{17}$ | Myosin essential light chains |
| $MLC_{20}$ | Myosin regulatory light chains |
| MLCK | Myosin Light Chain Kinase |

| | |
|---|---|
| MMPs | Metalloproteinases |
| MRCK | Myotonic Dystrophy Kinase-related CDC42-binding Kinase |
| mTOR | Mammalian target of rapamycin |
| MYPT1 | Myosin Phosphatase Target Subunit 1 |
| NMII | Non-muscle myosin II |
| NPF | Nucleation-promoting factors |
| NPR2 | Natriuretic peptide receptor 2 |
| OHSS | Ovarian hyperstimulation syndrome |
| OOX | Oocytectomized Cumulus-oocyte complexes |
| PBS | Phosphate-buffered Saline |
| PCOS | Polycystic Ovary Syndrome |
| PCR | Polymerase Chain Reaction |
| PDE3A | Phosphodiesterase 3A |
| PDE5 | Phosphodiesterase 5 |
| PDK1 | Phosphoinositide-dependent kinase 1 |
| PGC | Primordial Germ Cells |
| $PGE_2$ | Prostaglandin $E_2$ |
| PH | C-terminal pleckstrin homology domain |
| PI3K | Phosphoinositide 3-kinase |
| PIP3 | Phosphatidylinositol-3,4-triphosphate |
| PKA | Protein Kinase A |
| POF | Premature Ovarian Failure |
| POI | Primary Ovarian Insufficiency |
| PRL | Prolactin |
| PTEN | Phosphatase and tensin homolog |
| PTGS2 | Prostaglandin-endoperoxide synthase 2 |
| PTX3 | Pentraxin 3 |

| | |
|---|---|
| qPCR | Quantitative Polymerase Chain Reaction |
| RBD | Rho-binding domain |
| RHAMM | Receptor for Hyaluronan-Mediated Motility |
| RhoA | Ras Homolog Family Member A |
| ROCK1/2 | Rho-associated coiled-coil containing Kinase 1 and 2 |
| ROS | Reactive oxygen species |
| R-SMAD | Receptor SMADs |
| RSPO1 | R-spondin 1 |
| S6K | Ribosomal S6 kinase |
| SDF-1 | Stromal-cell-derived factor 1 |
| SEM | Standard Error of the Mean |
| Stra8 | Stimulated by retinoic acid 8 |
| TGFβ | Transforming Growth Factor β |
| TLR | Toll-like receptors |
| TNFAIP6 | Tumour necrosis factor α-induced protein 6 |
| TRPM7 | Transient Receptor Potential Melastatin 7 |
| TSC1/2 | Tuberous Sclerosis 1 and 2 |
| TSH | Thyroid Stimulating Hormone |
| TZP | Transzonal projections |
| WRC | WAVE Regulatory Complex |
| WT | Wild type |
| ZIPK | Leucine Zipper Interacting Kinase |

## List of Figures

# List of Tables

*Chapter 1:*

# Introduction

# 1. The female reproductive system in mammals

The term reproduction describes the generation of offspring. In asexual species, this act is carried on by, for example, cloning, a process during which one organism gives rise to another with the same genetic constitution. On the other hand, in sexually reproducing species, an individual is the product of combined genetic information from the progenitors and is genetically unique. Therefore, this mode of reproduction requires specialized reproductive cells, termed gametes, produced by the male and female reproductive tracts.

The female reproductive system in mammals includes the ovaries, the oviducts, the uterus, the vagina, accessory glands, and external genital organs. All these components work synergistically to generate competent female gametes, transport them to the fertilization site, produce sex hormones, support fetus development, give birth and, finally, nourish the newborn.

## 1.1. The hypothalamic-pituitary-gonadal axis

The hypothalamic-pituitary-gonadal (HPG) axis comprises the hypothalamus, the pituitary gland and the gonads, the primary reproductive organs. Its activity is crucial for the development and regulation of the female reproductive tract since its activity is required to *i*) produce and secrete sex hormones, *ii*) develop competent female gametes, called oocytes, and *iii*) trigger ovulation, the event that mediates their transportation to the fertilization site. The HPG axis and its components will be summarized in the following sections.

### 1.1.1. The hypothalamus

The hypothalamus is a small structure at the base of the third brain ventricle that harbours approximately 2,000 neurons in humans and 600 in mice, all responsible for producing and secreting neurohormones, including the gonadotropin-releasing hormone (GnRH) factors (1,2). GnRH, a decapeptide with a circulation half-life of 5 minutes, is released by the hypothalamus and binds its receptors on the surface of gonadotrope cells at the anterior pituitary. As a result, it will stimulate the synthesis and secretion of the gonadotropins Follicle Stimulating Hormone (FSH) and Luteinizing Hormone (LH) (3).

The hypothalamus releases GnRH in pulses or surges. After monitoring various environmental indicators such as body mass, nutritional status, stress levels and emotional state, the hypothalamus determines the frequency and amplitude of these GnRH secretory pulses,

except for right before ovulation, when it is released as a surge (4–6). The endocrine information is contained within the pulse's frequency and amplitude. For example, under normal physiological conditions, the menstrual cycle's follicular phase is characterized by GnRH pulses with a high frequency and a small amplitude. In contrast, the luteal phase relies on a lower frequency of large amplitude pulses.

### 1.1.2. The pituitary gland

The pituitary is an essential endocrine gland whose activity links the brain and ovarian function. That is because the pituitary translates the rhythm set by the hypothalamus into a gonadotropin signal that will control follicle development and ovulation. This gland contains three lobes: the posterior, the intermediate and the anterior (7–9). The anterior lobe harbours five different cell types that secrete either Thyroid Stimulating Hormone (TSH), Growth Hormone (GH), Adrenocorticotropic Hormone (ACTH), Prolactin (PRL) or the gonadotropins FSH and LH. The cells secreting FSH and LH in the circulatory system are termed gonadotropes (3).

Gonadotropins are glycoproteins composed of two subunits, termed α and β. The α subunit is common to all gonadotropins, namely FSH, LH, and human chorionic gonadotropin (hCG), mainly produced by placental cells. This subunit is non-covalently associated with a unique, hormone-specifying β subunit (10). While the α subunit is produced in excess by the gonadotropes, the β subunit synthesis is the rate-limiting step in producing FSH and LH (11,12). Moreover, both subunits have asparagine glycosylation sites, and the hormone's activity levels and circulation half-life are controlled by the extent and nature of the glycosylation (13–15). For instance, FSH tends to be less glycosylated during the follicular phase of the menstrual cycle, which increases its activity, favouring follicle development (16,17). Once secreted, FSH, LH and hCG will stimulate their target cells by binding to G-protein coupled receptors. The FSH receptor (FSHR) is expressed in granulosa cells, whereas the LHR, which binds both LH and hCG, is expressed in theca, mural granulosa and corpus luteal cells.

### 1.1.3. Ovaries: the female gonad

Ovaries are the primary female reproductive organs or gonads. Structurally, the ovaries are covered by an outer epithelium layer and are divided into two sections: cortex and medulla. The cortex is the outer portion of the organ, which often assumes a granular aspect due to the high concentration of ovarian follicles in various stages of development. The medulla is the

ovarian internal portion, which contains connective tissue and is highly vascularized. Functionally, the ovary produces and releases competent female gametes, the oocytes. To this end, each oocyte is enclosed in a follicle, the ovarian functional unit, that also harbours somatic cells responsible for integrating systemic hormonal and local paracrine signalling to support oocyte development.

#### 1.1.3.1. The human menstrual cycle

The menstrual cycle comprises a sequence of changes in hormone production and release that drives changes in the female reproductive tract – mainly in the ovaries and uterus. Therefore, it drives oocyte development and prepares the body for a possible pregnancy. The human menstrual cycle is characterized by a follicular phase, followed by midcycle ovulation and a luteal phase. In 1967, Treloar and colleagues (18) catalogued more than 275,000 menstrual cycles reported by Caucasian women attending the University of Minnesota. From this analysis, they determined that, for Caucasian women, the average duration of the menstrual cycle is 28 days, with the follicular and luteal phases each spanning approximately 14 days.

Throughout the female's reproductive life, small follicles on the cortex region of the ovaries will start to grow. Initially, their growth does not require gonadotropin stimulation. At the start of the follicular phase of the menstrual cycle, the increased secretion of FSH by the pituitary will stimulate follicle growth past these initial stages, supporting granulosa cell proliferation and follicle progression (19). At the end of the follicular phase, the high levels of estradiol produced by the granulosa cells of big antral follicles that grew in response to the gonadotropins will positively feedback the hypothalamus and the pituitary, leading to a surge in LH secretion (20,21).

The LH surge will trigger a series of changes inside the follicle: *i*) oocyte maturation, *ii*) cumulus layer expansion, *iii*) luteinization, and *iv*) release of the cumulus-oocyte complex after follicle rupture. Ovulation is then followed by the luteal phase, characterized by lower circulating levels of FSH and LH (4,22). During this phase, the remaining granulosa cells complete their differentiation and form the corpus luteum. This structure is an endocrine body that, in response to the hCG produced by placental cells in case of a successful pregnancy, will keep producing progesterone and sustain it (23).

#### 1.1.3.2. The rodent estrus cycle

While humans and non-primates have menstrual cycles, rodents have estrus cycles, representing the cyclical pattern of ovarian activity and behaviour that dictates reproductive receptibility. An estrus cycle, typically 4 to 5 days long for rodents, follows the same general mechanisms of a human menstrual cycle, with gonadotropins responsible for stimulating follicle growth and ovulation (24,25). The estrus cycle can be divided into 4 distinct phases: proestrus, estrus, metestrus and diestrus.

Proestrus is the phase during which late follicular development takes place, and a peak in estradiol produced by the granulosa cells from the rapidly growing antral follicles triggers a gonadotropin surge. In response to that, ovulation happens the following day, which is the estrus phase. The estrus phase is also accompanied by sexual receptivity behaviour. Next, the metestrus represents the early luteal phase, when the corpora lutea will continue to differentiate and grow until it reaches its maximum size, approximately 24 hours after ovulation. The next day, the female enters diestrus, a phase in which the uterus is ready for implantation and the corpora lutea are functional. If pregnancy does not occur, the uterine lining will be absorbed instead of shed, as is observed in a human menstrual cycle. However, if pregnancy ensues, the corpora lutea will be maintained by PRL, seeing that rodents do not produce hCG (26). Therefore, the rodent estrous cycle is also characterized by hormonal changes that drive gamete development and prepare the uterine environment for a possible pregnancy, supporting reproduction.

### 1.2. Female infertility

Infertility or subfertility is defined as failure to achieve pregnancy after 12 months of consecutive unprotected intercourse or therapeutic donor insemination (27,28). It has been estimated that infertility affects around 10-15% of couples in industrialized countries (29). Indeed, infertility prevalence among couples in Canada is estimated between 12 and 15% (30), and according to the American Society of Reproductive Medicine, at least 15% of couples in the United States are affected by it (31). Different from other health conditions, infertility involves two individuals, and there are a series of various underlying causes contributing to it that can spawn from both the male and female sides. While men continuously produce viable sperm throughout their lives, the most well-established factor affecting female fertility is age (32). Women's likelihood of bearing a child is stable from puberty to around 30 but declines rapidly

until menopause (33–35). This is increasingly more significant as socioeconomic factors raise the average age women have their first child (36). Other than age, alternative drivers of female infertility can include prematurely diminished ovarian reserve, ovulatory dysfunction, and uterine, pelvic or tubal abnormalities, which are illustrated in Figure 1 and will be briefly discussed below.

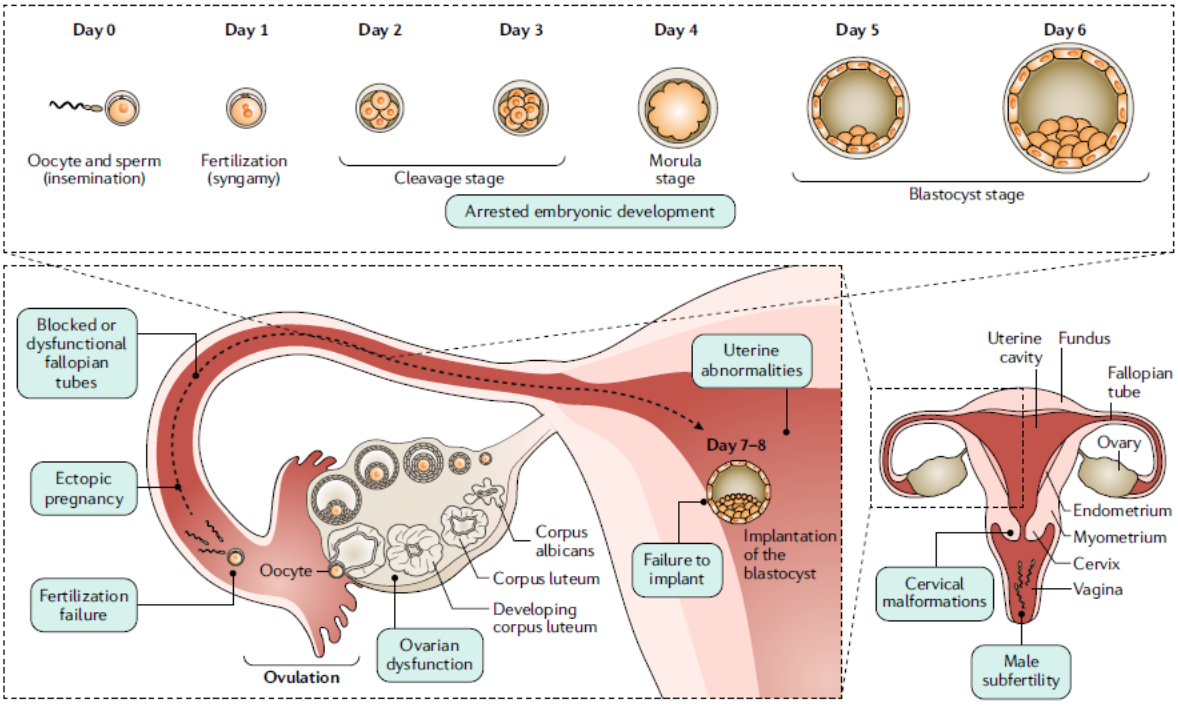


**Figure 1: The female genital tract and factors that affect fertility**. Several serial steps are required to establish a pregnancy, including developing and releasing a competent oocyte by the ovaries, fertilization by spermatozoa, passage through the oviducts (fallopian tubes), and implantation into the uterus. Oocyte or sperm abnormalities, or the failure of the sperm to reach and fertilize the oocyte, can prevent the generation of an embryo. Embryo development inside the oviducts can fail during the preimplantation stages, and implantation can fail or happen outside of the uterus (ectopic pregnancy). Uterine abnormalities deviate from a receptive uterine environment, a requirement for proper embryo implantation and development. Adapted from Farquhar *et al*. (29).

Prematurely diminished ovarian reserve is termed Premature Ovarian Failure (POF) or Primary Ovarian Insufficiency (POI). POF is usually observed due to an initial low ovarian reserve, an increased rate of follicle atresia or cytotoxic therapies, such as chemotherapy (37).

Anovulation is caused by ovulatory defects that can be related to obesity, hypothalamus-pituitary-gonad axis dysfunction, Polycystic Ovary Syndrome (PCOS) and other causes. PCOS, however, has been highlighted as the most common cause of anovulation (38,39). Although the exact causes of PCOS are still unknown, women with the condition have increased frequency of GnRH pulses that alter the FSH:LH secretion ratio, leading to higher androgen levels, lower oocyte maturation and anovulation (40). Tubal, pelvic and uterine abnormalities include scarring, adhesions, fibroids or endometriosis, a condition in which the uterine lining grows outside the uterus on different peritoneal surfaces (41).

Despite recent advances, approximately 30% of infertile couples are diagnosed with unexplained infertility. This happens in cases where ovulation and sperm quality have been confirmed, but no pregnancy was observed (42). Since ovaries are a crucial organ in maintaining fertility, this scenario warrants further in-depth studies to understand their functioning and prompt the development of better treatment for reproductive disorders.

Infertility management starts with a medical workup, which includes the assessment of lifestyle, health conditions, and medical history, plus sperm assessment when recommended. Initially, the approach can be non-interventional, and the clinician will check the couple's awareness of basic fertility concepts and can also calculate the chances of non-assisted conception using predictive models. These models, such as the Hunault model, consider female age, sperm motility, and duration of the period they have been trying to conceive, among others, to calculate the chances of natural conception throughout a year (43). However, if the prognostic is not good – lower than 30% chance of unassisted pregnancy in one year – options for active intervention to promote pregnancy include Intrauterine Insemination (IUI) and *In Vitro* Fertilization (IVF) and its associated techniques such as intracytoplasmic sperm injection (ICSI) and *in vitro* maturation (IVM), also known collectively as Assisted Reproductive Technologies (ARTs).

Over the past 20 to 30 years, a steady increase in the demand for ARTs has been observed due to the higher number of couples that are referred to the procedures, both due to identified or unexplained infertility diagnoses (44). Another contributing factor to this observation comes from single persons, gender non-conforming individuals, and members of the lesbian, gay, bisexual, transgender, queer, intersex, and asexual (LGBTQIA) community seeking fertility treatments. Single persons and members of the LGBTQIA community have the same

interest in having children as heteronormative couples, and family building for these groups includes different approaches, some requiring ARTs (45,46).

### 1.3. Assisted reproductive technologies

During the most fertile stages of a woman's life, the chances of non-assisted pregnancy during a given menstrual cycle are up to 30% due to the short window of oocyte viability after ovulation (47). Moreover, lifestyle, age, and health conditions can decrease this likelihood. Therefore, assisted reproductive technologies were designed to aid individuals in achieving pregnancy. By definition, these techniques involve any procedure in which oocytes and/or embryos are manipulated.

Standard IVF is a fertility treatment in which mature oocytes are fertilized outside of the body, and the resulting embryos that are deemed to have the best chances of establishing a pregnancy are transferred into the uterus (Figure 2). The first IVF procedure in humans was performed in 1978 with a single oocyte collected during a laparoscopic procedure (48). In this case and the ones that shortly followed, a natural menstrual cycle was monitored for the collection of a single oocyte. However, controlled ovarian stimulation (COS) with exogenous gonadotropin administration has become more common since then, as it allows for the development of multiple follicles, increasing the number of mature oocytes retrieved and the chances of success (49). Once the eggs are collected, they are incubated with sperm so fertilization can happen *in vitro*. For couples with a male infertility factor, including low sperm motility or count, ICSI is considered an alternative. In this procedure, individual sperm are selected based on morphological parameters and injected directly into the oocyte cytoplasm (50). The developing embryos are then incubated and transferred on day 3 after cleavage or on day 5 after reaching the blastocyst stage. Day 5 transfers are more common since the morphological analyses to predict implantation success are more accurate at this stage (51,52).

Analysis of more than 144,000 embryo transfers performed in European fertility centers in 2013 reported an overall pregnancy rate of 34.5%, regardless of the infertility cause (53). According to the last report published in June of 2023 by the Human Fertilisation and Embryology Authority (UFEA, in the UK), the average pregnancy rate for women under 34 years of age undergoing IVF was 41%, but 28% for women aged between 35-39 years. In addition to this relatively low success rate, IVF is a lengthy process with multiple critical steps,

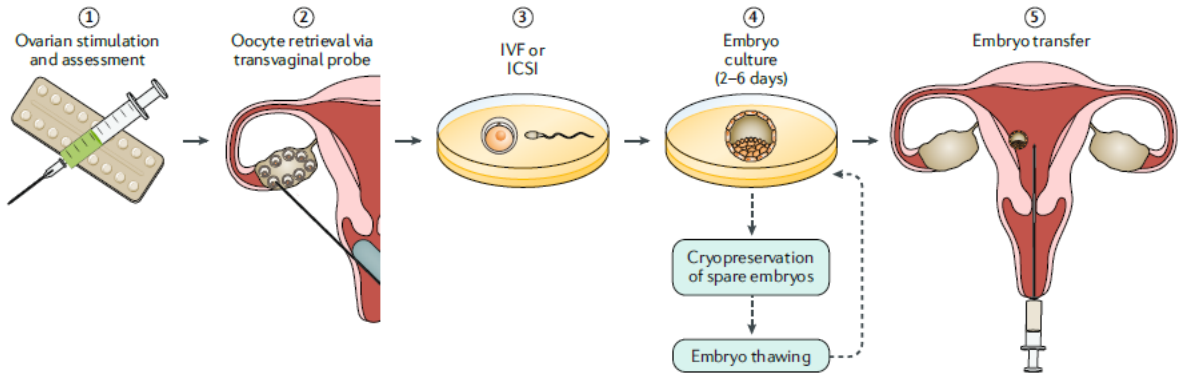


**Figure 2: The IVF protocol**. In step 1, gonadotropins are administered to stimulate follicle growth, and gonadotropin-releasing hormone (GnRH) agonists are given to suppress the natural menstrual cycle and downregulate the pituitary gland. When the follicles have reached an appropriate size, final maturation of the oocytes is induced, usually with hCG injections. In step 2, oocytes are collected with a transvaginal ultrasonography probe for guidance under general or local anesthesia with sedation. Step 3 is fertilization, which can be done by incubating the oocytes with sperm or intracytoplasmic sperm injection (ICSI). Once the oocytes have been fertilized, the developing embryos are cultured, which constitutes step 4. One is selected for transfer from the pool of available embryos in step 5. The leftover good-quality embryos can be cryopreserved for posterior use if the pregnancy is not established or if the couple desires another child. Adapted from Farquhar *et al*. (29).

and varied factors can hinder it and increase the risk factors. For instance, some women do not respond to COS or are at risk of ovarian hyperstimulation syndrome (OHSS)(49,54). OHSS is a serious condition where the ovaries swell in response to exogenous hormonal treatment and produce an excess of growth factors, possibly leading to renal injury or thromboembolism. Patients with PCOS, the most common cause of anovulation-related infertility cases, are at particular risk for OHSS when undergoing IVF (55,56).

Alternatively, to avoid such risks, immature oocytes can be retrieved from the ovaries, matured outside the body, and only then submitted to ICSI or incubated with sperm. This approach is a mild version of the standard IVF protocol (57) and is indicated for patients at high risk of OHSS, including the ones with PCOS, or women who do not respond to COS. Additionally, the milder hormonal stimulation and the consequently lower associated costs are reasons why the IVM approach may gain increased interest. However, the pregnancy rates of

IVM procedures are still considerably low when compared to the standard IVF protocol (58–62). This discrepancy in outcomes has been, at least partially, associated with varied protocols employed in different fertility centers (63). While some centers will only use a short course of FSH to stimulate follicle growth, others will also administer hCG right before oocyte retrieval (63–65) in a strategy termed "hCG triggered-IVM" or "truncated IVM" (66). This results in a heterogeneous population of collected oocytes that can be at the GV, MI or MII stages, impeding IVM protocol standardization and success. However, despite the protocol, the overall quality of the IVM oocytes tends to be inferior to *in vivo* matured ones (67).

Romero and colleagues (68) proposed an alternative approach to overcome IVM's low yield of good-quality embryos. Their aim was also to develop a method with little to no hormonal stimulation, which would be a good alternative for PCOS patients and women who do not respond to COS. In this work, they collected immature oocytes associated with their surrounding support somatic cells, the cumulus. These cumulus-oocyte complexes (COCs) were obtained from small and medium antral follicles of unprimed mice and were then submitted to a pre-maturation culture period before *in vitro* fertilization. Presumably due to the presence of the cumulus cells, which play a vital role in oocyte development during folliculogenesis, the oocytes continued growing during the pre-IVM culture, aiding their capacitation. For this reason, the procedure is denominated capacitation (CAPA-) IVM. The oocytes submitted to this process presented higher maturation and blastocyst formation rates. So far, this approach has been tested in livestock animals (69) and humans upon brief FSH stimulation (70,71).

The improvement in survival rates of cancer patients has contributed to the increased demand for ARTs due to the gonadotoxic nature of cancer treatment. Currently, adult and postpubertal patients can freeze mature oocytes for future IVF procedures or choose to cryopreserve embryos for future implantation. However, if the treatment cannot be postponed for two weeks or the patient is prepubertal, those are not valid options. In these cases, ovarian tissue cryopreservation can be performed for future reimplantation. Nonetheless, this approach is still experimental (72,73) and requires additional surgeries and, depending on the cancer type, this is not recommended due to the risk of reintroducing cancerous cells (74–77).

Transgender individuals represent a small but growing population that seeks fertility clinics. Currently, the available options for fertility preservation in transmen are similar to the ones available for cancer patients and include oocyte or embryo cryopreservation, ovarian tissue

cryopreservation, and IVM (78). Thus, the same obstacles regarding puberty are also at play for this group, in addition to the fact that gender-affirming treatments, including hormone therapy and surgery, have significant impacts on fertility. Additionally, there is a growing number of patients presenting for gender-affirming treatment and a trend toward decreasing age at the time of presentation (79). Therefore, the development of a reliable and efficient IVM protocol would benefit couples struggling with infertility, single persons and members of the LGBTQIA community wishing to conceive, and cancer survival patients. All these different groups would greatly benefit from a good alternative for *in vitro* oocyte capacitation, maturation and fertilization. This possibility requires further study of the processes involved in producing a mature and fertilizable oocyte.

## 2. Folliculogenesis and oogenesis

In mammals, the female germ cell undergoes a long differentiation journey before being fertilized and giving rise to viable offspring. This process starts during embryo development when oocytes differentiate from primordial germ cells that had previously migrated to the genital ridges to become oogonia. At this stage, the prophase I-arrested oocytes associate with pre-granulosa cells and form the primordial follicles, which can remain quiescent for years. But once recruited to the growing follicle pool, they will develop into primary, secondary, antral, and preovulatory follicles, finally giving rise to a developmentally competent oocyte (Figure 3). Therefore, folliculogenesis guarantees the production of fertilizable female gametes, an essential process for mammalian fertility.

### 2.1. Primordial germ cell differentiation

Primordial Germ Cells, or PGCs, are essential for fertility as they initiate the process of transferring genetic and epigenetic information from one generation to the next. In some species, such as *Drosophila* and *C. elegans*, PGCs differentiate through pre-formation (80). In this process, the germ cell fate is acquired by inheriting a specific subset of RNAs and proteins from the fertilized oocyte while the remaining cells differentiate into somatic cells. Mammals, on the other hand, specify PGCs by a different process, denoted induction (81).

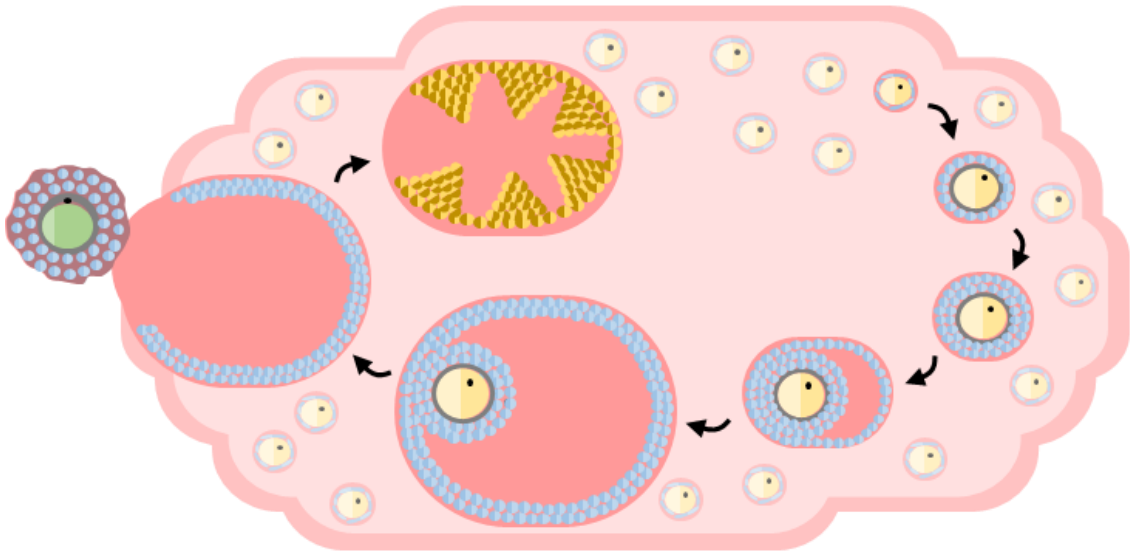

**Figure 3: Folliculogenesis**. Starting at the top right-hand side, a primordial follicle from the follicle reserve is recruited to the growing pool, developing past the primary, secondary, early antral, and antral stages. A mature and fertilizable oocyte is ovulated upon the ovulatory stimulus, while the remaining follicular cells undergo luteinization and form the corpus luteum (CL).

The induction of PGCs in mammals starts after the differentiation of the trophectoderm and the primitive endoderm (82,83). From embryonic day 6.5 (E6.5) in mice, signals from the extraembryonic ectoderm and visceral endoderm modulate the transcriptional activity of underlying epiblast cells (84). Among these signals, Bone Morphogenetic Protein 4 (BMP4) is primarily responsible for initiating specification (81,85). It signals through canonical BMP receptors in the epiblast cells (82,86,87) and activin A receptor type I on the visceral endoderm cells to indirectly facilitate the specification process (88). According to information obtained by studying knockout mouse models, BMP8b secreted by the extraembryonic cells and BMP2 secreted by the visceral endoderm also play indispensable roles in the induction of PGCs (89,90). As a result of this integrated signalling network, a cluster of PGCs can be first detected on E7.5 (91).

Once the germ cell fate is acquired, the PGCs gain motility, a valuable tool to reach the genital ridges, where the gonad develops in the embryo. A change in the adhesion dynamics of PGCs marks the onset of migration. For example, the cell-cell adhesion protein E-cadherin is required for PGC differentiation (92), but its expression decreases as soon as the PGCs acquire mobility and become incorporated in the hindgut epithelium (93,94). Similarly, PGCs' adhesion

to the extracellular matrix (ECM) also changes, and a lower affinity for laminin and fibronectin is observed (95). In parallel with decreasing their adhesion, PGCs assume a round morphology, a hallmark of an ancestral migration mode termed amoeboid (96). Further details on this migration mode will be provided in section 4.5.2 of this document.

Despite observed divergence regarding germ cell migration paths, general features are found in the most studied species. For example, most PGCs are induced at the posterior edge of the embryo or between embryonic or extraembryonic tissues. After induction, gastrulation often causes translocation initiation, which can be passive, as observed in drosophila (97), or active, as suggested by studies in mice (98,99). This initial translocation gets the PGCs to the center of the embryo, from where they must migrate through an epithelial barrier. Once this barrier has been crossed, they migrate further, both dorsally and laterally, to form the two distinct groups of germ cells that will integrate each developing gonad.

Although the migratory phenotype is essential for fertility, it is not sufficient: to reach the developing gonad, PGCs also need guidance. The existence of such a mechanism was postulated after observations of the high fidelity with which PGCs reach their destination (100). The idea was corroborated by solid evidence demonstrating the power of mouse genital ridge explants to attract PGCs across a significant distance *in vitro* (101–103). A central guidance mechanism was first uncovered in zebrafish (104,105) but was soon also identified in mice (106–108), chicken(108), and other marine species (109,110). This signalling mechanism is mediated by a gradient of the small chemokine stromal-cell-derived factor 1 (SDF-1, also called CXCL12) that binds and activates the GPCR receptor 4 (CXCR4) expressed by the migrating PGCs. Later, it was also shown that a steep gradient of SDF-1 is needed to properly guide the migrating PGCs, with an ectopic expression of *sdf-1* by the germ cells being enough to sterilize zebrafish (111). Further investigation showed *sdf-1* to have a dynamic expression at its peak just in front of the migrating germ cells (104,107,108), which is crucial in establishing the steep gradient required for successful signalling and PGC guidance.

All these changes allow the PGCs to translocate from one part of the embryo to another and invade through gaps and openings in their environment, following the cues to maintain their migratory phenotype and reach their destination. By E9.5, the PGCs will have emerged from the hindgut and colonized the genital ridges before migrating inwards to form the primitive medulla

and the sex cords (91). In females, this is where PGCs lose their motility and become oogonia (112,113).

### 2.2. Primordial follicle formation

Oogonia give rise to the germ cell population in the ovary. They do so by dividing mitotically to increase in number. However, this mitotic process differs from the one observed in other tissues or developmental stages, as these cells do not undergo complete cytokinesis but remain connected by intercellular bridges, forming germ cell cysts (114–116). At E13.5, following an anterior-to-posterior pattern in the murine ovary, the inter-connected oogonia will start entering meiosis (117,118). Retinoic acid, an active vitamin A derivative, is a key signalling molecule in this process. It binds its intracellular receptors to stimulate *Stra8* (stimulated by retinoic acid 8) expression, promoting germ cell chromatin replication and the official entry in the meiotic division (119–122). Activin A, a member of the Transforming Growth Factor β (TGFβ) superfamily, may cooperate with retinoic acid in promoting the meiosis of oogonia since it stimulates the expression of premeiotic and meiotic genes, including *Stra8* (123). Moreover, signalling molecules produced by ovarian somatic cells, including the canonical wingless-type MMTV integration site family member 4 (WNT4) and R-spondin 1 (RSPO1), have also been shown to be involved in oogonia meiosis entry (124). RSPO1 deficient ovaries lack *Stra8* expression, compromising PGC proliferation and oogonia meiosis entry (125). Once meiosis is initiated, the oogonia will progress through the leptotene, zygotene, and pachytene, getting arrested at the diplotene stage of meiotic prophase I, giving rise to primary oocytes. The meiotic arrest of mouse oocytes at this stage is crucial for primordial follicle formation (126).

Besides oocyte differentiation, primordial follicle formation also depends on proper pre-granulosa cell recruitment and differentiation into granulosa cells. It is an event coordinated by a set of secreted factors, including the previously mentioned WNT4 and RSPO1 signalling molecules and additional ones, such as the transcriptional regulator FOXL2 (124). Schmidt *et al*. (127) have identified expression of the granulosa cell marker FOXL2 as soon as E12.5 until primordial follicle formation. *Foxl2* deficiency impairs primordial follicle formation by interfering with granulosa cell differentiation and proper basal lamina formation (128). Additional work done by Padua *et al*. (129) showed that the deletion of transcription factors

*Gata4* and *Gata6* decreased FOXL2 expression, preventing the formation of the primordial follicle pool. At E17.5, only FOXL2-positive pre-granulosa cells succeed in invading cysts to start forming the primordial follicles (130). However, as mentioned above, FOXL2 is not the only factor required for pre-granulosa cell differentiation. Loss of function of WNT4 and RSPO1 leads to sex reversal of the gonad, denoted by expression of Sertoli cell markers SOX9 or *Dhh* (131,132). Oocyte-specific transcription factors such as *Figla* (133,134) and *Nobox* (135,136) have also been implicated in oocyte survival, primordial follicle formation and male germline gene expression prevention. These studies demonstrate how expressing different transcription factors at the right time and cell type during embryonic development paves the road for proper follicle formation and development.

In mice, the germ cell cysts undergo programmed breakdown at birth (137). During this period, the mitotically arrested pre-granulosa cells infiltrate the cysts, and degradation of the oocyte population leads to a significant decrease in the ovarian germ cell content (115). The remaining oocytes will then be enveloped by flattened pre-granulosa cells, giving rise to the primordial follicles. A basement membrane will also enclose these follicles, separating them from the stromal-interstitial tissue environment (138,139).

### 2.3. Primordial follicle activation

Primordial follicle activation designates the commitment of a small follicle to growth, as it will eventually lead to either the ovulation of a mature oocyte or to follicle atresia (140). It has been described to happen both before and after a female reaches sexual maturity. For example, a subset of primordial follicles in cows and sheep will be activated and further differentiate into primary, preantral and antral stages during late gestation (141,142). Before birth, however, these follicles will undergo atresia so that only primordial follicles remain in the ovary. A similar pattern is observed in mice, where two main classes of primordial follicles have been identified: the medullary and the cortical primordial follicles (143). The medullary follicles are activated right after birth and proceed through the folliculogenesis stages but are not ovulated. Once the female reaches sexual maturity, however, a subset of the cortical primordial follicles is continuously recruited to the growing follicle pool while the rest remains in the quiescent state.

Initially, there were conflicting data regarding the role of gonadotropins in primordial follicle activation. For example, it was reported by Halpin and Charlton in 1988 that a transgenic

mouse model with impaired GnRH signalling had a smaller population of early-growing follicles (144). FSH analogue injections rescued this effect. However, it had been previously shown that gonadotropin injection in young mice does not alter the rate of primordial follicle activation (145). In fact, studies carried out on mouse models deficient for FSH production or FSHR expression showed that the primordial follicles could still develop up to the preantral stage, indicating the absence of gonadotropin signalling did not affect primordial follicle activation (146,147). Therefore, primordial follicle activation is believed to rely on intraovarian factors rather than on direct gonadotropin signalling.

The first morphological indicator of primordial follicle activation is the remodelling of granulosa cell shape: previously squamous, the granulosa cells become cuboidal as they re-enter the mitotic cycle (148). Oocyte growth, which will be covered in more detail in the next section, starts shortly after the morphological changes in the granulosa cells are observed (149). Although vastly studied, the molecular mechanism behind the selective activation of primordial follicles is still poorly understood. Different lines of investigation point to a model in which local ovarian factors stimulate activation of the phosphoinositide 3-kinase (PI3K) pathway in granulosa cells, increasing protein synthesis, ultimately leading to granulosa cell morphology changes and enabling oocyte growth initiation.

The PI3K signalling pathway, illustrated in Figure 4, is reported to control cell growth, metabolism, and proliferation (150). Active PI3K stimulates a series of downstream effectors, namely the phosphoinositide-dependent kinase 1 (PDK1), AKT, also known as protein kinase B, the mammalian target of rapamycin (mTOR), and the ribosomal S6 kinase (S6K)(150). AKT is a central player of the canonical PI3K signalling and, upon activation, will localize to the membrane and phosphorylate its targets, including tuberous sclerosis 1 and 2 (TSC1/2)(151). When active, these factors inhibit protein synthesis by preventing mTOR and S6K activity, and direct phosphorylation by AKT will readily inactivate TSC1/2, lifting the inhibitory activity over the PI3K pathway. Besides TSC1/2, the phosphatase and tensin homolog (PTEN) and the transcription factor Forkhead box O3 (FOXO3) are critical negative regulators of the PI3K pathway. PTEN catalyzes the hydrolysis of one phosphate group from Phosphatidylinositol-3,4-triphosphate (PIP3), a product of PI3K activity, which in turn impairs the recruitment of PDK1, a kinase required for AKT phosphorylation (152). Without PTEN signalling, PI3K-AKT will be active and phosphorylate FOXO3. The phosphorylation of FOXO3 leads to its inactivation and

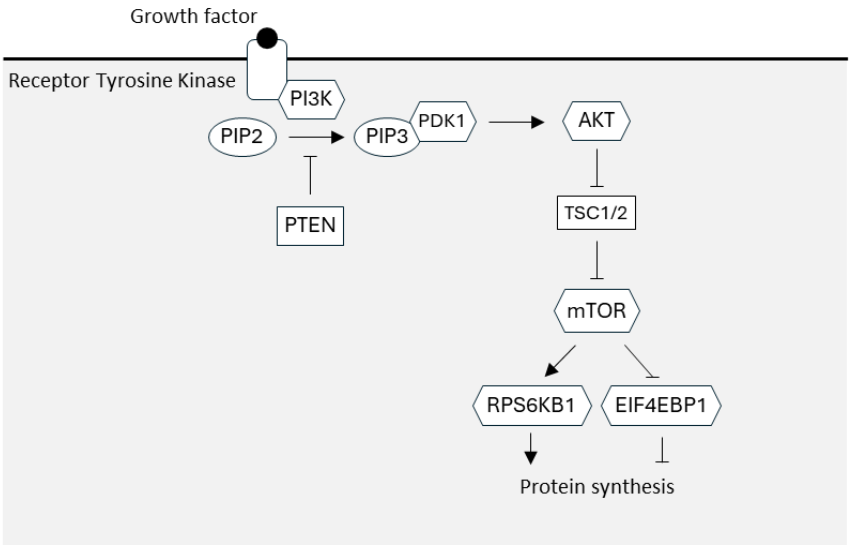


**Figure 4: The canonical phosphoinositide 3-kinase (PI3-Kinase) signalling pathway**. Upon growth factor binding to tyrosine kinase cell receptors, PI3K initiates the conversion of PIP2 into PIP3, a reaction that PTEN can undo. Increased PIP3 concentration at the membrane recruits and activates PDK1, which, in turn, phosphorylates AKT. AKT relieves the inhibitory pressure of TSC1/2 on mTOR, triggering protein synthesis.

translocation to the cytoplasm, where it can no longer promote the expression of cell cycle arrest genes (153). Therefore, PI3K-AKT-mTOR-S6K signalling suppresses cell cycle arrest and leads to increased protein synthesis by the cell.

In the ovary, deletion of *Pten* or *Foxo3* leads to a similar phenotype characterized by increased primordial follicle activation and oocyte overgrowth (154,155). Consistently, specific deletion of *Tsc1* in granulosa cells of mouse primordial follicles leads to PI3K activation and the transition of granulosa cells from squamous to cuboidal morphology (156). These results strongly suggest that the finely regulated recruitment of dormant primordial follicles to the growing pool depends on activating the PI3K signalling pathway on the flattened granulosa cells.

### 2.3.1. Oocyte growth initiation

Just as PI3K activity is required in the granulosa cells for primordial follicle activation, it might also be essential in oocyte growth initiation. In fact, multiple lines of evidence suggest that the signal initiating oocyte growth comes from the granulosa cells and activates the PI3K signalling pathway in the oocyte. An upstream regulator of PI3K, the growth factor Kit ligand

(KITL), is constitutively expressed by granulosa cells (157,158), and its receptor, the Kit receptor (KIT), is expressed by oocytes (159,160). The relationship between KITL-KIT signalling and oocyte growth initiation has been investigated by different approaches. For example, the expression of a constitutively active form of KIT was first targeted to mouse oocytes (161). Upon investigation, it was shown that granulosa cells remained flattened around the oocyte, indicating that the primordial follicles were not activated due to oocyte-activated KIT. Nonetheless, almost all oocytes started growing shortly after birth, which was corroborated by phosphorylated AKT detection in these cells, confirming the correlation between activated oocyte PI3K signalling and oocyte growth. In a different approach, functional KIT expression in the oocyte was ablated by deleting the exon encoding the kinase domain (161). In this system, the oocytes failed to grow even when the granulosa cells assumed a cuboidal morphology, denoting follicle activation and indicating that the KIT-deficient oocytes could not respond to the growth-promoting factor produced by the granulosa cells. Taken together, these results suggest that KITL, while not required for granulosa cell cuboidalisation, integrates the paracrine signal loop necessary for oocyte growth initiation shortly after primordial follicle activation.

Since KITL-KIT signalling activates the PI3K pathway in oocytes, its implications for oocyte growth were also closely investigated. This was done by targeting negative regulators of PI3K signalling, such as PTEN, TSC1/2 or FOXO3 (refer to Figure 4 for an overview of the PI3K signalling pathway). *Pten* deletion from the oocyte of primordial follicles led to global oocyte growth shortly after birth (154,162). The detection of increased phosphorylated AKT levels supported the implications of PI3K signalling. Similarly, oocyte deletion of *Tsc1* or *Tsc2* also triggered global oocyte growth and promoted the phosphorylation of ribosomal protein 6, a downstream target of AKT (163,164). In these cases, the granulosa cells tended to keep the flattened morphology, further corroborating the model in which oocyte PI3K signalling downstream of KITL-KIT binding is required for oocyte growth initiation.

### 2.4. Progression from the primary to the preovulatory follicle

As the primordial follicle enters the growing pool and gives rise to the primary follicle, the granulosa cells will continue proliferating to cover the expanding surface of the ever-increasing oocyte (165,166). As two layers of granulosa cells surround the oocyte, a new population of somatic cells starts to differentiate: the theca. At this point, the basement

membrane separates the layers of epithelial-like granulosa cells from the newly formed mesenchymal-derived theca, as it surrounds the whole follicle. This new compartment is responsible for capturing cholesterol and catalyzing its conversion into androgens, a critical substrate the granulosa cells use to produce estrogens (167). Blood supply is limited to the theca cells at this stage and does not penetrate the basement membrane (168).

Early follicular development was believed to be FSH-independent since follicles from *Fshr*-null can develop normally up to the preantral stage (169). However, treatment of young rats with a GnRH antagonist led to decreased ovarian weight, characterized by a reduced number of developing follicles and increased atresia (170). In contrast, FSH injections in rats under the same GnRH treatment increased ovarian weight and preantral follicle development. Additionally, preantral follicles of different species have been shown to be responsive to FSH exposure (171–174). Therefore, folliculogenesis can be divided into gonadotropin-responsive stages, from primary to preantral, and gonadotropin-dependent stages, early antral to preovulatory stages, as illustrated in Figure 5.

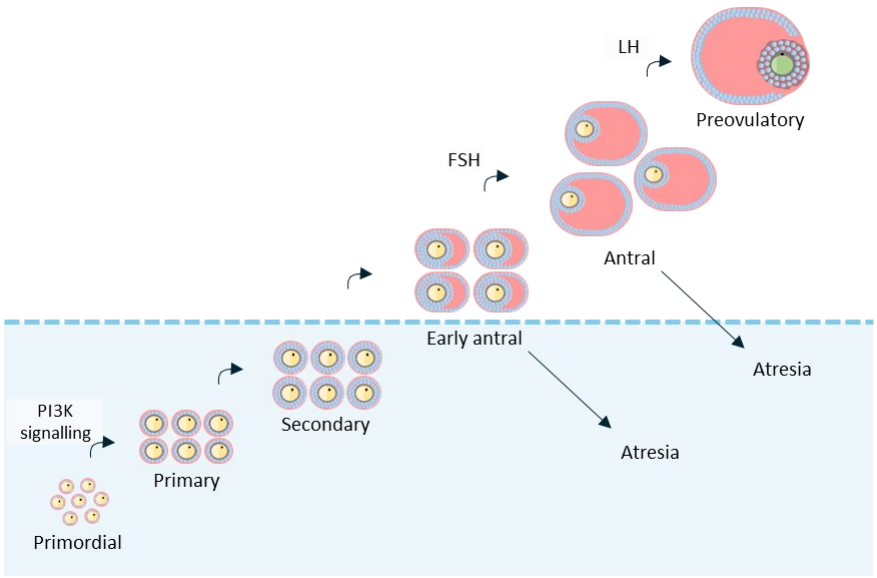


**Figure 5: Hormonal regulation of follicular growth**. After activation, follicle growth and development go through the gonadotropin-responsive primary and secondary stages (below the dashed line) and then progress to the gonadotropin-dependent stages, namely early antral, antral and preovulatory (above the dashed line).

Follicle growth up to the preantral stage is mainly regulated by bidirectional communication intermediated by paracrine factors originating from both the oocyte and the somatic cells. While the oocyte plays a vital role in the proliferation, differentiation and metabolism of the somatic follicular components, they, in turn, support oocyte growth and development (35,175,176). The details regarding this interaction will be explored in the oocyte growth section.

As the granulosa cells proliferate and accumulate around the oocyte, small fluid-filled cavities start to appear within the cell layers. Each cavity grows up to the point where they merge, creating one antrum that characterizes the new follicle stage. The antrum physically separates the granulosa cells into two populations: the mural granulosa cells, which line up the follicular wall, and the cumulus cells, found in close association with the growing oocyte. Most follicles will fail to respond to FSH and consequently undergo atresia (175,177,178). However, successful FSH stimulation activates many signalling pathways to *i*) prevent granulosa cell apoptosis (179–181), *ii*) stimulate their proliferation (182,183), and *iii*) promote estrogen production (184). As previously shown, a mouse model lacking expression of functional FSHR presents underdeveloped accessory sex tissues and significantly smaller ovaries characterized by arrested follicular development at the preantral stage and anovulation (169). Moreover, FSHR activation leads to the expression of various genes throughout the follicle, including the *Lhcgr* by the mural granulosa cells (185,186) and the *Egfr* by the cumulus cells (187). Thus, FSH exposure is not only required for follicle growth up to the preovulatory stage but also vital for guaranteeing granulosa cells' further differentiation and responsiveness to the LH surge.

### 2.4.1. Oocyte growth

The oocyte growth phase in mice spans around 3 weeks, a period during which the oocyte diameter increases from 12 to 80µm, representing a 500-fold increase in volume (188–191). This significant growth reflects continuous synthesis and storage of *i*) RNAs and proteins, *ii*) new organelles, including mitochondria and Golgi complex, and *iii*) new cytoplasmic structures, such as cortical granules and lipid droplets (192–194). The production and storage of these components are essential to support oocyte maturation and early embryo development (191,195–199). However, the oocyte is not solely responsible for its growth or nutrient accumulation. The role of granulosa cells in sustaining oocyte development was singled out early on when

Granulosa-Oocyte Complexes (GOCs) were collected and cultured in three configurations: intact GOCs, denuded oocytes in coculture with granulosa cells, or only denuded oocytes. While the oocytes within the intact GOCs continued growing, the ones in coculture with the granulosa cells or cultured alone failed to grow (200). Therefore, it is not only the physical proximity to granulosa cells but also their physical contact with oocytes that play a critical role in providing the developing gamete with essential nutrients (160,201).

During growth, granulosa cells and oocytes have a complementary metabolic profile. For example, while oocytes lack the machinery to metabolize glucose as their primary energy source (202), granulosa and cumulus cells present high expression of glycolytic enzymes and reportedly metabolize glucose to pyruvate and transfer these molecules to the oocyte, which can utilize them as an energy source (203). Similarly, oocytes rely on the granulosa cells to obtain certain amino acids and cholesterol since it also presents a low expression of alanine transporters (204) and enzymes of the cholesterol biosynthesis pathway (205). Therefore, the oocyte not only receives signals and nutrients from its neighbouring cells but also regulates their differentiation and metabolism (194). It does so in a paracrine fashion by producing and secreting growth factors that bind receptors on the plasma membrane of granulosa cells to stimulate their proliferation and shape their metabolic profile.

Growth Differentiation Factor 9 (GDF9) and Bone Morphogenetic Protein 15 (BMP15) are TGFβ superfamily members expressed by the growing oocyte (206,207). These factors, such as other TGFβ superfamily members, are biologically active as homo- or heterodimers (208,209) and their signalling is carried out after binding a heteromeric complex of type I and type II serine-threonine kinase receptors. Type II receptors phosphorylate type I receptors after heterodimerization, which is stimulated upon ligand binding. This will lead to the recruitment and phosphorylation of SMAD proteins. SMADs are signal transducers of downstream TGFβ ligands signalling and can be called receptor SMADs (R-SMADs), such as SMAD2/3 or SMAD1/5/8, or common SMAD (Co-SMAD), the SMAD4. Depending on the combination of ligand, type I, and II receptors, different SMADs will be activated. For example, GDF9 binding to the receptors will recruit and phosphorylate SMAD2/3 and BMP15, SMAD1/5/8 (210). The phosphorylated SMADs will then bind SMAD4, forming a complex that will translocate to the nucleus and regulate the expression of target genes.

GDF9 can be detected in oocytes starting on primary follicles (206). Ovaries of female mice with global deletion of *Gdf9* harbour only primordial and one-layer primary follicles that cannot progress to later stages of folliculogenesis (211). GDF9-deficient oocytes grew at a higher rate when compared to WT ones, reaching a bigger diameter despite the folliculogenesis arrest. Although most oocytes from mutant mice could complete meiosis during *in vitro* maturation experiments, they failed to produce cortical granules (212). Moreover, the study of this mouse lineage suggested possible targets for GDF9 signalling in the granulosa cells since granulosa cells from the mutant mice present upregulated expression of KITL and inhibin α (213). The deletion of inhibin α on the GDF9-deficient background lifted the folliculogenesis block, and follicles could develop until the late preantral phase (213). Therefore, a key role for GDF9 in mice during early folliculogenesis is the downregulation of inhibin α, leading to granulosa cell proliferation and consequent follicle development.

*Bmp15* is also detected in the cytoplasm of murine oocytes shortly after growth initiation (214). However, its expression remains relatively low until around ovulation (215). Consistently, female mice harbouring a null mutation in the *Bmp15* gene present ovaries with follicles at different developmental stages, including corpora lutea (216). However, after ovulatory stimulation, oocytes tended to remain trapped inside the follicles, and these females ovulated less than their WT counterparts. Overall, the loss of BMP15 does not seem to affect folliculogenesis, and defects are limited to ovulation and subsequent fertilization, leading to a subfertility phenotype in mice. As *Gdf9* expression was not upregulated in *Bmp15*-deficient mice, increased GDF9 signalling was most likely not responsible for the described mild ovarian phenotype of *Bmp15* knockout compared to the *Gdf9* one. The generation of a double knockout mouse lineage for *Bmp15* and *Gdf9* (*Bmp15*$^{-/-}$; *Gdf9*$^{-/+)}$ aided in deciphering the possible interactions between BMP15 and GDF9 during folliculogenesis (216). Double mutant animals presented seemingly normal early folliculogenesis development and ovulation in response to hormonal stimulation. However, the presence of late-stage follicles decreased, and *in vivo* fertilization rates were dramatically reduced compared to the control group, thus confirming the synergistic roles played by GDF9 and BMP15 throughout folliculogenesis.

The study of *Bmp15* point mutations in sheep suggested species-specific roles for this protein. Whereas homozygous carriers of one of these mutations are infertile, with ovaries harbouring follicles arrested at the primary stage, heterozygous carriers show higher ovulation

rates and larger litters compared to controls (217–222). Experiments immunizing WT sheep with synthetic peptides derived from the mature BMP15 for short-term replicated the increased ovulatory phenotype, while longer-term or higher dose treatment impaired ovulation (223,224). Therefore, besides controlling early folliculogenesis, BMP15 seems to restrain the number of dominant follicles, determining the ovulation and litter size in sheep (225).

The relationship between oocyte paracrine factors and cumulus cells' metabolic profile modulation has been explored by employing oocytectomy (OOX). In this technique, the oocyte is removed from a COC while preserving the cumulus shell structurally untouched. Initially, it was determined that oocyte removal led to decreased glycolysis activity in the cumulus cells, possibly driven by lowered expression of glycolytic enzymes (203,226). This phenotype is rescued by coculturing growing oocytes with the cumulus shells. Consistently, cumulus cells from *Bmp15*$^{-/-}$; *Gdf9*$^{-/+}$ mice also showed the same glycolytic defects (227) in addition to lower levels of cholesterol synthesis due to decreased expression of cholesterol biosynthesis enzymes (205). Therefore, the oocyte influences its companion cells' metabolism by producing and secreting paracrine factors that modulate their metabolism to complement the oocyte's nutritional needs.

#### 2.4.1.1. Meiotic prophase arrest

Throughout the growth period, the oocyte remains arrested at the prophase of meiosis I and is characterized by the presence of the nucleus, called germinal vesicle (GV), and a prominent nucleolus. During early folliculogenesis, the oocyte maintains meiotic arrest, partly due to the low expression of cyclin-dependent kinase 1 (CDK1), which is required for normal progression from prophase to metaphase (228–231). However, as the follicle approaches the preovulatory stage, the oocyte increases CDK1 expression, and its ability to resume meiosis when isolated from the follicle rises gradually (232). Nonetheless, meiosis will only resume after the LH surge. As the follicle develops, another mechanism is put in place to keep oocytes arrested at the prophase of the first meiotic division.

The meiotic prophase arrest system in antral and preovulatory follicles relies on a gap junction network connecting the follicular somatic and germ cell compartments. This was shown after gap junction inhibitors (233–236) or blocking antibodies targeting connexins 37 or 43 (233,236) promoted meiosis resumption of preovulatory enclosed oocytes. Indeed, the secondary

messengers cyclic adenosine monophosphate (cAMP) and cyclic guanosine monophosphate (cGMP) can diffuse from one cell to the other via gap junctions and are implicated in maintaining meiosis arrest. In the oocyte, meiosis arrest is kept by high levels of cAMP, produced by adenylyl cyclase AC3, which is, in turn, activated by the G-coupled receptor GPR3 (237). However, in the absence of contact with the somatic compartment of the follicle, the phosphodiesterase 3A (PDE3A) hydrolyses the cAMP, promoting meiotic resumption (238–241). This is prevented by the diffusion through gap junctions of granulosa cell-derived cGMP, which is produced by the guanylyl cyclase natriuretic peptide receptor 2 (NPR2) after the binding of C-type natriuretic peptide (CNP) originated from the mural granulosa cells (242). Therefore, granulosa cells cooperate to produce high levels of cGMP that are transferred to the oocyte, where it prevents a decrease in the cAMP levels, maintaining the meiotic cycle arrested at prophase I.

### 2.4.2. Transzonal Projections

The sole layer of flattened granulosa cells observed in the primordial follicle is in direct contact with the oocyte, with the former expressing N-cadherin and the latter E-cadherin, allowing them to establish cell-cell adhesions (243). As the follicle is activated and the granulosa cells proliferate, they give rise to several tightly packed layers around the oocyte, where cells from the innermost layers are in direct contact with the oocyte (244,245). However, as the oocyte grows, it secretes glycoproteins that form an extracellular coat around it, termed the zona pellucida (246–248). Even though the zona pellucida surrounds the oocyte, it is still in contact with the granulosa cells, possibly due to their ability to extend projections and overcome the physical barrier between them and the oocyte. For this reason, these structures are called transzonal projections (TZPs).

Previously described in various mammalian and non-mammalian species (249–256), TZPs are evolutionarily conserved thin cytoplasmic projections with cytoskeletal actin backbone (253,257–261). However, TZPs with a tubulin backbone have also been described, even though it is unclear whether they have overlapping or complementary functions (257). Structural analyses based on electron micrographs have shown TZPs to have enlarged tips cradled by the oocyte membrane (246,259). This feature increases the contact area between the two cell types, potentially enhancing TZPs' functions, which are two-fold. First, they are essential to maintain

adhesion between the two cell types, contributing to the follicle's three-dimensional structure (243). Second, these processes establish gap junctions with the oocyte and mediate the exchange of nutrients and growth factors (257,262). Consistent with this crucial function, the number of TZPs connecting the somatic and the germ cell compartments increases steadily as the oocyte grows (263). Oocyte-secreted factors potentially drive such an increase in the TZP number since oocytes lacking GDF9 are surrounded by a network of TZPs that are ill-oriented and decreased in number (212). Thus, TZP extension could be a part of the oocyte growth program to enhance communication with the granulosa cells and provide a bridge for the exchange of nutritional factors.

### 2.5. Ovulation

Successful ovulation is the timely release of a fully grown and developmentally competent female gamete from a preovulatory follicle. This complex process includes oocyte maturation, the production and secretion of a new ECM by the cumulus cells, and a local inflammatory response at the apical follicular wall, causing it to rupture and release the mature cumulus-oocyte complex. These processes, which are required for the future establishment of pregnancy and embryo development, are all initiated by a single trigger: the gonadotropin surge of luteinizing hormone.

The formation of the antrum during follicular development leads to the differentiation of distinct populations of somatic cells inside the follicle, the mural granulosa and the cumulus cells. These two cell populations respond differently to the LH surge. While the mural granulosa cells start differentiating and luteinize, cumulus cells undergo a mucification process called cumulus layer expansion before being released from the follicle. However, hCG can only induce luteinization of mural granulosa cells *in vitro*, not cumulus layer expansion (264,265). Specifically, the mRNA expression levels of LHR (*Lhcgr*) are one order of magnitude higher in the mural granulosa cells than in cumulus cells, and the binding of hCG to LHR is at least 9-fold higher in murine mural granulosa cells (266). This suggests that the mural granulosa primarily receives the ovulatory signal and relays it to the cumulus through secondary signals.

The binding of LH to its receptor in the mural granulosa cells triggers a spike in the intracellular secondary messenger cAMP. This readily activates the cAMP-dependent serine kinase protein kinase A (PKA) pathway (267,268). PKA is essential for activating another key

LHR signalling mediator, the extracellular regulated kinases 1 and 2 (ERK1/2)(269,270). Despite evidence that ERK1/2 are only phosphorylated for a short window of 2 hours after LHR activation (271–273), their deletion in granulosa cells suggests that these molecules are essential for the oocyte to resume meiosis, ovulation and luteinization (274). More specifically, *Erk1/2* deletion halts the ovulatory programme, failing to stop granulosa cell proliferation and differentiation and also impairing the expression of LH-induced genes such as the Epidermal Growth Factor (EGF)-like factors amphiregulin (*Areg*), epiregulin (*Ereg*), and betacellulin (*Btc*).

The production of EGF-like factors by the mural granulosa cells is, at least in part, an answer to the longstanding mystery of how the LH surge triggers cumulus layer expansion and oocyte maturation. The binding of these factors to the EGF receptor (EGFR) localized on the cumulus cells triggers additional preovulatory specific gene expression (275–277) and ERK1/2 phosphorylation (278). EGFR activation carries over the signalling for oocyte maturation and triggers cumulus layer expansion, a process central to this work that will be described extensively in section 3 of this document.

### 2.5.1. Oocyte maturation

The first morphological sign of oocyte meiosis resumption is the germinal vesicle breakdown (GVBD), which in mice happens around 2 hours after the LH surge, leading to the completion of the oocyte first meiotic division at 10-12h post-LH (279). During this first division, a set of chromosomes is extruded into a small non-functional cell called the first polar body, reducing the oocyte chromosome number from 2N to N. The remainder of the chromosomes then assemble in a spindle, reaching the metaphase II stage, when the cell cycle is arrested again. The oocyte is now ready to be ovulated and fertilized. Fertilization is the stimulus required for a new cell cycle resumption and second polar body extrusion, which separates the sister chromatids and leaves only one copy of oocyte-derived chromosomes in the recently formed zygote.

Up until the ovulatory signal, cGMP was produced in the granulosa cells and diffused into the oocyte, preventing degradation of the cAMP synthesized by the oocyte and keeping it in prophase of the first meiotic division. Consistently, the cellular signalling behind meiosis resumption was tied to a rapid decrease in cGMP (280,281) and cAMP (235,281,282) in response to LH stimulation. The cGMP drop is first detected in the outer mural granulosa cells,

then in the cumulus cells and, lastly, in the oocyte (283). This can be explained by observations regarding the cGMP-generating (CNP/NPR2) and cGMP-degrading (Phosphodiesterase 5) machinery and the gap junction network.

The rapid initial cGMP decrease was shown to happen without any change in the NPR2 or CNP protein content (284,285). By 30 minutes after LHR activation, NPR2 activity decreases by around 50% (284,285). This was explained by the fact that LH action causes the dephosphorylation of NPR2, reducing its activity (283,285). Following this initial activity reduction, follicular CNP starts decreasing around 2h after the ovulatory wave (284,286), which is shortly accompanied by a drop in *Npr2* transcript levels (287,288). Although slower, a reduction in the NPR2 small peptide agonist, CNP, has also been described to happen after 2h of LH receptor activation, driven by a decrease in the *Nppc* transcripts encoding the CNP peptide (284,286,289). Thus, the reduction in the preovulatory follicle cGMP content is due, at least in part, to the inhibition of the NPR2-CNP signalling in the granulosa cells, which had been responsible for generating high cGMP quantities up to this point.

The observation that the inhibition of NPR2 dephosphorylation could not wholly prevent this initial drop in cGMP levels suggested the existence of different mechanisms contributing to this effect (283,285). The phosphodiesterase 5 (PDE5), activated by the LHR effector PKA, was an excellent driving candidate. PDE5 is phosphorylated only 10 minutes after LH exposure and remains activated for at least 4h (290–292). Indeed, LH action increases PDE5's activity by 70% (293), which contributes to increasing cGMP degradation in the follicle. Due to these mechanisms regulating cGMP production and diffusion, its concentration inside the oocyte drops, lifting its inhibitory effect on PDE3A. PDE3A will rapidly hydrolyze cAMP within the oocyte, which leads to the dephosphorylation and activation of CDK1 (294). CDK1, in turn, will drive cell cycle resumption, ultimately leading to the first polar body extrusion, the morphological sign of oocyte maturation completion.

### 2.5.2. Release of the expanded cumulus-oocyte complex

After oocyte maturation and the expansion of the cumulus mass, the basement membrane and the ovarian wall pose a significant physical barrier to ovulation. As part of the ovulatory stimulus, this barrier undergoes gradual programmed thinning and degradation at the follicular apex. This process results from the synergistic action of infiltrated and local immune cells,

proteolysis, angiogenesis, and ultimate tissue remodelling that culminate in the release of the expanded COC.

Proteases secreted by the granulosa cells in response to the LH surge weaken the basement membrane, which has its major components - laminin, collagen type IV and fibronectin (295) - digested after LHR activation (296). This is followed by the development of a follicular capillary network that, despite not being connected to the central vasculature, might help provide the periovulatory follicle with serum and blood cells, which become enriched in the follicular fluid during the ovulatory process (297,298). In addition to proteolytic activity, cell death and migration also wear down the physical barrier to ovulation. Thecal fibroblasts migrate away from the follicular apical site (299), and surface epithelial cells undergo apoptosis and are subsequently shed from the same region (300,301). Thus, the complex ovulatory signal restructures the follicle, converging in the thinning of the ovarian and follicular walls, which culminates in the release of a mature and fertilizable oocyte.

## 3. Cumulus layer expansion

Within the preovulatory ovarian follicle, the oocyte is surrounded by tightly packed and well-organized layers of cumulus granulosa cells, connected to each other and the oocyte via intercellular processes and gap junctions. In response to the ovulatory LH surge, the cumulus cells produce and secrete a hyaluronan-rich extracellular matrix, the cumulus matrix. It assembles in the intercellular space, ultimately driving the cumulus cells away from the oocyte and increasing the cumulus-oocyte complex volume (Figure 6). Thus, right before ovulation, this new coat envelops both the oocyte and the displaced cumulus cells. This process, which encompasses the cumulus matrix production and the consequent cumulus cell displacement, is called *cumulus layer expansion* and will be reviewed in detail in this section.

### 3.1. Cumulus extracellular matrix

#### 3.1.1. Hyaluronan

The initial observation that hyaluronidase, an enzyme that digests hyaluronan, could break down the viscoelastic substance involving ovulated oocytes suggested Hyaluronan to be the major component of the cumulus matrix (302). Hyaluronan (HA), a non-sulfated linear glycosaminoglycan, is composed of repeated disaccharide units of glucuronic acid (GlcA) and

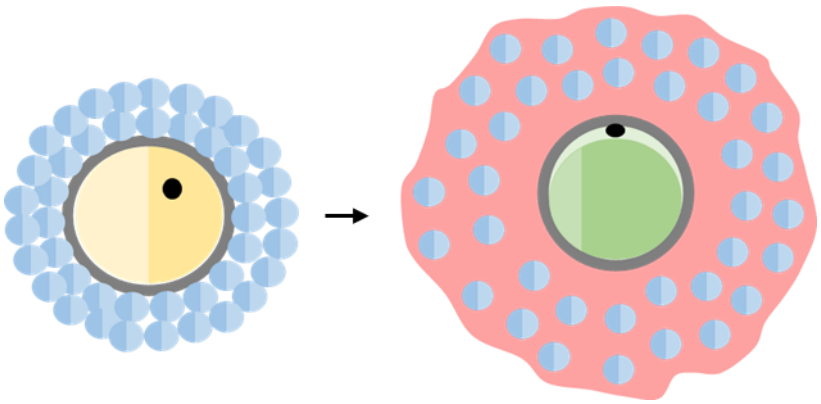

**Figure 6: Cumulus layer expansion.**

N-acetylglucosamine (GlcNAc) (303) (Figure 7a). In the cell, HA synthesis is closely associated with glucose metabolism since GlcA is synthesized from glucose-6-phosphate, an intermediate glycolysis metabolite, and GlcNAc is synthesized via the hexosamine biosynthetic pathway (HBP), a branch of the central glycolytic pathway.

HA synthesis is catalyzed by HA synthases (HAS), and three HAS isoforms have been identified so far: HAS1, HAS2, and HAS3 (304). These isoforms have a conserved structure, which contains clusters of hydrophobic amino acids, indicating they are transmembrane proteins (305,306). This structure makes HA unique among glycosaminoglycans since it is formed at the plasma membrane and immediately extruded from the cell, while other glycosaminoglycans are assembled inside the Golgi apparatus and only then secreted to the extracellular space (307,308) (Figure 7b). The HAS isoforms differ in processivity, producing HA molecules with different lengths (306). In culture, HAS1 and HAS3 elongated HA molecules of about $10^5$ kDa, and HAS2 catalyzes the extension of longer HA molecules of up to $10^7$ kDa (306). On the other hand, hyaluronidases (HYAL) catalyze the breaking down of HA chains. To date, six types of HYAL have been identified: HYAL1-4, PH-20 and HYALP1 (307). These enzymes are usually widely expressed in mammalian tissues, except for PH20, which is only found in sperm and plays a crucial role in digesting the cumulus matrix at fertilization (309). Therefore, HA can be present in a broad range of molecular weights, which dictates its physical properties and results from the combined activities of hyaluronan synthases and hyaluronidases (304).

a) b)

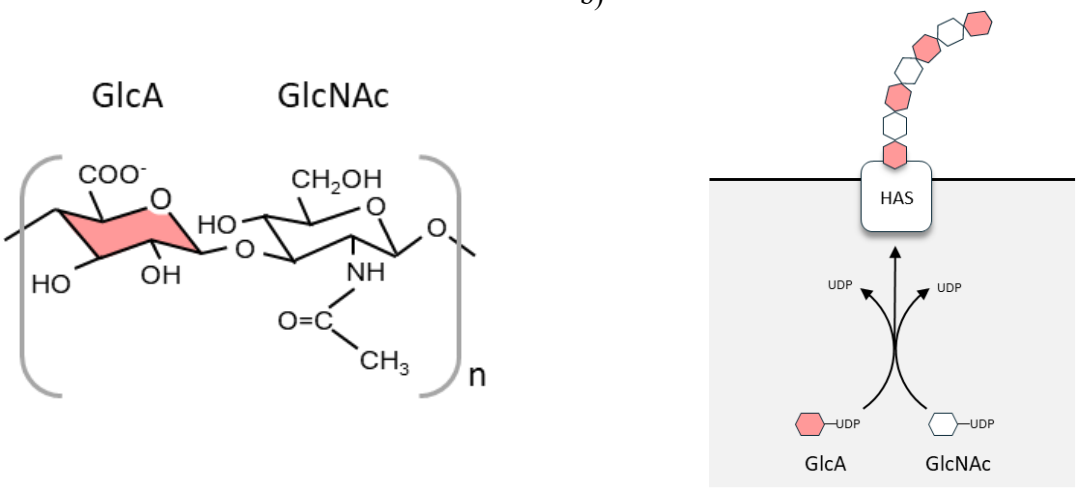


**Figure 7: Hyaluronan structure and synthesis**. a) The molecular structure of an HA is composed of repeating disaccharide units of glucuronic acid (GlcA; pink) and N-acetylglucosamine (GlcNAc). b) HA synthesis and secretion. HAS enzymes catalyze the addition of UDP-GlcA and UDP-GlcNAc to the nascent HA chain and extrude it through the plasma membrane directly into the extracellular space.

In the preovulatory follicle, the transcriptional activation of *Has2* is detectable in the cumulus cells within 3h of the LH surge (310). This leads to a 30-fold increase in HA synthesis, which is maximal between 3-12h after the ovulatory stimulus (311–313). Consistently, LH also stimulates glucose uptake by the cumulus cells, which drives the glycolytic and the hexosamine pathways, leading to the production of GlcA and GlcNAc, the saccharides that compose HA (314–318). As HA is a highly polyanionic molecule, it promotes the formation of highly hydrated ECMs, a property that is also observed in the cumulus matrix. Electron microscopy analyses have shown the cumulus matrix to be highly porous and fibrous, which suggests it is organized in a mesh-like network (319). In fact, protease digestion destabilizes the cumulus matrix, which further supports this hypothesis and reveals the role of accessory proteins in organizing the long HA chains (320).

### 3.1.2. Hyaluronan cross-linking proteins and proteoglycans

The cumulus matrix incorporates essential crosslinking proteins derived from the serum, such as the heavy chains of inter-α trypsin inhibitor (IαI), or locally synthesized by the cumulus cells, including the tumour necrosis factor α-induced protein 6 (TNFAIP6) and pentraxin 3 (PTX3) (Figure 8).

The fact that FSH could induce cumulus layer expansion *in vitro* when serum was added to the culture medium (264) suggested that a serum component was required to stimulate HA synthesis. In fact, Salustri and colleagues (313) showed that FSH fails to promote the expansion of compact COCs in the absence of serum. However, they also showed that the amount of HA synthesized in both conditions was comparable, but only 20% was incorporated into the cumulus matrix in the absence of serum, compared to 80% of HA incorporation in the controls. This suggested that unknown serum factors are essential in stabilizing the cumulus matrix. The identification of the serum proteoglycan IαI confirmed this theory, as purified IαI from the blood could rescue cumulus matrix assembly in the absence of serum, and conversely, IαI-free serum failed to support the matrix assembly (321).

Usually produced in the liver by hepatocytes, IαI is formed by two heavy chain proteins (HCs) linked by an ester bond to a glycosaminoglycan – a single chondroitin sulfate chain - carried by the core protein bikunin (322). IαI is a normal component of the blood serum and enters the follicle after the breakdown of the follicle-blood barrier stimulated by the LH surge (323,324). Once inside the follicle, the HCs linked to the glycosaminoglycan in the IαI are covalently transferred to the HA chains (325,326). This transfer occurs by breaking the ester bonds tying the HCs to the chondroitin sulfate, and remaking them to bind the HCs to the HA molecules, forming HC-HA complexes (322). The importance of these complexes was demonstrated by the bikunin-null mouse lineage, in which cumulus expansion fails due to a loosely assembled cumulus matrix, leading to the ovulation of almost completely denuded oocytes (327,328). In these animals, IαI is not appropriately formed in the liver, and HCs are found as free proteins in the blood due to the absence of bikunin. Intraperitoneal injections of purified bikunin failed to rescue the phenotype, further showing that bikunin does not play a role in stabilizing the cumulus matrix itself. Still, it is required for the transesterification reaction responsible for transferring the HCs chains from the chondroitin sulfate to the HA molecule. The HC-HA complexes help stabilize the cumulus matrix by cross-linking HA chains via ionic bounds (326,329) (Figure 8).

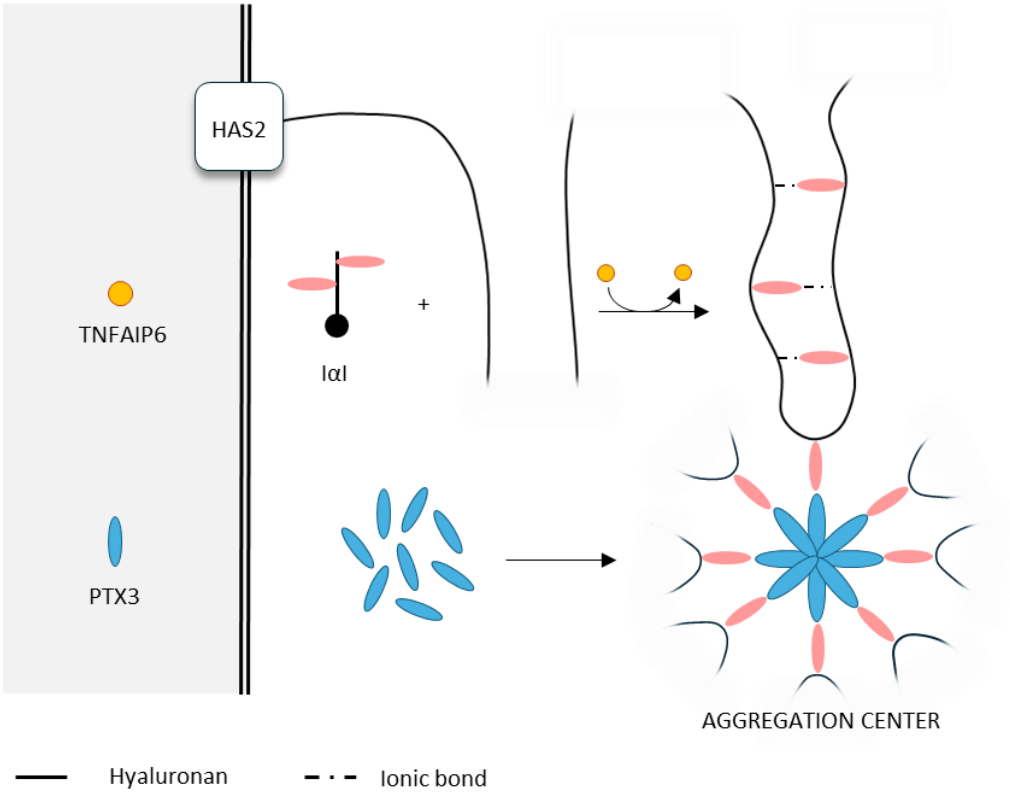


**Figure 8: Hyaluronan cross-linking proteins and cumulus matrix structure**. Upper portion of the panel: Hyaluronan (black solid line) is synthesized by Hyaluronan Synthase 2 (HAS2) at the cumulus cell membrane. In the intercellular space, TNFAIP6 catalyzes the transesterification reaction that transfers the Heavy Chains (HC - pink oval shapes) from the bikunin core to the HA molecules. The HC chains also establish ionic bonds with neighbouring HA molecules, further helping in stabilizing the cumulus matrix. Bottom portion of the panel: 8 PTX3 monomers organize in a structure that binds HCs that had been transferred to the HA chains, creating aggregation centers.

TNFAIP6, a small glycoprotein known to modulate inflammatory responses (330), is another protein that is essential for cumulus matrix formation. After the ovulatory stimulus, TNFAIP6 is rapidly translated by cumulus and mural granulosa cells (310,331–334). The importance of TNFAIP6 to the cumulus matrix is two-fold. First, the TNFAIP6 structure contains an N-terminal link module that binds HA with high affinity, further aiding cumulus matrix assembly in its mesh-like functional network (335). Second, it catalyzes the transesterification reaction that forms the HC-HA complexes (336–339). A series of different experiments demonstrated this. Initially, TNFAIP6, HA, and IαI were shown to colocalize in the cumulus matrix of hCG-stimulated ovary sections. Immunoblotting of ovulated COCs revealed

that an antibody raised against TNFAIP6 would identify 2 different bands: one containing TNFAIP6 as a free protein and a heavier one that was also recognized by antibodies raised against IαI (332,333). Further mass spectrometry analysis of the heavier band demonstrated that it contained TNFAIP6 and HCs (333). Finally, HCs were only transferred to HA *in vitro* in the presence of recombinant TNFAIP6, thus indicating the role played by TNFAIP6 in catalyzing this reaction (336). A TNFAIP6-deficient mouse lineage, just as observed in the females lacking bikunin, ovulated disintegrating COCs that failed to be fertilized, rendering the females sterile.

PTX3, a product of the *Ptx3* gene, is a protein upregulated in the cumulus cells after the LH surge (332,340) that also localizes to the cumulus matrix (341,342). The absence of PTX3 from the preovulatory follicle following the deletion of *Ptx3* leads to the formation of a disorganized cumulus layer that disintegrates shortly after ovulation (341,342). This dispersed COC fails to support fertilization and renders the *Ptx3*-null mice sterile. HA synthesis is normal in these mice, and HCs from IαI are adequately incorporated into the matrix (342). When *Ptx3*-null COCs are expanded *in vitro*, the addition of recombinant and purified PTX3 rescues expansion and the cumulus matrix organization (342). These results indicate that PTX3 is also required to link the HA chains and stabilize the matrix, but it might do so through a different mechanism than the one observed with the HCs from IαI and TNFAIP6.

PTX3 structure, which consists of 8 monomers linked by disulfide bonds, lacks a motif to bind HA directly (343). Nonetheless, the recombinant N-terminal portion of PTX3 fully substitutes whole PTX3, binding HCs and TNFAIP6 and supporting proper cumulus matrix assembly (342,344). An antibody raised against this portion of the PTX3 molecule blocks the ability of full-length PTX3 to rescue cumulus matrix assembly in *Ptx3*-null COCs (344). Therefore, it was initially proposed that each PTX3 subunit in the octameric complex could bind one TNFAIP6 unit (345,346), which would bind HA chains (335). However, additional evidence goes against this theory. For example, TNFAIP6-HC complexes, but not free TNFAIP6, are found in the cumulus matrix right before ovulation, suggesting this protein primarily transfers HCs to HA instead of physically integrating the matrix (334). Additionally, TNFAIP6 harbouring targeted mutations to its link site that did not affect their catalytic function could still support matrix assembly of *Tnfaip6*-null COCs (347), which strongly downplays the importance of the binding between TNFAIP6 and HA to stabilizing the cumulus matrix. Therefore, considering that PTX3 can bind HCs (343,345), it is likely that PTX3 might substantially

strengthen and stabilize the HA network by binding several HCs covalently linked to distinct HA molecules, creating “aggregation centers” (Figure 8).

Besides HCs, TNFAIP6 and PTX3, other components have been identified in the cumulus matrix, including versican, cartilage link protein, fibronectin, tenascin-C, and laminin (348–351). Versican is a proteoglycan synthesized by the mural granulosa cells, being highly expressed after the LH surge (352,353). The link protein facilitates versican’s incorporation in the cumulus matrix, conferring its higher resistance to enzymatic digestion (348,354). However, before ovulation, increased expression of ADAMTS (a disintegrin and metalloproteinase with thrombospondin-like motifs) 1 and 4 coincides with increased versican cleavage in the cumulus matrix (349,352). This correlation was further supported by studies conducted on ADAMTS1-null female mice. These animals ovulated expanded COCs that presented clumped cumulus cells inside an extracellular matrix characterized by non-uniform distribution of versican and HA, contrasting with the ovulated COCs from the control group with uniform ECM components and cumulus cell distribution (355). Therefore, the proper assembly and degradation of the cumulus matrix are essential for expansion, ovulation, fertilization, and overall fertility.

### 3.1.3. Hyaluronan binding receptors

Besides interacting with stabilizing proteins, HA can also bind cell surface proteins. The most studied HA receptors are Cluster of Differentiation 44 (CD44) and the Receptor for Hyaluronan-Mediated Motility (RHAMM). CD44 is a non-kinase transmembrane glycoprotein and interacts with HA on two conserved HA-binding domains (356). CD44 is encoded by a single gene, *Cd44*, and the resulting mRNA can undergo alternative splicing, giving rise to at least 9 different CD44 variants, in addition to possible post-translational modifications such as glycosylation (357). CD44 mediates HA internalization and degradation, contributing to its local turnover (358). Upon HA binding, CD44 becomes active and undergoes conformational changes, facilitating coupling with different cytoplasmic targets. These can be small Rho GTPase proteins - which will be reviewed in section 4.4 - or cytoskeletal anchor proteins, potentially triggering cytoskeleton rearrangement, cell migration, or cell growth and survival (359).

RHAMM, also known as Cluster of Differentiation 168 (CD168) or hyaluronan-mediated motility receptor (HMMP), is not ubiquitously expressed, being transiently detected during tissue repair (360) or in cancer cells (361–363). Like CD44, RHAMM is also encoded by

one gene, *Rhamm*, that can generate different RHAMM variants through alternative splicing, different start codons, and post-translational modifications (364). Structurally, RHAMM contains HA-binding motifs at the C-terminal region but does not have a membrane insertion domain (361). Interestingly, RHAMM can be found at different subcellular locations, such as cytoplasm, nucleus and cell surface (365,366). Cell surface RHAMM is usually associated with other proteins, including the non-tyrosine kinase receptor CD44 (367–369). HA binding to RHAMM/CD44 cell surface complexes increases migration and invasion partially due to its power to influence the expression of hyaluronan synthases and hyaluronidases, which increases the local concentration and processing of HA, creating a positive feedback pro motility (363). Alternatively, intracellular RHAMM can bind to different cell structures, including actin filaments, microtubules, and the mitotic spindle, thus affecting cell motility and proliferation (365,370,371). Fibroblast-based studies showed intracellular RHAMM could modulate ERK1/2 signalling, controlling spindle integrity, cell cycle progression, and random motility (362,367).

In the mammalian ovary, the expression of *Cd44* in cumulus cells quickly rises in response to the LH surge in humans (372), cattle (373), and pigs (374). In pigs, the binding of HA to CD44 on the membrane of cumulus cells has been linked to oocyte meiosis resumption (375). This functional coupling between the cumulus matrix and the oocyte maturational process was initially hinted at by the fact that inhibiting HA synthesis during *in vitro* expansion of porcine COCs prevented the phosphorylation of connexin 43 (Cx43). Connexins are transmembrane proteins that form gap junctions and allow cells to exchange ions and small molecules (376). Reportedly, phosphorylation of Cx43, the predominant connexin expressed by cumulus cells (377), has been associated with decreased cell-to-cell communication (378,379). Therefore, the authors hypothesized that CD44-HA binding after the ovulatory LH surge leads to Cx43 phosphorylation and consequent gap junction closure, interrupting the flow of cAMP to the oocyte and inducing GVBD. Indeed, blocking CD44 with the antibody brought the GVBD rate to approximately 13% when the control group had 64% of its oocytes undergoing GVBD. Therefore, during IVM of porcine COCs, CD44-HA signalling plays a role in oocyte maturation by interfering with the COC gap junction network. This highlights a key species-specific difference between rodents and pigs: in mice and rats, GVBD takes place before the cumulus matrix is deposited (312,380); however, in pigs, the matrix is deposited before the oocyte resumes the cell cycle (381). In mice, however, the role of CD44 during expansion has not been

investigated: a CD44-null lineage showed embryos develop normally in the absence of CD44 and its different variants (382), but no specific and detailed evaluation of their ovarian function has been performed.

On the other hand, *Rhamm* expression has been reported in cumulus cells of cattle (373) and buffalo (383) during cumulus layer expansion. In mice, it is expressed in granulosa cells and localizes to their mitotic spindle during the oocyte growth phase (384). Global deletion of both the centrosome and the HA-binding domains of RHAMM does not affect primordial follicle formation. Instead, it impaired granulosa cells' spindle orientation, interfering with their replication. As a result, folliculogenesis was impaired, and the ovaries isolated from mutant mice presented decreased numbers of antral and preovulatory follicles, leading to a subfertility phenotype (384). However, due to the folliculogenesis defects observed, the potential role of RHAMM during cumulus layer expansion – the process encompassing the deposition of an HA-rich extracellular matrix – has not been assessed yet.

### 3.2. Cumulus extracellular matrix gene expression and regulation

Cumulus layer expansion is physiologically triggered by the gonadotropin surge, but experimentally, it can be induced by hCG injections (385). However, as cumulus cells and oocytes express low to undetectable levels of the LHR, exposing COCs to LH/hCG *in vitro* fails to trigger expansion (386). This suggests that the effect of the LH in triggering cumulus layer expansion is not direct. LHR, a G-coupled protein receptor, rapidly triggers adenylate cyclase upon its activation, which increases the cAMP content inside the granulosa cells (387,388). Notably, factors such as FSH, prostaglandin $E_2$ or permeable cAMP analogs have been described to increase cumulus cell cAMP content and trigger cumulus layer expansion *in vitro* (264,389,390). Therefore, cAMP was considered a good candidate to mediate the intrafollicular effects of the LH surge, either by diffusing to the cumulus cells through gap junctions or by inducing the production of factors that can increase the cAMP content inside the cumulus cells.

The ovulatory stimulus induces the expression of prostaglandin-endoperoxide synthase 2 (PTGS2) in granulosa and cumulus cells within 2h of the LH surge (391). This enzyme catalyzes the rate-limiting step in prostaglandin $E_2$ ($PGE_2$) production. $PGE_2$ acts in an autocrine fashion by binding its receptor on the surface of mural granulosa and cumulus cells. Experiments carried out by incubating compact mouse COCs with purified $PGE_2$ showed that it stimulated cumulus

cells' cAMP production and induced cumulus layer expansion (390), further supporting the theory that $PGE_2$ is the intrafollicular mediator for LH. Consistently, the generation of a knockout mouse model for *Ptgs2* showed that impaired $PGE_2$ synthesis led to severely reduced ovulation rates due to decreased cumulus layer expansion, ultimately rendering the females infertile (392,393). Additionally, mice deficient for the $PGE_2$ receptor showed a similar phenotype with diminished expansion, reduced ovulation rates and overall infertility (394–396). Further investigation established that both models expressed normal levels of *Has2* but showed decreased mRNA and protein levels of TNFAIP6, compromising cumulus matrix assembly (397). However, despite the infertility phenotype, the fact that cumulus layer expansion was not completely impaired in these animals suggests that $PGE_2$/cAMP signalling is not the sole factor responsible for promoting cumulus layer expansion after the ovulatory stimulus.

Alternatively, purified EGF was established as a potent cumulus layer expansion promoter for COCs isolated from mice, rats and cattle (398–400). These observations strongly supported its role as an additional intrafollicular mediator of LH function. However, when Inoue and colleagues (401) analyzed the follicular fluid of 98 patients who underwent IVF procedures, they found that EGF was not enriched in the follicular fluid after hCG stimulation. Instead, the hormonal injections caused the follicular fluid to accumulate amphiregulin, a peptide member of the EGF-like factor family. EGF-like factors are closely related small proteins that share a structural motif, the EGF domain, required to bind and activate the EGF receptor (EGFR) (402). It is now established that a set of three EGF-like factors is induced in the preovulatory follicle after the LH surge, consisting of amphiregulin (AREG), epiregulin (EREG), and betacellulin (BTC) (275,276,403,404). These are rapidly expressed in mural granulosa cells as transmembrane precursors that are cleaved and released in the follicular fluid by metalloproteases (276,403,405). Later, these factors are also expressed by the cumulus cells as a consequence of $PGE_2$/cAMP signalling (406).

As shown by Park *et al*. (276), culture media containing AREG, EREG or BTC could stimulate cumulus matrix production and cumulus layer expansion on cultured antral follicles. These effects were comparable to the ones observed in the control group, where the antral follicles were exposed to LH alone. Conversely, inhibiting EGFR activity with AG1478 or C56 blocked LH-induced cumulus layer expansion. These results indicate that EGF-like factors are important mediators of intrafollicular LH signalling, as they activate the EGF receptor (EGFR)

on cumulus cells and propagate the effects of LH stimulation. Further evidence of this role was provided by Hsieh *et al.* (407) upon *in vivo* disruption of the ovarian EGF signalling. They first showed that amphiregulin null mice (*Areg*$^{-/-}$) present decreased cumulus expansion after intraperitoneal hCG injections. As EREG or BTC could potentially compensate for the lack of AREG, they also evaluated the effect of *Areg* deletion on a hypomorphic EGFR background (*Egfr*$^{wa2/wa2}$), in which EGFR had reduced overall activity. These animals presented severely decreased expansion-related gene expression and ovulation, and the few ovulated COCs obtained were mostly unexpanded.

The evidence presented thus far suggests a model for how LH controls the expansion of the cumulus layer (Figure 9)(408). According to this model, initial LHR activation increases cAMP production in the mural granulosa cells, leading to the transcription of para- and autocrine signalling molecules, including AREG, EREG, BTC, and $PGE_2$. Once secreted in the follicular fluid, these molecules activate their receptors on the cumulus cells. $PGE_2$ will induce cAMP production, also leading to the activation of the genes encoding AREG, EREG, and BTC in the cumulus cells. As a result, the EGF-like factor molecules that accumulate in the follicular fluid activate the EGFR in the cumulus cells, carrying over the LH signalling to trigger the deposition of the cumulus matrix. The primary genes involved in producing HA and mediating its organization into the cumulus matrix are *Has2*, *Tnfaip6*, *Ptx3* and *Ptgs2*.

Upon stimulation, the intrinsic EGFR tyrosine kinase activity is triggered, resulting in autophosphorylation and activation of the Mitogen-Activated Protein Kinase (MAPK) pathway. It comprises a series of proteins that transduce extracellular signals and culminate in the phosphorylation and activation of the Extracellular Related Kinases 1 and 2 (ERK1/2), also termed MAPK3/1. As LH and hCG stimulation produces an increase in ERK1/2 phosphorylation, which is required for oocyte maturation (409), it has been proposed that ERK1/2 are key EGFR downstream effectors in cumulus layer expansion. In fact, pharmacological inhibition of ERK1/2 activity in cumulus cells of COCs exposed to FSH or EGF blocked expansion and oocyte maturation (409,410). *In vivo* evidence that supports this claim was provided by Fan and colleagues (274) after conditionally deleting *Erk2* from granulosa cells in an *Erk1* global knockout model. In these animals, the absence of ERK1/2 from the granulosa cells completely prevented the expression of the cumulus matrix-related genes *Has2*, *Tnfaip6*, *Ptx3* and *Ptgs2*, besides impairing cumulus layer expansion. Thus, these results

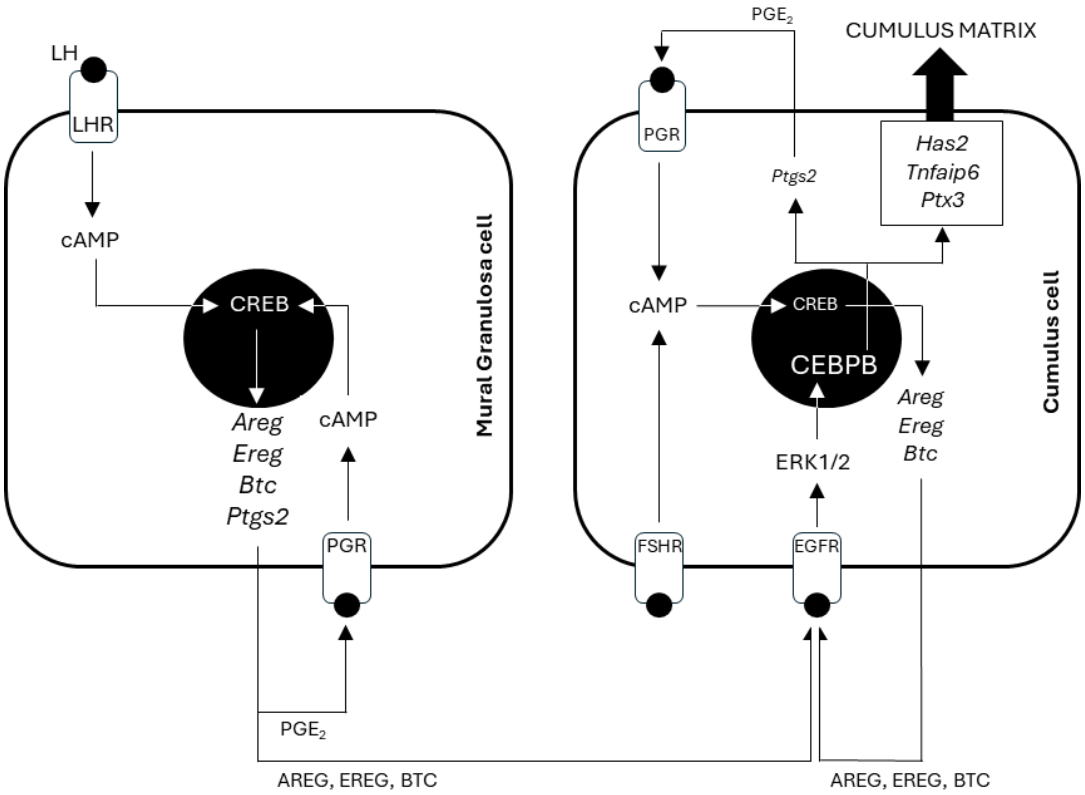


**Figure 9: Cumulus layer expansion regulation**. LHR activation triggers adenylate cyclase, elevating intracellular levels of cAMP and activating PKA signalling that leads to EGF-like factors (*Areg*, *Ereg*, and *Btc*) expression through the transcription factor cAMP response element-binding protein (CREB). $PGE_2$ positive feedback reinforces this signalling and EGF-like factors expression. FSHR activation on the cumulus cells also triggers cAMP production and leads to *Areg*, *Ereg* and *Btc* expression. Once secreted, EGF-like factors bind EGFR receptors on the cumulus cells, activating the MAPK signalling pathway, which leads to *Has2*, *Tnfaip6*, *Ptx3* and *Ptgs2* expression via the transcription factor CCAAT/enhancer binding protein beta (CEBPB).

highlight the importance of ERK1/2 for cumulus layer expansion and emphasize its contribution to intrafollicular LH signalling.

Even though LHR and EGFR activation are essential for cumulus layer expansion, they are not sufficient. In an early report, Buccione and colleagues (411) investigated the role of oocytes in the function of cumulus cells. To do so, they collected compact COCs from mice and microsurgically removed the oocyte in a technique called oocytectomy. The cumulus shells, or oocytectomized complexes (OOX), failed to undergo expansion and produce HA when exposed to FSH or EGF *in vitro*. Additionally, removing the oocyte did not affect cumulus cell cAMP

production in response to FSH. However, when the OOX were exposed to FSH or EGF in the presence of denuded oocytes, their ability to induce cumulus layer expansion was restored, and the cumulus shells expanded. The same was observed when the medium drop used for the experiment had been previously used to culture denuded oocytes, a practice termed conditioning the culture media. Moreover, the degree of expansion observed in the OOX was directly related to the number of oocytes used to condition the media. Therefore, these results provided strong evidence that the oocyte participates in regulating cumulus layer expansion, and their action is probably mediated by secreting soluble factors since physical contact between the oocyte and the cumulus cells does not seem to be a requirement. Moreover, the action of such oocyte-derived expansion enabling factors is downstream of cAMP production. BMP15 and GDF9 are two oocyte-secreted factors that are likely involved in enabling cumulus layer expansion, in addition to their role in modulating cumulus cell metabolism during the oocyte growth phase (412,413) (reviewed in section 2.4.1).

Peng *et al.* (208) cloned mouse and human *Gdf9* and *Bmp15* to express GDF9, BMP15 homodimers, and GDF9:BMP15 heterodimers and investigate their role in enabling cumulus layer expansion. Strikingly, human and mouse heterodimers GDF9:BMP15 were more effective than GDF9 or BMP15 homodimers in stimulating expansion-related gene expression in cultured granulosa cells. As GDF9 and BMP15 usually signal through different intracellular pathways, respectively SMAD2/3 and SMAD1/5/8, the authors investigated which pathway the heterodimer GDF9:BMP15 was signalling through. Treatment of granulosa cells in culture with mouse GDF9:BMP15 stimulated high levels of SMAD2/3 phosphorylation, while SMAD1/5/8 phosphorylation levels remained low. This suggested that GDF9:BMP15 signalling was probably mediated by SMAD2/3. Indeed, pharmacological inhibition of receptors ALK4/5/7, which phosphorylate and activate SMAD2/3, impaired the expression of *Has2*, *Ptx3* and *Ptgs2*, all genes related to producing the cumulus matrix during cumulus layer expansion. And consistently, when ALK2/3/6 were inhibited pharmacologically, gene expression was not affected. However, the absence of ALK6, made possible using granulosa cells collected from *Alk6*$^{-/-}$ mice, completely blocked SMAD2/3 phosphorylation after heterodimer treatment. For this reason, the authors proposed that mouse GDF9:BMP15 activity in cumulus cells probably requires structural support of the type 1 receptor ALK6 and the kinase activity of type 1

receptors ALK4/5/7 to phosphorylate and activate SMAD2/3, leading to the production of the cumulus matrix.

Oocyte-dependent signalling is also implicated in the activation of ERK1/2 in the cumulus cells (410). After confirming that preventing ERK1/2 activation impairs the expansion of compact COCs cultured in the presence of FSH, the authors investigated if oocytes played any roles in enabling this signalling. To do so, they used a system in which cultured cumulus cells could be treated with FSH in the presence or absence of oocytes. First, they determined that adding oocytes to cultured cumulus cells in the presence of FSH can induce ERK1/2 phosphorylation and the expression of *Has2* and *Ptgs2*. Then, when oocytes were added to a cumulus cell culture in the presence of FSH and U0126, they noticed that the expression of *Has2* and *Ptgs2* was impaired. They also showed that coculture with denuded oocytes or the addition of purified GDF9 to the culture medium induced ERK1/2 phosphorylation. Thus, these results show a requirement for oocyte-derived signalling in order to activate the MAP Kinase pathway in the cumulus cells.

So, even though EGF-like factors, FSH and oocyte-secreted factors act through different transduction pathways, they all activate ERK1/2 in cumulus cells, making ERK1/2 activation in the cumulus cells an essential step in cumulus layer expansion. Therefore, gonadotropins and oocyte-secreted factors work in synergy to activate the transcription of genes such as *Has2*, *Ptx3*, *Tnfaip6*, and *Ptgs2* in the cumulus cells, resulting in the deposition of the new extracellular matrix.

### 3.3. Key properties and function of the cumulus extracellular matrix

To support the generation of offspring, the female reproductive tract produces mature fertilizable oocytes and then mediates their transportation to the fertilization site. Thus, the LH surge will trigger oocyte maturation and the release of the expanded COC from the follicle, followed by the ovulated COC uptake by the oviduct. *In vivo* and *in vitro* evidence support an essential role for cumulus layer expansion and the cumulus matrix in both these processes. For example, an early study reported drastically decreased ovulation rates in mice injected with 6-diazo-5-oxo-l-norleucine (DON) (414). This inhibitor interferes with glucosamine synthesis, a building block of HA. Afterwards, mouse models deficient for components involved in forming the cumulus matrix - such as TNFAIP6 or bikunin, discussed in section 3.1.2 - presented

decreased ovulation rates compared to their WT counterparts (327,328,336). Therefore, this shows that cumulus layer expansion impairment interferes with the release of the cumulus mass from the follicle, thus impacting fertility. Moreover, an analysis of *in vitro* ovulation suggested that the cumulus matrix protects the oocyte as it exits the follicle, preventing COC dissociation as it is transferred to the fertilization site inside the oviduct (415).

Expanded COCs are ovulated into the peritoneum in humans and the bursa in rodents (416). Failure to properly transport them into the oviduct can impede fertilization or lead to ectopic pregnancies in women. Initially, it was hypothesized that the beating motion of cilia in the epithelial cells at the outermost portion of the oviduct - the infundibulum - created a fluid flow responsible for conducting the ovulated COC into the oviduct. However, while a fluid flow is produced, it can only move small particles, such as *Lycopodium* spores, but not more prominent structures like the expanded COC (417,418). Electron microscopy analyses showed that adhesions were formed between the cumulus matrix and the infundibular epithelium (419,420). Therefore, it was proposed that these adhesions can mediate the transportation of the expanded COC into the oviduct. This theory was further supported by the observation that oviduct uptake failed when structures that lack a cumulus matrix were used, such as denuded oocytes or unexpanded COCs (421,422).

An early study evaluated the relationship between cumulus layer expansion and fertilization. Chen and colleagues (423) first showed that supplementing the *in vitro* maturation medium with substrates for HA synthesis increased the degree of expansion. Next, these conditions were employed to assess the impact of the expansion degree in fertilization, defined as the percentage of 2-cell embryos in each group (414). Indeed, they found the fertilization to be higher in the groups where the COCs were expanded in the presence of HA substrates, which, as previously determined, led to a more pronounced expansion. To date, accumulated evidence supports this finding and extrapolates it to *in vivo* conditions. For example, in mouse models where cumulus matrix assembly was disrupted after deletion of either bikunin (322), TNFAIP6 (336) or PTX3 (341,342), fertilization was severely compromised, leading these animals to infertility. Moreover, zona-free or denuded oocytes from *Ptx3*$^{+/+}$ and *Ptx3*$^{-/-}$ females showed similar maturation rates and, when submitted to IVF, no differences in the rate of fertilization, progression to the two-cell stage or blastocyst formation were observed (342). Additionally, zygotes obtained from *in vitro* fertilized *Ptx3*$^{-/-}$ oocytes successfully developed when

transplanted into the uterus of pseudo-pregnant WT females, thus showing that the defects in fertilization observed *in vivo* are probably due to cumulus matrix abnormalities and not underlying oocyte developmental defects.

These observations are consistent with other crucial roles assigned to the cumulus matrix and cumulus cells during fertilization. In some mammals, such as primates, ruminants and rabbits, the sperm is deposited inside the vagina; while for others, including rodents and pigs, it is ejaculated inside the uterus (424). From these locations, sperm use a combination of passive drag and active swimming to reach the isthmus, a specific region of the oviduct (or fallopian tubes in humans) that works like a sperm reservoir (425). The sperm that accumulates in the isthmus binds to the local epithelial cells and remains viable for a period of time, which depends on the species (426). However, once ovulation happens, the sperm will leave the isthmus and start migrating towards the ampulla, the oviduct section where fertilization occurs. Recently, Wang and colleagues (427) uncovered an additional mechanism describing how cumulus cells from ovulated COCs control sperm migration inside the oviduct.

The authors showed that the same signalling responsible for triggering cumulus layer expansion – the gonadotropin surge in combination with oocyte-secreted factors - induces the transcription of TGFβ ligand 1 by the cumulus cells. In parallel, LH action also promotes the transcription of the TGFβ receptor *Tgfbr2* in the oviductal cells of the ampulla. Knowing that TGFβ can stimulate CNP production in other cell types (428) and that sperm derived from animals deficient for the CNP receptor NPR2 are unable to reach the ampulla before fertilization (429), the authors proposed a model to describe how the cumulus cells could control sperm migration. Therefore, the proposed model involves the binding of cumulus cell-derived TGFβ1 to the TGFβR2 in the cells of the ampulla, which induces CNP production and secretion that, in turn, would stimulate the sperm to leave the isthmus and migrate towards the expanded COC located at the ampulla. To test this model, a mouse lineage with cumulus cell conditional knockout of *Tgfb1* and an epithelial cell conditional knockout of *Tgbr2* was generated. The goal was to impair TGFβ1-TGFBR2 signalling and consequently decrease CNP production at the ampulla to evaluate the effect on sperm migration. As expected, sperm migration out of the isthmus was dramatically reduced in the double knockout mice in comparison to their WT counterparts, further supporting the idea that cumulus cell-derived TGFβ1 promotes the expression of CNP in the oviductal ampulla, a critical step for sperm migration and fertilization.

As the mature oocyte is located at the center of the expanded COC, sperm first interacts with the matrix before reaching the oocyte (430,431). This is especially relevant *in vivo*, where the sperm-oocyte ratio is closer to one and not nearly as high as in IVF conditions (432). Work carried out by Shimada and colleagues (433) characterized a regulatory feedback loop between sperm and COCs involving the HA in the cumulus matrix. Cumulus cells of ovulated COCs express toll-like receptors (TLR) - a family of receptors that bind HA and increase the production and secretion of chemokines, substances known to stimulate cell migration. Therefore, by incubating ovulated COCs with either hyaluronidase or sperm – a biological source of hyaluronidase - they tested whether this signalling pathway plays any role in sperm migration and fertilization. They showed that the low molecular weight HA molecules generated by exogenous hyaluronidase activated the TLR2 and 4 on the cumulus cells. This induced the transcription of interleukin 6, C-C Motif Chemokine Ligands 4 and 5 mRNAs, an effect that was prevented by adding TLR2 and TLR4 blocking antibodies. Interestingly, the increased chemokine production led to elevated levels of protein tyrosine phosphorylation in the sperm, a measurement of sperm capacitation. So, the proposed model involves sperm-derived hyaluronidase generating low molecular weight HA, which activates its specific receptors on the cumulus cells that produce and secrete chemokines, which will induce further sperm capacitation and consequently increase fertilization. Therefore, cumulus layer expansion is essential so the oocyte is protected when exiting the follicle, so the oviduct pickup is facilitated, and, finally, so the sperm is fully capacitated and adequately guided to the oocyte right before fertilization.

### 3.4. Cumulus cell actin cytoskeletal rearrangement

The actin cytoskeleton is a complex network of F-actin filaments that give cells their shape, enabling internal organization and aiding in essential functions such as cell division or migration. The actin cytoskeleton will be reviewed in detail in section 4.2.1 of this document. Early work with expanding bovine COCs investigated the redistribution of the F-actin filaments during expansion (434). The authors identified extensive changes in the actin cytoskeleton during the first half of expansion, with the appearance of large F-actin bundles on the cumulus cells. Upon further investigation, it was determined that the changes identified in the cumulus cells coincided with oocyte GVBD and included cytoplasmic F-actin assembly, membrane ruffling, cell polarization and extension of membrane protrusions (435). The addition to the culture media of cytochalasin B, a drug that promotes the disorganization of F-actin filaments,

prevented all these changes, as well as cumulus layer expansion altogether (436). Therefore, these results indicate that the observed reorganization of the F-actin cytoskeleton is essential for cumulus layer expansion.

Additional evidence regarding cumulus cell morphology and cellular protrusions supports this theory. During the oocyte growth phase, the cumulus cells conserve a round morphology and extend actin-rich TZPs to enhance communication with the oocyte (437). These filopodia-like structures retract after the LH surge triggers cumulus layer expansion, and the gap junction network is lost (438,439). Concomitantly, cumulus cells have been described to assume an elongated morphology in cattle (436) and pigs (440) COCs, in addition to also extending different cell protrusions, including filopodia, membrane blebs and microvilli (319,351,434,441,442). All these changes depend on the assembly and disassembly of actin filaments. Therefore, cumulus layer expansion, besides the intense extracellular matrix deposition, is also characterized by an extensive rearrangement of actin filaments in the cumulus cells.

Although this mechanism is essential for oocyte developmental competence, the mechanisms driving TZP retraction and cumulus cell cytoskeletal rearrangement are still elusive. Cumulus cells have been described to extend different cellular protrusions during expansion, such as filopodia, membrane blebs and microvilli (319,351,434,441,442). The generation of these structures is intimately dependent on the assembly and disassembly of actin filaments, implying an extensive cytoskeletal rearrangement concomitant to their elaboration.

To further investigate cumulus cell detachment during expansion, Kawashima and colleagues (442) evaluated the role of the protease calpain, which is usually involved in degrading adherent junction proteins (443). After LHR activation, calpain activity increased in cumulus cells, which detached from one another and presented bleb-like membrane protrusions. Immunofluorescence experiments showed calpain's localization shifted from the cytoplasm to foci along the membrane, colocalizing with paxillin, a common calpain target that integrated adherent junctions. Pharmacological inhibition of calpain activity blocked cumulus cell detachment, membrane bleb formation, and cumulus layer expansion altogether. But while the inhibitor treatment impaired the expansion process, it did not alter *Has2* expression levels. This seminal work indicated cumulus layer expansion to be mediated by two distinct processes: one

leading to cumulus matrix production and another responsible for cumulus cell detachment and movement.

Work done by Akison *et al.* (444) supports and further develops the theory proposed by Kawashima and colleagues (442). Mouse COCs were collected over 14h after hCG injections and used to characterize their migratory behaviour. To do this, they employed Transwell Migration Assays, in which samples are incubated on top of standing cell culture membranes and might migrate to the bottom chamber in case they respond to the chemoattractant component added to it (445). In this case, the chemoattractants used were EGF and serum. While cumulus cells from unexpanded COCs showed very low migration, samples collected within 4 and 8h showed increased migratory capacity that peaked at 12h post-hCG injection. Additionally, the ability of cumulus cells to migrate decreased rapidly in samples collected from the oviduct. Therefore, these results demonstrate that the LH surge instills a highly migratory phenotype in the cumulus cells of preovulatory follicles. This phenotype may play a role in cumulus layer expansion or be required for successful ovulation. However, the mechanism behind this displacement is still unknown.

## 4. Cell migration

Cell migration refers to the movement of cells throughout the body, and its study is highly relevant to our understanding of both normal and pathological processes (446,447). During embryonic development, for example, coordinated cell migration guides gastrulation and the formation of the ectoderm, mesoderm and endoderm (448). In cancers, tumour cells travel to colonize new tissues - a process termed metastasis that dramatically affects cancer treatment and patient survival. Therefore, understanding the cellular and molecular mechanisms behind cell migration is of utmost importance for diagnostic and therapeutic purposes.

### 4.1. 1D, 2D and 3D cell migration and their physiological relevance

One-dimensional, or 1D, cell migration is a term that refers to cells migrating along a narrow linear structure. *In vivo*, it is termed contact guidance (449,450) and can be observed, for example, on collagen fibrils that irradiate from highly invasive human breast tumours (451). The poor prognosis assigned to these patients and the observation that tumour cells, stem cancer cells, and leukocytes will preferentially migrate along these collagen arrays have suggested this specific ECM deposition to enhance cell migration (452,453). Moreover, *in vitro* evidence

showed that glioblastoma cells migrate more rapidly on 1D nanofiber grids when compared to two-dimensional substrates made of the same material (454), further supporting this theory.

Two-dimensional (2D) cell migration has been extensively studied in cell culture (455,456). In this system, cells follow a general and well-characterized migration mechanism involving repetitive protrusion, adhesion and contraction (455,457–459). Briefly, actin polymerization driven by small Rho GTPases like Rac1 and CDC42 mediate lamellipodia extension and/or filopodia at the leading edge. This causes the leading edge to protrude and adhere to the substrate, followed by cell body translocation, mediated by another small Rho GTPase, RhoA. This standard migration mechanism has been described for different cell types, cancerous or not, migrating on flat 2D surfaces. However, 2D migration is rarely observed *in vivo* and does not constitute a good physiological model for investigating cell locomotion.

As tridimensional (3D) cell culture systems were studied more and more, it became clear that the standard 2D migration mode was a specialized and stereotypical version of cell locomotion. In fact, the more physiological the environment the cells are inserted in, the more flexible they become and can easily switch between different migration modes – namely mesenchymal and amoeboid. It is now known that the migratory mode of a cell navigating complex and intricate ECMs of living tissues is determined by three primary parameters: *i*) adhesion to the substrate, *ii*) actin protrusion, and *iii*) actomyosin contraction. According to cell-based or environmental-derived factors, these key parameters can assume different spatiotemporal dynamics that define each migration mode, reviewed in section 4.5.

### 4.2. Actomyosin, the motor behind cell migration

In 1970, Michael Abercrombie suggested that cells propel themselves forward by adding material to their front, which leads to an internal rearward flow that, coupled with adhesion to the substrate, results in a net movement forward (460). Schematically, it can be compared to a war tank propelling itself forward while its tracks roll backward. We now know that this backward flow inside the cell results from the extension/disassembly of membrane-associated actin filaments. But that is not the only tool the cell has to generate force: it also relies on the activity of molecular motors to contract actin filaments and, for example, pull the back of the cell forward (461). Therefore, actin polymerization (pushing) and the contraction of antiparallel actin filaments (pulling) are the two sources of mechanical force inside the cell. The relative

contribution of these pushing and pulling forces to actual movement varies according to the migration mode at play. In mesenchymal migrating cells, for instance, lamellipodia extension at the cell's leading edge will push the membrane forward, and the contraction of stress fibres – longitudinal cellular actin cables – will pull the cell body forward. Amoeboid migratory cells, however, tend to rely mostly on contraction to propel themselves forward. Cortical actin contraction increases the cytoplasmic hydrostatic pressure and promotes the protrusion of different cellular structures, leading to a bleb-based cell motility (462), reviewed in section 4.5.2. Therefore, despite the migration mode, the underlying mechanisms for force generation are conserved and dependent on the actomyosin cytoskeleton. This structure results from the association between actin filaments and molecular motors such as myosin (463).

### 4.2.1. Actin cytoskeleton dynamics

The actin cytoskeleton is a vast and complex network of actin filaments and associated proteins (464). It defines cell shape, facilitates intracellular organization and cargo transportation, drives cytokinesis and motility and enables cell adhesions. Despite its complexity, the actin cytoskeleton is dynamic and can reorganize in response to extracellular signals, including growth factors and chemotactic cues, to promote and support cell migration, adhesion and division.

Globular actin (G-actin) exists in free form before being assembled into an actin filament (F-actin). This process comprises three key steps: *i*) nucleation, *ii*) elongation and *iii*) steady-state phase. While nucleation is the rate-limiting step, during elongation, G-actin monomers are added to the oligomer until the steady-state phase, when the rate of assembly on one end of the filament equals the rate of disassembly on the opposite one. The opposing ends of an actin filament harbour distinct polymerization dynamics: assembly of G-actin monomers happens at the *barbed* or (+) end of the filament, while disassembly is concentrated on the *pointed* or (-) end (465). As a result, the actin filament conserves an average length, with the G-actin subunits treadmilling from the barbed to the pointed end (466).

F-actin polymerization happens spontaneously in a G-actin solution, given that it is maintained in physiological conditions (Figure 10a). Therefore, cells have developed strategies to curb this trend and guide actin assembly/disassembly to suit their needs (Figure 10b). To prevent spontaneous polymerization, G-actin monomers are in constant association with

a)

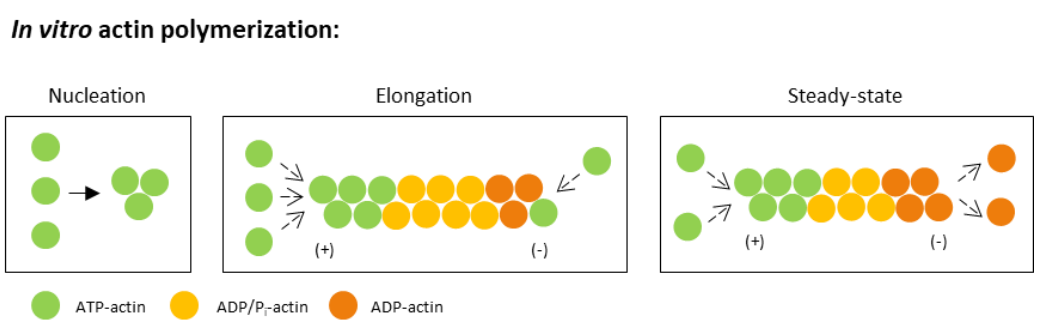


b)

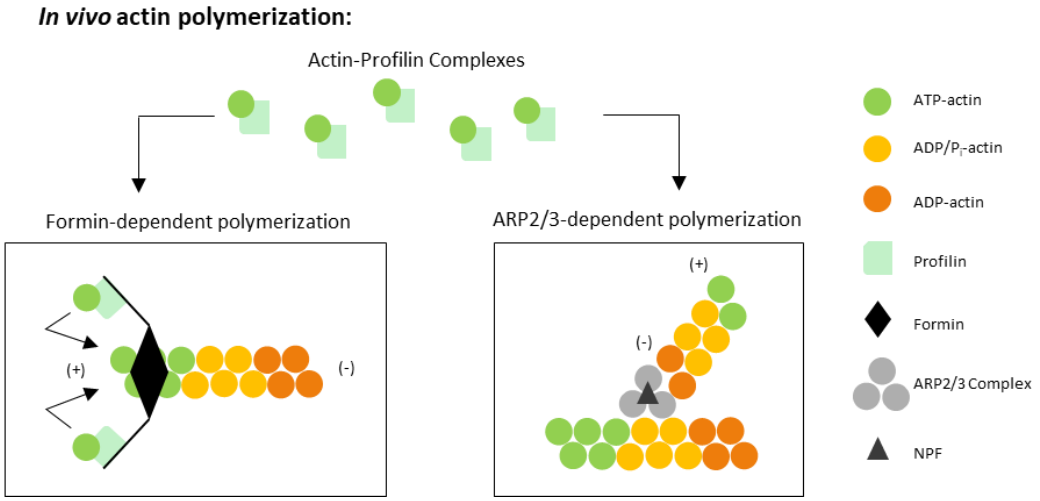


**Figure 10: *In vitro* and *in vivo* actin polymerization**. a) After G-actin spontaneously nucleates *in vitro*, filaments are elongated by adding more G-actin subunits, mostly at the barbed (+) end. The ATP molecules present in the incorporated subunits undergo hydrolysis and phosphate release, creating an "age-dependent" gradient of nucleotides along the filament. The ATP-actin subunits (green) are mostly localized at the barbed end, while the ADP-actin subunits (orange) are localized in the center of the filament. Once the filament reaches equilibrium, it enters the so-called treadmilling or steady state. b) *In vivo*, free ATP-actin subunits are associated with actin-sequestering proteins (e.g. profilin, light green). Nucleation and elongation can occur by formin-dependent or Arp2/3-dependent mechanisms.

sequestering proteins, such as the members of the profilin family, decreasing the concentration of free G-actin monomers (467). Moreover, specific proteins control and facilitate directed actin polymerization. To do so, they mimic an actin trimer or tetramer, whose formation is the most critical step in F-actin elongation (468). A prominent group of actin nucleators is the formin family, which is responsible for the nucleation of linear actin strands. With the help of their conserved formin homology 2 (FH2) domain, these proteins stabilize an actin dimer and recruit

profilin-actin complexes, which promotes elongation of the stabilized dimer (469). Another well-studied actin nucleator is the Actin-Related Protein (Arp) 2/3. This complex comprises seven subunits, two of which (Arp2 and Arp3) are structurally similar to actin (470). They attach to pre-existing actin filaments and nucleate the elongation of a branched new actin strand (471). Intrinsically inactive, Arp2 and 3 activities can be stimulated by at least 8 known factors, called nucleation-promoting factors (NPFs). These factors share a so-called WCA domain, which harbours an actin-monomer binding WH2 region and can bind Arp2/3, leading to a conformational change and consequent activation (472).

Once actin monomers are incorporated into the filaments, they start ageing, a process mediated by the hydrolysis of actin-bound ATP. This favours the binding of disassembly factors, leading to increased G-actin dissociation towards the filament pointed end (473). Actin disassembly can occur in different ways, namely by debranching of whole Arp2/3-containing actin filaments by members of the coronin and GMF protein families (474) or as a result of ADF/cofilin activity, which has been described as disassemble, sever and depolymerize actin filaments (475–477). Once removed from the filament, the ADP binding the actin monomers can be swapped by ATP by profilin proteins (478–480) or by cyclase-associated proteins (481), replenishing the pool of ATP-bound G-protein monomers.

### 4.2.2. Non-Muscle Myosin II

Myosins are ubiquitously expressed motor proteins that play crucial roles in cellular processes that require force generation, such as cargo transportation and contraction (482). This activity requires energy provided by the hydrolysis of ATP, which is catalyzed by myosin's ATPase activity. Most known myosins belong to class II and, in association with actin filaments, they make up the contractile machinery in cardiac, skeletal, and smooth muscle cells (482). Additionally, this class also harbours the non-muscle myosin II (NMII). This molecule shares its structure with its muscle counterparts, but instead of muscle contraction, it is usually involved in cellular processes that require reshaping, such as cell division and migration. NMII is expressed in all non-muscle eukaryotic cells (483,484) and can also be found in muscle cells, where they play pivotal roles during their development and differentiation (485).

Each NMII is a complex that encompasses six subunits: two heavy chains (MHC) and two pairs of light chains, one commonly referred to as the regulatory light chains (20kDa MLC,

$MLC_{20}$) and the other as the essential light chains (17kDa MLC, $MLC_{17}$) (Figure 11a). The two MHC form homodimers through charge-driven interactions between their coiled-coil regions, giving rise to an extended coiled-coil rod domain that ends in a short, non-helical tail. The light chains interact with the MHC chains at their other extremity, called the neck domain, a short junction that separates the coiled-coil rod domain from the motor one formed by the light chains. Thus, the resulting hexamer assembles into a polar structure, with the globular motor domain on one end of the molecule and the coiled-coil rod domain on the other (482).

Three NMII isoforms have been identified, each characterized by a different heavy chain: MHC-A, MHC-B, and MHC-C (482). Two main properties differ among the different NMII isoforms: the actin-triggered ATPase activity, which is the increase in ATP hydrolysis by myosin upon binding to acting, and the duty ratio, defined as the time that myosin is binding actin in a force-generating state. Among the three isoforms, NMII-A has the highest ATP hydrolysis rate (486). NMII-B has a higher duty ratio when compared to NMII-A (487,488). Also, NMII-B has a much higher affinity to ADP than the other isoforms, which means it releases ADP at a lower rate. These kinetic differences could help explain why some cellular functions seem isoform-dependent while others seem redundant (489,490).

As described above, the N-terminal region of NMII harbours the actin and the ATP binding domains and, therefore, determines the kinetic parameters of the molecule. On the other hand, the C-terminal region of NMII comprises the coiled-coil rod domain and the non-helical regions, which can bind to the coiled-coil rod domain of a second NMII, associating into bipolar mini-filaments (491) (Figure 11b). When the head domains of these bipolar NMII mini-filaments interact with actin filaments, tethering them, they form actomyosin. Then, the energy provided by ATP hydrolysis powers NMII folding, ultimately causing the actin filaments to slide in opposite ways and creating tension inside the cell.

Actomyosin assembly and ATPase activity are tightly regulated. While skeletal and cardiac myosins are regulated by a separate set of proteins attached to the actin filaments, NMII polar mini-filament formation and the ATP hydrolysis are under the control of the reversible phosphorylation of specific residues located on $MLC_{20}$ and MHC. In turn, there is no evidence that the $MLC_{17}$ undergoes reversible phosphorylation, and its primary function seems to be binding and stabilizing the MHC (484). For simplicity, from this point on, the regulatory light chains $MLC_{17}$ are going to be referred to as MLCs.

a)

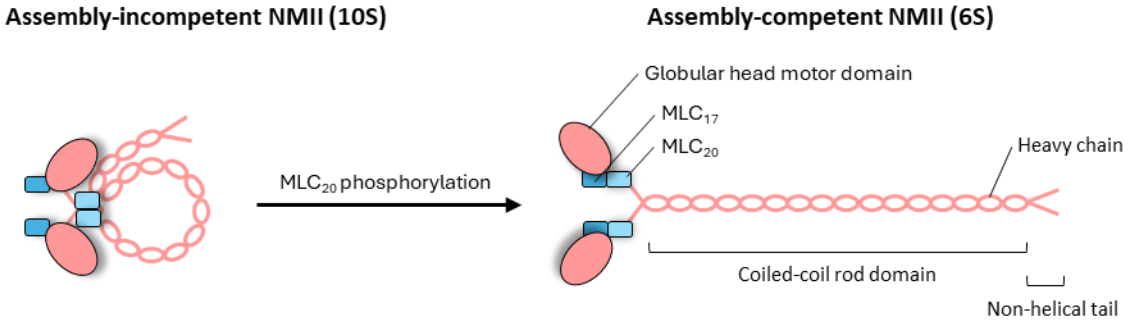


b)

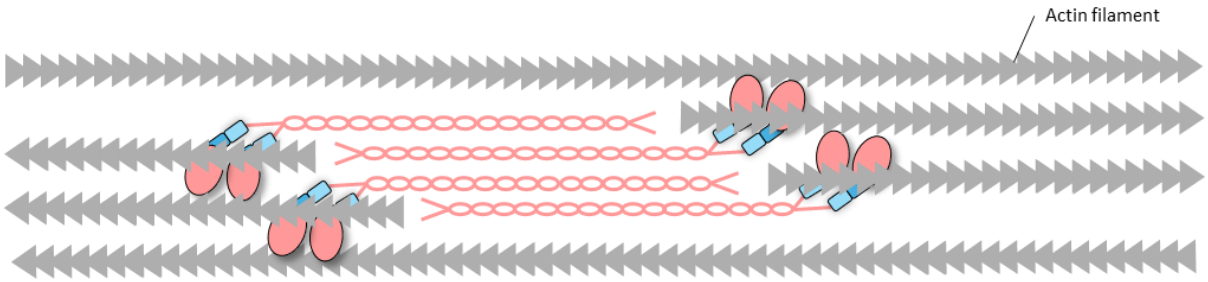


**Figure 11: Structure, assembly, and activation of NMII**. a) The subunit and domain structure of Non-muscle Myosin II (NMII). The globular head domain contains the actin-binding regions and the motor domains. The essential light chains ($MLC_{17}$) and the regulatory light chains ($MLC_{20}$) bind to the heavy chains at the lever arms that link the head and coiled-coil rod domains. Left panel: In the absence of $MLC_{20}$ phosphorylation, NMII folds and forms a compact structure through a head-to-tail interaction, resulting in an assembly incompetent form (10S) that is unable to associate with other NMII. Right panel: After $MLC_{20}$ phosphorylation, the 10S structure unfolds and becomes assembly-competent(6S). b) NMII molecules assemble into bipolar mini-filaments through interactions between their coiled-coil rod domains. These mini-filaments bind to actin through their head domains, and the ATPase activity of the head enables a conformational change that moves actin filaments in an anti-parallel manner. Bipolar myosin mini-filaments link actin filaments together in thick bundles, forming actomyosin.

Even though the role of MHC reversible phosphorylation has only been well established in *Dictyostelium* and *Acanthamoeba* (492,493), mammalian cells seem to follow the same trend, with MHC phosphorylation negatively regulating NMII activity. Phosphorylation sites have been identified near the C-terminus of the MHC, more specifically, both in the coiled-coil region, which forms the rod domain and the non-helical tail (494–496). *In vitro* assays have shown that

these residues can be phosphorylated by either PKC (494), Casein II (495) or Transient Receptor Potential Melastatin 7 (TRPM7)(496). In each of these cases, the phosphorylation either causes the subunits of NMII to dissociate or prevents their assembly. Additionally, the phosphorylation promoted by TRPM7 on the helical portion of the rod, Thr1800, has been shown to guide the subcellular localization of NMII (496).

On the other hand, the positive regulation of NMII activity is controlled by reversible phosphorylation of the MLC. Evidence from extensive *in vitro* experimentation shows that MLC phosphorylation controls NMII mini-filament assembly by regulating its conformational state. Assembled and MLC-nonphosphorylated NMII is folded into a compact conformation, where the rod domain tail folds over and binds the two head domains, which also bind each other in an asymmetrical manner (497–501). This conformational state is assembly-incompetent, as illustrated in Figure 11a. However, introducing a negative charge by phosphorylation of MLC disrupts the head-head and the head-tail interactions (497), causing the 10S fast sedimenting structure to convert to the 6S slow sedimenting one (Figure 11a). Additionally, the 6S conformation is assembly-competent and can form mini-filaments with other NMII molecules and interact with actin filaments, forming actomyosin (Figure 11b). The phosphorylation responsible for these changes occurs at the Ser19 of the MLC, and even though this event increases NMII's ATPase activity (502), it does not seem to increase NMII affinity to actin (503). Additional phosphorylation on Thr18 is also observed, and its function is twofold. First, Thr18 phosphorylation increases NMII ATPase activity and its affinity to actin, besides stabilizing NMII 6S conformation, which decreases the chances of actomyosin disassembly (504,505). In cells, di-phosphorylation of MLC is usually observed in regions with increased tension, suggesting the double Ser19/Thr18 phosphorylation produces actomyosin that, besides generating, can also withstand great tension (506). Therefore, in opposition to the MHC phosphorylation, adding phosphates to amino acid residues located on the MLC stimulates NMII mini-filament formation and ATP hydrolysis that power NMII activity.

The fact that F-actin can be polymerized as a linear or a branched structure gives rise to two main actomyosin varieties: networks and bundles. Actomyosin bundles occur when NMII mini-filaments associate with linear actin, giving rise to stress fibres (507). The actin filaments in the stress fibres are aligned and overlap but conserve the possibility of being oriented in opposite directions within the bundle (508,509). Different categories of stress fibres have been described

mainly based on their location inside the cell and how they align with the movement direction (510). Although stress fibres are sometimes observed in cells migrating through 3D ECMs, they are often observed in cells migrating on 2D hard substrates (511). In these scenarios, stress fibres generate pulling forces responsible for detaching adhesions to the substrate and retracting the cell's rear end.

On the other hand, many cell types migrate without stress fibre formation. These rely on forces generated by actomyosin networks, formed after a mixture of randomly positioned linear and branched actin filaments bind NMII mini-filaments (512). These actomyosin networks are frequently formed in association with the plasma membrane, generating what is referred to as the actin cell cortex (513). Despite the lack of alignment, the sliding of NMII mini-filaments along randomly oriented actin filaments can produce overall network contraction and power cell migration (514). Cortical tension is mainly controlled by NMII activity (515), and NMII inhibition can reduce it by up to 80% (516). All three NMII isoforms have been shown to localize to the cell cortex (517).

Different kinases have been reported to phosphorylate the MLC subunit of NMII. These include the Myosin Light Chain Kinase (MLCK), the Citron Kinase (CITK), the Leucine Zipper Interacting Kinase (ZIPK), the Rho-associated coiled-coil containing Kinase (ROCK), and the Myotonic Dystrophy Kinase-related CDC42-binding Kinase (MRCK)(484,502,518,519). MLCK was the first reported kinase to phosphorylate the Ser19 of MLC in smooth muscle myosin II (520). While MLCK can also phosphorylate the MLC of NMII, it does so with a much lower affinity, and smooth muscle myosin II is its main substrate (521). For this reason, the depletion of MLCK in non-muscle cells usually leads to a mild phenotype (522). CITK plays a crucial role in cytokinesis, but its expression is restricted to the testis, kidneys and spleen, and therefore, it might not be required for cell migration (523,524). Similarly, ZIPK has been mainly associated with the onset of apoptosis and has not been reported to contribute to NMII during cell migration (525). Therefore, the primary known NMII kinases involved in controlling actomyosin contractility during cell migration are ROCK and MRCK.

ROCK, a Serine/Threonine kinase, can control NMII activity by either directly phosphorylating the MLC (526) or by phosphorylating and inactivating Myosin Phosphatase Target Subunit 1 (MYPT1), which is the phosphatase responsible for dephosphorylating MLC (527). Structurally, ROCK has an N-terminal kinase domain, a coiled-coil region containing a

Rho-binding domain (RBD) and a C-terminal pleckstrin homology (PH) domain, as illustrated in Figure 12. ROCK is usually found folded in an autoinhibited conformation, where a head-to-tail interaction blocks its catalytic site (528). Association with the active (GTP-bound) small Rho GTPase RhoA (Ras Homolog Family Member A), which binds the RBD domain, induces a conformational change, transiently activating ROCK (529,530). In the cell, two ROCK isoforms can be found and are here referred to as ROCK1 and ROCK2. While they have an overall homology of 62%, their kinase domain is nearly the same, with 92% identity (531). But even though ROCK1 and ROCK2 are structurally very similar, they might have nonredundant functions. For example, in mesenchymal migratory cells, both ROCK1/2 can phosphorylate MLC, but ROCK1 seems to accumulate at the back of the cell, defining front-back polarity, while ROCK2 localizes to the leading edge (532).

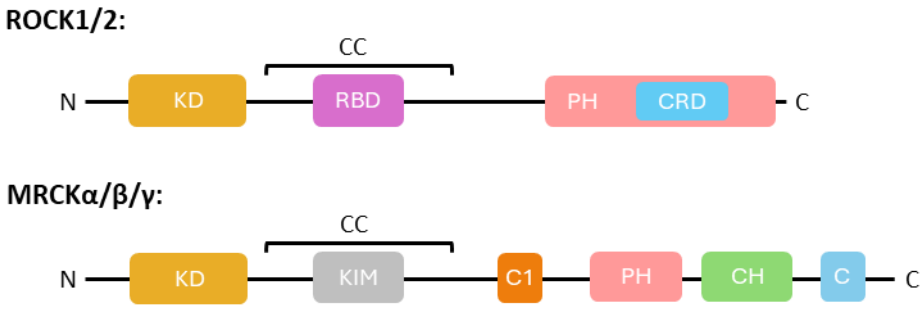


**Figure 12: Domain and Structure of ROCK and MRCK**. Domains: KD, CC, coiled-coil region; kinase domain; RBD, Rho-binding domain; PH, pleckstrin homology domain; CRD, cysteine-rich domain; C1, C1 domain; CH, citron homology domain; C, CDC42- and Rac-Interactive Binding (CRIB).

MRCKs integrate a group of Serine/Threonine kinases that is evolutionarily related to ROCK1/2 and also play a crucial role in regulating actomyosin contractility (533). Among the three MRCK isoforms - α, β, and γ - MRCKα/β are ubiquitously expressed and present kinase domains with 85% identity, while MRCKγ is more divergent and has a restricted expression pattern (534). Despite that, all three isoforms have an N-terminal kinase domain that is followed by C-terminal kinase C conserved region (C1), PH-like domain, citron homology (CH) domain and CRIB domain (Figure 12). MRCKs are found at the plasma membrane (535), possibly due to the presence of the C1 domain, which has been described to bind plasma membrane components and mediate the anchoring of cytosolic proteins to it (536). MRCK forms a tetrameric complex in

the inactive state and undergoes a head-to-tail autoinhibitory conformation (533,535). Binding to active CDC42 will relieve the autoinhibition by inducing a conformational change and guiding the active MRCK to a specific cell location (537). Similar to ROCK1/2, MRCKs can also directly phosphorylate MLC on Ser19 and Thr18, in addition to inhibiting MYPT1 activity as well (537,538) ROCK1/2 and MRCK have highly related kinase domains and a similar set of substrates (533). However, their activities are not redundant, partially due to their differential regulation, which will be discussed in section 4.4.

### 4.3. Cell protrusions

Cell migration is driven by the cytoskeleton, which combines protrusive (pushing) and contractile (pulling) forces to move cells forward, whether in protist amoebas or multicellular organisms. Different actin assembly/disassembly and actomyosin contractility control will translate into different protrusion types. The protrusion of the plasma membrane can be mainly achieved by three distinct mechanisms involving actin filaments (Figure 13). The first one generates a broad and complex network of branched actin filaments at the cell's leading edge, forming the lamellipodium. The second mechanism involves the linear growth of small actin bundles that polymerize and extend the membrane to form filopodia. Finally, the third mechanism does not require active actin polymerization but high actomyosin contractility, increasing the internal hydrostatic pressure and driving the protrusion of structures termed membrane blebs. Therefore, the actin-based cellular protrusions that aid cell migration can be polymerization-driven, as lamellipodia and filopodia, or contractility-generated, as the membrane blebs.

#### 4.3.1. Lamellipodia

Lamellipodia are the most extensively studied structure driving cell migration. They consist of a flat membrane protrusion that can be observed at the leading edge of fibroblasts, neurons, and epithelial, endothelial, and immune cells. They are formed when cells migrate on solid surfaces both *in vitro* and *in vivo* and can also be tridimensional depending on the substrate and the cell’s capacity to adhere to it (473,539). These 3D lamellipodia are referred to as membrane ruffles but are generated by the same mechanisms controlling the extension of lamellipodia on hard 2D surfaces (468).

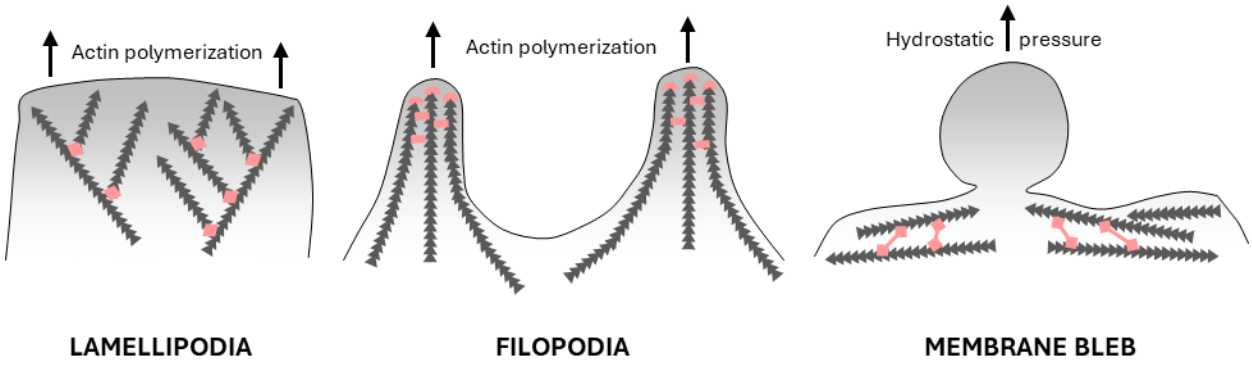


**Figure 13: Types of actin-based protrusions**. Representative examples of plasma membrane protrusion types - lamellipodia, filopodia, and membrane blebs. Protrusion of the plasma membrane can be achieved by actin polymerization forces, in the case of lamellipodia and filopodia, or by hydrostatic pressure created by actomyosin contractility for membrane blebs. Accessory proteins illustrated in pink will be reviewed in the next sections.

Lamellipodia formation is usually associated with the mesenchymal mode of migration and is, therefore, formed downstream of Rac GTPases (540), whose signalling will be reviewed in detail in section 4.4. Briefly, when a cell detects the presence of growth factors, lamellipodia will be extended in response to the stimulus to initiate migration. Therefore, after the growth factor binds and activates its receptors on the cell surface, its tyrosine kinase activity will transduce the signal and activate small Rho GTPases such as Rac1 and RhoA (541). At the leading edge, Rac1 interacts with the WAVE complex, which undergoes a conformational change before binding and activating another protein complex, the Arp2/3. Arp2/3 will then bind to pre-existing actin filaments close to the membrane and catalyze the extension of an extensive network of branched actin filaments, which create a pushing force that drives membrane protrusion (542–544) (Figure 14). This force generation depends on actin polymerization and is uncoupled from NMII activity (545). Once extended, the membrane establishes adhesive interactions when integrin receptors at the lamellipodia tip interact with the underlying substrate (546,547). These adhesion sites serve as anchoring points for linear bundles of actomyosin that constitute the stress fibres, which are synthesized by the formins mDia1 and 3, activated downstream of RhoA (456). The stress fibres connect the nascent adhesion sites to those located at the cell's rear, enabling RhoA-mediated actomyosin contraction, detaching the rear adhesions and retracting the cell body.

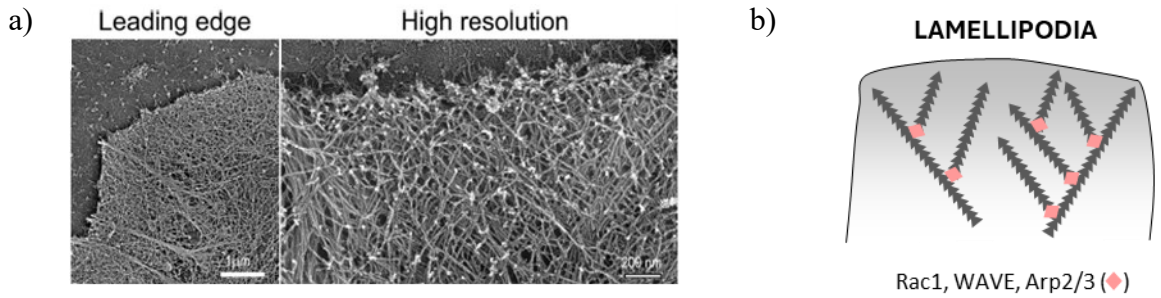


**Figure 14: Actin cytoskeleton structure of lamellipodia**. a) Platinum replica electron microscopy adapted from Alexandrova *et al*. (554). Left panel: the cell leading edge; right panel: high magnification of the leading edge. b) Diagram of actin organization in lamellipodia. The cytoskeleton of lamellipodia consists of a dense branched actin network generated by Rac1>WAVE>Arp2/3 signalling. Arp2/3 complex (pink) is positioned at the sites of initiation of new actin filament branches at the side of the mother filament.

The stabilization of a lamellipodium depends on cell contact with the substrate. For example, if two mesenchymal migrating cells meet, their lamellipodia will stop extending and retract (548,549). Alternatively, a lamellipodium will also retract to the cell body if the cell's ability to adhere to the underlying substrate is reduced (539). Moreover, the formation and stabilization of a lamellipodium also depend on the internal delicate balance of actin polymerization at the leading edge and in the cytosol: increased actin assembly in the cytosol can affect the availability of G-actin subunits at the leading edge, which drives lamellipodia retraction (550).

### 4.3.2. Filopodia

Filopodia are thin, fingerlike cellular projections that usually protrude from the edge of lamellipodia. Functionally, they probe the extracellular environment for cues to direct cellular motility or to mediate cell-cell contact (551,552). Structurally, filopodia are built of long, linear actin filaments that are bundled up by actin-binding proteins such as Fascin (553). Cross-linking the actin bundle is essential to building the filopodia backbone (552) (Figure 15).

Two models have been proposed to describe filopodia initiation development: the tip nucleation model and the convergence elongation model (553). The tip nucleation model is based on the direct actin filament nucleation at the membrane by formins. As the filaments are extended, they are bundled up by actin-binding proteins. Alternatively, filopodia protrusion can

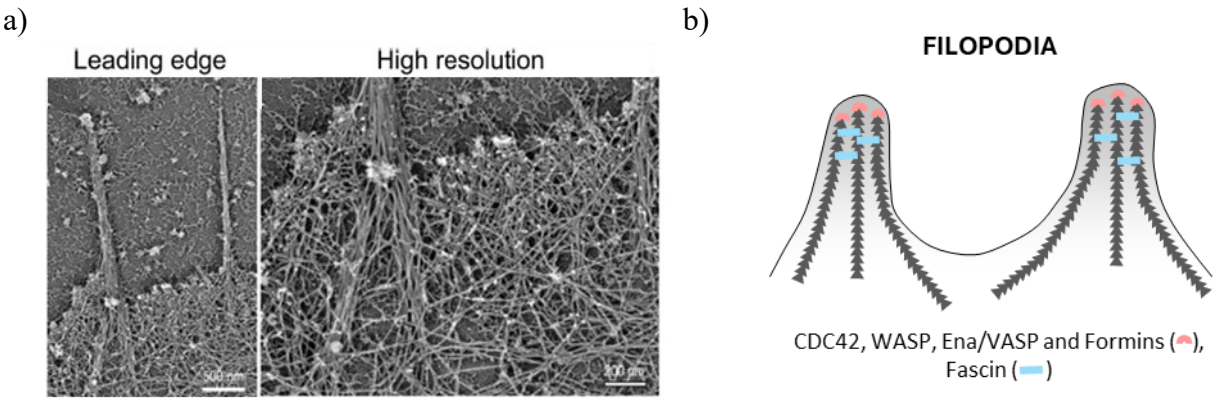


**Figure 15: Actin cytoskeleton structure of filopodia**. a) Platinum replica electron microscopy adapted from Alexandrova *et al*. (554). Left panel: the cell leading edge; right panel: high magnification of the leading edge. b) Diagram of actin organization in filopodia. The Cytoskeleton of filopodia consists of a bundle of actin filaments elongated by actin elongation factors such as Ena/VASP and formins (pink). The filaments are cross-linked by actin binding protein such as fascin (blue) and oriented with their barbed ends to the tip of the filopodium.

be explained by the convergence of the branched-actin network that comprises the lamellipodia. In this model, actin elongation factors such as Ena/VASP and formins associate with the barbed end of actin filaments that constitute the lamellipodia and promote their reorganization and elongation. The filaments will be extended as long as the elongation factors are binding. Next, the protein Fascin will cross-link the filaments, organizing the bundles and giving the rising filopodia a functional backbone.

Regardless of the initiation model, the formation of filopodia has been found to depend on specific proteins, including the small Rho GTPase CDC42. CDC42 is crucial to this process as it recruits and triggers the activation of WASP/N-WASP and the formin mDia2 to promote actin polymerization (555). Additionally, the CDC42 effector Inverse-Bin-Amphiphysin-Rvs (I-BAR) domain-containing protein IRSp53 (insulin receptor phosphotyrosine 53 kDa) has also been implicated in filopodia formation as it creates a curvature on the plasma membrane, a prerequisite to forming the filopodial tip (556). Filopodia stop extending and retract into the cell when the elongation factors dissociate and actin polymerization stops (557).

### 4.3.3. Membrane blebs

Membrane blebs are spherical membrane protrusions that form on the surface of the cell (558). Once considered a hallmark of apoptosis and necrosis (559), blebs are also consistently observed during cell division and cancer cell migration (560). These highly distinct processes have something in common: high cortical pressure, later identified as the driving force behind membrane bleb protrusion. In fact, further studies of migrating cancer cells pointed out that while they usually extend lamellipodia and filopodia when cultured on hard substrates, they'll preferentially use membrane blebs to migrate inside 3D soft extracellular matrices (462,561,562). This conclusion led membrane blebs to be recognized as a standard cell protrusion type. Therefore, in addition to lamellipodia and filopodia, membrane blebs constitute a third protrusion type and do not require actin polymerization for their extension as they are driven by the cell's internal hydrostatic pressure.

Membrane blebbing can be divided into three distinct stages: initiation, expansion, and retraction (561), as illustrated in Figure 16. Bleb initiation occurs as a small area of the plasma membrane detaches from the underlying cell cortex in response to increased cortical tension. This gives way to the expansion phase, during which the cytoplasm flow inflates the membrane, causing it to detach even further (563). Besides the increase in the detached area, the unfolding of plasma membrane invaginations also helps increase the membrane area available to expand, according to the research conducted by Gourdazi *et al*. (564). Towards the end of bleb expansion, which happens in tens of seconds (565), the actomyosin cortex is reassembled underneath the plasma membrane that constitutes the bleb, and its contraction drives bleb retraction back into the cell body (561,566).

Repeated measurements and analysis of bleb number and volume showed that its formation depends on hydrostatic pressure. For instance, the volume of a single bleb decreased when multiple consecutive blebs were formed, or the intracellular hydrostatic pressure was disturbed by electroporation (567,568). The high hydrostatic pressure observed in blebbing cells results from increased contractility of the actomyosin cell cortex, driven by NMII contraction (565). RhoA and its downstream effectors ROCK1/2 are critical activators of NMII activity whose activity has been described to trigger blebbing activity (569,570). Consistent with this observation, inhibiting NMII activity significantly interferes with membrane bleb formation (571–573).

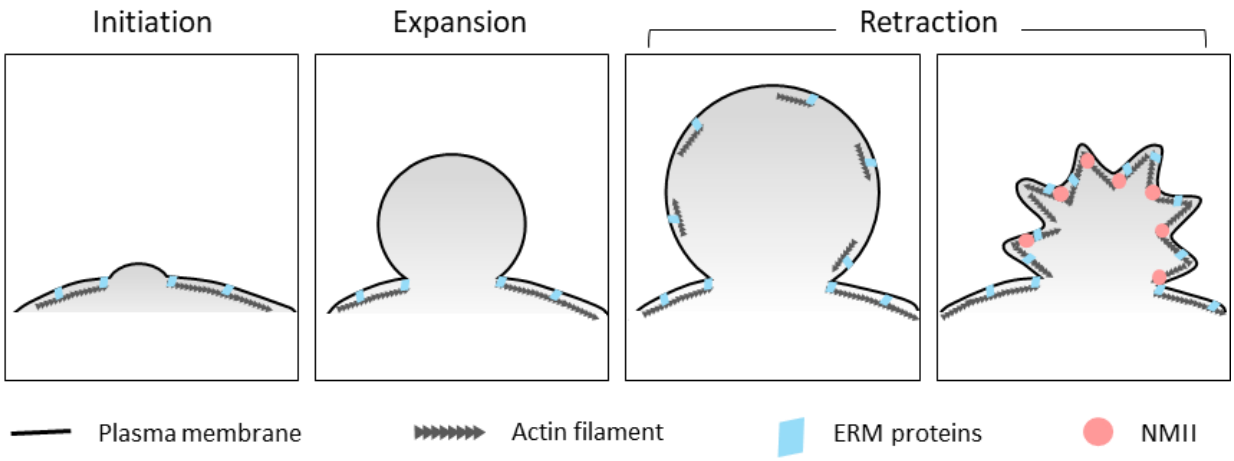


**Figure 16: The life cycle of a membrane bleb.** Membrane blebs are formed when the plasma membrane (black solid line) detaches from the underlying actin cytoskeleton (dark grey). The detachment can happen due to increased intracellular pressure or the local rupture of actin filaments. After the expansion of membrane protrusion, ERM family proteins (blue) are recruited to the protruded bleb membrane, and reassembly of actin filaments occurs rapidly and covers the protruded membrane. Finally, NMII (pink) is recruited to the freshly assembled actin cortex inside the protruded membrane, and contraction of this actomyosin cortex mediates bleb retraction.

Further study of blebs dynamic led to the hypothesis that they tend to occur at points where the link between the cell cortex and the plasma membrane is weaker. To test this hypothesis, the association membrane-cortex was manipulated in different ways. Initially, experiments using laser ablation (572,574) or small molecules that induce actin depolymerization (574,575) were shown to undermine the association between the membrane and the cortex, leading to bleb formation. The proteins Ezrin, Radixin and Moesin (ERM) have as their primary function mediating the tethering of the plasma membrane to the actomyosin cell cortex (576). Therefore, researchers next investigated their role in controlling bleb initiation. In fact, Ezrin overexpression significantly reduced bleb formation (577). Conversely, biasing the membrane lipid composition to molecules that cannot bind ERM proteins showed increased blebbing activity (578,579).

In addition to discovering the mechanism of bleb initiation, research has also focused on unveiling how the actin cortex reassembly inside the bleb unfolds. To this effect, Charras *et al.* (577) used an exogenous GFP-tagged protein expression system to track the localization of

critical regulators of actin assembly during the bleb life cycle. The results showed that as soon as expansion ceased, Ezrin was the first protein recruited to the inner side of the bleb membrane, followed by actin and only then NMII, identified by the GFP-tagged regulatory light chain subunit. Markedly, the recruitment of NMII coincided with the onset of bleb retraction. Later, proteins from the formin family were identified as responsible for resynthesizing the F-actin inside the bleb (580,581), integrating the key factors required for inner bleb actin cortex repopulation and subsequent bleb retraction.

Ikenouch and Aoki proposed a unique model to describe the membrane bleb life cycle regulation by two distinct small Rho GTPases, RhoA and Rnd3 (Figure 17)(558). Rnd3 is a constitutively active small GTPase reported to negatively regulate RhoA activity (582,583). The authors observed that Rnd3 is highly enriched on the membrane of expanding blebs but quickly disappears as the expansion phase ends. Therefore, the proposed model states that, during the expansion phase, the high concentration of Rnd3 on the membrane inhibits RhoA, preventing actin re-polymerization and actomyosin contraction that it would promote otherwise. However, as the membrane expands, Rnd3 concentration on the membrane drops, which locally relieves the inhibition over RhoA. As RhoA is transiently activated, it phosphorylates its downstream effectors ROCK1/2 and promotes actin re-polymerization inside the bleb. In turn, ROCK1/2 phosphorylates Rnd3 on Serine 240, which sequesters it into the cytoplasm (563,584,585), entirely preventing its inhibitory activity over RhoA. This enables RhoA to promote extensive actin re-polymerization and subsequent contraction to retract the bleb. Therefore, this model describes a feedback system between Rnd3 and RhoA that controls bleb expansion, actin re-polymerization and bleb retraction.

### 4.4. The family of Small Rho GTPases and their role in cell migration

Rho GTPases were first identified to control cell migration during the 80's. Ever since, extensive studies have expanded our understanding of how different members of the Rho GTPase family control migration through different substrates and conditions, first using 2D *in vitro* culture conditions and later based on 3D and *in vivo* systems.

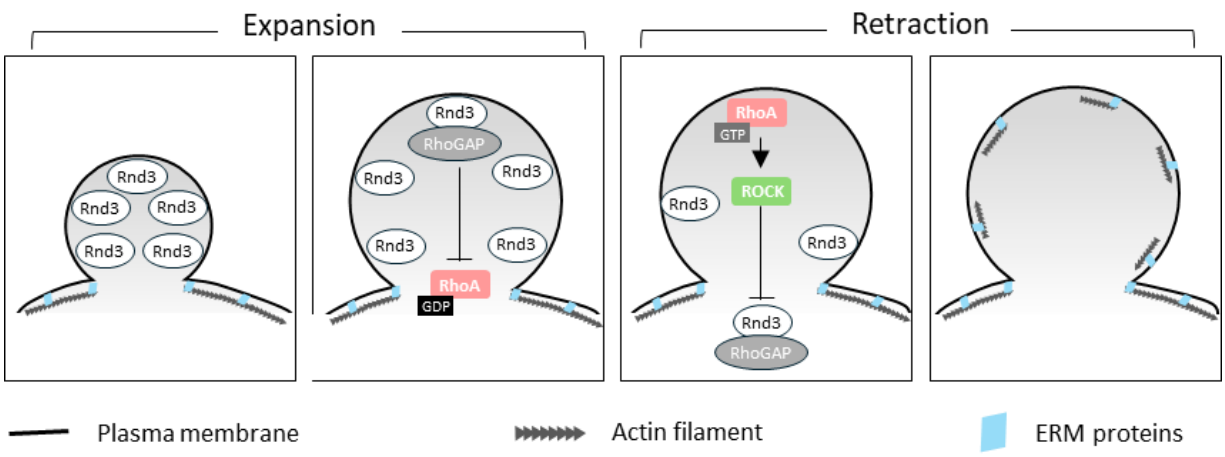


**Figure 17: Regulation of the actin cortex by Rnd3 and RhoA during membrane blebbing**. In the expansion phase of membrane blebs, Rnd3 and a RhoGAP (p190RhoGAP) inhibit the activation of RhoA and consequent regrowth of actin filaments. As the surface area of the protruded membrane increases during expansion, the concentration of Rnd3 at the plasma membrane decreases and locally activation of RhoA may occur. Activated RhoA activates ROCK that, in turn, phosphorylates Rnd3, leading to its removal from the plasma membrane. Thus, RhoA activation is amplified and sustained by a positive feedback loop, initiating the retraction phase of the membrane bleb life cycle.

Rho GTPases are small proteins (approximately 21kDa) that are part of the Ras superfamily of small GTPases. When localized at the plasma membrane, they can be activated by extracellular stimuli and proceed to modulate the activity of different downstream effectors, functioning as a signal transducer (586). Most Rho GTPases work as a molecular switch, assuming an active conformation when bound to GTP and an inactive one when GTP is hydrolyzed to GDP. Rho GTPases have an intrinsic GTPase activity, but the rate of this reaction is low (587). Therefore, the regulation of the Rho GTPases depends on the activity of other proteins, namely guanine nucleotide exchange factors (GEFs), GTPase-activating proteins (GAPs) and guanine nucleotide dissociation inhibitors (GDIs) (586) (Figure 18). GEFs catalyze the exchange of GDP by GTP, therefore activating the Rho GTPase. GAPs, in turn, inactivate the Rho GTPase by stimulating the hydrolysis of GTP to GDP. Finally, GDIs sequester Rho GTPases to the cytosol by solubilizing them, which prevents their localization to the plasma membrane and impairs signalling (588).

The most extensively studied small Rho GTPases are Rac1, CDC42 and RhoA. These are conserved and found in plants, fungi and animals (589). Seminal studies of cells migrating on 2D

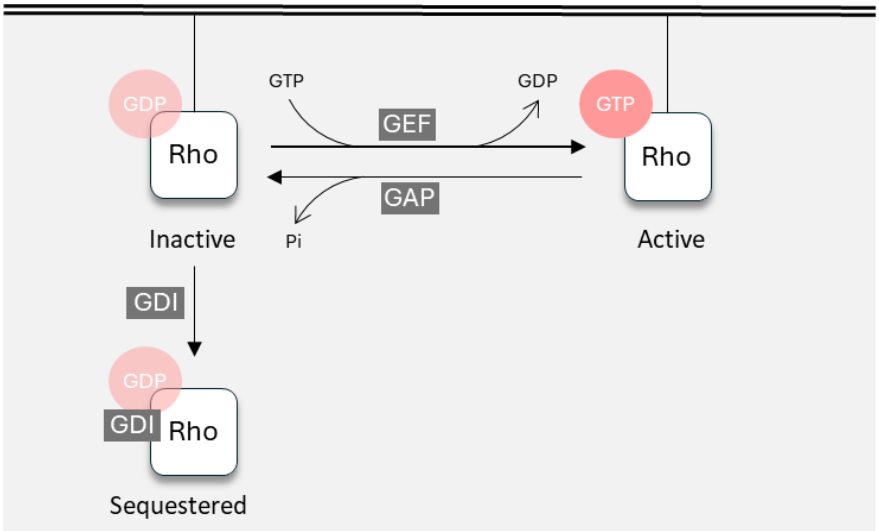


**Figure 18: The regulation of small Rho GTPases**. Small Rho GTPases are active at cellular membranes (double black line), where they function as signal transducers. A guanine nucleotide exchange factor (GEF) exchanges GDP for GTP, thereby bringing Rho into its GTP-bound, active state. A GTPase-activating protein (GAP) hydrolyses the Rho-bound GTP, thereby cleaving off a phosphate group (Pi) and bringing Rho to its GDP-bound, inactive state. A guanine nucleotide dissociation inhibitor (GDI) extracts GDP-bound Rho from the membrane and sequesters it to the cytosol, thereby preventing Rho GTPases from being activated.

substrates established Rac1 signalling to be responsible for generating lamellipodia (590), RhoA to be linked to contractile actomyosin fibres (548), and CDC42 to promote filopodia formation (591). The following decades of study unveiled a series of downstream effectors for Rac1, RhoA and CDC42 and, most importantly, their crosstalk to generate actin polymerization and actomyosin contractility during cell migration (Figure 19).

Rac1 involvement in lamellipodia formation is characterized by its ability to bind the WAVE Regulatory Complex (WRC). This leads to a conformational change that exposes the VCA motif, now free to bind and activate Arp2/3, promoting branched actin assembly and consequent lamellipodial extension (592,593). Rac1 activity also translates into a negative feedback loop controlling RhoA activation levels: increased reactive oxygen species (ROS) mediated by NOX downstream of Rac1 will increase the affinity of p190RhoGAP to GTP-bound RhoA and hydrolyze the GTP, leading to a decrease in RhoA activation levels (594). In opposition to Rac1, RhoA promotes linear actin polymerization and actomyosin contractility. It does so by binding and activating the formins mDia, which will elongate linear actin filaments,

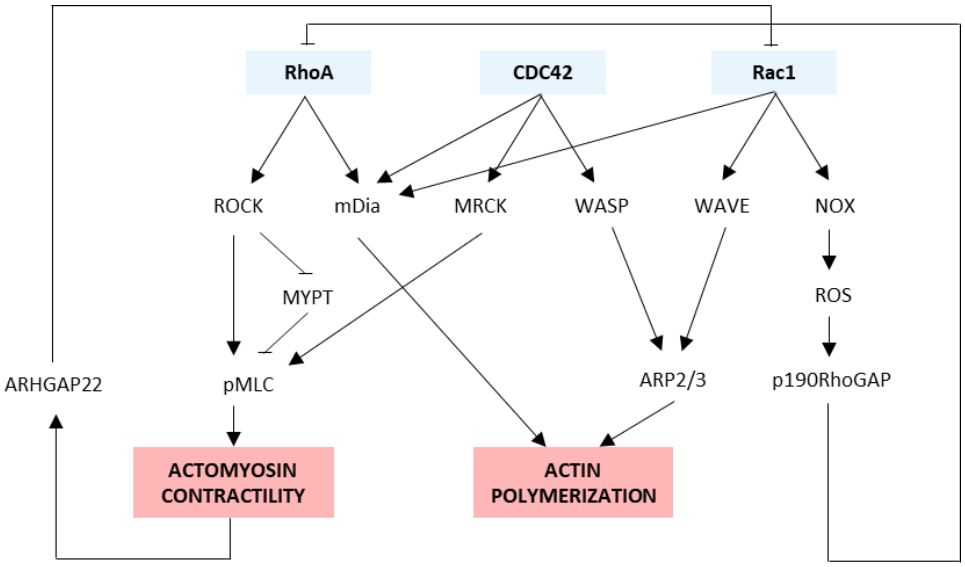


**Figure 19: Crosstalk between classical small Rho GTPases regulates the actin cytoskeleton remodelling and contraction during cell migration**. RhoA promotes actomyosin contractility through ROCK-dependent phosphorylation of MLC and inhibition of the MLC phosphatase MYPT. Another RhoA effector is the formin mDia, which promotes actin polymerization. RhoA antagonizes Rac1 signalling through ROCK/contractility-dependent activation of the Rac1 GAP ARHGAP22. Rac1 promotes actin polymerization and lamellipodia formation through activation of WAVE. Rac1 also antagonizes RhoA-mediated signalling through the activation of NOX-dependent ROS production, which activates p190RhoGAP, leading to the inhibition of RhoA. CDC42 connects with both Rac1 and RhoA, promoting actomyosin contractility through activation of MRCK, which directly phosphorylates MLC and also inactivates MYPT, besides inducing filopodia formation via WASP-mediated activation of Arp2/3.

and also by activating its downstream effectors ROCK1/2, whose activity increases NMII phosphorylation levels (described in section 4.2)(527,595). The elevated actomyosin tension that derives from activating RhoA was shown to cause FilGAP, a member of the ARGHGAP22 protein family, to dissociate from the actin filaments (596) and relocate to the plasma membrane, where it binds and inactivates Rac1 (597,598).

Similarly to RhoA, CDC42 is also responsible for enhanced actin polymerization and increased actomyosin contractility, but it does so through different downstream effectors. CDC42 can activate Arp2/3 and promote branched actin polymerization by activating its effector WASP (599). Moreover, CDC42 can cooperate with RhoA in increasing actomyosin contractility by activating a different set of NMII kinases, the MRCK (also described in section 4.2.2).

Therefore, the inter-connected and varied functions of the small Rho GTPases reaffirm their role in regulating the actin cytoskeleton and actomyosin contractility.

### 4.5. Single-cell migration modes

The betterment and continuously growing use of 3D cell culture enabled the characterization of two distinct single-cell migration modes, mesenchymal and amoeboid. It is important to note that although they require different contractility levels, both depend on the actin cytoskeleton to generate the forces needed for migration. As discussed in section 4.2, these are pushing and pulling forces from actin polymerization and actomyosin contraction. Therefore, the actin cytoskeleton integrates signals from the physical (rigidity, confinement, homogeneity) and chemical (ligands, gradient) characteristics of the environment to drive either mesenchymal or amoeboid migration.

#### 4.5.1. Mesenchymal

Mesenchymal migration involves the repetitive process of extending and attaching the front of the cell, followed by the detachment and retraction of the cell's rear (600,601). These activities depend on pushing and pulling forces created by the actin cytoskeleton. The first relies on protrusive actin filaments at the leading edge, which are involved in forming the main types of cell protrusions related to mesenchymal migration: lamellipodia and filopodia (602). In turn, NMII associates with long actin filament bundles, forming actomyosin cables that, upon the right stimuli, contract and generate the pulling forces necessary to translocate the cell body (603). These bundles, referred to as stress fibres, were described in section 4.2.1 of this document. For these reasons, mesenchymal migration is intimately associated with the opposing activity of the small Rho GTPases Rac1 and RhoA since Rac1 is needed at the leading edge to stimulate lamellipodia extension. At the same time, RhoA is required at the cell’s rear to promote actomyosin contractility along the stress fibres and mediate cell body retraction (Figure 20).

Another hallmark feature of mesenchymal migration is the adhesion to the substrate, which helps convert the protrusive and contractile forces into traction. For cells migrating on an ECM, the adhesion is usually mediated by receptors of the integrin protein family (604,605) In contrast, cells migrating over other cells usually rely on cadherin receptors for cell-cell adhesion (606,607). In both cases, the receptors' intracellular portion is associated with the actin cytoskeleton (606), usually with the tip of stress fibres, forming a focal adhesion (507,608).

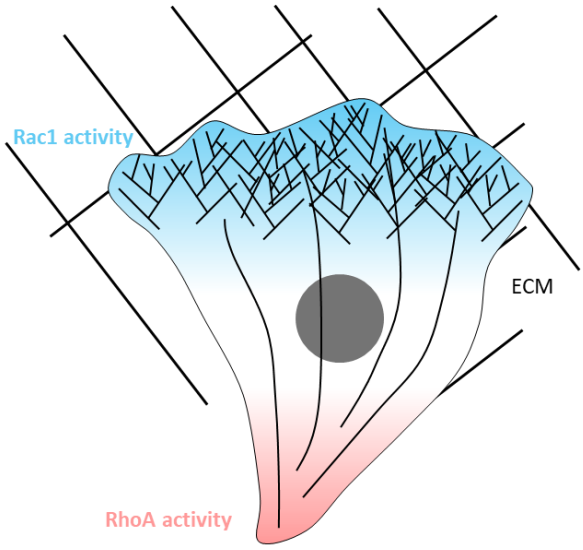


**Figure 20: Mesenchymal migration.** The small GTPases Rac1 and RhoA - the best-studied family representatives in mammals - ultimately control mesenchymal migration. While Rac1 activity dominates at the leading edge (blue) and leads to the formation of a lamellipodium at the leading edge, RhoA signalling (pink) is enhanced toward the cell rear and controls tail detachment and retraction. The actin cytoskeleton is represented by black solid lines.

Besides serving as anchor points, focal adhesions are also useful signalling hubs. For instance, focal adhesion formation stimulates Rac1 activation, thus functioning as a positive feedback site for protrusion-based migration (609,610). Conversely, lack of adhesion has been described to inhibit lamellipodia extension (462). Moreover, direct contact with the substrate allows cells to follow specific physical environmental cues. For example, in addition to a chemoattractant gradient (chemotaxis)(611), mesenchymal migration *in vivo* can be guided by adhesiveness (haptotaxis)(612) or substrate stiffness (durotaxis)(613,614).

Most data describing the mechanisms behind mesenchymal migration come from studies of cells on 2D substrates *in vitro*. These mechanisms are well conserved in 3D ECMs, with the additional discovery of the critical role played by metalloproteinases (MMPs). When produced and secreted by migratory cells, these proteins can break down extracellular matrix barriers and modify their composition, interfering with cell adhesion and modulating migration(615). Therefore, the hallmarks of mesenchymal migration include the formation of actin-rich protrusions at the leading edge of the cell, strong adhesion to the substrate, strong dependence on

MMP-mediated substrate modification, and low actomyosin contractibility requirement, usually paired up with an elongated cell shape.

### 4.5.2. Amoeboid

Amoeboid migration was named after the free-living organism amoebae due to inherent similarities with how they move. However, this type of migration is also observed in eukaryotic cells, such as embryonic PGCs (573) and tumour cells (616). In opposition to mesenchymal motility, amoeboid migration is defined by a high dependency on actomyosin contractility rather than actin polymerization to generate intracellular forces and translocate the cell forward. It is also referred to as bleb-based migration, as membrane blebs are the cell protrusion most often associated with this type of migration. Additionally, bleb-based migration does not rely on MMP secretion or adhesions to the substrate. This absence of substrate adhesion can be advantageous since it allows cells to migrate inside an ECM to which they do not express specific receptors.

The enhanced actomyosin contractility required for amoeboid migration is promoted by the small GTPase RhoA (562,616–618). Through its downstream effectors mDia1 and ROCK1/2, RhoA promotes cortical actomyosin formation and activation, a process described in detail in section 4.4 of this document. Besides giving the amoeboid cell its usual round morphology (619), this tension is essential for the initial separation of the plasma membrane from the underlying actin cortex, the event that marks the first stage of the bleb life cycle (567,573,620). RhoA activation is also required to contract the expanded bleb back into the cell body (577). Therefore, increased cortical tension leads to increased blebbing activity, which explains why high RhoA activity and blebbing are hallmarks of amoeboid migration (Figure 21). CDC42 and its effector MRCK have recently been implicated in maintaining high actomyosin contractility in amoeboid migratory cancer cells (616,621).

While the mechanism of how lamellipodia promote cell body translocation is well described, we still do not know how membrane blebs contribute to cell locomotion. Nonetheless, several models have been created to try and explain how blebbing cells can generate traction force and move forward without adhesion to the substrate (622). For instance, it has been proposed that cells extend blebs through the membrane pores, using it as a pivoting point or proceeding to squeeze themselves through it (623,624). This mechanism also helps explain why amoeboid motility does not depend on the expression and secretion of MMPs. This simple,

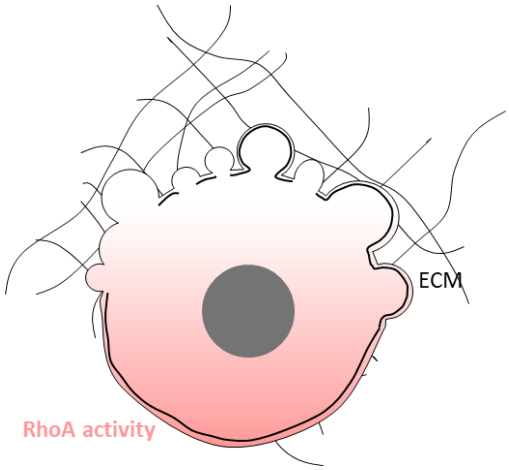


**Figure 21: Amoeboid migration**. The small GTPase RhoA controls amoeboid migration. RhoA signalling (pink) guides cortical actin synthesis (black solid lines) and NMII activity, rising cortical tension and cellular hydrostatic pressure. As a result, membrane blebs are extended and mediate the translocation of the cell body forward.

gliding migration mode enables cells to achieve high speeds inside 3D substrates: 2μm/min for A375m2 melanoma cells (616) or an impressive 25 μm/min for lymphocytes inside collagen gels (625). For reference, the speed range reported for mesenchymal cells is 0.1-0.5 μm/min (626).

Alternatively, the possibility that membrane bleb elaboration could exert lateral forces on the substrate was also proposed, and that, coupled with the extension of additional protrusions at the leading edge, could amount to forward cell movement (462,561,627). However, bleb extension would not necessarily be required to create lateral forces. This ultimately opened the question of whether blebs are required for migration or a byproduct of the inherent higher cortical contractility observed during migration. To further investigate this question, Tozluoğlu and colleagues (628) used mathematical models to assess the significance of different protrusion types in various substrates. Initially, they confirmed that actin polymerization-driven protrusions or membrane blebs could aid migration inside a continuous confined environment by modelling cells migrating between two planar sheets. Surprisingly, they found that the bleb-based migration inside a discontinuous confining environment - which models for a collagen mesh ECM - would be more effective for generating traction and promoting translocation. Thus, cell migration dependent solely on membrane blebbing is possible - and even advantageous - in specific environments.

Asymmetry is a prerequisite for cell movement and, therefore, needs to be established at some level (629). In fact, Keller and Bebie described the bleb formation site to determine the direction of movement (630). Therefore, cells must have different mechanisms to bias bleb formation to the leading edge. Since bleb formation often happens at sites where the link between the cell cortex and the membrane is weak, it was hypothesized that the cell would accumulate membrane linker protein to the rear end to bias bleb formation at the front (631,632). As expected, elevated levels of Ezrin were observed at the rear end of migratory cancer cells (633) and PGCs (632). However, some cells, such as the melanoma lineage A375, do not seem to limit bleb formation to their leading edge. Lorentzen and colleagues (634) investigated the A375 cells and identified that, even though it is not as apparent as in other cells, they do present some level of polarization. This is due to a rigid structure rich in actin, plasma membrane and Ezrin along a small portion of the membrane. The authors noticed that the placement of this region would always oppose the direction of the movement. Therefore, their model states that this rigid membrane patch prevents local bleb formation, which ultimately biases the blebbing activity towards the leading edge and functions as an intracellular compass to guide cell motility.

### 4.6. Migration plasticity

Migration plasticity refers to cells' capability to change their migration mode. The most studied type of migration plasticity is the Epithelial-to-Mesenchymal Transition (EMT). During EMT, non-migratory epithelial cells connected by cell-cell adhesions detach from each other and start migrating in a mesenchymal mode (635–637). In normal conditions, EMT occurs during embryo development or wound healing processes, for example. However, it can also be observed in pathological conditions: it is considered to be the first step in the metastasis process, where tumour cells acquire the migratory phenotype and migrate to colonize secondary tumour sites (638). EMT is a relatively lengthy process since it involves changes in gene expression and post-translational modifications (639). However, once segregated, cells may maintain the mesenchymal phenotype or transition to amoeboid migration. This different process of migration plasticity is called the Mesenchymal-to-Amoeboid Transition (MAT)(640,641).

The transition between the migration modes is usually reversible. For example, breast cancer cells that underwent EMT were found to go through a Mesenchymal-to-Epithelial Transition (MET) once they reached distant lymph nodes and developed secondary lesions

whose morphology resembled the primary tumour (642,643). Reversibility is especially characteristic of MAT and Amoeboid-to-Mesenchymal Transition (AMT) since these processes rely on protein activity regulation and happen in a relatively short time scale when compared to EMT (644,645).

Once the cell has started migrating, it is believed that MAT and AMT are demonstrations of the plasticity that aids in adapting to different environments and conditions, whether the cell in question is from a healthy embryo or a tumour. Cells face an immense diversity of environmental conditions, and efficient migration depends on their ability to adapt to these conditions. Additionally, migration plasticity also helps tumour cells to escape medical treatment. In fact, initial promising cancer treatments, such as small molecules that inhibit the activity of MMPs, were found extensively ineffective. This is because they only block mesenchymal migration and induce a MAT, and the tumour cells can still disseminate (554).

As discussed previously, different small Rho GTPases control the mesenchymal and amoeboid modes of migration. Briefly, amoeboid motility depends on high actomyosin contractility, mainly driven by RhoA activity, while cells migrating mesenchimally present high levels of Rac1 activity that, in turn, drives the actin polymerization responsible for lamellipodia formation. Therefore, a slight shift in the RhoA/Rac1 activity balance can lead to changes in actin polymerization and actomyosin contractility. These are two main mechanisms described to induce a transition in migration modes, along with changes in the connectivity between the membrane and the underlying actin cortex (554). Numerous environmental triggers for MAT/AMT exert their effects through one of these three mechanisms (569,616,644,646–648).

So far, different experimental outcomes support this concept. Initially, the experiments targeted the activity of the Rho GTPases or their direct downstream effectors. For example, it was shown that blebbing cells treated with the ROCK inhibitor Y27632 or the NMII inhibitor blebbistatin fail to elaborate membrane blebs further and start migrating with an elongated shape and mesenchymal manner (616,649). Small interference RNA (siRNA) was also applied to reduce RhoA, ROCK1 or ROCK2 expression in the typically amoeboid A375 melanoma cell line that also assumed a mesenchymal phenotype (569,616,650). As GAPs and GEFs control the activity of Rho GTPases, their role in promoting AMT/MAT was also investigated. For example, silencing the Rac1 inactivator GAP ARHGAP22 in the same A375 amoeboid cell line caused

them to assume a mesenchymal phenotype that was characterized by decreased actomyosin contractility levels, evidenced by lower MLC phosphorylation (569).

Besides RhoA and Rac1, CDC42 was also shown to regulate migration plasticity. The seminal work published by Wilkinson and colleagues (649) indicates that CDC42 can activate the NMII kinase MRCK, which cooperates with ROCK1/2 in increasing actomyosin contractility. The authors showed that stimulation of the CDC42/MRCK pathway in the usually elongated and mesenchymal BE colorectal carcinoma cell line leads to a MAT, where the cells showed improved invasion after assuming a round morphology and starting to elaborate membrane blebs. Additionally, similar results were observed when RhoA/ROCK1/2 was activated in the same cell line. These results suggest that different groups of NMII kinases can contribute to maintaining actomyosin contractility during amoeboid migration. Treating amoeboid A375 cells with high doses of the NMII inhibitor blebbistatin completely impaired cell blebbing and motility (649). Conversely, lower doses only partially inhibited NMII, leading the cells to assume an elongated shape and undergo an AMT. These results, in turn, lead to the conclusion that while amoeboid migration relies on high actomyosin contractility, it is required for mesenchymal motility, even if at lower levels. The authors propose that inhibiting ROCK activity to stop cancer cell migration would be ineffective, as the cells could still rely on MRCK to generate actomyosin contractility and support mesenchymal migration, aiding the spread of cancer.

This same principle was applied years later when researchers proposed the creation of a new cancer treatment category: migrastatics (651). A migrastatic is defined as an inhibitor – or a set of inhibitors – capable of inhibiting both mesenchymal and amoeboid cancer cell migration, as they would ultimately impair the cancer cell's ability to invade other tissues and spread the disease. Good candidate targets for migrastatic drugs are proteins involved in promoting actomyosin contractility, like ROCK1/2 and MRCK. This drug would inhibit actomyosin contractility, which, as discussed, is necessary for all migration modes.

## 5. Rationale, hypothesis, and objectives

Cumulus layer expansion is a process that encompasses extensive extracellular matrix production and secretion, which is accompanied by cumulus cell displacement away from the oocyte. These processes are crucial for releasing the fertilizable oocyte, which is enclosed inside

the cumulus matrix that also contains the dispersed cumulus cells. This configuration enables the prompt transfer of the ovulated complex to the fertilization site, where both the cumulus cells and cumulus matrix aid in guiding the sperm to the ovulated oocyte. Therefore, cumulus layer expansion is an essential process for female fertility. However, while some studies suggest cumulus cell displacement could be an active migration process, the mechanism behind this displacement is still elusive. Therefore, it was hypothesized that **cumulus cell displacement during expansion requires active migration, which depends on an extensive actin cytoskeleton rearrangement that mediates the extension of actin-related cellular protrusions and is powered by Non-muscle Myosin II**. The following objectives will test this hypothesis.

**Objective 1**: To investigate cumulus matrix production, cumulus cell displacement, detachment, and cytoskeletal rearrangement during cumulus layer expansion (Chapter 3).

**Objective 2**: To determine if cumulus cell displacement during cumulus layer expansion depends on the same cellular mechanisms that control cancer cell migration inside soft 3D extracellular matrices (Chapter 4).

*Chapter 2:*

# Material and Methods

## 1. Animals

This study was performed using CD-1 mice obtained from Charles River (St-Constant, QC). All experiments were executed in compliance with the regulations and policies of the Canadian Council on Animal Care and were approved by the Animal Care Committee of the Research Institute of the McGill University Health Centre (RI-MUHC, protocol 7783).

## 2. Cumulus-Oocyte Complexes collection

To study the morphological and molecular events unfolding during the process of cumulus layer expansion, 19-day-old mice were injected peritoneally with 5 IU of equine chorionic gonadotropin (eCG, Sigma), hereafter termed *primed mice*. Forty-four hours later, ovaries were harvested and dissected in pre-warmed HEPES-buffered αMEM (Thermo Scientific, 11900024). Ovaries were then transferred to a 35 mm petri dish containing 2 ml of pre-warmed HEPES-buffered αMEM supplemented with CNP (100 nM, Sigma N8768) to prevent oocyte meiotic resumption. Large antral follicles were punctured with an insulin needle, and COCs with numerous layers of cumulus cells around the oocyte were transferred to a new dish containing clean and pre-warmed HEPES-buffered αMEM, also supplemented with CNP. Depending on the experiment, the primed mice were injected with 5 IU of human chorionic gonadotropin (hCG) to trigger cumulus expansion *in vivo* instead of being submitted to ovary harvest. Ovaries were then harvested, and the expanding COCs were collected similarly. Five to ten female mice were used for each experimental replicate.

## 3. *In vitro* cumulus layer expansion

After collection, the selected COCs were washed twice in pre-warmed bicarbonate-buffered αMEM and then incubated for 8h in Expansion Media at 37°C in an atmosphere of 5% $CO_2$/95% air. The Expansion Media was composed of bicarbonate-buffered αMEM supplemented with recombinant human EGF (10 ng/ml, BD Biosciences 354052) to trigger cumulus layer expansion and FBS (1%, Gibco A3840001) to supply the serum components required for proper cumulus matrix assembly. Depending on the experiment, the Expansion Media was also supplemented with components listed in Table 1.

| | Final concentration | Manufacturer | Catalog number |
|---|---|---|---|
| **AG1478** | 1 µM | Selleck | S2728 |
| **SB431542** | 1 µM | Tocris | 1614 |
| **U0126** | 25 µM | Sigma | U120 |
| **Calpain Inhibitor I** | 5, 50 µM | Millipore | 11086090001 |
| **Rho activator II** | 0.25, 1 µg/ml | Cytoskeleton | CN03 |
| **Para-amino Blebbistatin** | 10, 50, 100 µM | Cayman Chemical | 22699 |
| **Y27632** | 1, 10, 50 µM | Tocris | 1254 |
| **BDP9066** | 1, 10, 50 µM | MCE | HY-111424 |

**Table 1: List of additional Expansion Media components.**

### 3.1. Live imaging

Alternatively, COCs were also submitted to live imaging during expansion. In these cases, the COCs were washed twice in pre-warmed bicarbonate-buffered αMEM and then initially incubated in Live Imaging Expansion Media at 37°C and a 5% $CO_2$ atmosphere. The Live Imaging Expansion Media was composed of bicarbonate-buffered αMEM supplemented with recombinant human EGF (10 ng/ml, BD Biosciences 354052), FBS (1%, Gibco A3840001), Ascorbic Acid (30 mM, Sigma V-038), and HEPES (20 mM, Sigma H3784) to guarantee a stable pH throughout the experiment. After the initial culture, the dish containing the COCs in Live Imaging Expansion Media was transferred to a Spinning Disk microscope (Zeiss) equipped with an incubator and temperature control system so samples could be maintained at 37°C and an atmosphere of 5% $CO_2$/95% air. Brightfield images of the samples were then obtained every 5 minutes, spawning different tiles and Z positions. The timelapses obtained were analyzed using the Zen Lite Software (Zeiss) version 3.9. Only COCs that were not in contact with other COCs throughout the whole live imaging period were selected for COC area quantification. That is because pictures containing the expanding COC and the surrounding area were exported and used to measure the COC area with ImageJ. The images were transformed into 8-bit grayscale, and a threshold value was chosen for each COC, so the background was excluded. Next, the area covered by the pixels with a grayscale value above the background was measured for each picture, and the data was compiled in a graph using GraphPad Prism 10.1.0.

## 4. Brightfield imaging and analysis

Immediately before and after incubation, the COCs of each experimental group were imaged with a brightfield microscope (Leica DMi6000). The images were later used to quantify the area covered by each COC at different time points and conditions. The quantification was carried out with ImageJ, as shown in Figure 22.

a)

b)

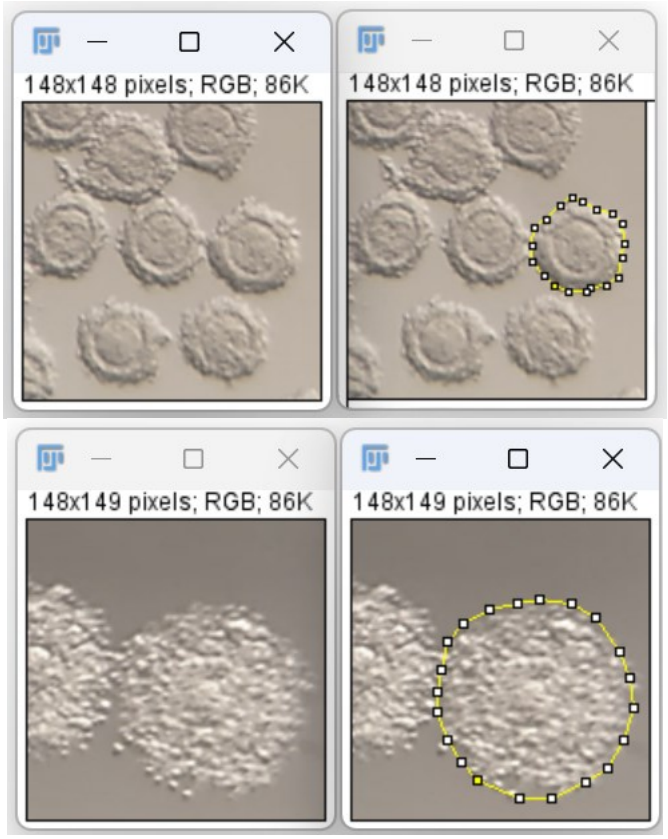


**Figure 22: Cumulus-Oocyte Complexes area quantification**. The left panels show a section of a brightfield image taken from freshly collected COCs (a) and *in vitro* expanded COCs (b), and right panels show an example of how the 'polygon selections' tool from ImageJ was used to obtain the area covered by each COC.

After quantification, the average COC area obtained for the COCs at the start of the experiment (freshly collected, 0h time point) was used to normalize the measurements obtained for the COCs in the other experimental groups and time points from the same replicate. Therefore, the normalized values for each replicate were used for the statistical comparison.

## 5. Gene expression analysis

In this work, gene expression analysis was carried out at the mRNA level by Quantitative Real-time PCR (qPCR) and at the protein level by Immunofluorescence of wholemount samples or Western Blot analyses.

### 5.1. Quantitative Real-time PCR

To assess gene expression by qPCR, COCs were collected, cultured, and then submitted to RNA extraction, reverse transcription and quantitative real-time PCR. The PicoPure RNA isolation kit (Applied Biosystems) was used according to the manufacturer's instructions. Briefly, the samples were pelleted in Eppendorf tubes, and after removing the supernatant, 40 µl of the lysis buffer was added to each tube. The tubes were incubated at 42°C for 30 minutes, and then moved to a -80°C freezer until further processing. Once all the replicates for a given experiment were collected, the samples were thawed in ice. Forty µl of ethanol 70% was added to each sample to precipitate the nucleic acid molecules, and the mixture was then transferred to a microcolumn. After brief centrifugation, the microcolumns were washed with Wash Buffer 1 and treated with DNAse I (Qiagen) at room temperature for 15 minutes to remove the genomic DNA. Following an additional wash step with Wash Buffer 1, the microcolumns were also washed with Wash Buffer 2 and centrifuged at maximum speed to eliminate buffer traces. Finally, 11 µl of the Elution buffer was pipetted onto the microcolumns that were transferred to new tubes and submitted to a final centrifugation to collect the RNA solution.

According to the manufacturer's instructions, the SuperScript IV Reverse Transcription kit (Thermo Fisher, 18091050) was employed for the reverse transcription step. Briefly, 1 µl of a random hexamers solution (50 µM) and 1 µl of dNTP mix (10 mM) were added to each tube containing the eluted RNA. The mixture was incubated at 65°C for 5 minutes and then kept on ice for an additional one. Each cDNA synthesis reaction was completed by adding 4 µl of the SuperScript IV RT Buffer (5x), 1 µl of DTT solution (100 mM), 1 µl of RNAseOUT, and 1 µl of the SuperScript IV Reverse Transcriptase solution (200 U/µl). Next, they were incubated at 23°C for 10 minutes to allow the random hexamers to anneal to the RNA molecules, at 55°C for another 10 minutes so the Reverse Transcriptase can synthesize the cDNA, and final 10 minutes at 80°C to inactivate the reaction.

The primers used in the qPCR reactions were designed with the Primer Blast tool (NCBI). The primers were preferentially targeted to an exon/exon junction to reduce the chances of amplifying remaining genomic DNA. For internal control, the expression of *Rpl19* and *Atpb5* was used to normalize for the amount of total cDNA per sample. Table 2 contains the sequences of the primers used in this work and their target genes.

| | **Forward primer (5' → 3')** | **Reverse Primer (5' → 3')** |
|---|---|---|
| ***Has2*** | GGCCGGTCGTCTCAAATTCA | ACAATGCATCTTGTTCAGCTCC |
| ***Tnfaip6*** | GATGGCCAAGGGTAGAGTCG | ACACTCCTTTGCATGTGGGT |
| ***Ptx3*** | CTGCCCGCAGGTTGTGAA | TGGTCTCACAGGATGCACG |
| ***Ptgs2*** | AGCCAGGCAGCAAATCCTT | CAGTCCGGGTACAGTCACAC |
| ***Rpl19*** | TCAGGCTACAGAAGAGGCTTGC | ATCAGCCCATCCTTGATCAGC |
| ***Atpb5*** | GAGGTCTTCACGGGTCACAT | CCCACCATGTAGAAGGCTTG |

**Table 2: List of Forward and Reverse Primers used in this study.**

The SsoAdvanced Universal SYBR Green qPCR Master Mix (2x) (Bio-Rad, 1725271) was used for the qPCR reactions according to the manufacturer's guidelines. Each reaction contained 10 µl of the qPCR Master Mix (2x), 5 µl of premixed Forward and Reverse primers (250 µM each) and 5 µl of cDNA solution diluted 1:10. Cycling conditions were set as follows: Activation step at 95°C for 30 seconds and then 40 cycles of amplification (15 seconds at 95°C for DNA denaturation, 60 seconds at 60°C for primer annealing and extension) in an LC480 II LightCycler (Roche). Fold changes were calculated using the $2^{-\Delta\Delta Ct}$ method (652).

### 5.2. Immunofluorescence

Cultured or recently collected COCs were fixed in freshly prepared Fixative Solution (2% (w/v) paraformaldehyde (Fisher Scientific 04042) in phosphate-buffered saline (PBS, pH 7.2) containing 0.1% Triton X-100 (ACROS 9002-93-1)) for 15 minutes at room temperature. Next, samples were washed in Blocking Buffer (BB: 3% Bovine Serum Albumin (Sigma) in PBS containing 0.1% Triton X-100) three times for 15 minutes each and finally incubated in 400 µl of BB as the blocking step at 4°C overnight. The following day, the samples were transferred to a primary antibody solution (Table 3) in BB and incubated overnight at 4°C.

| | Stock concentration | Dilution | Host species | Manufacturer | Catalog number |
|---|---|---|---|---|---|
| **Anti-phosphorylated Myosin Light Chain (Ser19/Thr18) (pMLC)** | 20 µg/ml | 1:100 | Rabbit | Cell Signalling | 3674 |

**Table 3: Primary antibody used for immunofluorescence analyses**.

The following day samples were washed three times in BB for 15 minutes each and then transferred to a secondary antibody solution (Table 4) in BB that also contained DAPI (Roche 10236276001) and Alexa Fluor 555-conjugated Phalloidin (Thermo Fisher, A34055) at room temperature and protected from light. After an hour, samples were washed three times with BB for 15 minutes each, also protected from light.

| | Stock concentration | Dilution | Host species | Manufacturer | Catalog number |
|---|---|---|---|---|---|
| **Anti-Rabbit Alexa 488** | 2 mg/ml | 1:100 | Goat | Thermo Fisher | A-11008 |

**Table 4: Secondary antibody used for immunofluorescence analyses**.

After washing, samples were rinsed in PBS and incubated for 30 minutes in a 1:1 solution of Vectashield (Vector Laboratories, H-1900) in PBS. The samples were then mounted in 0.5 µl of Vectashield on a 35 mm glass bottom dish and examined at the RI-MUHC Imaging Core Facility with an LSM 880 confocal microscope (Zeiss, Toronto, ON).

### 5.2.1. TZP quantification

The F-actin immunofluorescence images obtained after using the Alexa 555-conjugated Phalloidin evidenced the Transzonal Projections (TZPs) and were, therefore, used for their quantification. To do so, the images were opened in ImageJ (National Institutes of Health, NIH)(653), and a segmented circle was created around the oocyte circumference in the middle of the zona pellucida. The fluorescence intensity at each point on the line was obtained and only kept if it was above the background value, set to match the oocyte cytoplasm. Each remaining fluorescent point whose value was higher than each of its immediately neighbouring points was counted as a TZP. The total number of TZPs counted by this method does not represent the total number of TZPs in a given COC, but was considered as the TZP number associated with it.

### 5.2.2. Membrane blebbing and Cell Elongation Index quantification

Immunofluorescence staining is also useful to assess cell morphology and cell protrusions. Therefore, the Phalloidin staining of the F-actin cytoskeleton was first used to analyze and quantify the percentage of blebbing cells per COC. Using ImageJ (National Institutes of Health, NIH)(653), the channel containing the Phalloidin staining was split into four quadrants. Zooming in into each quadrant, each cell on the image was assessed and characterized as either *i*) blebbing, defined by the presence of at least one membrane bleb, *ii*) non-blebbing, defined as a smooth actin cortex devoid of membrane blebs, and *iii*) out of the focal plane, defined as the cell whose nucleus was not sectioned by the focal plane chosen, as exemplified in Figure 23.

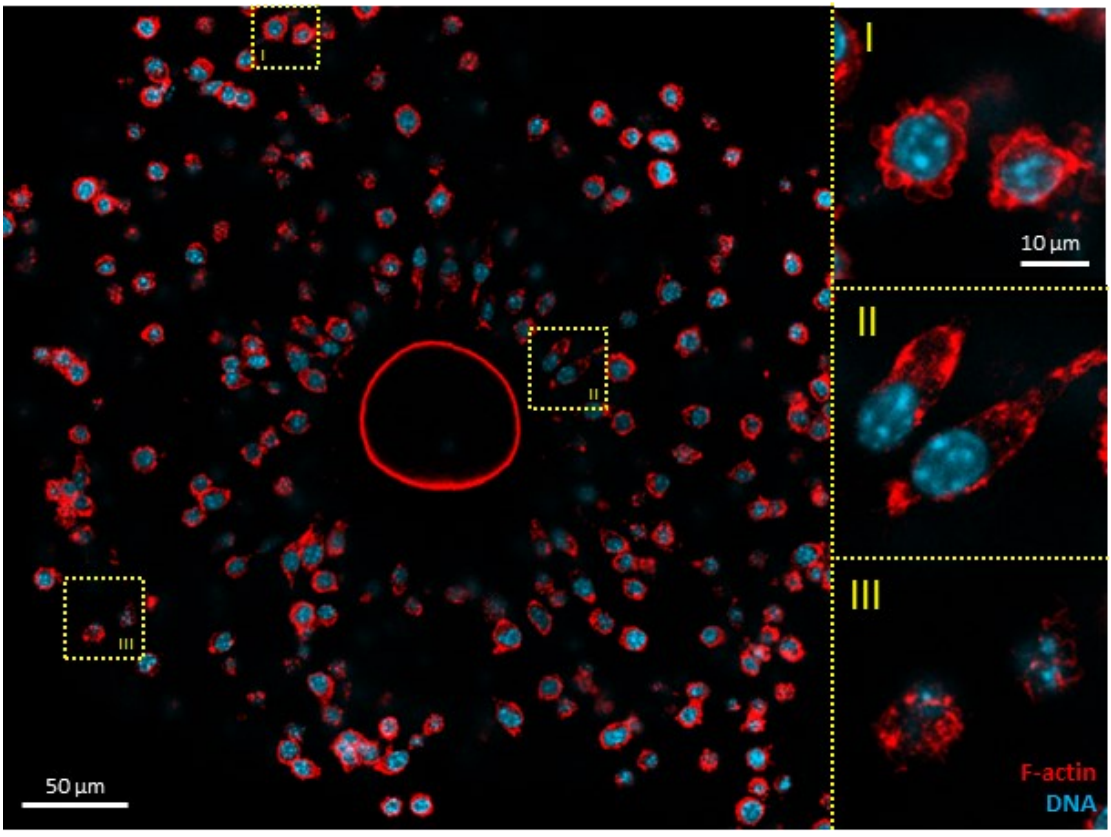


**Figure 23: Membrane blebbing quantification**. Example of an *in vitro* expanded COC and cumulus cells classified as I) blebbing, II) non-blebbing and III) out of the focal plane. F-actin is shown in red and DNA in blue.

At the end of the quantification process, the numbers obtained for each quadrant were compiled, and an overall percentage of blebbing cells for each COC was calculated following the formula: $Percentage\ of\ blebbing\ cells = \frac{blebbing\ cells}{blebbing\ cells + non{-}blebbing\ cells}\ x\ 100.$

The F-actin staining was also used to calculate a morphological descriptor, the Cell Elongation Index (CEI). The CEI is defined as the ratio between the cell's length and width. As an EI of 1 represents a perfect circle, values between 0 and 2 describe a round cell, while values above 2 refer to an elongated one. As illustrated in Figure 24, the length of the cumulus cells was measured along the radial axis of the COC, and the width was measured along the nucleus, perpendicular to the length.

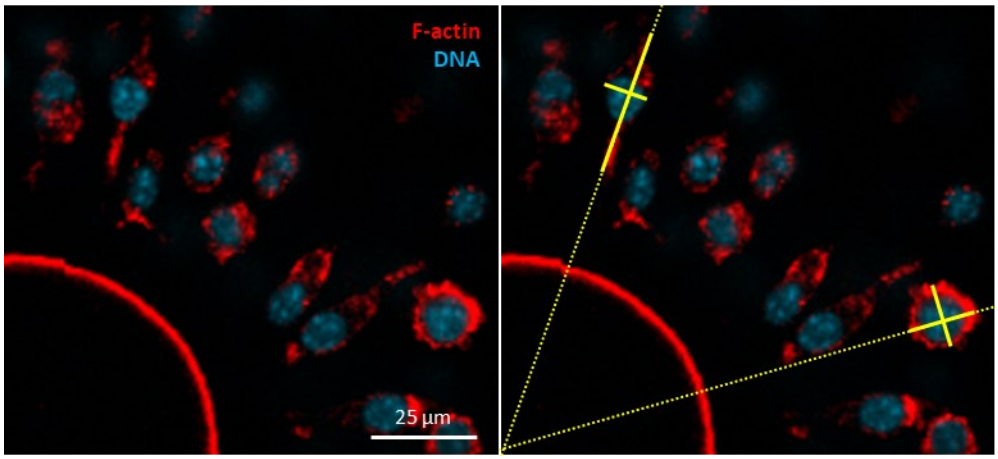


**Figure 24: Cell Elongation Index measurement.** The length of cumulus cells was measured along the oocyte radial axis, and the width was obtained by tracing a line perpendicular to it, at the height of the cell nucleus. The EI is calculated by the ratio between length and width.

### 5.2.3. pMLC foci number quantification

The mean number of pMLC foci per cumulus cell in a given COC was quantified using ImageJ. First, since NMII is active during cytokinesis and pMLC staining can be visualized at the base of the first polar body as it is extruded (Figure 25a), the oocyte was selected and cropped out of every image. Next, to eliminate background noise, the images were converted to 8-bit grayscale, which gives each image pixel a gray value between 0 and 255 based on the intensity of the fluorescence signal. The threshold for the green channel was set to 40 (Figure 25b), which means that any pixel with a gray value lower than 40 was not considered for the

analysis, only the ones above 40. Then, the "Analyze particles" tool was used to count the number of pMLC foci in each image, respecting the previously set threshold. This value was normalized by the number of cumulus cells in each picture, which was calculated by counting the number of nuclei in each blue channel (Figure 25b). Within each replicate, the pMLC foci per cell value for a COC was normalized by the mean value obtained for the COCs from the 0h experimental group. This normalization generated a "Relative pMLC foci per cumulus cell" metric, which was used for comparison between the experimental groups.

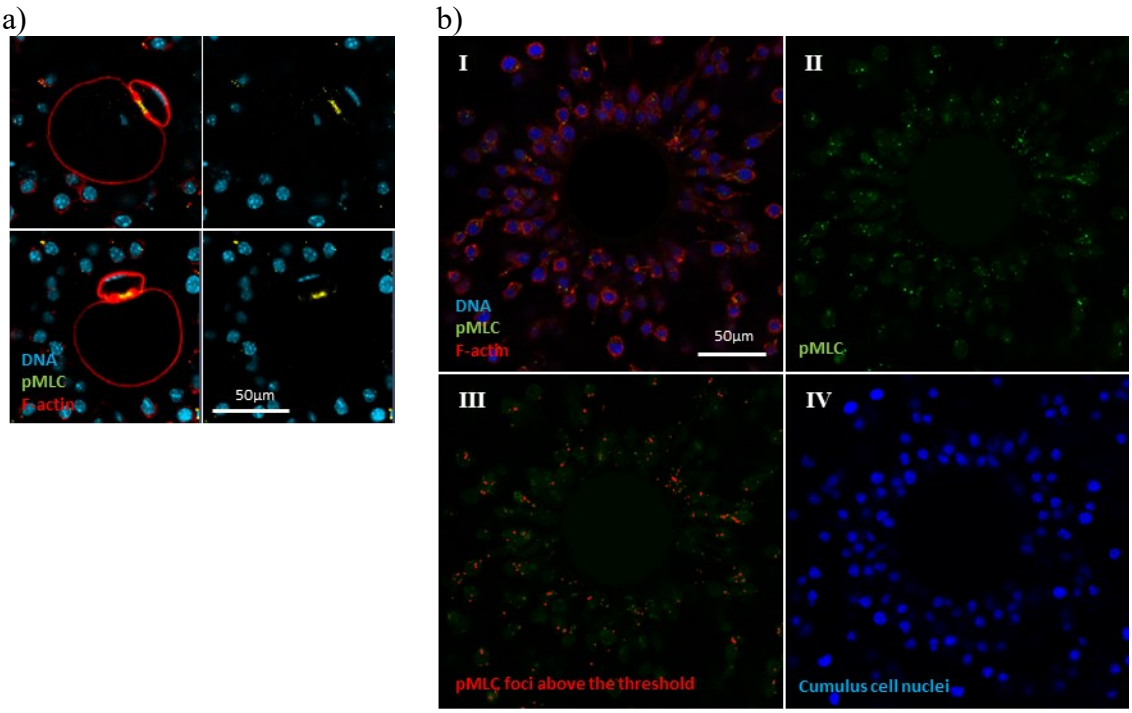


**Figure 25: Phosphorylated Myosin Light Chain staining**. Example of an in vitro expanded COC. Staining for pMLC can be observed at the base of the first polar body (a), and also along the cortex of cumulus cells (b). After cropping the oocyte (panel bI), the green channel was isolated (panel bII) and a threshold was applied (panel bIII) before using the ImageJ tool 'Analyze Particles' to measure the number of pMLC foci. This number was divided by the total number of cumulus cells in the picture, calculated by counting the number of visible cumulus cell nuclei (panel bIV). F-actin is shown in red, pMLC in green and DNA in blue.

### 5.3. Western blot

To compare protein levels in different time points and conditions, samples were separated by SDS-page electrophoresis, transferred onto a membrane, and immunodetected. To this end, COCs were collected and cultured as described in sections 2 and 3. Samples were then pelleted in Eppendorf tubes, the supernatants removed, and 20 µl of Laemmli Buffer (0.0625M Tris base, SDS 2%, β-Mercaptoethanol 5%, Bromophenol Blue 0.002%) was added. The tubes were incubated at 95°C for 5 minutes and briefly spun down to collect the liquid that accumulated on the tube walls and lid. The proteins were separated in precast 4-15% polyacrylamide gels (Bio-Rad, 4568081). The electrophoresis was performed at 120V for 2 hours, and proteins were transferred to a PVDF membrane using a wet transfer system for 1 hour.

After transfer, the membranes were trimmed, washed with PBS-Tween (PBST: Tween 20 0.01% in PBS) and blocked in BSA solution (5% in PBST) for 1 hour at room temperature. After blocking, the membranes were incubated overnight at 4°C with a primary antibody (Table 5) diluted in BSA (5% in PBST). The next day, the membranes were washed in PBST three times for 15 minutes each and then incubated with a secondary antibody solution in PBST (Table 6) at room temperature. After 1 hour, the membranes were washed in PBST three times, for 15 minutes each. Blots were developed using Pierce™ ECL Plus Western Blotting Substrate (Thermo Scientific, PI32134) according to the manufacturer's instructions and imaged with an Amersham Imager 600 (GE Healthcare Life Sciences). The resulting images were analyzed using ImageJ.

| | **Stock concentration** | **Dilution** | **Host species** | **Manufacturer** | **Catalog number** |
|---|---|---|---|---|---|
| **Anti-total SMAD2/3** | 72 µg/ml | 1:1000 | Rabbit | Cell Signalling | 8685T |
| **Anti-pSMAD3** | 0.576 mg/ml | 1:1000 | Rabbit | Abcam | ab52903 |
| **Anti-pSMAD2** | 120 µg/ml | 1:200 | Rabbit | Sigma | ZRB04953 |

**Table 5: List of primary antibodies used for Western Blot analyses**.

| | Stock concentration | Dilution | Host species | Manufacturer | Catalog number |
|---|---|---|---|---|---|
| **Anti-Rabbit HRP-conjugated** | 1 mg/ml | 1:5000 | Goat | Fisher Scientific | PR-W4011 |

**Table 6: HRP-conjugated secondary antibody used for Western Blot analyses**.

## 6. Transwell Migration Assay

The Transwell Migration Assay is widely used to assess cell migration when faced with a chemoattractant gradient of, for example, chemokines or growth factors. To this end, two medium-filled chambers divided by a porous membrane are used to create a gradient of the tested chemoattractant (Figure 26). The chemoattractant is diluted in the bottom chamber, and the cells are seeded at the top. Following incubation, cells can be detected on the underside of the membrane if they acquire a migratory phenotype in response to the chemoattractant gradient.

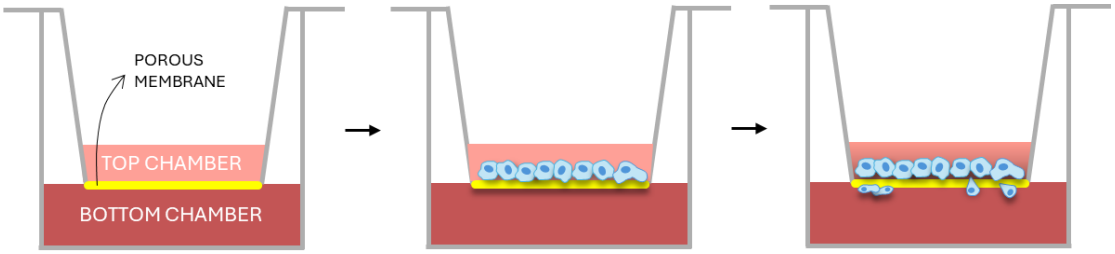


**Figure 26: Transwell Migration Assay**. A cell culture insert with a porous membrane (highlighted in yellow) is inserted into a well in a 24-well culture plate. The top chamber is filled with plain culture medium, while the bottom chamber is filled with culture medium containing a chemoattractant. Cells are seeded in the top chamber. If they respond to the chemoattractant gradient by acquiring a migratory trait, they will be detected on the underside of the membrane after incubation.

Here, this assay was adapted to assess if the cumulus cells *i*) acquire a migratory phenotype in response to an EGF gradient and *ii*) if this migration requires NMII activity. Thus, COCs were collected and submitted to a pre-assay incubation of 4 hours before being thoroughly washed and transferred to the top of the standing cell culture inserts (12 µm pore size, Millipore, PIXP01250). Each insert containing 20 COCs was placed in a well of 24-well culture plates that were then incubated overnight at 37°C and 5% $CO_2$ atmosphere.

The basal culture media for all groups was bicarbonate-buffered αMEM supplemented with FBS (1%) to supply the expanding COCs with the serum components needed for cumulus matrix assembly and to ensure that different groups are submitted to similar culture conditions. Table 7 summarizes the complete media composition for the different experimental groups. Briefly, to account for random cumulus cell migration that was not stimulated by the EGF gradient, the COCs in the negative control (CNP experimental group) were only exposed to the basal culture media supplemented with CNP during the pre-assay incubation and in the top and bottom chambers. On the other hand, the COCs in the positive control (EGF experimental group) were cultured in basal media supplemented with EGF during the pre-assay incubation to trigger cumulus layer expansion, then washed to eliminate EGF traces and placed in plain basal media in the top chamber. The bottom chamber contained basal media with EGF, the chemoattractant. In the further experimental groups, the setting was the same except for the addition of the molecular inhibitors targeting NMII and its activators. Therefore, the pre-assay incubation media contained EGF and a molecular inhibitor either targeting NMII (PAB), ROCK1/2 (Y27632), MRCK (BDP9066) or both ROCK1/2 and MRCK (Y27632 and BDP9066). Similarly, the molecular inhibitor was also added to the top and bottom chamber media for these groups to sustain the inhibition throughout the experiment.

After the overnight incubation, cotton swabs were used to scrape the cells remaining at the top of the inserts, and the membranes were fixed in 1 ml of chilled methanol for 5 minutes. Following fixing, the inserts were moved to a well containing 1 ml of crystal violet solution (2% in 20% methanol solution in distilled water) for staining at room temperature. After 5 minutes, the inserts were moved to a clean well and washed three times in distilled water for 15 minutes each. Finally, the membranes were removed from the inserts, mounted on slides and imaged with a brightfield microscope (Leica DMi6000).

| Experimental Group | Pre-assay incubation | Top chamber | Bottom chamber |
|---|---|---|---|
| **CNP** | CNP | CNP | CNP |
| **EGF** | EGF | - | EGF |
| **EGF+PAB** | EGF + PAB | PAB | EGF + PAB |
| **EGF+Y27** | EGF + Y27632 | Y27632 | EGF + Y27632 |
| **EGF+BDP** | EGF + BDP9066 | BDP9066 | EGF + BDP9066 |
| **EGF+Y27+BDP** | EGF + Y27632 + BDP9066 | Y27632 + BDP9066 | EGF + Y27632 + BDP9066 |

**Table 7: Media composition for pre-assay incubation, top and bottom chambers in the Transwell Migration assay**. Basal culture media was bicarbonate-buffered αMEM supplemented with FBS (1%). The additional components were added at the following concentration: CNP (100 nM), human recombinant EGF (10ng/ml), PAB (100 μM), Y27632 (50 μM), and BDP9066 (50 μM).

### 6.1. Transwell Migration assay quantification

Transwell Migration assays performed after seeding a cell suspension on the top chamber usually present a homogenous cell distribution on the underside of the membrane in case they acquire the migratory phenotype in the presence of the chemoattractant. Thus, the quantification of the cells' migratory behaviour can be done by measuring the area covered by stained cells on three or five random brightfield pictures taken from the underside of the membrane. In this work, however, the placement of 20 COCs on the top chamber prevents a homogeneous distribution of cumulus cells on the underside of the membrane. Therefore, the quantification of this assay was carried out based on 12 individual 5x brightfield pictures taken so they cover almost the whole area of the membrane, as illustrated in Figure 27.

To measure the area covered by the crystal violet-stained cumulus cells, the brightfield images were first submitted to a colour deconvolution process. In diagnostic brightfield microscopy, this technique is used to decompose RGB images of multiple stained biological samples into different images that show individual stains. This is possible when the RGB composition of a specific stain is known. Petrachi and colleagues (654) used a similar approach to analyze crystal violet stains using Ruifrok and Johnston's colour deconvolution algorithm,

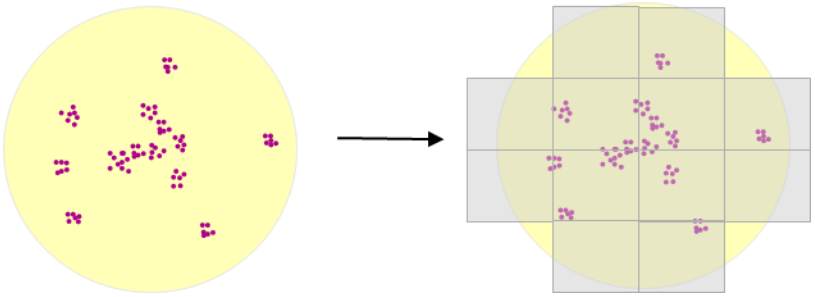

**Figure 27: Transwell Migration Assay membrane imaging**. The left diagram showcases the membrane after it has been fixed and stained. The violet dots indicate the clusters of cumulus cells that have migrated to the bottom chamber. On the right, the membrane is overlapped with an image grid consisting of 12 fields of view, which was used to capture images of all the membranes from all the replicates.

which describes crystal violet RGB composition to be 0.5 Red, 0.55 Green and 0.65 Blue. Therefore, these parameters were applied to decompose the brightfield images obtained and isolate the crystal violet staining, as shown in Figure 28. The area covered by the stained cells was measured in square micrometres, and each replicate was normalized to their respective Positive Control mean value to generate the 'Relative Migration Index' metric.

a) b)

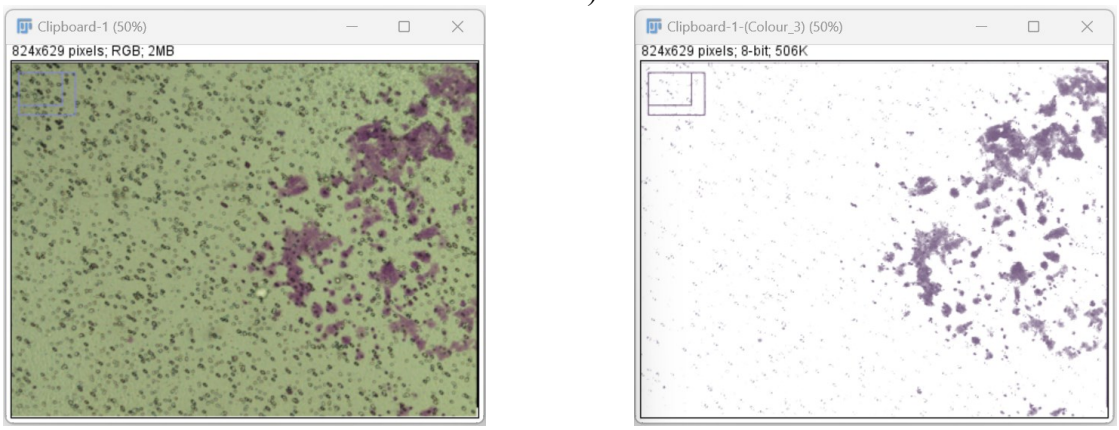


**Figure 28: Transwell Migration Assay quantification**. Sample brightfield picture from a Transwell Migration Assay run (a) was submitted to a colour deconvolution to isolate the crystal violet staining (b). The area covered by the crystal violet staining was quantified to make up the Migration Index.

## 7. Sperm Penetration Assay

The sperm penetration assay was used to analyze the ability of capacitated sperm to penetrate the cumulus layer of COCs that were expanded under different conditions. To this end, COCs were collected and cultured in expansion media, as described in sections 2 and 3. Approximately 6 hours into the COC culture, epididymides of two 5-week-old male mice were collected in pre-warmed bicarbonate-buffered αMEM medium. Each epididymis was dissected and had its content squeezed into a 300 µl drop of pre-warmed Capacitation Medium (bicarbonate-buffered αMEM supplemented with 0.9% BSA) and incubated at 37°C. After 1h, the drops were checked under the microscope, and the ones that contained capacitated sperm were selected for the experiment. Thirty µl of a HOECHST solution (0.01 mg/ml) was added to each drop, and the plates were incubated at 37°C for an additional 10 minutes. During this incubation, the COCs were removed from the culture and washed in pre-warmed IVF media (bicarbonate-buffered αMEM supplemented with 0.4% BSA) three times to eliminate traces of FBS and molecular inhibitors.

For the assay, groups of 15 COCs for each experimental group were placed in 50 µl drops of pre-warmed IVF medium under mineral oil. Ten µl of capacitated sperm was added to each drop, and the plates were placed back in the incubator for an hour. At the end of this incubation step, the COCs were fixed in freshly prepared Fixative Solution, washed three times for 15 minutes in Blocking Buffer, stained with Alexa Fluor 555-conjugated Phalloidin and mounted as described in section 5.2. The dishes were imaged using an LSM780 Confocal microscope (Zeiss), and detailed Z-stacks containing brightfield images, as well as the blue and red channels, were captured for each COC (Figure 29).

### 7.1. Sperm penetration assay quantification

The ability of capacitated sperm to penetrate the cumulus layer was defined as the number of sperm that reached the zona pellucida. For this quantification, the red (Alexa Fluor 555-conjugated Phalloidin) and blue (HOECHST) channels of the Z-stacks obtained for each COC were compiled into Maximal intensity projections. A circle with a diameter 15% bigger than the oocyte was traced on the maximal intensity projection of the red channel (Figure 30a, b). This circle was then transferred to the maximal intensity projection of the blue channel (Figure 30c). The sperm located inside the circle were considered successful in the goal of reaching the zona.

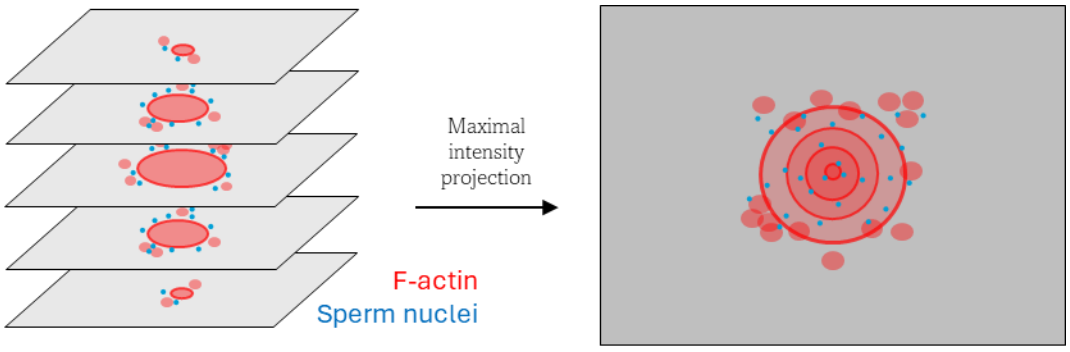


**Figure 29: Sperm Penetration Assay imaging**. COCs submitted to the Sperm Penetration Assay were stained with Alexa Fluor 555-conjugated Phalloidin. At confocal, detailed Z-stacks were taken of each COC (left panel), and the stacks were used to obtain maximal intensity projections of the red and blue channels to obtain the files used for quantification.

They were, therefore, counted to obtain the "Number of penetrating sperm" metric. The values obtained for each experimental group were normalized by the mean of the positive control group (where the COCs were expanded in the presence of EGF and FBS only, control conditions), giving rise to the "Relative number of penetrating sperm".

a) b) c)

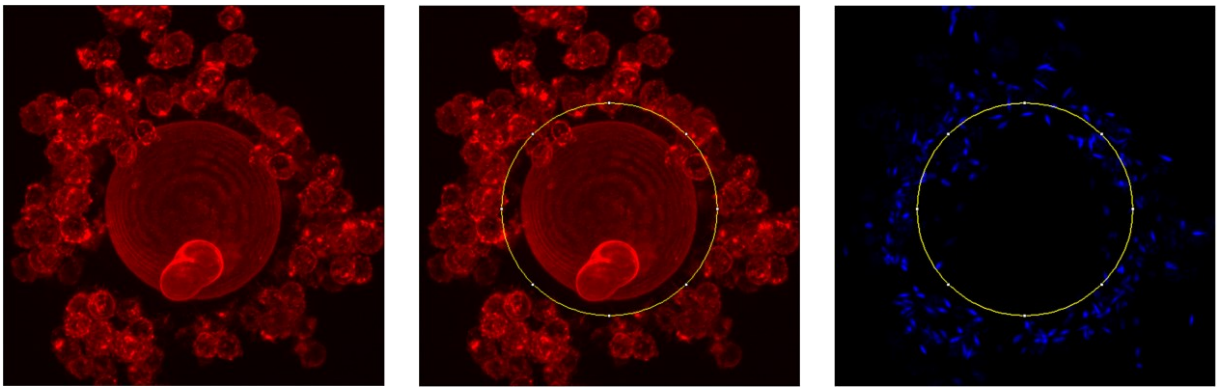

**Figure 30: Sperm penetration assay quantification**. A Maximal Intensity Projection was obtained from a sample Z-stack from the positive control group. The red channel Maximal Intensity Projection was used as a reference to trace a circle with a diameter 15% bigger than the oocyte's (b). This circle was transferred to the blue channel Maximal Intensity Projection, and the sperm located inside it were considered successful in penetrating the cumulus layer and reaching the zona pellucida.

## 8. Statistical analyses

The experiments were repeated a minimum of three times, and the values are expressed as mean ± the standard error of the mean (SEM). The quantitative data obtained were analyzed using one-way ANOVA followed by Tukey's Honest Significance Difference post-hoc test using GraphPad Prism 10.1.0. Differences were considered statistically significant when $P < 0.05$ and are denoted by different letters on the graphs.

*Chapter 3*:

# Cumulus matrix production, cumulus cell detachment, cytoskeletal rearrangement, and displacement during cumulus layer expansion

## 1. Sustained cumulus matrix gene expression depends on oocyte-secreted factors, not EGF signalling.

Cumulus layer expansion has been described to depend on oocyte-secreted factors and gonadotropin signalling, which triggers the production of EGF-like factors that propagate the gonadotropin stimulation effects inside the follicle. Therefore, to start investigating the relative roles of EGF-like and oocyte-derived factors in cumulus matrix production, COCs were initially collected and exposed to recombinant EGF *in vitro* to trigger expansion. At different time points, a subpopulation of COCs was processed to assess the transcriptional activation of the genes related to producing the cumulus matrix.

The transcriptional activity of all four genes analyzed – *Has2*, *Tnfaip6*, *Ptx3* and *Ptgs2* – rapidly increased during the first 3 hours of culture (Figure 31). Over the next 3 hours, however, the mRNA quantity either started to decrease, as observed for *Has2*, *Tnfaip6* and *Ptgs2* or remained constant as per the data regarding *Ptx3* expression levels. Moreover, during the last 3 hours of culture in the presence of EGF, the mRNA levels of the assessed genes declined. This pattern of sharp initial increase during the first hours of expansion followed by a steady decline over the following hours has been observed before (310,341,397).

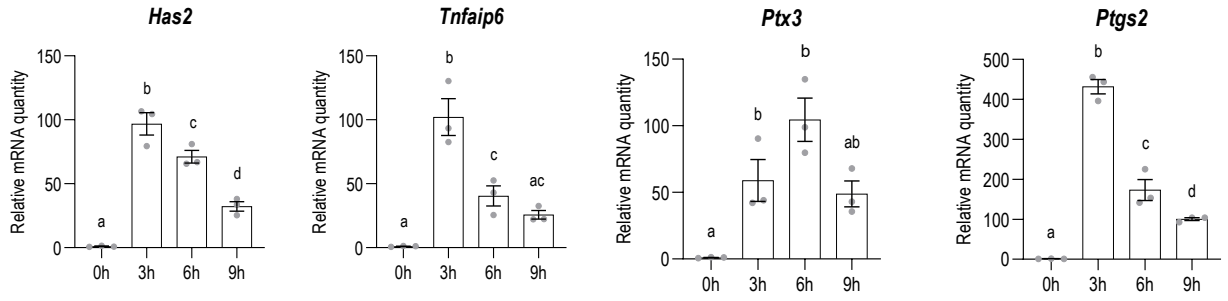


**Figure 31: EGF exposure triggers the transcriptional activation of the cumulus matrix-related genes *Has2*, *Tnfaip6*, *Ptx3*, and *Ptgs2* during cumulus layer expansion**. COCs were collected from primed mice and incubated with recombinant EGF for 9h. At 0, 3, or 6h after initial exposure to EGF, samples were collected for quantitative PCR analysis to assess mRNA quantity of cumulus matrix-related genes *Has2*, *Tnfaip6*, *Ptx3* and *Ptgs2*.

These results suggest a more intense production of the cumulus matrix during the first 3 hours of cumulus layer expansion. Two simple theories could justify the observed subsequent drop in the steady-state levels of transcripts. First, assuming synthesis stays relatively constant, a shift in transcript degradation could explain the drop in total mRNA quantity. Alternatively, a drop in the synthesis rate, assuming degradation stays relatively constant, could also account for the data obtained. Even though both scenarios are possible, the nature of the experiment performed does not permit such distinction to be made.

Since oocyte-secreted factors signal through ALK4/5/7 receptors to promote cumulus matrix production, we assessed their role in maintaining cumulus matrix-related gene expression throughout expansion. To this end, COCs were cultured with EGF and SB431542, a small molecule that competes for the ATP binding site and inhibits ALK4/5/7 activity (655). The inhibitor was added to the media 0, 3 or 6 hours after the start of the culture, and at the end of 9 hours, all samples were processed and submitted to qPCR analysis.

The inhibitor addition from the start of the culture (Figure 32, SB431452 0-9h group) completely prevented the upregulation of *Has2*, *Ptx3* and *Ptgs2* that was observed in the No inhibitor group. Moreover, the transcripts for *Has2* and *Ptx3* were virtually absent at 9 h, whether the ALK4/5/7 blocker was added at 3 or 6 hours after the start of the culture. Similarly, the mRNA quantity for *Ptgs2* was severely reduced. These results confirm the role of oocyte-driven TGFβ signalling in triggering cumulus matrix-related gene expression. Additionally, they also indicate that ALK4/5/7 activity is needed throughout the process to maintain this gene expression.

Next, we evaluated the role of EGFR signalling in cumulus matrix production throughout expansion. To this end, COCs were cultured with EGF and 0, 3 or 6 hours into the culture, the small molecule AG1478 was added to the media. AG1478 binds EGFR and blocks its tyrosine kinase activity, preventing its autophosphorylation and activation (656). After a total of 9 hours of culture, the samples were collected and submitted to qPCR analysis.

The COCs cultured in the presence of the inhibitor for 9h (Figure 33, AG1478 0-9h group) did not undergo transcriptional activation of the cumulus matrix-related genes observed in the No inhibitor group. Surprisingly, adding the EGFR blocker 3 or 6 hours into the start of the culture did not have a strong effect as the one observed when the ALK4/5/7 blocker was used and only partially prevented the accumulation of transcripts compared to the No inhibitor group.

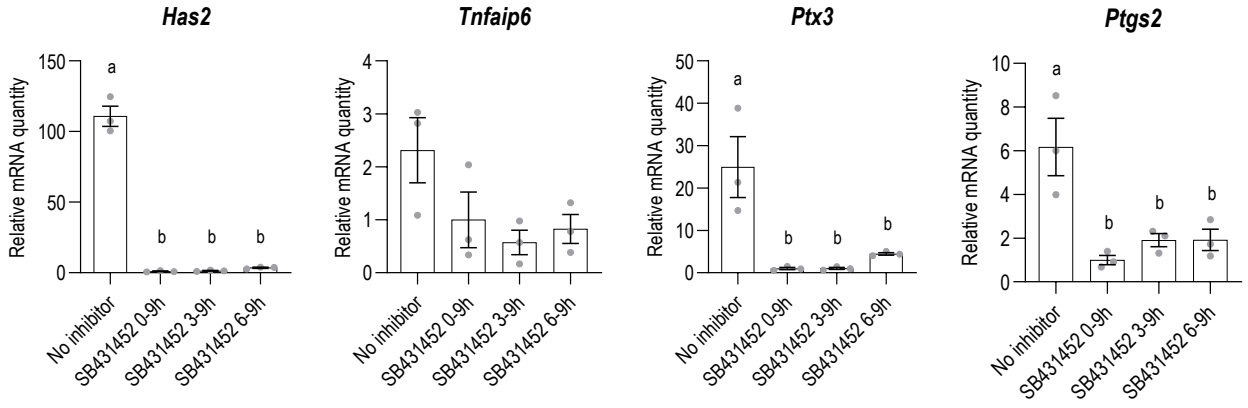


**Figure 32: Inhibiting ALK4/5/7 at different times after initial EGF exposure prevents the transcriptional activity of cumulus matrix-related genes**. COCs were collected from primed mice and incubated with recombinant EGF for 9h. At 0, 3, or 6h after initial EGF exposure, the ALK4/5/7 molecular inhibitor SB431452 was added to the culture medium at a final concentration of 1 µM, and samples were harvested at the end of 9h for quantitative PCR analysis to assess mRNA quantity of cumulus matrix-related genes *Has2*, *Tnfaip6*, *Ptx3* and *Ptgs2*.

Although these experiments measure steady-state mRNA levels and do not distinguish between mRNA synthesis and degradation, they suggest differential regulation of cumulus-matrix production by EGFR and oocyte-secreted factors. The results obtained suggest that once EGF triggers cumulus layer expansion and induces matrix-related gene expression alongside oocyte-secreted factors, the TGFβ signalling promoted by the oocyte is the primary pathway responsible for maintaining their expression throughout the process.

## 2. EGF exposure triggers cumulus cell displacement and the extension of actin-related cell protrusions.

Cumulus layer expansion is a process during which the cumulus cells produce and secrete copious amounts of an HA-rich extracellular matrix, which is accompanied by cumulus cell displacement away from the oocyte. However, how cumulus cells get displaced away from the oocyte over time is still unknown. To investigate this, COCs were collected, cultured with EGF and live imaged. Starting 1.5h into the culture, a brightfield picture was taken every 5 minutes until 8.5h of culture was completed. The images were then used to measure the area covered by

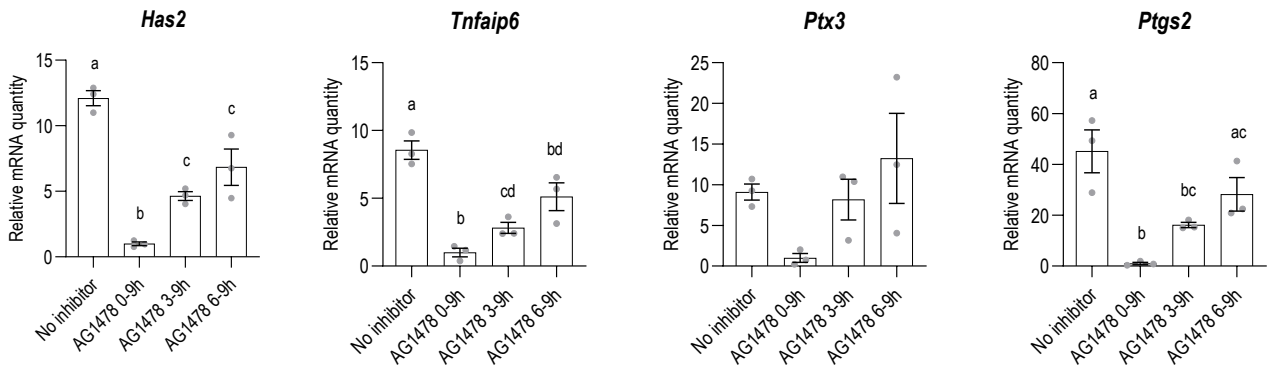


**Figure 33: Inhibiting EGFR at different times after initial EGF exposure partially prevents transcriptional activity of cumulus matrix-related genes**. COCs were collected from primed mice and incubated with recombinant EGF for 9h. At 0, 3, or 6h after initial exposure to EGF, the EGFR molecular inhibitor AG1478 was added to the culture medium at a final concentration of 1 μM, and samples were harvested at the end of 9h for quantitative PCR analysis to assess mRNA quantity of cumulus matrix-related genes *Has2*, *Tnfaip6*, *Ptx3* and *Ptgs2*.

each COC to assess how much the cumulus cells had been displaced away from the oocyte at each time point (Figure 34).

This analysis yielded detailed data, according to which the COC area undergoes small cycles of brief expansion and contraction during the first 4 hours of culture (Figure 34b). After this period, the COC area increases steadily, indicating that cumulus cell displacement only takes place 4 hours after initial exposure to EGF. Therefore, we next focused on this interval.

To closely analyze cumulus cells during the last few hours of expansion, COCs were collected, incubated with EGF, and live imaged between 6.5 and 8.5h after initial EGF exposure, this time with greater magnification so cumulus cell morphology could be analyzed (Figure 35). Throughout the time analyzed, the cumulus cells maintained a round morphology and were often observed to extend membrane blebs, an actin-related cell structure that aids cell migration (511) (Figure 35a). The membrane blebbing was dynamic and seemed to stem around the cell's perimeter. Even though most of the cumulus cells elaborated membrane blebs, some were also observed to extend membrane ruffles and filopodia, additional cell structures also related to cell migration (Figure 35b). These observations, along with our knowledge surrounding actin-related

a) b)

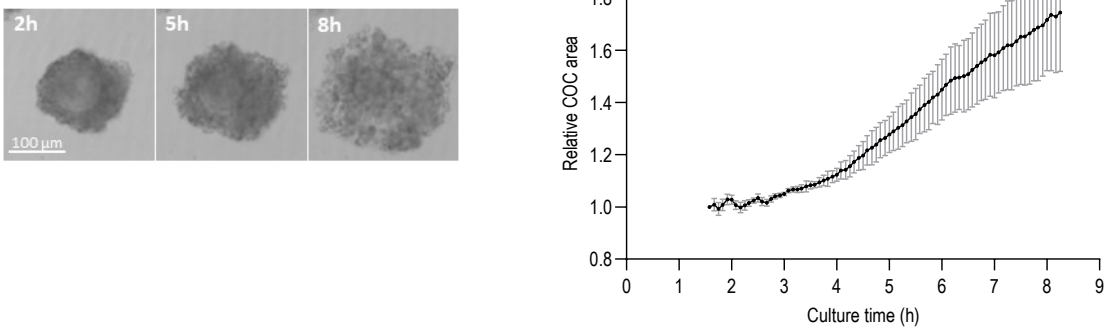


**Figure 34: EGF exposure triggers cumulus cell displacement during cumulus layer expansion**. COCs were collected from primed mice, incubated with recombinant EGF for 8.5, and live-imaged from 1.5 to 8.5h of culture. Throughout this period, a brightfield image was taken every 5 minutes and used to quantify the area covered by the COC to assess cumulus cell displacement.

cell structures like blebs, ruffles and filopodia suggest that cumulus cells undergo extensive actin cytoskeletal rearrangement during cumulus layer expansion.

## 3. LH and EGF signalling trigger cumulus cell actin cytoskeletal rearrangement.

Throughout the oocyte growth phase, the granulosa and cumulus cells elaborate thin, filopodia-like structures called Transzonal Projections (TZPs). These structures traverse the zona pellucida and establish cell contact with the growing oocyte (263). After the ovulatory stimulus, however, communication between the somatic and the germ compartments is interrupted, and the TZPs retract into the cumulus cells' cell bodies. As TZP's backbones are mainly constituted of actin, we investigated whether the timing of TZP retraction coincides with the onset of cumulus cell displacement and the extension of actin-related structures. To do so, 19-day-old female CD1 mice were primed with eCG, an FSH analog, to promote late follicle development, followed by the LH analog, hCG, to stimulate ovulation. Four and eight hours after the hCG injection, the COCs were collected, fixed, and stained with Phalloidin so TZPs could be assessed (Figure 36).

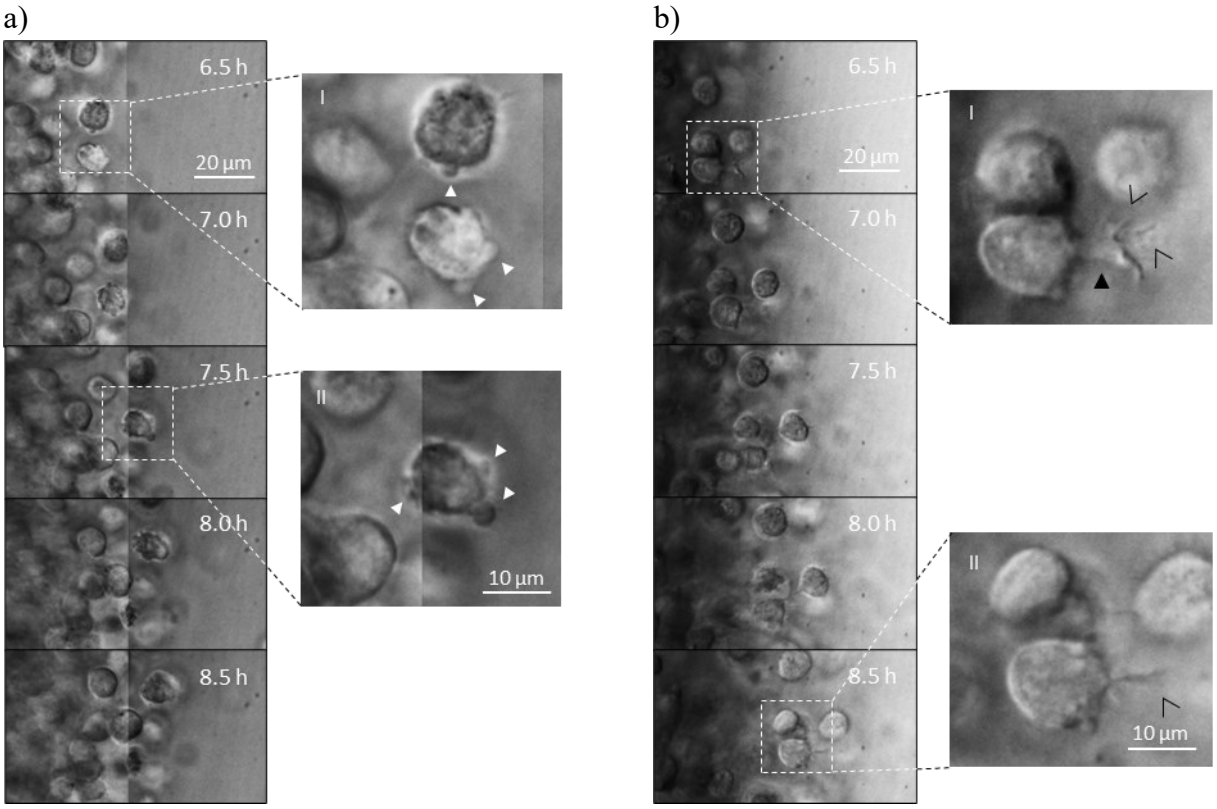


**Figure 35: EGF exposure triggers the extension of actin-related cell protrusions by the cumulus cells during cumulus layer expansion**. COCs were collected from primed mice, incubated with recombinant EGF for 8.5h, and live-imaged from 6 to 8.5h of culture. Throughout this period, a brightfield image was taken every 5 minutes and used to assess cumulus cell morphology and the presence of (a) membrane blebs and (b) membrane ruffles and filopodia during cumulus cell displacement observed in cumulus layer expansion. White arrowheads indicate membrane blebs, black arrowheads indicate membrane ruffles and black arrows indicate filopodia.

Before the hCG injection, the COCs harboured a vast TZP network connecting the cumulus cells to the oocyte (Figure 36a, b). Four hours after the injection, the number of TZPs remained stable ($1.00 \pm 0.25$ vs. $1.00 \pm 0.13$, $p \leq 0.9974$). Nonetheless, virtually no TZPs could be detected 8h after the injection ($0.004 \pm 0.007$ vs. $1.00 \pm 0.13$, $p < 0.0001$). This indicates that TZP retraction, and therefore actin cytoskeletal reorganization, occur between 4 and 8h after the ovulatory stimulus.

Cumulus cells do not express LH receptors (LHR) (386). Instead, they express EGFR and respond to EGF-like factors, the main mediators of LH signalling inside the preovulatory follicle

a) b)

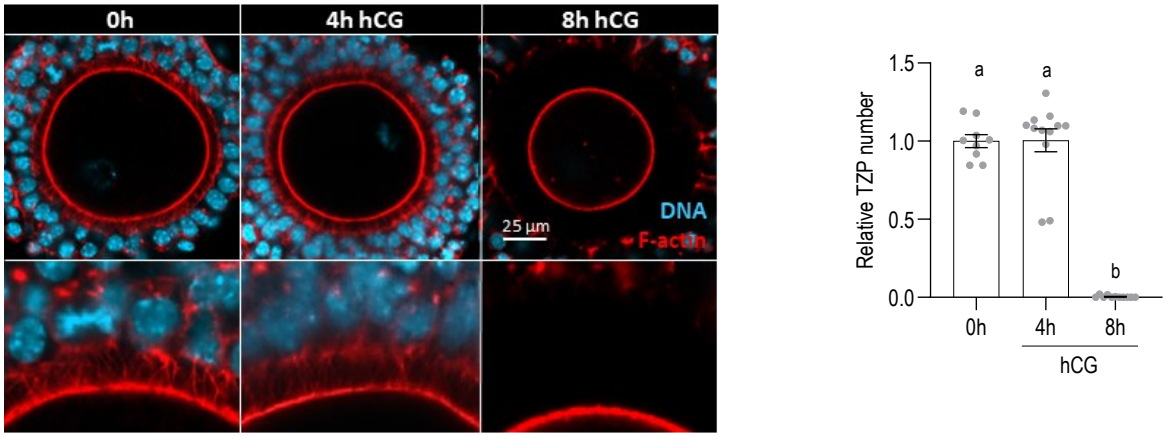


**Figure 36: The ovulatory stimulus triggers TZP retraction during cumulus layer expansion**. Forty-eight hours after being primed with eCG, mice were injected with hCG to trigger ovulation. COCs were collected at 0, 4, and 8h after the hCG injection, fixed, and (a) stained with phalloidin. The fluorescent images were used to quantify the (b) TZP number.

(276). To investigate if EGF signalling also mediates TZP retraction, COCs were collected and cultured with recombinant EGF and AG1478, an EGFR molecular inhibitor (656) (Figure 37).

The dense TZP network present in the fresh COCs was substantially decreased after 8h of culture with EGF (1.00 ± 0.19 vs. 0.14 ± 0.15, $p < 0.0001$). The COCs exposed to EGF and the EGFR blocker, however, still harboured 0.76 ± 0.23 of the initial TZP population ($p \leq 0.0002$). Therefore, TZP retraction not only temporally coincides with the appearance of actin-related and with the onset of cumulus cell displacement, but it is also controlled by EGF signalling. This indicates that LH/EGF signalling triggers a wide process of cytoskeletal rearrangement within the cumulus cells.

## 4. Branched actin is required for cumulus cell actin cytoskeletal rearrangement.

Cytoskeletal rearrangement relies on the coordinated assembly and disassembly of actin filaments on specific sites, promoting cell protrusion extension/retraction (464,468). The actin polymerization required for this process is usually controlled by the Arp2/3 complex, responsible for nucleating branched actin filaments (657). To test if Arp2/3 plays a role in the cumulus cell

a) b)

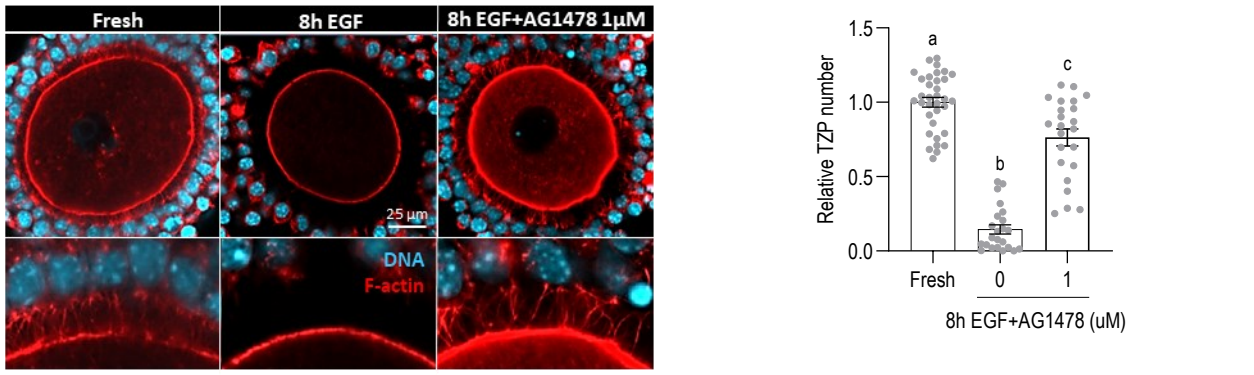


**Figure 37: EGFR signalling is required for TZP retraction during cumulus layer expansion**. COCs were collected from primed mice and incubated with recombinant EGF for 8h in the presence or absence of the EGFR molecular inhibitor AG1478 (1 µM). The COCs were fixed and stained with phalloidin (a) so the actin cytoskeletal rearrangement could be assessed by quantifying the TZP number of each COC (b).

actin cytoskeletal reorganization, COCs were then expanded in the presence of CK-666, a known and widely used Arp2/3 molecular inhibitor (658). After culture, the COCs were fixed, stained with Phalloidin, and submitted to TZP quantification to assess actin cytoskeletal reorganization (Figure 38).

a) b)

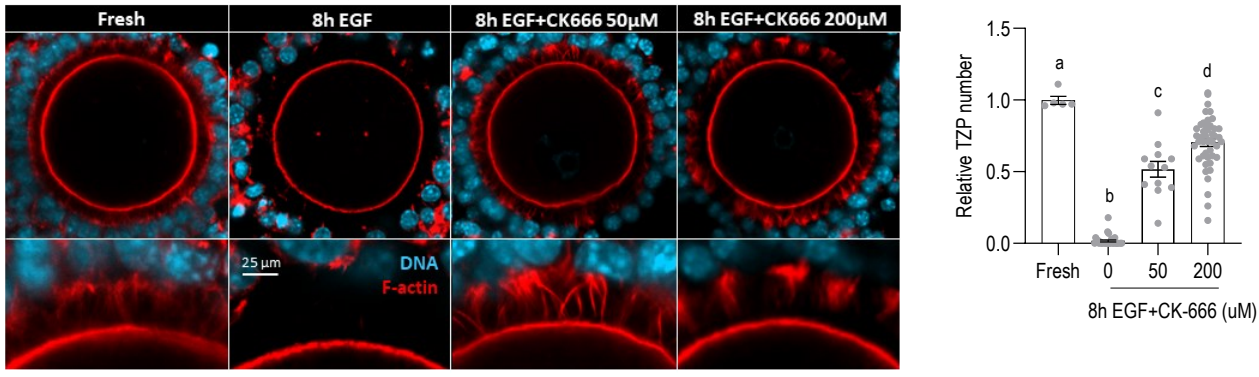


**Figure 38: Full cumulus cell actin cytoskeletal rearrangement requires Arp2/3 activity**. COCs were collected from primed mice and incubated with recombinant EGF for 8h in the presence or absence of the Arp2/3 molecular inhibitor CK-666 at a final concentration of 50 or 200 µM. The COCs were then fixed and stained with phalloidin (a) so that the actin cytoskeletal rearrangement could be assessed by quantifying the TZP number of each COC (b).

As expected, the high number of TZPs observed before culture almost completely disappeared after the 8-hour incubation with EGF (1.00 ± 0.06 vs. 0.02 ± 0.04, $p < 0.0001$). However, when the Arp2/3 blocker was added to the culture media, this loss decreased dose-dependently, reaching 0.52 ± 0.19 and 0.70 ± 0.18 at CK-666 final concentration of 50 and 200 µM, respectively ($p < 0.0001$ and $p \leq 0.0004$).

Close analysis of the immunofluorescence pictures reveals that, while the TZPs on the fresh COCs seem closely associated with the oocyte plasma membrane, the TZPs in the CK-666-treated COCs seemed slightly shortened and no longer connected to the oocyte, as illustrated in Figure 39. Additionally, the actin cortex of the cumulus cells treated with the inhibitor seemed virtually absent, apart from a few spots with high actin concentration, as evidenced by the phalloidin staining.

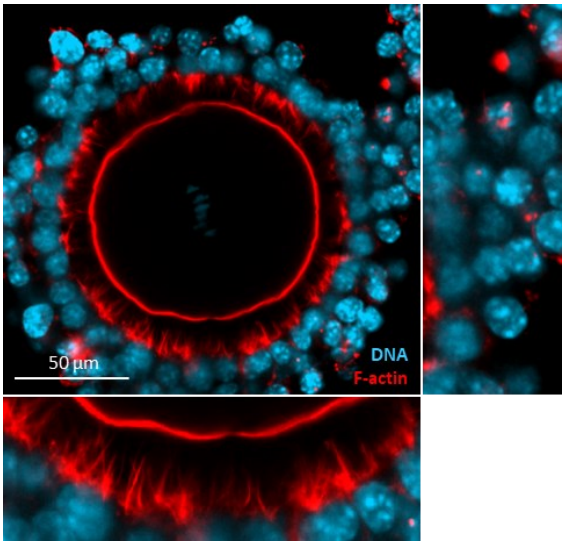


**Figure 39: Cumulus cell actin cytoskeleton after Arp2/3 inhibitor treatment.** COCs were collected from primed mice and incubated with recombinant EGF for 8h in the presence or absence of the Arp2/3 molecular inhibitor CK-666 at a final concentration of 200 µM. The COCs were then fixed and stained with phalloidin.

To verify if the phenotype observed in the Arp2/3-inhibited COCs was due to impaired cumulus matrix production, we cultured COCs with either EGF or EGF plus CK-666 at the final concentration of 200 µM. We then evaluated the mRNA levels of key genes related to cumulus matrix production. As illustrated in Figure 40, the Arp2/3 blocker addition to the culture media

did not impair the transcriptional activation of *Has2*, *Tnfaip6* or *Ptgs2*, suggesting cumulus matrix production is not dependent on Arp2/3 activity.

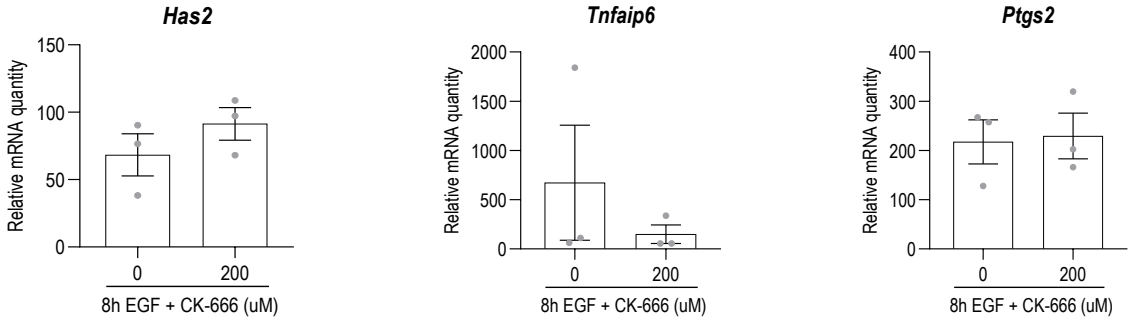


**Figure 40: Transcription of the cumulus matrix-related genes does not depend on Arp2/3 activity**. COCs were collected from primed mice and incubated with recombinant EGF for 8h in the presence or absence of the Arp2/3 molecular inhibitor CK-666 (200 μM). Samples were harvested for quantitative PCR analysis to assess the mRNA quantity of the cumulus matrix-related genes *Has2*, *Tnfaip6*, and *Ptgs2*.

## 5. Control of cumulus cell attachment is key for actin cytoskeletal rearrangement and cumulus matrix production.

The observation that TZPs did not retract but still lost connection to the oocyte plasma membrane after Arp2/3 inhibition suggested that programmed cell detachment precedes cytoskeletal rearrangement. In fact, cell detachment is considered the first step in metastasis, when cancer cells detach from the primary tumour before migrating and establishing secondary tumours in other tissues (659). That is because the cytoplasmic portion of cadherins, the proteins that mediate cell-cell attachment, are connected to the actin cytoskeleton, stabilizing it and preventing its reorganization (660).

The link between cadherins and the cytoskeleton is mediated by so-called adaptor proteins, such as talin and paxillin (661). The protease Calpain targets adaptor proteins and aids in disassembling cell-cell adhesions (662,663). Calpain is expressed in granulosa cells, and its activity has been reported to increase after hCG (442). Therefore, we reasoned that Calpain activity must be required for cumulus cells and TZP tip detachment so actin cytoskeletal rearrangement can occur. To test this hypothesis, COCs were exposed to EGF in combination

with Calpain Inhibitor I (CI-I), a small molecule that inhibits Calpain activity. COCs were then fixed and stained with phalloidin. The images obtained then were used to quantify the number of TZPs to assess the extent of the actin cytoskeletal rearrangement (Figure 41).

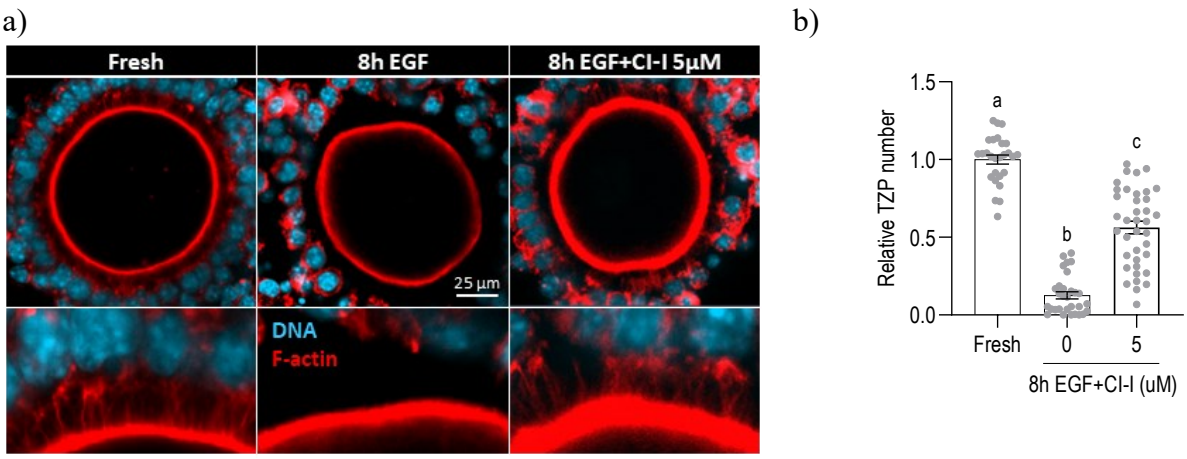


**Figure 41: Full cumulus cell actin cytoskeletal rearrangement requires Calpain activity**. COCs were collected from primed mice and incubated with recombinant EGF for 8h in the presence or absence of the Calpain molecular inhibitor CI-I (5 µM). The COCs were fixed and stained with phalloidin (a), and the actin cytoskeletal rearrangement could be assessed by quantifying the TZP number of each COC (b).

The quantification of the TZP number showed that the cumulus cells from the COCs incubated solely with EGF underwent cytoskeletal rearrangement and lost their TZPs (1.00 ± 0.15 vs. 0.13 ± 0.12, $p < 0.0001$). On the other hand, as predicted according to our hypothesis, the COCs cultured with EGF and CI-I retained most of their TZPs until the end of the culture (0.56 ± 0.25 vs. 0.13 ± 0.12, $p < 0.0001$). This result indicates that Calpain activity is required to promote cumulus cell detachment and enable actin cytoskeletal rearrangement, which is required for their displacement.

To confirm that the phenotype observed was not due to interference with cumulus matrix production, we evaluated the mRNA levels of key genes related to cumulus matrix production after culture with EGF and CI-I. As illustrated in Figure 42, the small inhibitor did not block the transcriptional activity of *Has2*, *Tnfaip6*, *Ptx3*, and *Ptgs2*, which were present at the same levels as those detected in the control samples.

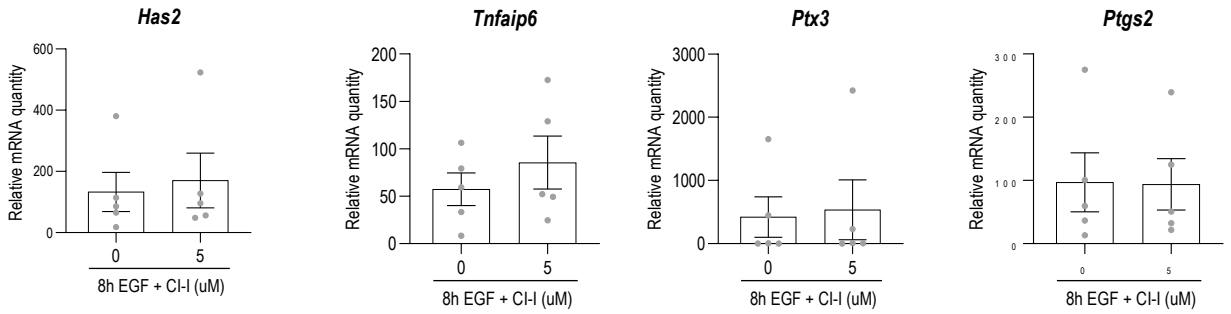


**Figure 42: Transcription of the cumulus matrix-related genes does not depend on Calpain activity**. COCs were collected from primed mice and incubated with recombinant EGF for 8h in the presence or absence of CI-I (5 μM). Samples were harvested for quantitative PCR analysis to assess mRNA quantity of cumulus matrix-related genes *Has2*, *Tnfaip6*, *Ptx3* and *Ptgs2*.

In the first section of this chapter, we investigated the transcription of cumulus matrix-related genes over the course of an 8-hour incubation with EGF. Almost unanimously, the transcript levels steeply increase during the first 3 hours of culture and proceed to decrease over the course of the next 6 hours of culture. This result could reflect a gradual decrease in the transcription rate for the analyzed genes after the observed 3h peak. It is known that oocyte-secreted factors signal through ALK4/5/7 receptors, leading to the phosphorylation of SMAD2/3 (208) that is increased 4 hours after initial EGF exposure and decreased by the 8-hour culture mark (664). Despite being regulated by EGFR signalling, the protease Calpain follows the same activation pattern, reaching peak activity 8h after initial EGF exposure (442). Given that SMAD2 phosphorylation and gene transcription decrease as cumulus cells detach from each other and the oocyte, we hypothesized that cell attachment is required to maintain high SMAD2 signalling and cumulus matrix-related gene transcription.

To start testing this hypothesis, COCs were collected and cultured with EGF plus CI-I for a period of 12h and then submitted to western blot analyses. This was done to examine if extended EGF exposure paired with Calpain inhibition could prevent cell-cell detachment and, therefore, sustain SMAD2 phosphorylation levels. As illustrated in Figure 43, at the end of a 12-hour incubation with EGF, pSMAD2 was virtually no longer detectable. However, the COCs cultured for 12h in the presence of EGF and 5 or 50 μM of CI-I presented detectable levels of

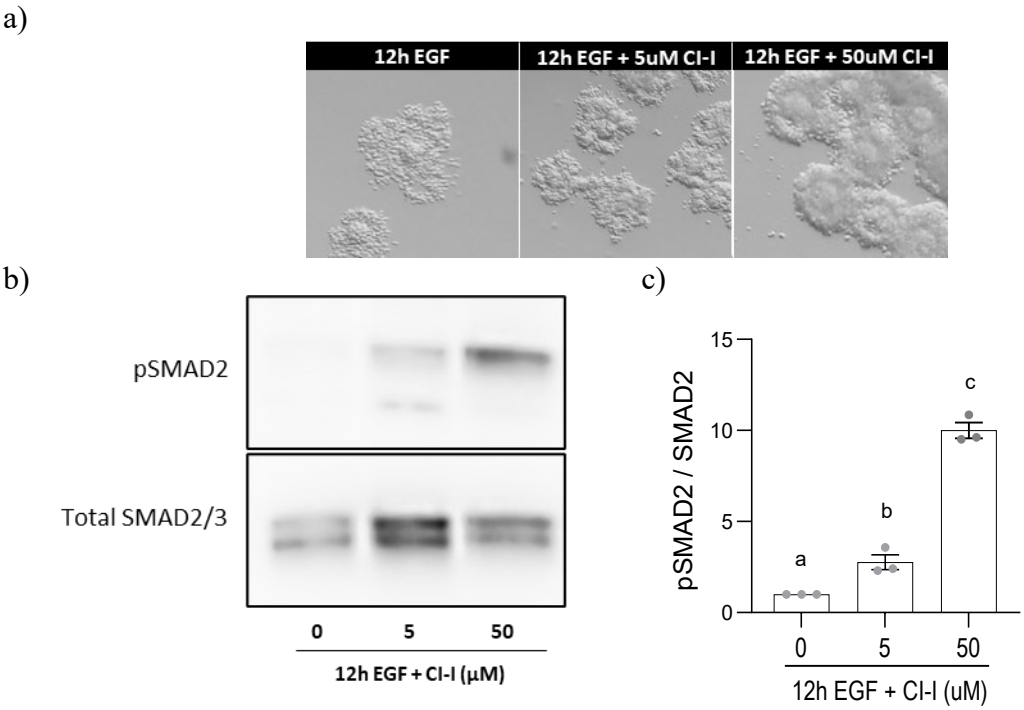


**Figure 43: Inhibiting cumulus cell detachment by blocking Calpain activity maintains TGFβ signalling**. COCs were collected from primed mice and incubated with recombinant EGF for 12h in the presence or absence of CI-I (5 or 50 µM). Brightfield images (a) were obtained before samples were submitted to western blot analysis (b) for quantification of pSMAD2 levels (c).

pSMAD2 that were significantly elevated compared to the 12h EGF group (2.76 ± 0.40, $p \leq 0.0252$ and 10.00 ± 0.43, $p < 0.0001$, respectively).

Next, to further test the role cell-cell attachment in TGFβ signalling and cumulus matrix-related gene expression, we turned to cadherins. The tethering between cumulus cells and the cumulus cells and the oocyte was described to be mediated by cadherins (243,665). Since cadherins are calcium-dependent molecules, calcium-free culture media was employed to challenge cadherin-based cell contact within the COC. Therefore, COCs were collected and pre-incubated in either normal or calcium-free culture media, both containing CNP to prevent GVBD. After 30 minutes, the complexes were washed and transferred to new dishes containing normal or calcium-free culture media supplemented with EGF. The COCs were then cultured for 3h before being submitted to western blot analyses (Figure 44a, b).

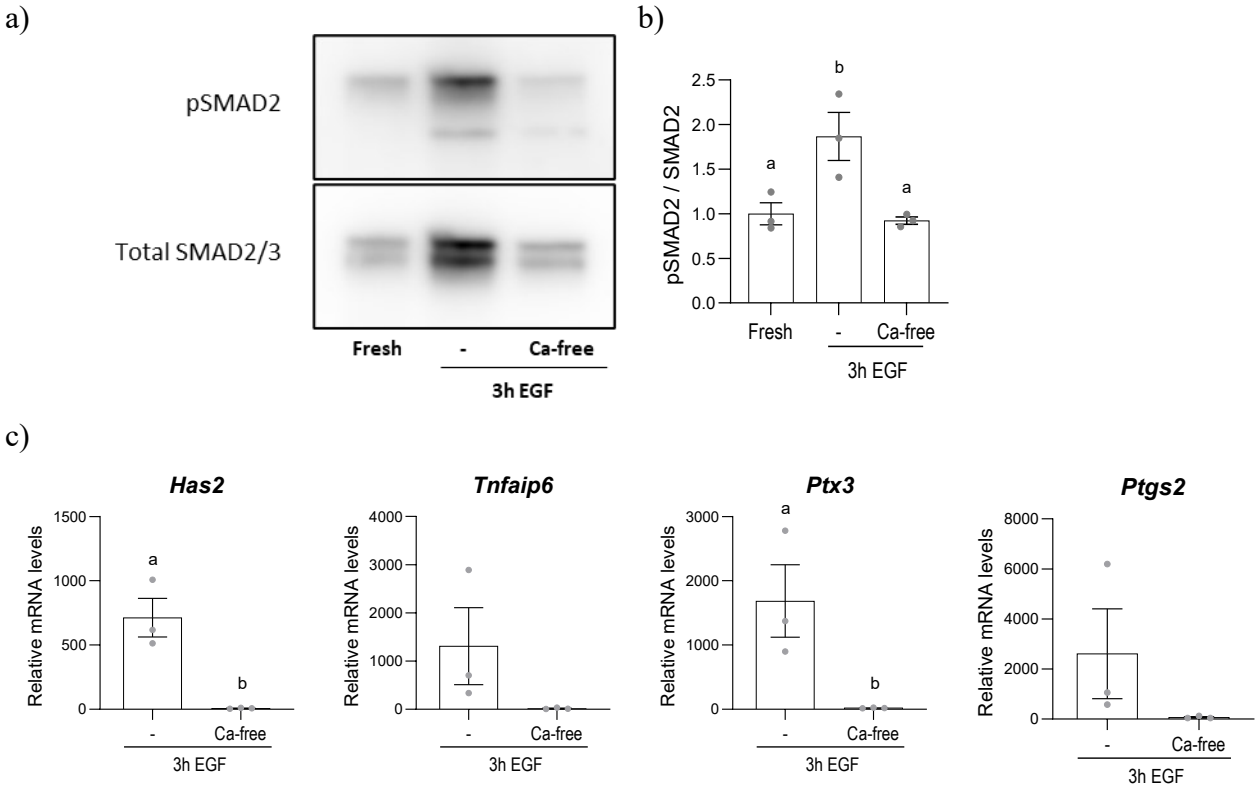


**Figure 44: Cumulus cell attachment is required for cumulus matrix-related gene expression**. COCs were collected from primed mice and incubated with recombinant EGF for 3h in normal or Ca-free culture media. After culture, samples were submitted to western blot analysis (a) for quantification of pSMAD2 levels (b). Samples cultured in the same conditions and harvested for (c) quantitative PCR analysis to assess mRNA quantity of cumulus matrix-related genes *Has2*, *Tnfaip6*, *Ptx3* and *Ptgs2*.

As expected based on previous results, EGF exposure led to a spike in pSMAD2 levels ($1.87 \pm 0.27$ vs. $1.00 \pm 0.12$, $p \leq 0.0282$). However, this increase was not observed in the COCs that were cultured in the calcium-free media ($0.92 \pm 0.04$, $p \leq 0.9480$ vs. Fresh and $p \leq 0.0196$ vs. EGF in complete media). These results suggest that TGFβ signalling is disrupted when COCs are cultured in calcium-free media, impacting cell-cell attachment that depends on $Ca^{2+}$ ions. Therefore, we next assessed the impact of this treatment on SMAD2-driven gene expression. For this, COCs were cultured in the same conditions and submitted to quantitative PCR analyses to measure the transcript levels of the cumulus matrix-related genes (Figure 44c). In accordance with previous results, the COCs exposed to EGF for 3h in complete culture media presented a steep increase in transcript levels of *Has2*, *Tnfaip6*, *Ptx3* and *Ptgs2*. This increase, however, was

virtually absent in the COCs cultured in the calcium-free media, even though it was also supplemented with EGF. These results suggest that cell-cell attachment is a prerequisite to maintaining the high TGFβ signalling responsible for phosphorylating SMAD2 and promoting cumulus matrix-related gene transcription during the early stages of cumulus layer expansion. However, as the expansion process advances, cell detachment is required so the actin cytoskeletal rearrangement can take place, allowing cumulus cell displacement to take place.

The results presented in this chapter regard the signalling controlling cumulus matrix production, the dynamics of cumulus cell displacement during expansion, and both extension and retraction of their cellular structures, which underlines a complex cytoskeletal rearrangement process. Collectively, these observations strongly indicate that cumulus cell displacement has an active component. Therefore, the molecular mechanisms responsible for cumulus cell displacement during expansion will be investigated in the next chapter.

*Chapter 4:*

# Molecular mechanisms controlling cumulus cell displacement during cumulus layer expansion

## 1. EGF-triggered activation of Non-muscle Myosin II is required for cumulus cell displacement during cumulus layer expansion.

To start investigating the molecular mechanism behind cumulus cell displacement we first collected COCs, incubated them with EGF and assessed cumulus cell displacement at 0, 4 and 8h. This was done by measuring the COC area based on brightfield pictures, as done previously (Figure 45a, b). No significant change was observed in the COC area between the start of the culture and the 4-hour mark ($p \leq 0.8968$, Fresh vs. 4h EGF). However, by the end of 8 hours of culture, the COC area had increased to $3.18 \pm 0.15$ ($p<0.0001$ vs. Fresh $1.00 \pm 0.02$). These results confirm the pattern previously observed after live imaging of expanding COCs (Section 2, Chapter 3).

Cell migration requires actomyosin contractility, which is powered by NMII activity (666). Thus, we fixed these samples and stained them with an antibody that recognizes the active (phosphorylated) form of Myosin Light Chain (MLC). Before EGF exposure, the cumulus cells presented few fluorescent pMLC foci (Figure 45c, d). A similar pattern was observed for the samples fixed after 4 hours of culture with EGF. By the end of the 8h culture, however, the number of pMLC foci per cumulus cell had increased by a factor of $2.81 \pm 0.33$ ($p < 0.0001$ vs Fresh).

Alongside pMLC, the COCs were also stained with Phalloidin to label the cell cortex. Closely examining the pictures, it is possible to determine the percentage of cumulus cells extending membrane blebs. This ratio remained low and stable for the analyzed COCs at the 0 and 4-hour time points (Figure 45c, e). However, towards the end of the culture, it increased significantly and reached $68.06 \pm 5.37\%$ of cumulus cells positive for membrane blebs in the 8h EGF group compared to the Fresh samples ($p < 0.0001$). Therefore, these results indicate that NMII activity in the cumulus cells of COCs increases between 4 and 8 hr after initial exposure to EGF, which temporally coincides with cumulus cell displacement and an increase in membrane blebbing.

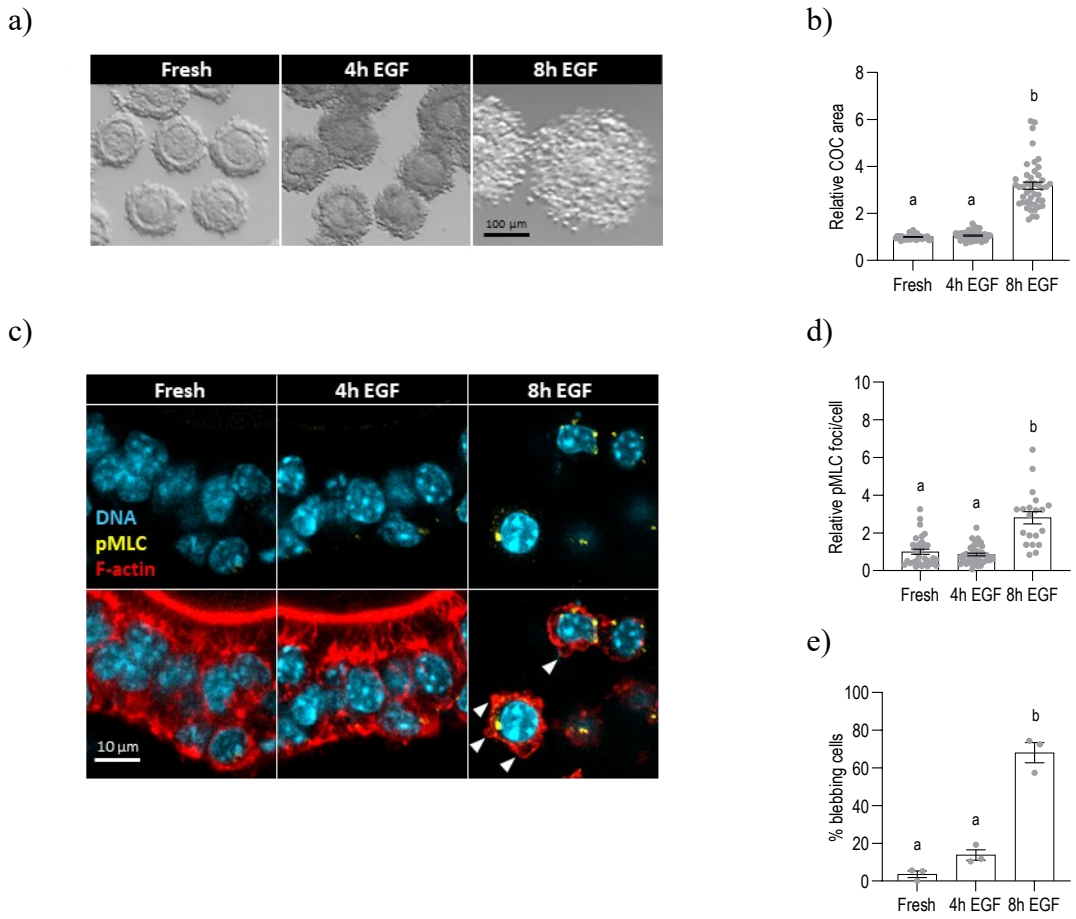


**Figure 45: EGF exposure induces cumulus cell displacement, upregulation of MLC phosphorylation and membrane blebbing.** COCs were collected from primed mice and incubated with recombinant EGF for 8h. At 0, 4 and 8h after initial EGF exposure, brightfield pictures (a) were taken to assess cumulus cell displacement by measuring the COC area (b). COCs were fixed and stained with an antibody raised against phosphorylated MLC (c) to assess NMII activation levels (d). COCs were also stained with phalloidin (c) to assess cell morphology and the percentage of membrane blebbing cells (e). DNA is shown in light blue, filamentous actin (F-actin) in red, and pMLC foci are shown in yellow. White arrowheads show membrane blebs.

To test whether this increase in NMII activity was triggered by EGFR signalling, we collected COCs and cultured them with EGF and AG1478, a known EGFR molecular inhibitor (656). As illustrated in Figure 46, inhibiting EGFR activity prevents full NMII activation compared to the 8h EGF group ($1.93 \pm 1.06$ vs. $3.34 \pm 1.66$, $p \leq 0.0003$). This indicates that EGFR activity is partially responsible for NMII activation in the cumulus cells during expansion.

a) b)

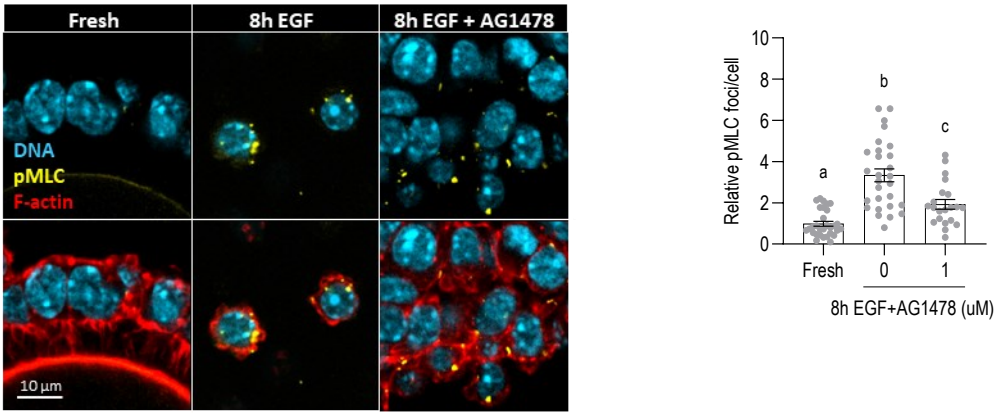


**Figure 46: Pharmacological inhibition of EGFR partially prevents pMLC upregulation.** COCs were collected from primed mice and incubated with recombinant EGF for 8h with or without the EGFR molecular inhibitor AG1478 at a final concentration of 1M. COCs were fixed and stained with an antibody raised against phosphorylated MLC (a) to assess NMII activation levels (b). DNA is shown in light blue and pMLC foci are shown in yellow.

Next, we examined whether NMII activity is required for cumulus cell displacement away from the oocyte during cumulus layer expansion. To do this, COCs were collected and incubated with EGF and Para-amino Blebbistatin (PAB), a permeable molecule that prevents actomyosin contraction by binding and inhibiting NMII's ATPase subunit (667). As PAB acts downstream of MLC phosphorylation, immunofluorescence could not be employed to assess the efficiency of the treatment. Instead, we analyzed the percentage of blebbing cells since NMII is responsible both for their extension and retraction (668). While membrane blebs were identified in around 60% of the cumulus cells exposed to EGF, they were virtually absent from the ones exposed to EGF and PAB, thus implying that the treatment succeeded in inhibiting NMII activity (Figure 47a, b).

Unexpectedly, the cumulus cells from the COCs exposed to EGF and PAB presented an elongated shape, which clashed with the usual round morphology observed for cumulus cells both before and after expansion (Figure 47a). To quantify this observation, we used the morphological descriptor Cell Elongation Index (CEI) (Figure 47c). The CEI is obtained by dividing the cell's length by its width. While a perfect circle has a CEI of 1, cells with a CEI between 0 and 2 are considered to have a round morphology, and CEI values above 2 describe an elongated cell. The CEI values for the Fresh and 8h EGF groups did not differ statistically and

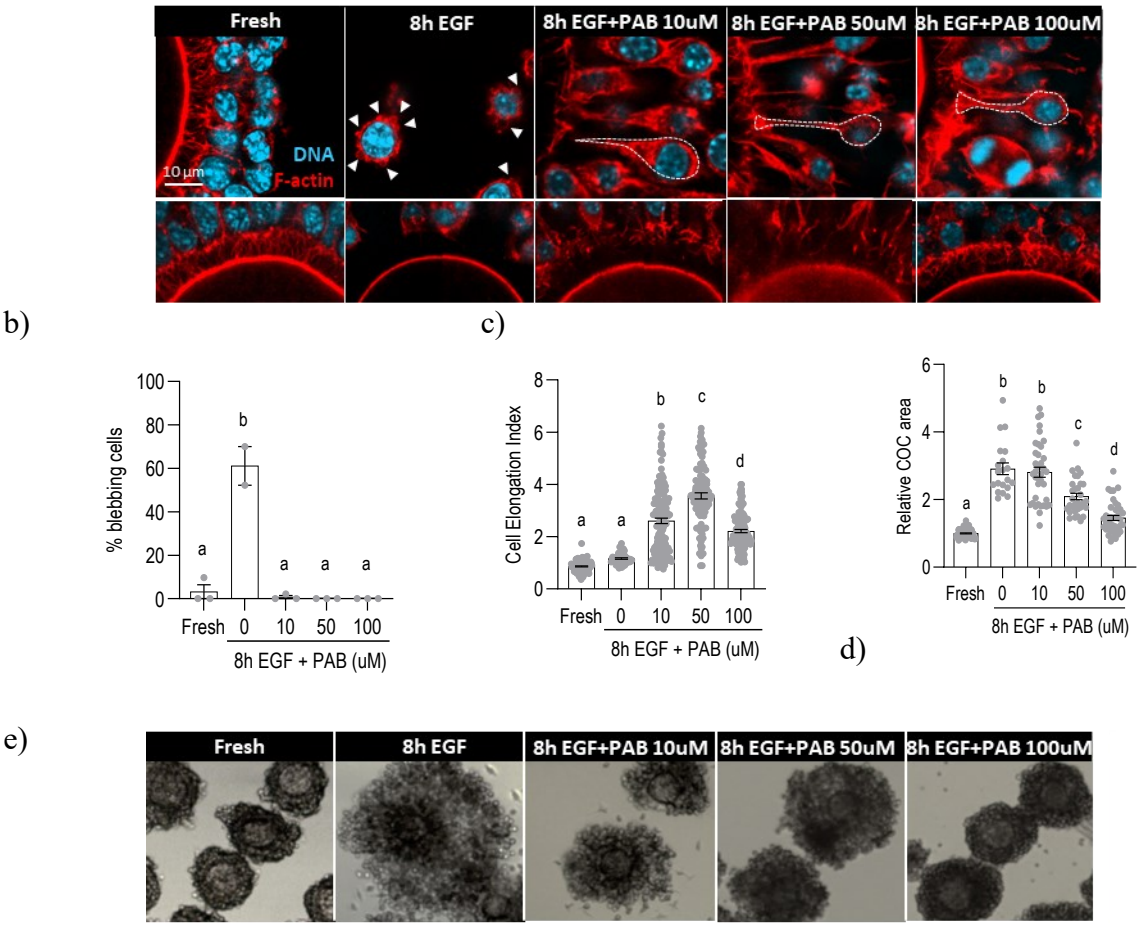


**Figure 47: Non-muscle Myosin II activity is required for full cumulus cell displacement during cumulus layer expansion**. COCs were collected from primed mice and incubated with recombinant EGF for 8h with or without the molecular inhibitor of NMII ATPase Para-amino Blebbistatin (PAB) at final concentrations of 10, 50 or 100 µM. COCs were fixed and stained with phalloidin (a) to assess the percentage of membrane blebbing cells (b) and cell morphology (c). Cumulus cell displacement was assessed by measuring the COC area (d) in brightfield pictures (e) obtained before and after the culture. DNA is shown in light blue, and filamentous actin (F-actin) in red. White arrowheads show membrane blebs, and dotted lines highlight cell morphology.

stayed below the 2 mark (0.86 ± 0.21 vs. 1.16 ± 0.21, $p \leq 0.2156$). The COCs exposed to PAB, however, harboured mainly elongated cells, with the highest mean CEI reaching 3.5 ± 1.18 when PAB was added to the medium at 50 µM. Besides the elongated shape, the cumulus cells from the COCs expanded in the presence of the NMII blocker also failed to fully retract their TZPs, which seemed detached from the oocyte (Figure 47a, bottom panel).

To assess the effects of decreased NMII on cumulus cell displacement, we measured the COC area before and after the treatment (Figure 47d, e). As expected, the mean COC area increased in the control EGF group when compared to the fresh COCs (2.91 ± 0.17 vs. 1.00 ± 0.01, $p < 0.0001$). This increase was reduced in a dose-dependent manner when PAB was present, reaching 1.46 ± 0.07 at 100 µM ($p < 0.0001$ vs EGF alone), suggesting NMII activity in the cumulus cells is required for full expansion.

It is well known that cumulus layer expansion relies on extensive cumulus matrix synthesis. For this reason, we tested whether PAB addition to the culture media affected the transcription of key genes involved in producing the cumulus matrix (Figure 48). This analysis detected no change in the quantity of the encoded mRNAs between the control and treatment groups, implying that the drug did not prevent the cells from producing the cumulus matrix. Therefore, these results indicate that NMII activity is required for cumulus cell displacement during expansion but not for cumulus matrix production.

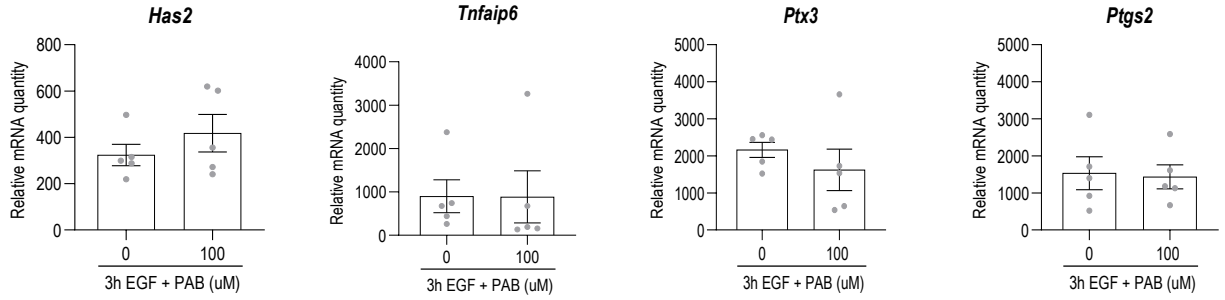


**Figure 48: Non-muscle Myosin II activity is not required for the transcriptional activation of cumulus matrix-related genes**. COCs were collected from primed mice and incubated with recombinant EGF for 3h with or without the molecular inhibitor of NMII ATPase Para-amino Blebbistatin (PAB) at a final concentration of 100 µM. COCs were harvested for quantitative PCR analysis to assess mRNA quantity of cumulus matrix-related genes Has2, Tnfaip6, Ptx3, and *Ptgs2*.

## 2. EGF-triggered activation of Non-muscle Myosin II is not mediated through ERK signaling.

The ERK pathway is a key downstream effector of the EGFR signalling. Previous studies have demonstrated that cumulus expansion is impaired when this pathway is pharmacologically inhibited or genetically disabled (409,410). Therefore, we tested whether ERK signalling mediates NMII activation in cumulus cells during expansion. To do this, we collected COCs and cultured them with EGF and U0126, a highly specific and noncompetitive inhibitor of MEK1 and MEK2, the members of the mitogen-activated protein kinase pathway that directly activate ERK kinases (669). First, we confirmed that the treatment with U0126 inhibited cumulus cell displacement (Figure 49a, b) and prevented the transcriptional activation of the cumulus matrix-related genes (Figure 49c), as expected.

Next, samples were cultured in the same conditions, fixed and stained for pMLC so NMII activation levels could be assessed (Figure 50a, b). Strikingly, the number of pMLC foci per cell in the COCs exposed to EGF and U0126 increased 2.5-fold when compared to the fresh samples ($2.67 \pm 0.24$ vs $1.00 \pm 0.08$, $p < 0.0001$), while it remained just below what was observed for the COCs treated with EGF alone ($3.51 \pm 0.23$, $p \leq 0.02$). The same pattern was observed for the percentage of blebbing cells that increased in EGF plus U0126-treated COCs when compared to the Fresh samples ($32.89 \pm 6.39$ vs $8.64 \pm 1.10$, $p \leq 0.01$) but not to the same extent as what was observed for the COCs treated solely with EGF ($73.16 \pm 1.70$, $p < 0.0001$) (Figure 50c). These results do not exclude a partial role for ERK, but they do indicate that there are other signalling pathways primarily responsible for promoting NMII activation and membrane blebbing in cumulus cells during expansion.

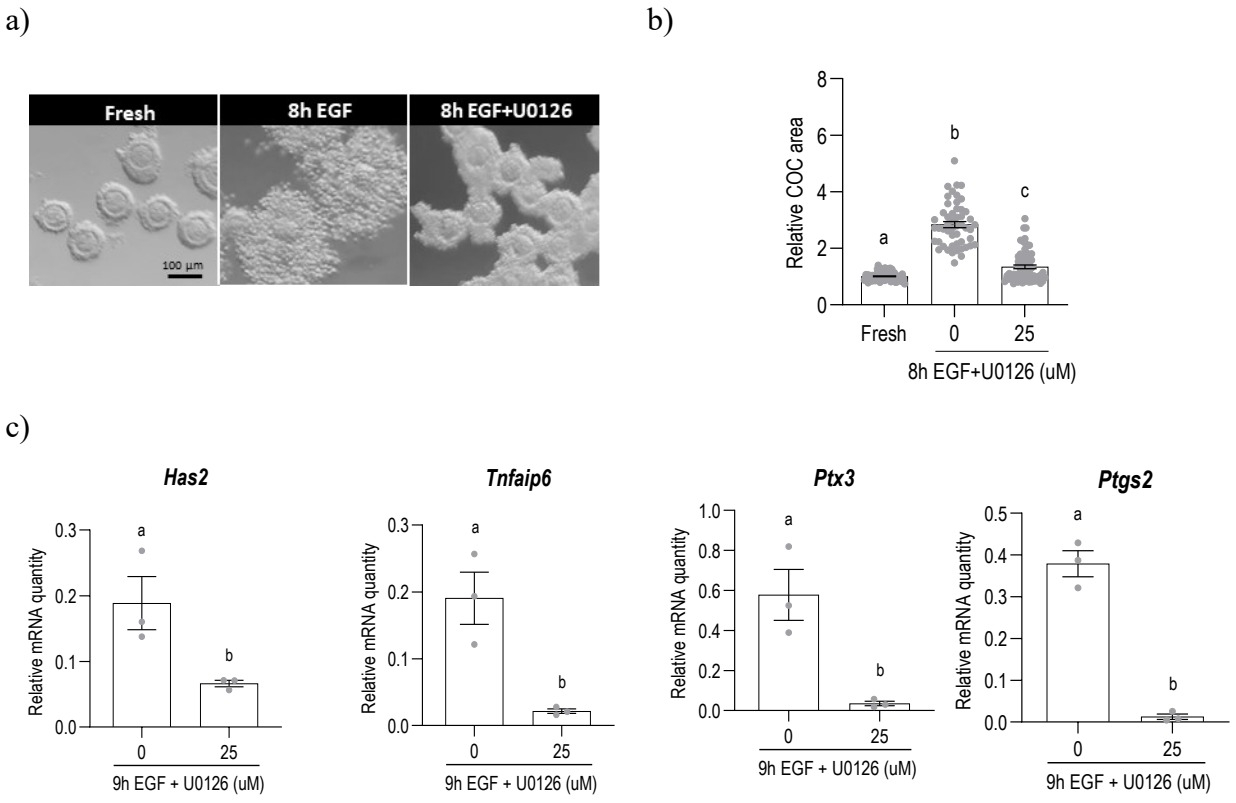


**Figure 49: Inhibition of ERK signalling prevents cumulus layer expansion.** COCs were collected from primed mice and incubated with recombinant EGF for 8h with or without the ERK molecular inhibitor U0126 at a final concentration of 25 µM. Brightfield images of the COCs (a) were acquired to assess cumulus cell displacement by measuring the COC area (b). COCs were harvested for quantitative PCR analysis (c) to assess mRNA quantity of cumulus matrix-related genes *Has2*, *Tnfaip6*, *Ptx3*, and *Ptgs2*.

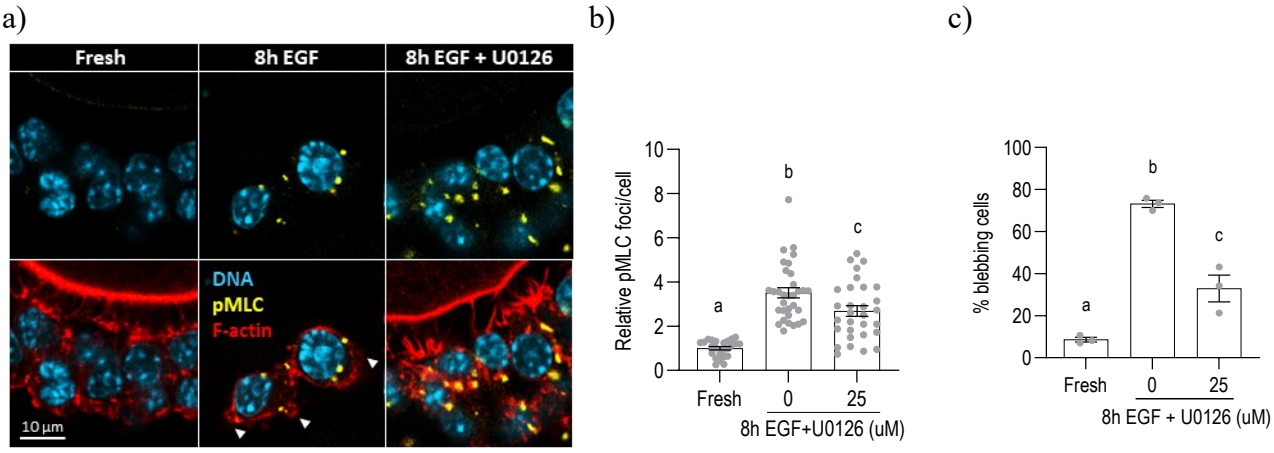


**Figure 50: EGF-triggered activation of NMII is not mediated through ERK signalling.** COCs were collected from primed mice and incubated with recombinant EGF for 8h with or without the MEK molecular inhibitor U0126 at a final concentration of 25µM. COCs were fixed and stained with an antibody raised against phosphorylated MLC (a) to assess NMII activation levels (b). COCs were also stained with phalloidin (a) to assess cell morphology and the percentage of membrane blebbing cells (c). DNA is shown in light blue, filamentous actin (F-actin) in red, and pMLC foci are shown in yellow. White arrowheads show membrane blebs.

## 3. RhoA signalling triggers Non-muscle Myosin II activation.

The small Rho GTPase RhoA has been implicated in different cell processes. These include cell migration, which is often accompanied by NMII activation and membrane blebbing, especially in highly invasive cancer-derived cell lines (616,670). For this reason, and the fact that RhoA can be activated by EGFR signalling (671,672), RhoA was considered a good candidate to mediate NMII activation in cumulus cells during expansion. To test this hypothesis, COCs were collected and cultured with Rho Activator II (RhoA act) in the absence of EGF. RhoA act is a small protein that selectively enters the cell and activates RhoA (673), showing the highest response 3 hours after initial exposure. Therefore, we incubated the COCs with two different doses of RhoA act for 3h in the absence of EGF, and assessed NMII activation levels (Figure 51).

Image analysis revealed a dose-dependent increase in the number of pMLC foci per cell in the COCs that were cultured with the Rho activator (1 µg/ml: 4.47 ± 0.55 vs 1.00 ± 0.07, $p < 0.0001$). This increase could not be attributed to culturing alone since the COCs incubated for 3h

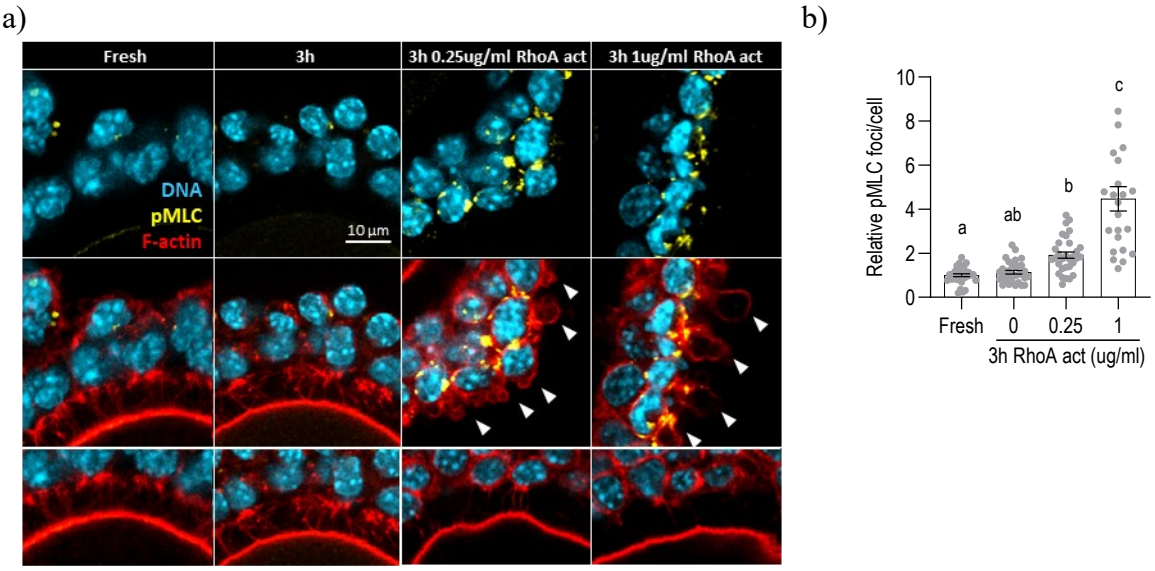


**Figure 51: RhoA signalling triggers NMII activation.** COCs were collected from primed mice and incubated with RhoA activator at final concentrations of 0, 0.25 or 1 µg/ml. COCs were fixed and stained with an antibody raised against phosphorylated MLC (a) to assess NMII activation levels (b). COCs were also stained with phalloidin (a) to assess cell morphology and membrane blebbing. DNA is shown in light blue, filamentous actin (F-actin) in red, and pMLC foci are shown in yellow. White arrowheads show membrane blebs.

without RhoA act kept pMLC levels comparable to the COCs in the Fresh group (1.140 ± 0.47 vs. 1.00 ± 0.38, $p \leq 0.9728$). Strikingly, the presence of the activator induced an actin cytoskeletal rearrangement, underlined by TZP retraction and intense membrane blebbing activity, as illustrated by the phalloidin staining in Figure 51a.

Despite being able to activate NMII and lead to membrane blebbing, the RhoA activator did not promote the transcriptional activation of the cumulus matrix-related genes, as verified by qPCR (Figure 52). Thus, these results indicate RhoA to be a good candidate for mediating NMII activation and membrane blebbing by EGFR signalling. Also, they suggest NMII activation and cumulus matrix production to be regulated through distinct pathways downstream of EGFR.

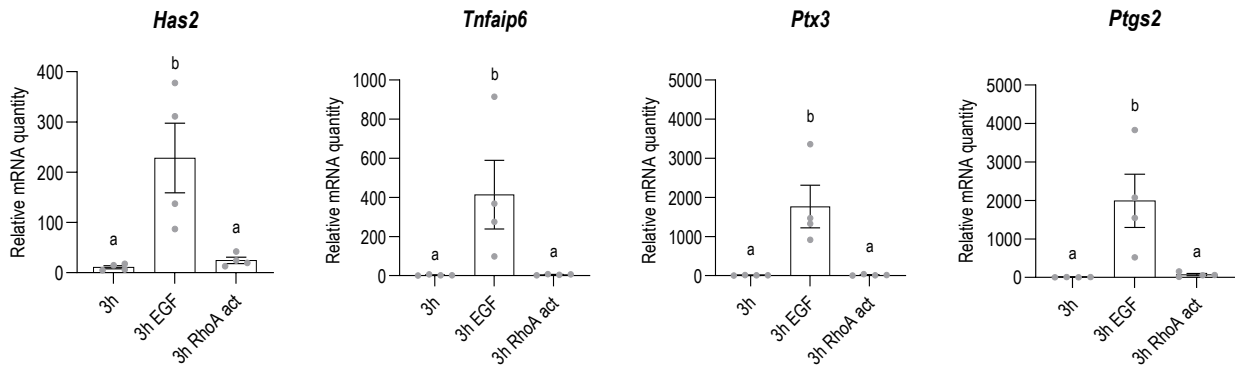


**Figure 52: RhoA signalling does not trigger transcriptional activation of cumulus matrix-related genes.** COCs were collected from primed mice and incubated for 3h either in plain media, with recombinant EGF or with RhoA activator (1µg/ml) alone. COCs were harvested for quantitative PCR analysis to assess mRNA quantity of ECM-related genes *Has2*, *Tnfaip6*, *Ptx3* and *Ptgs2*.

## 4. ROCK signalling partially mediates EGF-triggered Non-muscle Myosin II activation and cumulus cell displacement.

The Rho-associated kinases 1 and 2 (ROCK1/2) are the most well-characterized downstream effectors of RhoA (674). Upon activation, these kinases increase actomyosin contractility by phosphorylating the MLC subunit of NMII or by inhibiting myosin light chain phosphatase (MYPT) (526,527). Therefore, we next tested the role of ROCK1/2 kinase activity in cumulus cell displacement during expansion. We collected and cultured COCs for 8h in the presence of EGF and Y27632 (Y27), a highly selective small molecule that inhibits ROCK1/2 activity by competing for the ATP-binding site (675) (Figure 53).

After culture, the number of pMLC foci per cell in COCs treated with EGF alone increased by a factor of 5.13 ± 0.43 ($p < 0.0001$) when compared to the fresh samples (Figure 51a, b). The fold increase for the COCs exposed to EGF and Y27 at a concentration of 10 µM and 50 µM was only 3.26 ± 0.32 ($p \leq 0.0009$ vs EGF alone) and 3.17 ± 0.24 ($p \leq 0.0013$ vs EGF alone), respectively. Following a similar pattern, intense blebbing was observed in the COCs post-EGF treatment, but virtually no cumulus cell in the COCs exposed to EGF and Y27 presented membrane blebs (Figure 53c).

a)

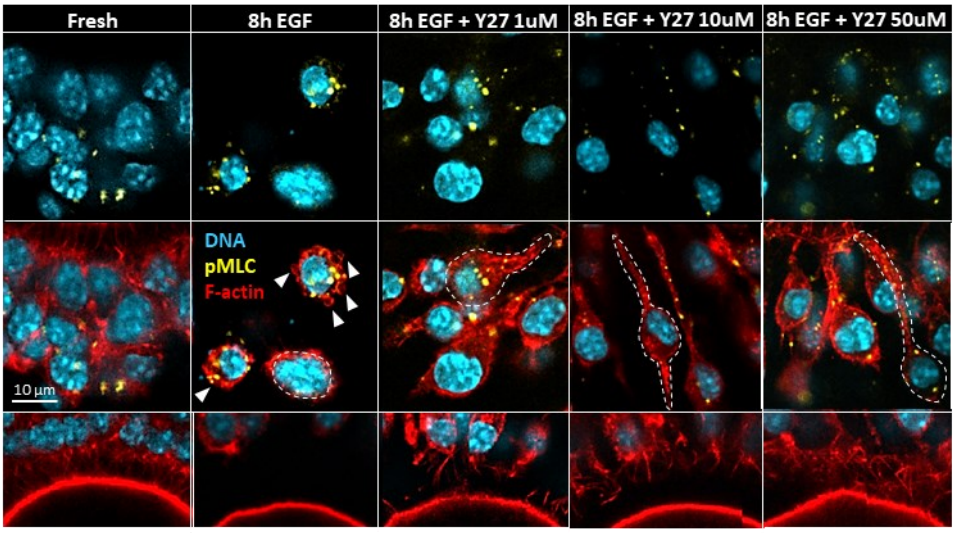


b)

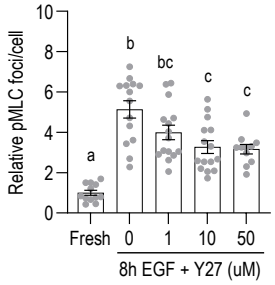


c)

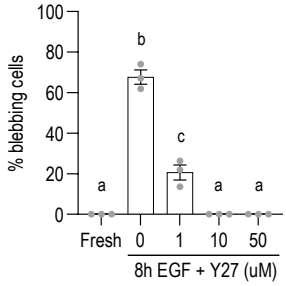


d)

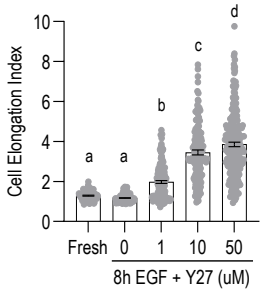


e)

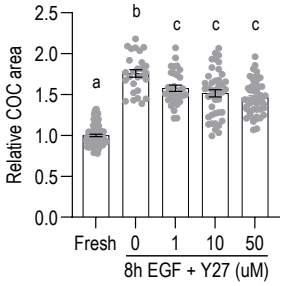


f)

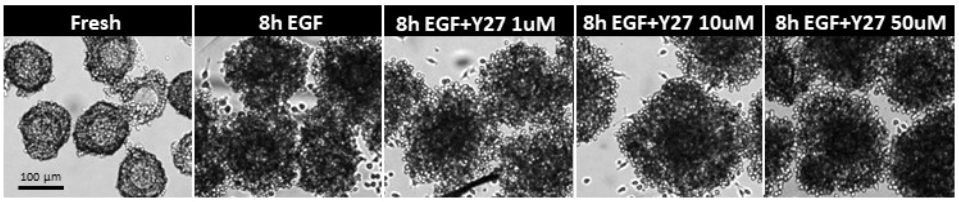


**Figure 53: ROCK signalling partially mediates EGF-triggered NMII activation and cumulus cell displacement.** COCs were collected from primed mice and incubated with recombinant EGF for 8h with or without Y27632, a ROCK molecular inhibitor, at final concentrations of 1, 10, or 50µM. COCs were fixed and stained with an antibody raised against phosphorylated MLC (a) to assess NMII activation levels (b). COCs were also stained with phalloidin (a) to assess the percentage of membrane blebbing cells (c) and cell morphology (d). Cumulus cell displacement was assessed by measuring the COC area (e) in brightfield pictures (f) obtained before and after the culture. DNA is shown in light blue, filamentous actin (F-actin) in red, and pMLC foci are shown in yellow. White arrowheads show membrane blebs and dotted white lines show cumulus cell morphology.

According to the phenotype observed when NMII activity was inhibited (Figure 47a, c), the cumulus cells cultured with Y27 seemed to successfully detach from the oocyte but failed to fully retract (Figure 53a, bottom panel). Additionally, they also presented a predominant elongated shape. This observation was confirmed by the Cell Elongation Index quantification that reached 3.45 ± 1.44 ($p < 0.0001$ vs. fresh) and 3.86 ± 1.62 ($p < 0.0001$ vs. fresh) at 10 μM and 50 μM of Y27 (Figure 53d). Moreover, cumulus cell displacement, as depicted by the relative COC area (Figure 53e, f), decreased in the presence of the inhibitor.

## 5. Both ROCK and MRCK signalling are required for full Non-muscle Myosin II activation and cumulus cell displacement.

Even though the treatment with Y27 decreased NMII activation levels and restricted cumulus cell displacement, it did not completely impair these processes. As shown in Figure 53b and e, pMLC phosphorylation and the Relative COC area were still significantly elevated in comparison to the fresh samples when the inhibitor was added at the final concentration of 50 μM. While these results could indicate an incomplete inhibition of ROCK1/2 by Y27, they could suggest that an additional pathway is also contributing to MLC phosphorylation in the cumulus cells. In fact, the Myotonic Dystrophy-Related CDC42-binding Kinases (MRCKs), a downstream effector of the small Rho GTPase CDC42, phosphorylate NMII and have been implicated in cancer cell motility and invasiveness (534,649). Thus, we next tested the role of MRCK in cumulus cell displacement during cumulus layer expansion.

COCs were collected and cultured in the presence of EGF and BDP9066 (BDP), a highly selective inhibitor of MRCK (676). After 8h of culture, the pMLC foci per cell increased by a factor of 3.81 ± 0.38 in the presence of EGF alone ($p < 0.0001$ vs. Fresh). In the presence of the inhibitor, however, this increase was significantly reduced (10 μM: 1.89 ± 0.16, $p < 0.0001$ vs. EGF alone; 50 μM: 2.08 ± 0.23, $p < 0.0001$ vs. EGF alone) (Figure 54a, b). Consistently, the sharp increase in the membrane blebbing observed in the EGF group was absent when the inhibitor was added at 10 or 50 μM (0 hr: 6.62 ± 3.73; 10 μM: 18.59 ± 4.71, $p \leq 0.4846$; 50 μM: 2.22 ± 2.22, $p \leq 0.9689$) (Figure 54a, c). Quantification of the Cell Elongation Index showed that cumulus cells exposed to 10 or 50 μM of BDP showed they assume an elongated morphology in comparison to the post-treatment control (10 μM: 2.00 ± 0.84, $p < 0.0001$ vs. EGF alone; 50 μM: 3.15 ± 1.13, $p < 0.0001$ vs. EGF alone) (Figure 54a, d). Additionally, as observed before, when

a)

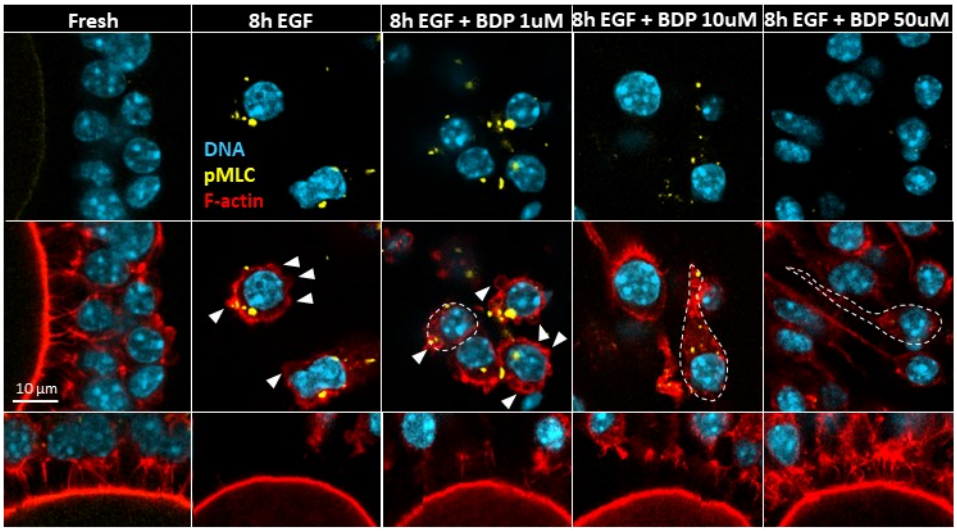


b)

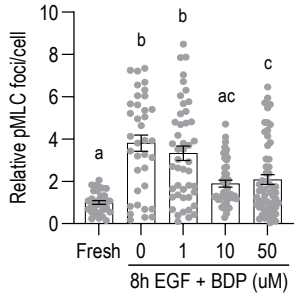


c)

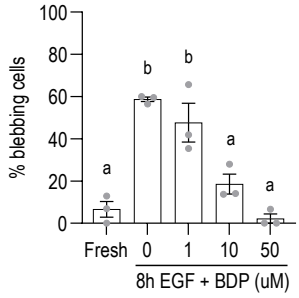


d)

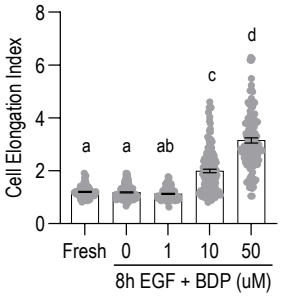


e)

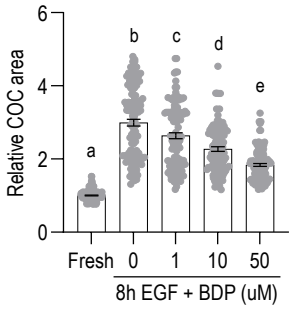


f)

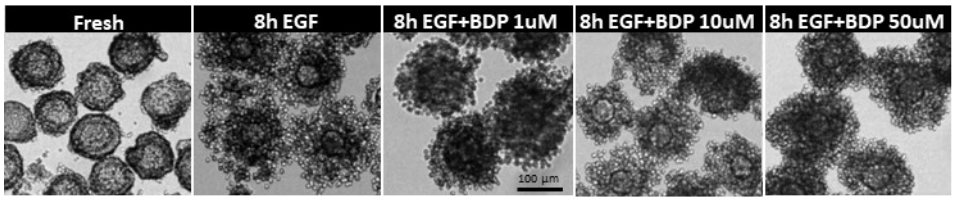


**Figure 54: MRCK partially mediates EGF-triggered NMII activation and cumulus cell displacement**. COCs were collected from primed mice and incubated with recombinant EGF for 8h with or without BDP9066, an MRCK molecular inhibitor, at final concentrations of 1, 10, or 50µM. COCs were fixed and stained with an antibody raised against phosphorylated MLC (a) to assess NMII activation levels (b). COCs were also stained with phalloidin (a) to assess the percentage of membrane blebbing cells (c) and cell morphology (d). Cumulus cell displacement was assessed by measuring the COC area (e) in brightfield pictures (f) obtained before and after the culture. DNA is shown in light blue, filamentous actin (F-actin) in red, and pMLC foci are shown in yellow. White arrowheads show membrane blebs, and dotted white lines show cumulus cell morphology.

NMII activity was impaired, the TZPs seemed to detach from the oocyte but failed to fully retract into the cumulus cell's body (Figure 54a, bottom panel). Moreover, the relative COC area was significantly reduced, dose-dependently, in all three groups exposed to EGF and the inhibitor (Figure 54e, f).

Since individually inhibiting ROCK and MRCK yields a partial impairment of cumulus cell displacement, we next blocked both. Therefore, COCs were exposed to either EGF alone or a combination of EGF plus Y27 and BDP at a final concentration of 50 μM each. The increase in pMLC observed in the COCs exposed to EGF alone was completely prevented when both NMII kinases were inhibited (1.35 ± 0.13 vs. 1.00 ± 0.10, $p \leq 0.3896$; $p > 0.0001$ vs. EGF alone) (Figure 55a, b). The same was true for cumulus cell blebbing, which was completely blocked, as membrane blebs were virtually absent from the COCs exposed to EGF and both inhibitors (Figure 55a, c). As expected, the block in membrane blebbing was accompanied by a lack of TZP retraction (Figure 55a, bottom panel) and an elongated morphology, evidenced by the Cell elongation Index, which increased more than three-fold in the inhibitor group in comparison to the pre-culture control (3.34 ± 0.89 vs. 1.21 ± 0.19; $p < 0.0001$). Moreover, cumulus cell displacement was substantially reduced (3.39 ± 0.13 vs 1.72 ± 0.05, $p < 0.0001$). Collectively, these results show that ROCK and MRCK are the main kinases responsible for phosphorylating and activating NMII in the cumulus cells during expansion, further supporting the hypothesis that NMII activity is required for cumulus cell displacement.

## 6. Non-muscle Myosin II activity is required for EGF-triggered cumulus cell migration.

Next, we investigated whether EGF exposure induces migratory capacity in the cumulus cells during cumulus layer expansion. To this end, COCs were submitted to Transwell Migration Assays, during which two medium-filled chambers divided by a porous membrane are used to create a gradient of the chemoattractant being tested. The chemoattractant is diluted in the bottom chamber, and the cells are seeded at the top. Following incubation, cells can be detected on the underside of the membrane if they acquire a migratory phenotype in response to the chemoattractant. Therefore, COCs were initially incubated with CNP to prevent oocyte maturation or with EGF to induce cumulus layer expansion. After 4h, the COCs were transferred to the top of cell culture inserts placed in wells containing media supplemented with either CNP,

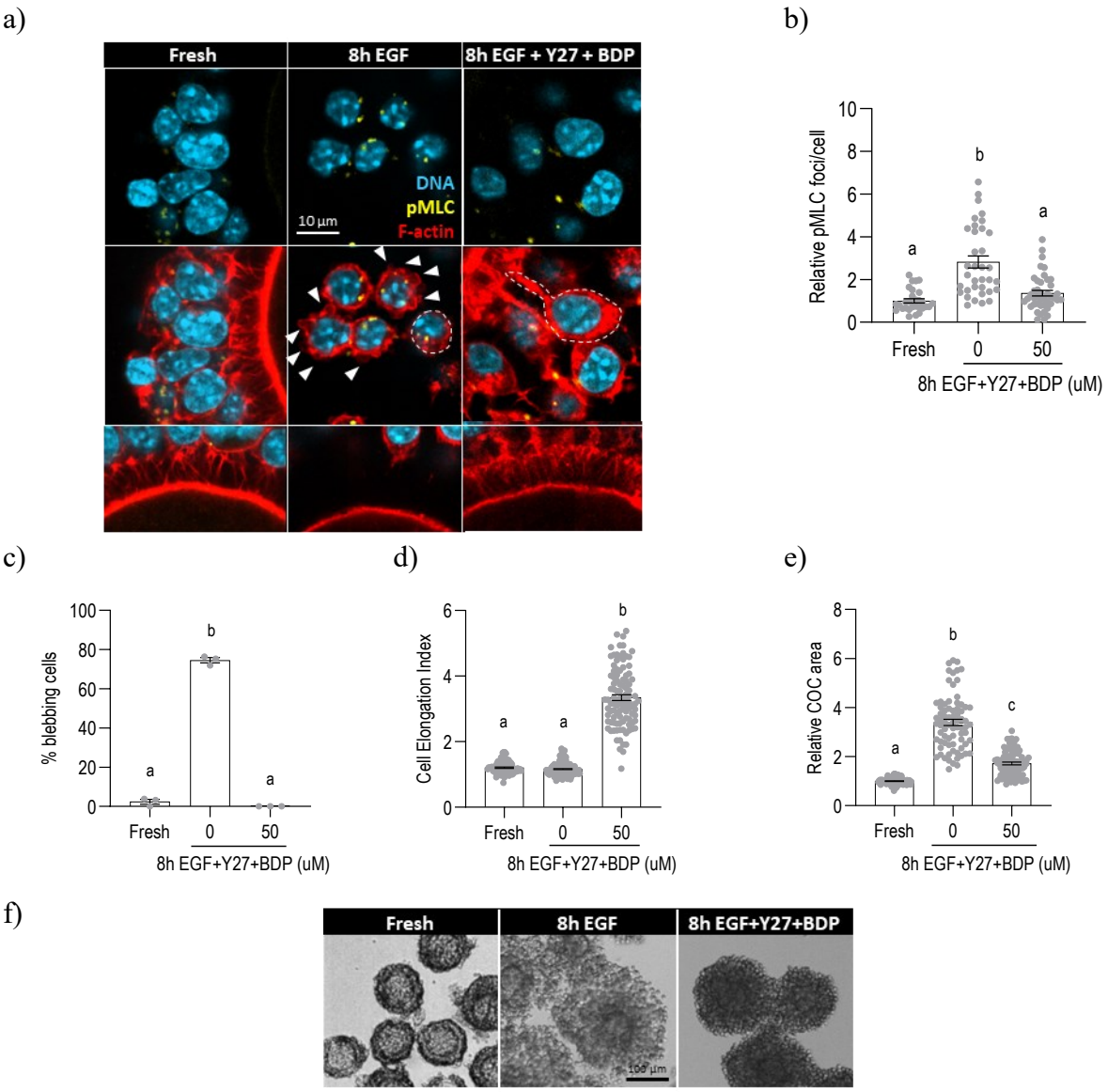


**Figure 55: Both ROCK and MRCK signalling are required for full NMII activation and cumulus cell displacement**. COCs were collected from primed mice and incubated with recombinant EGF for 8h with or without a combination of Y27632 and BDP9066, a ROCK and MRCK molecular inhibitor, respectively, at a final concentration of 50 µM, each. COCs were fixed and stained with an antibody raised against phosphorylated MLC (a) to assess NMII activation levels (b). COCs were also stained with phalloidin (a) to assess the percentage of membrane blebbing cells (c) and cell morphology (d). Cumulus cell displacement was assessed by measuring the COC area (e) in brightfield pictures (f) obtained before and after the culture. DNA is shown in light blue, filamentous actin (F-actin) in red, and pMLC foci are shown in yellow. White arrowheads show membrane blebs and dotted white lines show cumulus cell morphology.

or EGF to act as the chemoattractant. As illustrated in Figure 56, the Migration Index obtained for the EGF group was substantially increased in comparison to the CNP one (11.02 ± 1.54 vs. 1.00 ± 0.32, $p < 0.0001$), indicating that the cumulus cells did acquire the ability to migrate and follow the EGF gradient established at the porous membrane during the assay.

We also used molecular inhibitors to determine the extent to which NMII activity is required for this migration. In the presence of each inhibitor, the migration index was comparable to the one obtained for the CNP group, ranging from 0.92 ± 0.30 in the presence of Y27 ($p > 0.9999$ vs CNP, $p < 0.0001$ vs EGF) to 1.46 ± 0.57 in the presence of PAB ($p \leq 0.9972$ vs. CNP, $p < 0.0001$ vs EGF). These results demonstrate that the cumulus cells' observed migratory behaviour and ability to follow the EGF gradient depend on NMII activity.

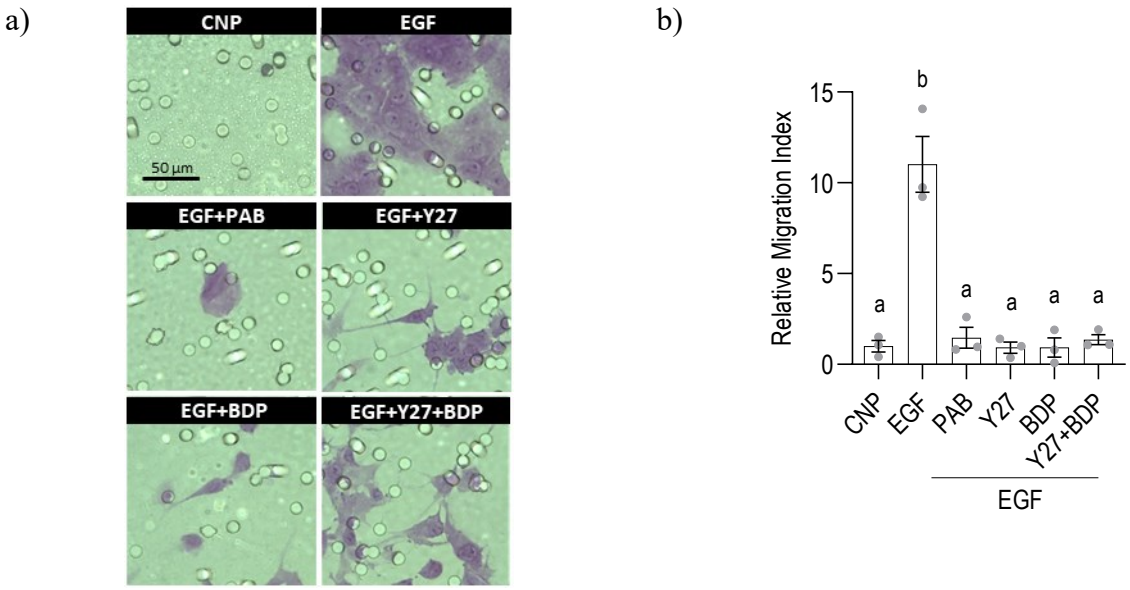


**Figure 56: NMII activity is required for EGF-triggered cumulus cell migration**. COCs were collected from primed mice and incubated for 4h in one of the following conditions: CNP (100 nM), recombinant EGF alone or with the addition of molecular inhibitors targeting either NMII (PAB, 100 µM), ROCK (Y27632, 50 µM), MRCK (BDP9066, 50 µM), and ROCK+MRCK (Y27632+BDP9066, 50 µM each). Transwell migration assays were then performed with either CNP or EGF in the bottom chamber, as well as the molecular inhibitors according to the experimental group condition. After an overnight incubation, the membranes were fixed, stained (a) and the images used to quantify the relative migration index for each condition (b).

## 7. Sperm penetration through the cumulus layer requires Non-muscle Myosin II activation.

Expansion of the cumulus layer is considered necessary for fertilization since it might facilitate sperm access to the mature oocyte. Thus, we next tested the importance of NMII-mediated cumulus cell migration in enabling sperm penetration of the cumulus layer. To do so, COCs were first collected and cultured with either EGF alone or EGF in combination with the different NMII activity inhibitors used in the previous experiments. During this period, sperm was collected, capacitated and stained with HOECHST, a live cell DNA fluorescent dye. COCs were then washed and incubated with the sperm for 1h, and then the complexes were fixed and imaged. That way, images were used to quantify the number of sperm able to penetrate the cumulus layer and reach the zona pellucida of COCs cultured in different conditions.

The number of sperm able to reach the zona pellucida decreased substantially in the presence of each inhibitor (Figure 57a, b). Notably, whereas the number of penetrating sperm was decreased by a factor of 0.5-fold (Y27: 0.48 ± 0.19 vs. 1.00 ± 0.32, $p < 0.0001$; BDP: 0.41 ± 0.32, $p < 0.0001$) when MLC phosphorylation was partial – e.g., when ROCK or MRCK were targeted individually – the decrease was more severe and reached a factor of 0.8-fold when NMII was almost completely inhibited (PAB: 0.19 ± 0.19 vs. 1.00 ± 0.32, $p < 0.0001$; Y27+BDP: 0.14 ± 0.15 vs. 1.00 ± 0.32, $p < 0.0001$) (Figure 55b). These results demonstrate that compromising expansion of the cumulus cell layer by blocking NMII activity and, therefore, cumulus cell migration substantially reduced the number of sperm that were able to reach the zona pellucida.

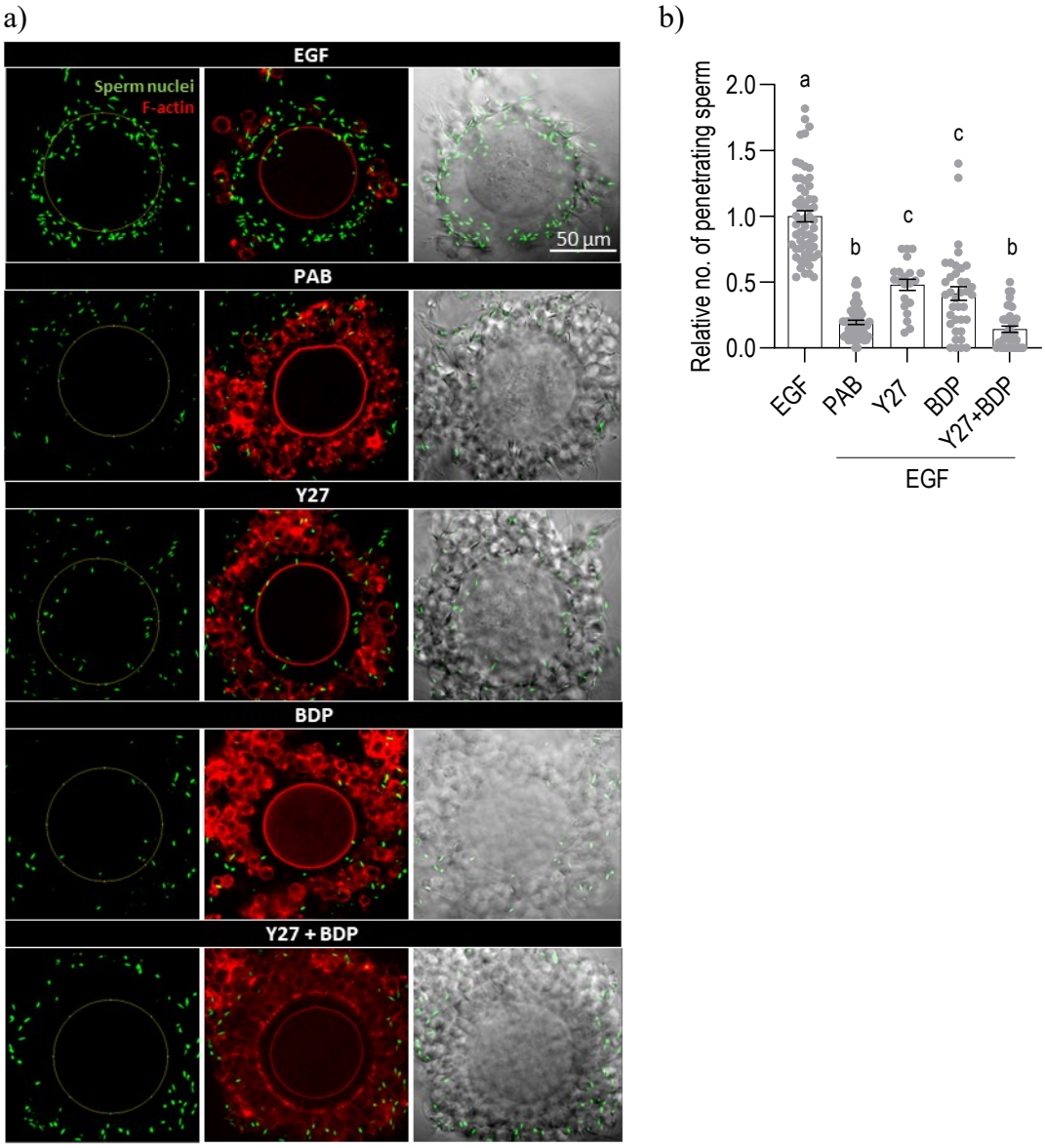


**Figure 57: Sperm penetration through the cumulus layer requires NMII activation**. COCs were collected from primed mice and incubated for 8h in one of the following conditions: recombinant EGF alone or with the addition of molecular inhibitors targeting either NMII (PAB, 100 µM), ROCK (Y27632, 50 µM), MRCK (BDP9066, 50 µM), and ROCK+MRCK (Y27632+BDP9066, 50 µM each). COCs were washed and incubated with nuclei-stained and capacitated sperm. After 1h, the complexes were fixed, stained with phalloidin and imaged (a). The images were used to quantify the number of sperm at the zona pellucida (b).

*Chapter 5:*

# Discussion

## 1. Thesis rationale

During the early phases of folliculogenesis, the granulosa cells are organized around the oocyte in dense layers. As they proliferate, small fluid-filled cavities start to appear within the cell layers. Each cavity grows up to the point where they merge, creating one antrum that separates the granulosa cells into cumulus and mural granulosa. The cumulus cell layers remain tightly packed around the oocyte in a configuration that will only change after the LH surge. This event, besides triggering oocyte maturation and ovulation, will also trigger cumulus layer expansion. This process encompasses extensive extracellular matrix production and secretion, which is accompanied by cumulus cell displacement away from the oocyte. Therefore, the new cumulus matrix envelops the mature oocyte and the now displaced cumulus cells, forming an expanded cumulus-oocyte complex, which will soon be ovulated.

After ovulation, the cumulus matrix mediates the uptake of the ovulated complex by the oviduct. Once it reaches the ampulla, the fertilization site within the oviduct, the cumulus cells and the cumulus matrix play crucial roles in attracting and guiding the sperm to the mature oocyte. Therefore, cumulus layer expansion is essential for female fertility. However, little is known about how the cumulus cells become displaced away from the oocyte during expansion. Previous work has described changes in the cumulus cell actin cytoskeleton, which involve intense F-actin assembly and the appearance of actin-related cellular structures, like membrane ruffling and blebbing (319,351,434,435,441,442). The fact that membrane ruffling and blebbing are usually observed in migratory cells prompted studies to characterize cumulus cells' behaviour during expansion. In fact, Akison *et al*. (444) determined that cumulus cells do assume a highly invasive and migratory phenotype after the LH surge. Moreover, it was found that cumulus layer expansion fails upon inhibition of calpain, a protease known for degrading cell adhesions and promoting cell migration (442,663). Even though these results suggest cumulus cell displacement could be an active migration process, the mechanism behind this displacement is still elusive. Therefore, we used an *in vitro* cumulus layer expansion system to first investigate the link between cumulus matrix production, cumulus cell displacement and actin cytoskeletal rearrangement during expansion (Chapter 3). Then, the use of molecular inhibitors targeting the cellular contractile machinery allowed us to address the question of whether cumulus cell displacement depends on the same cellular mechanisms that control cancer cell migration inside soft 3D extracellular matrices (Chapter 4).

## 2. Key findings

### 2.1. TGFβ signalling and cell-cell contact are essential for cumulus matrix production

Cumulus layer expansion depends on two different signalling pathways: *i*) TGFβ signalling promoted by oocyte-secreted factors, and *ii*) gonadotropin signalling, which triggers the production of EGF-like factors that propagate the gonadotropin stimulation effects within the follicle. These promote the transcriptional activity of genes related to producing the cumulus matrix, an essential event for cumulus layer expansion. According to our results, cumulus cells within COCs exposed to recombinant EGF *in vitro* rapidly accumulated transcripts for *Has2*, *Tnfaip6*, *Ptx3* and *Ptgs2* during the first 3 hours of culture. Over the next 6 hours, however, the steady-state level of the assessed mRNAs decreased. This pattern of sharp increase followed by a steady decline has been described by others using *in situ* hybridization (341,397) and semi-quantitative RT-PCR (310,397). These techniques, as well as the qPCR employed in this thesis, measure the steady-state mRNA quantity, that is, the balance between synthesis and degradation. A decrease in synthesis or an increase in degradation could explain the drop in the relative mRNA levels observed after the 3-hour culture mark. However, cumulus matrix-related genes are not expressed before the ovulatory stimulus (310,341,397), and SMAD signalling generally triggers a specific response that involves transcriptional gene activation (210). Therefore, it is more plausible that the observed drop in mRNA levels reflects a drop in synthesis and not an increase in degradation.

The cumulus matrix production requirement for TGFβ signalling, previously described elsewhere (208,411), was confirmed by us. Moreover, by inhibiting this pathway at different times after the start of the culture, we showed that TGFβ signalling is also required throughout the expansion process to maintain cumulus matrix-related transcriptional activity. However, when EGFR signalling was targeted similarly, the effect in inhibiting cumulus matrix-related gene expression was not as pronounced. These results suggested differential regulation of cumulus matrix-related gene transcription by TGFβ and EGFR signalling.

Work done by Sasseville *et al*. (677) showed that oocyte-induced expression of *Has2* by cultured granulosa cells can be completely prevented by inhibiting TGFβ signalling but only partially affected when EGFR is blocked. In fact, after further exploring the interaction between EGFR and TGFβ signalling, they proposed a model to explain the interaction between TGFβ and

EGFR signalling during folliculogenesis. In addition to the key phosphorylation of the C-terminal portion of SMAD2/3 proteins by the ALK receptors mediating TGFβ signalling, additional phosphorylation of the SMAD2/3 linker region can be promoted by EGFR downstream effectors. This additional phosphorylation of the SMAD2/3 linker region can boost TGFβ signalling (678). Therefore, throughout cumulus layer expansion, ALK receptors would mediate C-terminal SMAD2/3 phosphorylation to activate them and maintain cumulus matrix-related transcriptional activity, while EGFR would promote phosphorylation of the linker region of SMAD2/3, boosting the expression of the same genes.

Next, we showed that TGFβ signalling depends on cell-cell contact within the expanding COC. Phosphorylated SMAD2 levels, a result of oocyte-induced TGFβ signalling in the cumulus cells, start decreasing in expanding COCs around 8 hours after the start of the process (664). This coincides with the peak of calpain activity, a protease involved in degrading cell-cell adhesions (442). In fact, we showed that inhibiting calpain activity, and therefore preventing cell detachment, promoted high pSMAD2 levels that were not observed in the control without the calpain inhibitor. While this result supports the hypothesis that cell-cell contact is required for TGFβ signalling, an alternative explanation could also apply: as calpain inhibition prevents cumulus layer expansion, cumulus cell proximity to each other and to the oocyte could account for readily accessible oocyte-secreted ligands that would bind their receptors on the cumulus cells and lead to the increased pSMAD2 levels observed. Therefore, we employed calcium-free culture media to disturb cadherin-based cell-cell adherens junction within COCs cultured with EGF. Using a shorter time interval, we showed that, even though the cells were kept in proximity, disrupting cadherin-mediated cell-cell contact prevented both the increase in pSMAD2 and the transcriptional activity of cumulus matrix-related gene expression.

Even though this result further suggests that TGFβ signalling requires cell-cell attachment, it should be interpreted cautiously. That is because a wide spectrum of cell signalling is sensitive to $Ca^{2+}$ concentration fluctuation (679), and the culture of COCs in a calcium-free medium could disrupt any of these processes and consequently disturb TGFβ signalling and cumulus matrix production. However, these results suggest a model for further investigation in which cell adherens junctions play a role in receptor availability, thus controlling TGFβ signalling. Although not vast in the literature, an example of a similar model can be found in the work done by Rudini *et al*. (680). The authors determined that membrane clustering of the

adhesion molecule VE-cadherin promotes their assembly into an active complex, a key step in enabling TGFβ signalling-induced effects in endothelial cells.

### 2.2. EGFR signalling triggers cumulus cell detachment and actin cytoskeletal rearrangement during cumulus layer expansion

Cytoskeletal rearrangement reflects the balance between coordinated assembly and disassembly of actin filaments at specific sites as well as actomyosin contractility. These activities can promote the extension and/or retraction of cellular structures (464,468). Accordingly, we have determined that both Transzonal Projection (TZP) retraction and membrane blebbing can be first observed in the interval between 4 and 8 hours after cumulus layer expansion has been triggered. This observation suggests cumulus cell cytoskeletal reorganization takes place in the same interval. As the TZP number is a readily accessible and quantifiable metric, we explored this correlation and utilized TZP number measurement as a marker to assess cumulus cell cytoskeletal rearrangement during expansion and investigate the machinery controlling it. This approach allowed us to determine that EGFR signalling, triggered downstream of the ovulatory stimulus, initiates cumulus cell actin cytoskeletal rearrangement during expansion.

Following the same approach, we showed cumulus cell cytoskeletal reorganization to depend on branched actin synthesis as well as on actomyosin contractility. That is because inhibition of branched actin synthesis almost completely prevented TZP retraction and, consequently, actin cytoskeletal rearrangement. Moreover, we observed that interference with cumulus cell contractile machinery - which includes NMII, ROCK and MRCK - also prevented TZP retraction. In fact, actomyosin contractility is intimately related to actin cytoskeleton rearrangement because it aids in directing cytoskeleton components and guiding the formation of actin bundles or networks (681). Conversely, we have also shown that inducing actomyosin contraction by activating the small Rho GTPase RhoA also triggers actin cytoskeletal rearrangement, denoted by membrane blebbing and TZP retraction. Finally, it is important to point out that this phenotype arose in the absence of EGF, solely as a result of stimulating RhoA activity in the COCs over the course of a 3-hour incubation.

When associated with initiation of cell migration, actin cytoskeletal reorganization is preceded by cell detachment (635–637). That is because cell adherens junctions, such as the ones

mediated by cadherins, for example, are linked to the cytoskeleton and stabilize it (660). So, in order to modify their cytoskeleton and migrate, cells must first detach from their substrate, be it the extracellular matrix or other cells. Therefore, we reasoned that cumulus cells must undergo programmed cell detachment prior to rearranging their cytoskeleton and moving. In support of this principle, when actin synthesis or actomyosin contractility was impaired, the non-retracted TZPs often were no longer connected to the oocyte. This phenotype was most apparent after inhibition of branched actin synthesis by the Arp2/3 complex. Finally, we showed that preventing cumulus cell detachment prevented cytoskeletal rearrangement, as indicated by the TZP number that remained high in the COCs cultured with EGF and the inhibitor.

### 2.3. Cumulus cell migration during cumulus layer expansion depends on Non-muscle Myosin II

The displacement of the cumulus cells observed during cumulus layer expansion has been mainly described as a passive process that happens due to the intense cumulus matrix production, secretion and assembly into the intercellular space (682). However, evidence provided here and elsewhere (442,444) suggests that cumulus cells actively migrate inside the cumulus matrix and away from the oocyte. In other tissues, single cells navigate complex tridimensional ECMs by one of two modes: amoeboid or mesenchymal. These migration modes reflect different levels of certain characteristics, such as adhesion to the substrate, actin protrusion, and actomyosin contraction. In fact, mesenchymal migration is characterized by high adhesion to the substrate, high actin protrusion, and low actomyosin contractility, which translates into a lamellipodium-driven migration. On the other hand, amoeboid migrating cells present low adhesion to the substrate, low actin protrusion and high actomyosin contractility. The high actomyosin contractility on the cell cortex mediates a round cell morphology and promotes a membrane bleb-based movement.

Utilizing the Transwell Migration Assay, we confirmed that cumulus cells from expanding COCs do have the ability to migrate in response to EGF, as shown previously (444). Moreover, by adding a specific NMII inhibitor to the culture media during the experiment, we determined that this migration depends on NMII activity. Despite assessing cell motility, this test is not designed to distinguish between migration modes. Nevertheless, we showed that cumulus cells conserve their round morphology and undergo intense membrane blebbing during

expansion. These are strong indicators that they utilize the amoeboid migration mode to move inside the cumulus matrix. Additional evidence supporting this claim was obtained, for instance, by inhibiting NMII during *in vitro* cumulus layer expansion. This experiment yielded COCs containing cumulus cells that were completely devoid of membrane blebs and displayed an unusual, elongated morphology. Work done by Wilkinson *et al*. (649) investigates the behaviour of the melanoma cancer cell line A375m2. This amoeboid cell line lost its ability to extend membrane blebs and sustain their round morphology in a dose-dependent way when cultured in the presence of an NMII blocker. These phenotypes are compatible with changes in actomyosin and actin protrusive activities, which could be interpreted as an Amoeboid-to-Mesenchymal Transition, or AMT. In an AMT process, cells that originally displayed round morphology and membrane blebbing - both sustained by high actomyosin contractility - shift to an elongated morphology and lamellipodia-based motility mode, driven by actin protrusive forces. Therefore, due to the similarity of how cumulus cells and A375m2 cells react to the different doses of the NMII blocker, it can be reasoned that the cumulus cells also adapt to the decreased actomyosin contractility by switching from an amoeboid to a mesenchymal migration mode.

### 2.4. Non-muscle Myosin II activity required to support cumulus cell migration is promoted by MRCK and ROCK signalling

After determining that NMII activity is required for cumulus cell migration during cumulus layer expansion, we investigated the molecular pathway controlling its activation. We showed that ERK signalling, a key EGFR downstream effector and cumulus layer expansion mediator (409,410), plays a minor role in promoting NMII activation. Consistently, NMII activity is controlled by Small Rho GTPases such as RhoA in other cell types (616,670). In fact, we showed that induction of RhoA activation in the cumulus cells of freshly collected COCs promoted NMII activation and membrane blebbing without EGF present in the system. These results suggest RhoA as the main mediator of NMII activation in the cumulus cells during expansion. Indeed, EGFR has been described to activate RhoA (671,672) and constitutes a good candidate to control NMII activation in the cumulus cells during cumulus layer expansion.

ROCK, a Serine/Threonine kinase, is a downstream effector of RhoA and aids in controlling actomyosin contractility by regulating NMII activity (526,527). Here, we showed that ROCK inhibition during cumulus layer expansion led to a phenotype characterized by elongated

cells devoid of membrane blebs. This phenotype resembles the one observed when NMII activity was gradually impaired by increasing concentrations of the NMII blocker. However, the similarities stop there: the cells whose NMII activity was blocked had their migration restricted, which was denoted by the decreased COC area. On the other hand, ROCK inhibition led to a mild reduction in cumulus cell displacement, which was the same across all different inhibitor doses.

Studying the mesenchymal colorectal carcinoma cell line BE, Wilkinson and colleagues (649) determined that ROCK or the serine/threonine kinase MRCK, a downstream effector of the small Rho GTPase CDC42, could supply the low actomyosin levels required for mesenchymal migration. They initially showed that BE cell migration was impaired when exposed to an NMII inhibitor, which indicates that mesenchymal migration relies on actomyosin contractility. However, BE cells would migrate at their normal speed when they singularly inhibited ROCK or knocked MRCK down with small interference RNA technology. It was only when they simultaneously inhibited ROCK and knocked down MRCK that the cells failed to migrate and mimicked the migratory phenotype observed when NMII activity was blocked. Therefore, it can be inferred that the cumulus cells, once deprived of ROCK activity, underwent an AMT and relied on MRCK to promote the NMII activity required to fuel mesenchymal migration. This work led to the development of small molecule inhibitors aiming to block both ROCK and MRCK with the goal of preventing tumour cell migration and dissemination, *e.g.* metastasis (651). Therefore, work done by Kale and colleagues (683) identified and tested the small molecule inhibitor DJ4 that inhibits ROCK and MRCK by competing for their ATP-binding sites. When tested with multiple highly invasive cancer cell lines, DJ4 inhibited cell migration and invasion in a dose-dependent manner. Similar results were observed for BDP5290, a small molecule inhibitor developed by Unbekandt et al. (684) that also targets ROCK and MRCK, decreasing MLC phosphorylation, cell invasion and migration.

The partial effect observed after ROCK inhibition and the results found in the literature prompted us to test the role played by MRCK in cumulus cells during expansion. We showed that MRCK inhibition induces an elongated membrane bleb-free cell morphology that is accompanied by reduced migratory capacity. When ROCK and MRCK were simultaneously inhibited, the cumulus cells had their displacement severely affected besides the change in morphology and blebbing capacity. Thus, based on these results and the cited literature, a model

to explain the contributions of ROCK and MRCK to actomyosin contractility in cumulus cells during expansion can be created. Under normal *in vitro* culture conditions, where culture media has been supplemented with recombinant EGF and FBS to support expansion, ROCK and MRCK cooperate to produce the high levels of actomyosin required to sustain cumulus cell amoeboid migration away from the oocyte. If ROCK or MRCK are blocked, cumulus cells undergo an AMT and adapt to the lower actomyosin contractility levels. After this process, the activity of either ROCK or MRCK should generate enough actomyosin contractility to support cumulus cell mesenchymal migration away from the oocyte. However, if both ROCK and MRCK are blocked, cumulus cells have even lower actomyosin contractility that is not enough to sustain amoeboid or mesenchymal migration. Therefore, in this case, as well as when NMII is directly inhibited, cell migration is severely impaired.

### 2.5. Amoeboid cumulus cell migration during cumulus layer expansion is required for the sperm to reach the oocyte

After the LH surge, a complex containing the oocyte and the dispersed cumulus cells enveloped by the cumulus matrix is ovulated. Thus, before the sperm can breach the zona pellucida and fertilize the oocyte, it must first penetrate the cumulus layer. Here, we showed that decreased NMII activity - which translates into impaired cumulus cell migration during expansion - affects sperm's ability to penetrate the cumulus layer and reach the oocyte. We also showed this effect to be proportional to NMII inhibition levels: when NMII inhibition was partial due to targeting ROCK or MRCK individually, the number of sperm reaching the zona pellucida decreased by 50%; but if NMII activity was targeted directly or by inhibiting ROCK and MRCK simultaneously, the number of penetrating sperm dropped 80% in comparison to the control group.

The literature regarding sperm penetration of the cumulus layer describes the roles played by sperm-bound hyaluronidases. In mice, the hyaluronidases PH-20 and HYAL5 are expressed as glycosylphosphatidylinositol (GPI)-anchored membranous proteins and mediate the digestion of the hyaluronan backbone of the cumulus matrix, facilitating sperm penetration (685,686). However, we have evidence that cumulus matrix production is unaffected when either NMII activity, actin cytoskeletal rearrangement or cumulus cell detachment are inhibited. So, impairment of the interaction between the sperm hyaluronidase and the cumulus matrix

hyaluronan backbone is probably not the factor impeding sperm penetration of the cumulus layer of COCs with lower actomyosin contractility.

Closely examining the images obtained from the sperm penetration assay - a representative one for each group can be found in Figure 57a - it is possible to notice a negative correlation between the number of sperm close to the zona pellucida and the number of cumulus cells around the oocyte. That is because when the number of cumulus cells surrounding the oocyte is low, the number of sperm reaching the zona pellucida is high, as observed in the control EGF group. Conversely, when the number of cumulus cells is high, sperm reaching the zona pellucida is low. This analysis is in agreement with our key finding that cumulus cell displacement during cumulus layer expansion is, at least partially, due to active cumulus cell migration. Thus, it can be reasoned that, in normal conditions, the cumulus cells migrate away from the oocyte, which creates spaces between the cumulus cells and the cumulus cells and the oocyte. These spaces are filled up with the cumulus matrix, and before fertilization, sperm can swim through them with the help of their hyaluronidases and successfully make their way to the oocyte. However, when NMII activity is reduced, and cumulus cell migration is impaired, sperm can no longer swim between the cumulus cells and reach the oocyte.

This model generally applies to all the experimental groups analyzed, whether cumulus cell migration was partially affected – when ROCK or MRCK were targeted individually – or when cumulus cell migration was severely impaired – when NMII or ROCK+MRCK were inhibited. However, a specific distinction must be made: according to our results and interpretations, cumulus cells from COCs expanded in the presence of either ROCK or MRCK inhibitor were still able to migrate, even though they did not have the high actomyosin contractility to sustain the amoeboid migration and underwent an AMT process. This distinction is relevant because, even in these situations where the cumulus cells could migrate in a mesenchymal way, the average number of sperm able to reach the zona pellucida surroundings decreased by 50% in comparison to the control. It can be argued that the elongated cell tails of the mesenchymal migrating cumulus cells would constitute a physical barrier to the sperm, in opposition to the compact and round amoeboid cumulus cell’s bodies that would be present in normal conditions. Therefore, this analysis suggests that sperm penetration is not simply facilitated by cumulus cell migration but, more specifically, by amoeboid cumulus cell migration.

## 3. Limitations

The main limitation of the work presented in this thesis is the prevalence of *in vitro* treatments to test the raised hypotheses. *In vitro* cumulus layer experiments are limited because culture conditions do not closely recreate the preovulatory follicle environment for various reasons. Firstly, some key components present in the preovulatory follicle are missing in the tissue culture plate, such as mural granulosa or theca cells. These different cell types produce and secrete different components, known or unknown, that accumulate in the follicular fluid and could play a role in the process of cumulus layer expansion and be relevant to fertility. For example, the expression of Versican, a proteoglycan that integrates the cumulus matrix, and ADAMTS1, a metalloproteinase that participates in Versican's processing right before ovulation, is limited to the mural granulosa cells (349,687). Thus, COCs expanded *in vitro* in the absence of mural granulosa cells present cumulus matrices with altered composition (688). Secondly, even though the expansion culture media can induce cumulus layer expansion, it means that the COCs are exposed to a constant concentration of recombinant EGF, which differs from the varying expression pattern of the three EGF-like factors expressed in the periovulatory follicles (406). Similarly, the required FBS addition to the culture media could also misrepresent the blood serum components that enter the follicle upon the thinning of the follicular walls.

Perhaps equally important is the limitation of utilizing small-molecule inhibitors to test the hypotheses and models. Even though the straightforward pharmacological approach allowed us to target various proteins, it is not without flaws. For example, small molecule inhibitors usually have off-targets whose inhibition could contribute to the phenotype and make results hard to interpret. Moreover, due to the possibility of off-targets, the usage of small molecule inhibitors is usually done in different concentrations, in an approach called titration. While this allows phenotype confirmation, it also calls for more experimental groups, implicating a higher number of animals per replicate so a higher number of COCs can be collected.

Concerning other technical limitations, obtaining enough freshly collected COCs for each replicate was challenging. That is because there is a limited amount of full COCs that can be collected from an ovary without compromising sample quality. Thus, we aimed for every experimental group to have between 15-25 COCs, which limited the amount of protein or RNA extracted. However, after running some tests, we determined that some experiments required an

unattainably high number of COCs. For example, the relative quantification of pMLC by western blot was unsuccessful even with 100 COCs per group - hence why pMLC quantification was performed based on immunofluorescence experiments. Moreover, the type of samples employed also limited the utilization of other techniques, such as Small Interfering RNA (siRNA). For the siRNA-driven knockdown, the samples must be incubated with the siRNA for a period of 5 days, which impaired the tridimensional structure and developmental capacity of the COCs.

*Chapter 6:*

# Conclusion

## 1. General conclusion

This thesis aimed to determine if cumulus cell displacement during expansion is mediated by active cumulus cell migration. Based on the literature, this migration would depend on Non-muscle Myosin II (NMII) activity, which would power the rearrangement of the actin cytoskeleton and the extension of actin-related cellular protrusions. To investigate this central hypothesis, we devised two research objectives. The first aimed to investigate cumulus matrix production and how it relates both to cumulus cell displacement and regular hallmarks of cell migration, such as cell detachment and actin cytoskeletal rearrangement. The second objective sought to determine the molecular mechanism behind cumulus cell migration during cumulus layer expansion.

The results obtained are summarized in Figure 58. According to them, cumulus cells remain attached to each other and the oocyte during the first few hours of cumulus layer expansion. This attachment plays a role in maintaining high cumulus matrix production. However, after 4 hours of the start of the process, cumulus cells begin to display signs of migratory behaviour. For instance, they undergo an actin cytoskeletal reorganization, start extending actin-related cell structures such as membrane blebs and progressively become displaced away from the oocyte. Closely investigating this displacement, we confirmed that it does have an active cell migration component. Based on cumulus cell morphology, intense membrane blebbing and response to the molecular inhibitors targeting actomyosin contraction, we have determined that cumulus cells migrate using the amoeboid migration mode under normal *in vitro* culture conditions. This proved especially relevant when sperm penetration of the cumulus layer was investigated. We showed that sperm will not reach the oocyte at the same rate when cumulus cells assume an elongated morphology and migrate mesenchimally. In fact, sperm penetration is further affected if cumulus cell migration is impaired altogether.

## 2. Future work

The work presented in this thesis has established the foundations of a new molecular and cellular model for cumulus layer expansion. Future work can be proposed to further expand it and its potential clinical applications. Given that this model was established by employing an *in vitro* culture system for cumulus layer expansion, we would like to propose a series of experiments to validate it *in vivo*. For instance, cumulus pMLC levels could be measured before

a)

b)

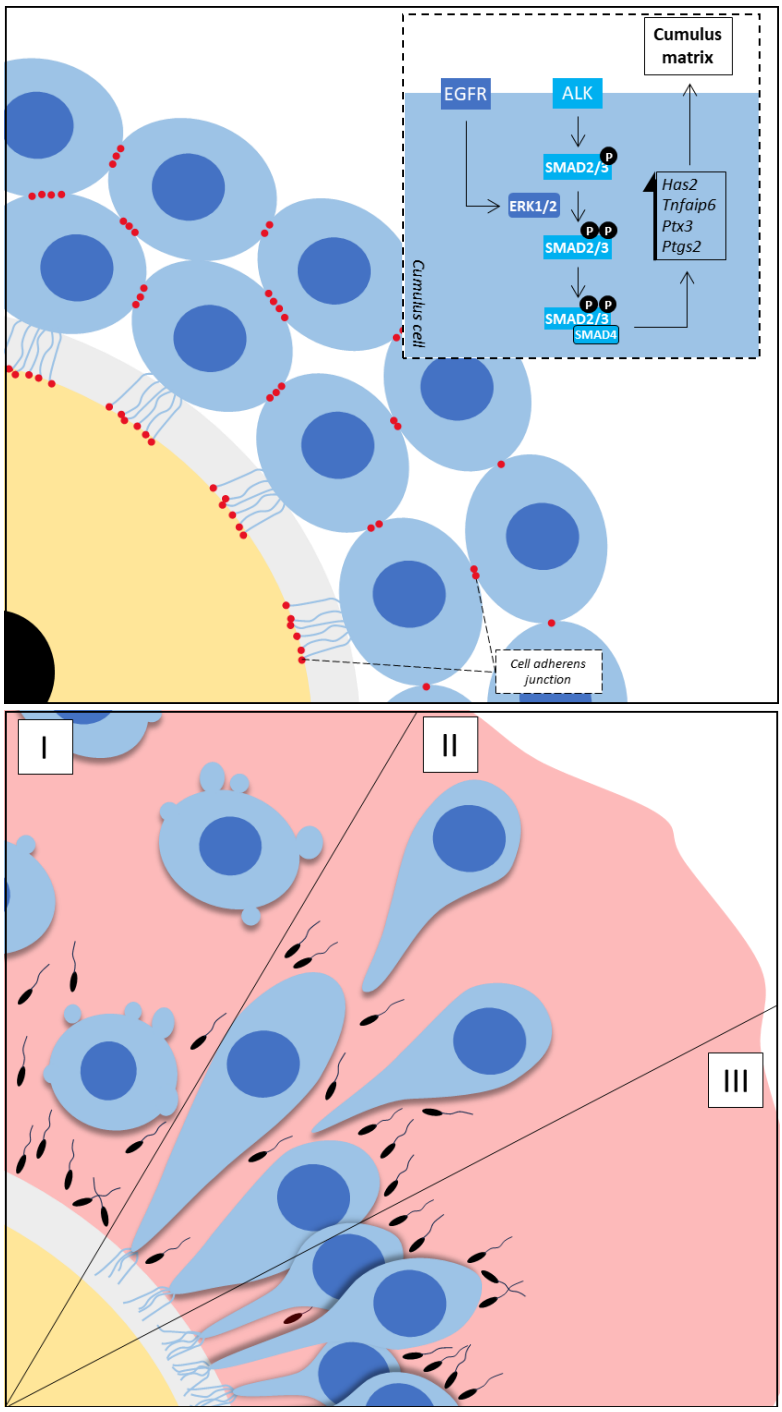


**Figure 58: Molecular and cellular mechanisms controlling cumulus layer expansion**. a) During the first few hours of the cumulus layer expansion process, cumulus cells remain attached to each other and the oocyte. This attachment aids in maintaining high TGFβ signalling that, paired with the boost provided by EGFR and ERK1/2 signalling, promotes the expression of genes related to producing the cumulus matrix - *Has2*, *Tnfaip6*, *Ptx3* and *Ptgs2*. b) After the 4-hour mark, cumulus cells start to exhibit phenotypical signs of migratory behaviour, such as actin cytoskeletal rearrangement, extension of actin-

related cellular protrusions and displacement away from the oocyte. According to the culture conditions and the level of Non-muscle Myosin II (NMII) activation, three different scenarios are possible. I: In normal culture conditions in which the media is supplemented with recombinant EGF and FBS, both NMII kinases - ROCK and MRCK - are active. Therefore, the cumulus cells are provided with the high actomyosin contractility required to sustain amoeboid migration, which creates enough space between the cumulus cells and the oocyte, facilitating sperm penetration of the cumulus layer. II: When either ROCK or MRCK is inhibited, NMII is only partially activated. This induces an Amoeboid to Mesenchymal Transition (AMT) in the cumulus cells that assume an elongated bleb-free morphology. This change in migration mode decreases the ability of the sperm to penetrate the cumulus layer and reach the oocyte. III: When NMII or both NMII kinases - ROCK and MRCK - are directly inhibited, actomyosin levels are too low to sustain even mesenchymal migration. Therefore, cumulus cells remain close to the zona pellucida, which impairs the ability of the sperm to penetrate the cumulus layer and reach the oocyte. The cumulus matrix, depicted in pink around the oocyte, is not affected by decreased NMII activity.

and after an exogenous ovulation stimulus to confirm that NMII also becomes activated during *in vivo* cumulus layer expansion.

NMII has three main isoforms – NMIIA, NMIIB, and NMIIC – that present slightly distinct kinetics, regulation and cell localization (603). Therefore, it could be advantageous to determine if a single isoform is the most predominant in cumulus cells during expansion. This information could facilitate the development of a conditional knockout model for NMII. Conditional deletion can be achieved by employing the *Cre/Lox* system, a site-specific recombinase technology based on the targeted expression of the Cre recombinase that recognizes specific *Lox* sequences and catalyzes the deletion of the region flanked by them (689). A granulosa cell-specific conditional knockout could be achieved by expressing the *Cre* recombinase under the control of the *Fshr* promoter, as done by Wang and colleagues (427), or under the control of the *Cyp19* promoter, as done by Fan and colleagues (274). This genetic model could be used to validate the *in vitro* findings presented here and also to further investigate the roles of NMII activity in the cumulus cells on ovulation and fertilization.

Lysophosphatidic acid (LPA) is a derivative phospholipid molecule that is found in the blood serum and has strong bioactive functions (690). After the ovulatory stimulus, the thinning of the follicular walls causes LPA to become enriched in the follicular fluid (691). This fact prompted studies to evaluate if the supplementation of *In Vitro* Maturation (IVM) culture media

with LPA could enhance oocyte development. In fact, it has been shown that adding LPA to culture media improves oocyte maturation, fertilization and blastocyst formation rates (692). As LPA main downstream signalling leads to the activation of RhoA and activation of NMII (690,693), we reason that LPA follicular fluid enrichment could play a role in enhancing NMII *in vivo* and further guaranteeing high NMII in the cumulus cells to support amoeboid migration during expansion. Moreover, it has been shown that LPA supplementation to denuded oocytes has a negative effect on maturation (694). Thus, the beneficial results observed after LPA addition to the IVM culture medium must be mediated by the cumulus cells, which suggests a role for cumulus cells' NMII activity in oocyte developmental competence. Therefore, the granulosa cell conditional knockout of NMII could also be employed to study oocyte developmental competence without granulosa cell NMII activity.

## 3. Clinical implications

The work presented in this thesis ties cellular and ovarian biology by determining a key role for active cumulus cell migration in the cumulus layer expansion process. In the broad scientific landscape, these results help expand the growing body of evidence supporting recently found key biological functions for MRCK (695). Regarding the ovary biology field, the knowledge herein described can hopefully be applied to clinical innovations in the future. Despite advances in diagnosis and treatments, unexplained infertility afflicts approximately 30% of infertile couples despite having had their ovulation and sperm quality confirmed (42). Therefore, unveiling this new molecular pathway that controls cumulus layer expansion and influences sperm penetration of the cumulus layer may offer new possibilities for further diagnosis and treatment of unexplained infertility.

Recent advances in Assisted Reproductive Techniques (ARTs) have helped infertile couples, single persons, and members of the LGBTQIA community achieve pregnancy. They have also aided young and adult women preserve their ovarian reserve while undergoing cancer treatment or natural aging processes. However, techniques such as IVM that require little to no exogenous hormonal stimulation still present low success rates. Therefore, effort has been put towards improving the culture conditions employed in IVM protocols in order to increase their similarity to physiological conditions and, therefore, improve overall success rates. The results presented here, alongside the proposed future work, offer the molecular basis to further support

the testing of culture media supplements that contribute to increasing NMII activity, such as LPA. Moreover, identified candidates responsible for boosting cumulus cells NMII during *in vivo* expansion, if produced in sufficient amounts in bodily fluids such as blood, for instance, may be employed as a fertility marker. Alternatively, further supplementation of these components could configure a less invasive and less costly approach to treating unexplained infertility cases.

## Bibliography


1. Casoni F, Malone SA, Belle M, Luzzati F, Collier F, Allet C, et al. Development of the neurons controlling fertility in humans: New insights from 3D imaging and transparent fetal brains. Development (Cambridge). 2016;143(21):3969-3981.
2. Gamble JA, Karunadasa DK, Pape JR, Skynner MJ, Todman MG, Bicknell RJ, et al. Disruption of ephrin signaling associates with disordered axophilic migration of the gonadotropin-releasing hormone neurons. Journal of Neuroscience. 2005;25(12):3142-50.
3. Bliss SP, Navratil AM, Xie J, Roberson MS. GnRH signaling, the gonadotrope and endocrine control of fertility. Frontiers in Neuroendocrinology. 2010;31(3):322-40.
4. Herbison AE. A simple model of estrous cycle negative and positive feedback regulation of GnRH secretion. Frontiers in Neuroendocrinology. 2020;57:100837.
5. Uenoyama Y, Nagae M, Tsuchida H, Inoue N, Tsukamura H. Role of KNDy Neurons Expressing Kisspeptin, Neurokinin B, and Dynorphin A as a GnRH Pulse Generator Controlling Mammalian Reproduction. Frontiers in Endocrinology. 2021;12:724632.
6. Herbison AE. The gonadotropin-releasing hormone pulse generator. Endocrinology. 2018; 159(11):3723-3736.
7. Di Iorgi N, Secco A, Napoli F, Calandra E, Rossi A, Maghnie M. Developmental abnormalities of the posterior pituitary gland. In: Endocrine Development. 2009;14:83-94.
8. Kelberman D, Rizzoti K, Lovell-Badge R, Robinson ICAF, Dattani MT. Genetic regulation of pituitary gland development in human and mouse. Endocrine Reviews. 2009; 30(7):790-829.
9. Zhu X, Gleiberman AS, Rosenfeld MG. Molecular physiology of pituitary development: Signaling and transcriptional networks. Physiological Reviews. 2007;87(3):933-63.
10. Talmadge K, Vamvakopoulos NC, Fiddes JC. Evolution of the genes for the β subunits of human chorionic gonadotropin and luteinizing hormone. Nature. 1984;307(5946).
11. Kourides IA, landon MB, hoffman BJ, Weintraub BD. Excess free alpha relative to beta subunits of the glycoprotein hormones in normal and abnormal human pituitary glands. Clin Endocrinol (Oxf). 1980;12(4).

12. Fetherston J, Boime I. Synthesis of bovine lutropin in cell-free lysates containing pituitary microsomes. Journal of Biological Chemistry. 1982;257(14).

13. Bousfield GR, Harvey DJ. Follicle-stimulating hormone glycobiology. Endocrinology. 2019;160(6):1515-1535.

14. Bousfield GR, Butnev VY, Butnev VY, Hiromasa Y, Harvey DJ, May J V. Hypo-glycosylated human follicle-stimulating hormone (hFSH21/18) is much more active in vitro than fully-glycosylated hFSH (hFSH24). Mol Cell Endocrinol. 2014;382(2):989-97.

15. Bishop LA, Robertson DM, Cahir N, Schofield PR. Specific roles for the asparagine-linked carbohydrate residues of recombinant human follicle stimulating hormone in receptor binding and signal transduction. Molecular Endocrinology. 1994;8(6):722-31.

16. Wide L, Eriksson K. Dynamic changes in glycosylation and glycan composition of serum FSH and LH during natural ovarian stimulation. Ups J Med Sci. 2013;118(3):153-64.

17. Butnev AY BG. Macro and Micro Heterogeneity in Pituitary and Urinary Follicle-Stimulating Hormone Glycosylation. J Glycomics Lipidomics. 2014;04(04):1000125.

18. Treloar AE, Boynton RE, Behn BG, Brown BW. Variation of the human menstrual cycle through reproductive life. Int J Fertil. 1970;12(1):77-126.

19. Robker RL, Richards JS. Hormone-Induced Proliferation and Differentiation of Granulosa Cells: A Coordinated Balance of the Cell Cycle Regulators Cyclin D2 and p27Kip1. Molecular Endocrinology. 1998;12(7):924-40.

20. Labhsetwar AP. Role of Estrogens in Ovulation: A Study Using the Estrogen-Antagonist, I.C.I. 46, 474. Endocrinology. 1970;87(3):542-51.

21. Chappell PE, Levine JE. Stimulation of gonadotropin-releasing hormone surges by estrogen. I. Role of hypothalamic progesterone receptors. Endocrinology. 2000;141(4):1477-85.

22. Woodruff TK, Besecke LM, Groome N, Draper LB, Schwartz NB, Weiss J. Inhibin A and Inhibin B Are Inversely Correlated to Follicle-Stimulating Hormone, Yet Are Discordant during the Follicular Phase of the Rat Estrous Cycle, and Inhibin A Is Expressed in a Sexually Dimorphic Manner. Endocrinology. 1996;137(12):5463-7.

23. Stocco C, Telleria C, Gibori G. The molecular control of corpus luteum formation, function, and regression. Endocrine Reviews. 2007;28(1):117-49.

24. Astwood EB. Changes in the weight and water content of the uterus of the normal adult rat. American Journal of Physiology-Legacy Content. 1939;126(1):1209-15.

25. Blandau RJ, Boling JL, Young WC. The length of heat in the albino rat as determined by the copulatory response. Anat Rec. 1941;79(4).

26. Bachelot A, Beaufaron J, Servel N, Kedzia C, Monget P, Kelly PA, et al. Prolactin independent rescue of mouse corpus luteum life span: Identification of prolactin and luteinizing hormone target genes. Am J Physiol Endocrinol Metab. 2009;297(3):E676-84.

27. Practice Committee of the American Society for Reproductive Medicine. Definitions of infertility and recurrent pregnancy loss: a committee opinion. Fertil Steril. 2020;113(3):533-535.

28. Zegers-Hochschild F, Adamson GD, Dyer S, Racowsky C, de Mouzon J, Sokol R, et al. The International Glossary on Infertility and Fertility Care. Fertil Steril. 2017;108(3):1786-1801.

29. Farquhar CM, Bhattacharya S, Repping S, Mastenbroek S et al. Female subfertility. Nature Reviews Disease Primers. 2019;5(1):7.

30. Bushnik T, Cook JL, Yuzpe AA, Tough S, Collins J. Estimating the prevalence of infertility in Canada. Human Reproduction. 2012;27(3):748-56.

31. Breitkopf DM, Hill M. Infertility Workup for the Women's Health Specialist. Obstetrics and Gynecology. 2019;133(6):1294-1295.

32. Eijkemans MJC, Van Poppel F, Habbema DF, Smith KR, Leridon H, Te Velde ER. Too old to have children? Lessons from natural fertility populations. Human Reproduction. 2014;29(6):1304-12.

33. Van Noord-Zaadstra BM, Looman CWN, Alsbach H, Habbema JDF, Te Velde ER, Karbaat J. Delaying childbearing: Effect of age on fecundity and outcome of pregnancy. Br Med J. 1991;302(6789):1361-5.

34. Norman RJ. Book Review Preservation of Fertility Edited by Togas Tulandi and Roger G. Gosden. 279 pp., illustrated. London, Taylor & Francis, 2004. New England Journal of Medicine. 2005;352(13).

35. Broekmans FJ, Soules MR, Fauser BC. Ovarian aging: Mechanisms and clinical consequences. Endocrine Reviews. 2009;30(5):465-93.

36. OECD. OECD Family Database. 2022. SF2.3: Age of mothers at childbirth and age-specific fertility.

37. Vassilakopoulou M, Boostandoost E, Papaxoinis G, de La Motte Rouge T, Khayat D, Psyrri A. Anticancer treatment and fertility: Effect of therapeutic modalities on reproductive system and functions. Vol. 97, Critical Reviews in Oncology/Hematology. 2016;97:328-34.

38. ACOG Practice Bulletin No. 194: Polycystic Ovary Syndrome. Obstetrics and gynecology. 2018;131(6):e157-e171.

39. Fauser BCJM, Tarlatzis BC, Rebar RW, Legro RS, Balen AH, Lobo R, et al. Consensus on women's health aspects of polycystic ovary syndrome (PCOS): The Amsterdam ESHRE/ASRM-Sponsored 3rd PCOS Consensus Workshop Group. In: Fertility and Sterility. 2012;97(1):28-38.e25.

40. Islam H, Masud J, Islam YN, Haque FKM. An update on polycystic ovary syndrome: A review of the current state of knowledge in diagnosis, genetic etiology, and emerging treatment options. Women's Health. 2022;18:17455057221117966.

41. Zondervan KT, Becker CM, Koga K, Missmer SA, Taylor RN, Viganò P. Endometriosis. Nature Reviews Disease Primers. 2018;4(1):9.

42. Ray A, Shah A, Gudi A, Homburg R. Unexplained infertility: An update and review of practice. Reproductive BioMedicine Online. 2012;24(6):591-602.

43. Hunault CC, Habbema JDF, Eijkemans MJC, Collins JA, Evers JLH, Velde ER. Two new prediction rules for spontaneous pregnancy leading to live birth among subfertile couple, based on the synthesis of three previous models. Human Reproduction. 2004;19(9):2019-26.

44. Stephen EH, Chandra A, King RB. Supply of and demand for assisted reproductive technologies in the United States: clinic- and population-based data, 1995–2010. In: Fertility and Sterility. 2016;105(2):451-8.

45. Ethics Committee of American Society for Reproductive Medicine. Access to fertility treatment by gays, lesbians, and unmarried persons: A committee opinion. Fertil Steril. 2013;100(6):1524-7.

46. Ethics Committee of American Society for Reproductive Medicine. Access to fertility services by transgender persons: An Ethics Committee opinion. Fertil Steril. 2015;104(5):874-878.

47. Wilcox AJ, Weinberg CR, Baird DD. Timing of Sexual Intercourse in Relation to Ovulation — Effects on the Probability of Conception, Survival of the Pregnancy, and Sex of the Baby. New England Journal of Medicine. 1995;333(23):1517-21.

48. Steptoe PC, Edwards RG. Birth after the reimplantation of a human embryo. Lancet. 1978;2(8085):366.

49. Steward RG, Lan L, Shah AA, Yeh JS, Price TM, Goldfarb JM, et al. Oocyte number as a predictor for ovarian hyperstimulation syndrome and live birth: An analysis of 256,381 in vitro fertilization cycles. Fertil Steril. 2014;101(4):967-73.

50. Van Der Westerlaken L, Helmerhorst F, Dieben S, Naaktgeboren N. Intracytoplasmic sperm injection as a treatment for unexplained total fertilization failure or low fertilization after conventional in vitro fertilization. Fertil Steril. 2005;83(3):612-7.

51. Gardner DK, Schoolcraft WB, Wagley L, Schlenker T, Stevens J, Hesla J. A prospective randomized trial of blastocyst culture and transfer in in-vitro fertilization. Human Reproduction. 1998;13(12):3434-40.

52. Glujovsky D, Quinteiro Retamar AM, Alvarez Sedo CR, Ciapponi A, Cornelisse S, Blake D. Cleavage-stage versus blastocyst-stage embryo transfer in assisted reproductive technology. Cochrane Database of Systematic Reviews. 2022;(6):CD002118.

53. Calhaz–Jorge C, De Geyter C, Kupka MS, De Mouzon J, Erb K, Mocanu E, et al. Assisted reproductive technology in Europe, 2013: Results generated from European registers by ESHRE. Human Reproduction. 2017;32(10):1957-1973.

54. Mourad S, Brown J, Farquhar C. Interventions for the prevention of OHSS in ART cycles: An overview of Cochrane reviews. Cochrane Database of Systematic Reviews. 2017;1(1):CD012103.

55. Kahnberg A, Enskog A, Brännström M, Lundin K, Bergh C. Prediction of ovarian hyperstimulation syndrome in women undergoing in vitro fertilization. Acta Obstet Gynecol Scand. 2009;88(12):1373-81.

56. Ashrafi M, Bahmanabadi A, Akhond MR, Arabipoor A. Predictive factors of early moderate/severe ovarian hyperstimulation syndrome in non-polycystic ovarian syndrome patients: a statistical model. Arch Gynecol Obstet. 2015;292(5):1145-52.

57. Trounson A, Wood C, Kausche A. In vitro maturation and the fertilization and developmental competence of oocytes recovered from untreated polycystic ovarian patients. Fertil Steril. 1994;62(2):353-62.

58. Ho VNA, Braam SC, Pham TD, Mol BW, Vuong LN. The effectiveness and safety of in vitro maturation of oocytes versus in vitro fertilization in women with a high antral follicle count. Human Reproduction. 2019;34(6):1055-1064.

59. Ortega-Hrepich C, Stoop D, Guzmán L, Van Landuyt L, Tournaye H, Smitz J, et al. A 'freeze-all' embryo strategy after in vitro maturation: A novel approach in women with polycystic ovary syndrome? Fertil Steril. 2013;100(4):1002-7.

60. Gremeau AS, Andreadis N, Fatum M, Craig J, Turner K, McVeigh E, et al. In vitro maturation or in vitro fertilization for women with polycystic ovaries? A case-control study of 194 treatment cycles. Fertil Steril. 2012;98(2):355-60.

61. Das M, Son WY, Buckett W, Tulandi T, Holzer H. In-vitro maturation versus IVF with GnRH antagonist for women with polycystic ovary syndrome: Treatment outcome and rates of ovarian hyperstimulation syndrome. Reprod Biomed Online. 2014;29(5):545-51.

62. Julania S, Walls ML, Hart R. The Place of in Vitro Maturation in PCO/PCOS. International Journal of Endocrinology. 2018:5750298.

63. Son WY, Tan SL. Laboratory and embryological aspects of hCG-primed in vitro maturation cycles for patients with polycystic ovaries. Hum Reprod Update. 2010;16(6):675-89.

64. Chian RC, Buckett WM, Tuiandi T, Tan SL. Prospective randomized study of human chorionic gonadotrophin priming before immature oocyte retrieval from unstimulated women with polycystic ovarian syndrome. Human Reproduction. 2000;15(1):165-70.

65. Ho VNA, Pham TD, Le AH, Ho TM, Vuong LN. Live birth rate after human chorionic gonadotropin priming in vitro maturation in women with polycystic ovary syndrome. J Ovarian Res. 2018;11(1):70.

66. De Vos M, Smitz J, Thompson JG, Gilchrist RB. The definition of IVM is clear - Variations need defining. Human Reproduction. 2016;31(11):2411-2415.

67. Gilchrist RB, Smitz J. Oocyte in vitro maturation: physiological basis and application to clinical practice. Fertility and Sterility. 2023;119(4):524-539.

68. Romero S, Sánchez F, Lolicato F, Van Ranst H, Smitz J. Immature oocytes from unprimed juvenile mice become a valuable source for embryo production when using C-type natriuretic peptide as essential component of culture medium. Biol Reprod. 2016;95(3):64.

69. Gilchrist RB, Luciano AM, Richani D, Zeng HT, Wang X, De Vos M, et al. Oocyte maturation and quality: Role of cyclic nucleotides. Reproduction. 2016;152(5):R143-57.

70. Sánchez F, Lolicato F, Romero S, De Vos M, Van Ranst H, Verheyen G, et al. An improved IVM method for cumulus-oocyte complexes from small follicles in polycystic ovary syndrome patients enhances oocyte competence and embryo yield. Human Reproduction. 2017;32(10):2056-2068.

71. Sanchez F, Le AH, Ho VNA, Romero S, Van Ranst H, De Vos M, et al. Biphasic in vitro maturation (CAPA-IVM) specifically improves the developmental capacity of oocytes from small antral follicles. J Assist Reprod Genet. 2019;36(10):2135-2144.

72. Grynberg M, Sonigo C, Santulli P. Fertility Preservation in Women. New England Journal of Medicine. 2018;378(4):400.

73. Practice Committee of American Society for Reproductive Medicine. Ovarian tissue cryopreservation: A committee opinion. Fertil Steril. 2014;101(5):1237-43.

74. Loren AW, Mangu PB, Beck LN, Brennan L, Magdalinski AJ, Partridge AH, et al. Fertility preservation for patients with cancer: American Society of Clinical Oncology clinical practice guideline update. Journal of Clinical Oncology. 2013;31(19):2500-10.

75. Bastings L, Beerendonk CCM, Westphal JR, Massuger LFAG, Kaal SEJ, van Leeuwen FE, et al. Autotransplantation of cryopreserved ovarian tissue in cancer survivors and the risk of reintroducing malignancy: A systematic review. Hum Reprod Update. 2013;19(5):483-506.

76. Dolmans MM, Luyckx V, Donnez J, Andersen CY, Greve T. Risk of transferring malignant cells with transplanted frozen-thawed ovarian tissue. Fertility and Sterility. 2013;99(6):1514-22.

77. Rosendahl M, Greve T, Andersen CY. The safety of transplanting cryopreserved ovarian tissue in cancer patients: A review of the literature. Journal of Assisted Reproduction and Genetics. 2013;30(1):11-24.

78. Ainsworth AJ, Allyse M, Khan Z. Fertility Preservation for Transgender Individuals: A Review. Mayo Clinic Proceedings. 2020;95(4):784-792.

79. Judge C, O'Donovan C, Callaghan G, Gaoatswe G, O'Shea D. Gender dysphoria - prevalence and co-morbidities in an Irish adult population. Front Endocrinol (Lausanne). 2014;5:87.

80. Extavour CG, Akam M. Mechanisms of germ cell specification across the metazoans: Epigenesis and preformation. Development. 2003;130(24):5869-84.

81. Lawson KA, Dunn NR, Roelen BAJ, Zeinstra LM, Davis AM, Wright CVE, et al. Bmp4 is required for the generation of primordial germ cells in the mouse embryo. Genes Dev. 1999;13(4):424-36.

82. Saitou M, Yamaji M. Germ cell specification in mice: Signaling, transcription regulation, and epigenetic consequences. Reproduction. 2010;139(6):931-42.

83. Sasaki K, Nakamura T, Okamoto I, Yabuta Y, Iwatani C, Tsuchiya H, et al. The Germ Cell Fate of Cynomolgus Monkeys Is Specified in the Nascent Amnion. Dev Cell. 2016;39(2):169-185.

84. Saga Y. Mouse germ cell development during embryogenesis. Current Opinion in Genetics and Development. 2008;18(4):337-41.

85. Ohinata Y, Payer B, O'Carroll D, Ancelin K, Ono Y, Sano M, et al. Blimp1 is a critical determinant of the germ cell lineage in mice. Nature. 2005;436(7048):207-13.

86. Zhao GQ. Consequences of knocking out BMP signaling in the mouse. Genesis (United States). 2003;35(1):43-56.

87. Senft AD, Bikoff EK, Robertson EJ, Costello I. Genetic dissection of Nodal and Bmp signalling requirements during primordial germ cell development in mouse. Nat Commun. 2019;10(1):1089.

88. Chuva De Sousa Lopes SM, Roelen BAJ, Monteiro RM, Emmens R, Lin HY, Li E, et al. BMP signaling mediated by ALK2 in the visceral endoderm is necessary for the generation of primordial germ cells in the mouse embryo. Genes Dev. 2004;18(15):1838-49.

89. Ying Y, Liu XM, Marble A, Lawson KA, Zhao GQ. Requirement of Bmp8b for the generation of primordial germ cells in the mouse. Molecular Endocrinology. 2000;14(7):1053-63.

90. Ying Y, Zhao GQ. Cooperation of endoderm-derived BMP2 and extraembryonic ectoderm-derived BMP4 in primordial germ cell generation in the mouse. Dev Biol. 2001;232(2):484-92.

91. Ginsburg M, Snow MHL, McLaren A. Primordial germ cells in the mouse embryo during gastrulation. Development. 1990;110(2):521-8.

92. Okamura D, Kimura T, Nakano T, Matsui Y. Cadherin-mediated cell interaction regulates germ cell determination in mice. Development. 2003;130(26):6423-30.

93. Bendel-Stenzel MR, Gomperts M, Anderson R, Heasman J, Wylie C. The role of cadherins during primordial germ cell migration and early gonad formation in the mouse. Mech Dev. 2000;91(1–2):143-52.

94. De Felici M, Scaldaferri ML, Farini D. Adhesion molecules for mouse primordial germ cells. Frontiers in bioscience: a journal and virtual library. 2005;10:542-51.

95. García-Castro MI, Anderson R, Heasman J, Wylie C. Interactions between germ cells and extracellular matrix glycoproteins during migration and gonad assembly in the mouse embryo. Journal of Cell Biology. 1997;138(2):471-80.

96. Lämmermann T, Sixt M. Mechanical modes of 'amoeboid' cell migration. Current Opinion in Cell Biology. 2009;21(5):636-44.

97. DeGennaro M, Hurd TR, Siekhaus DE, Biteau B, Jasper H, Lehmann R. Peroxiredoxin Stabilization of DE-Cadherin Promotes Primordial Germ Cell Adhesion. Dev Cell. 2011;20(2):233-43.

98. Anderson R, Copeland TK, Schöler H, Heasman J, Wylie C. The onset of germ cell migration in the mouse embryo. Mech Dev. 2000;91(1–2):61-8.

99. Molyneaux KA, Stallock J, Schaible K, Wylie C. Time-lapse analysis of living mouse germ cell migration. Dev Biol. 2001;240(2):488-98.

100. Chiquoine AD. The identification, origin, and migration of the primordial germ cells in the mouse embryo. Anat Rec. 1954;118(2):135-46.

101. Donovan PJ, Stott D, Cairns LA, Heasman J, Wylie CC. Migratory and postmigratory mouse primordial germ cells behave differently in culture. Cell. 1986;44(6):831-8.

102. Godin I, Wylie C, Heasman J. Genital ridges exert long-range effects on mouse primordial germ cell numbers and direction of migration in culture. Development. 1990;108(2):357-63.

103. Godin I, Wylie CC. TGFβ1 inhibits proliferation and has a chemotropic effect on mouse primordial germ cells in culture. Development. 1991;113(4):1451-7.

104. Doitsidou M, Reichman-Fried M, Stebler J, Köprunner M, Dörries J, Meyer D, et al. Guidance of primordial germ cell migration by the chemokine SDF-1. Cell. 2002;111(5):647-59.

105. Knaut H, Werz C, Geisler R, Busch-Nentwich E, Dahm R, Frohnhöfer HG, et al. A zebrafish homologue of the chemokine receptor Cxcr4 is a germ-cell guidance receptor. Nature. 2003;421(6920):279-82.

106. Ara T, Nakamura Y, Egawa T, Sugiyama T, Abe K, Kishimoto T, et al. Impaired colonization of the gonads by primordial germ cells in mice lacking a chemokine, stromal cell-derived factor-1 (SDF-1). Proc Natl Acad Sci U S A. 2003;100(9):5319-23.

107. Molyneaux KA, Zinszner H, Kunwar PS, Schaible K, Stebler J, Sunshine MJ, et al. The chemokine SDF1/CXCL12 and its receptor CXCR4 regulate mouse germ cell migration and survival. Development. 2003;130(18):4279-86.

108. Stebler J, Spieler D, Slanchev K, Molyneaux KA, Richter U, Cojocaru V, et al. Primordial germ cell migration in the chick and mouse embryo: The role of the chemokine SDF-1/CXCL12. Dev Biol. 2004;272(2):351-61.

109. Fernández JA, Bubner EJ, Takeuchi Y, Yoshizaki G, Wang T, Cummins SF, et al. Primordial germ cell migration in the yellowtail kingfish (Seriola lalandi) and identification of stromal cell-derived factor 1. Gen Comp Endocrinol. 2015;213:16-23.

110. Li M, Tan X, Jiao S, Wang Q, Wu Z, You F, et al. A new pattern of primordial germ cell migration in olive flounder (Paralichthys olivaceus) identified using nanos3. Dev Genes Evol. 2015;225(4):195-206.

111. Wong TT, Collodi P. Inducible Sterilization of Zebrafish by Disruption of Primordial Germ Cell Migration. PLoS One. 2013;8(6):e68455.

112. Baker TG, Franchi LL. The fine structure of oogonia and oocytes in human ovaries. J Cell Sci. 1967;2(2):213-24.

113. Sathananthan AH, Selvaraj K, Trounson A. Fine structure of human oogonia in the foetal ovary. Molecular and Cellular Endocrinology. 2000;161(1-2):3-8.

114. Pepling ME, Spradling AC. Female mouse germ cells form synchronously dividing cysts. Development. 1998;125(17):3323-8.

115. Pepling ME, Spradling AC. Mouse ovarian germ cell cysts undergo programmed breakdown to form primordial follicles. Dev Biol. 2001;234(2):339-51.

116. Pepling ME. From primordial germ cell to primordial follicle: Mammalian female germ cell development. Genesis (United States). 2006;44(12):622-32.

117. Suzuki H, Kanai-Azuma M, Kanai Y. From sex determination to initial folliculogenesis in mammalian ovaries: Morphogenetic waves along the anteroposterior and dorsoventral axes. Sexual Development. 2015;9(4):190-204.

118. Menke DB, Koubova J, Page DC. Sexual differentiation of germ cells in XX mouse gonads occurs in an anterior-to-posterior wave. Dev Biol. 2003;262(2):303-12.

119. Bowles J, Knight D, Smith C, Wilhelm D, Richman J, Mamiya S, et al. Retinoid signaling determines germ cell fate in mice. Science (1979). 2006;312(5773):596-600.

120. Koubova J, Menke DB, Zhou Q, Cape B, Griswold MD, Page DC. Retinoic acid regulates sex-specific timing of meiotic initiation in mice. Proc Natl Acad Sci U S A. 2006;103(8):2474-9.

121. Xu H, Beasley MD, Warren WD, van der Horst GTJ, McKay MJ. Absence of mouse REC8 cohesin promotes synapsis of sister chromatids in meiosis. Dev Cell. 2005;8(6):949-61.

122. Griswold MD, Hogarth CA, Bowles J, Koopman P. Initiating meiosis: The case for retinoic acid. Biology of Reproduction. 2012;86(2):35.

123. Liang GJ, Zhang XF, Wang JJ, Sun YC, Sun XF, Cheng SF, et al. Activin a accelerates the progression of fetal oocytes throughout meiosis and early oogenesis in the mouse. Stem Cells Dev. 2015;24(20):2455-65.

124. Nicol B, Yao HHC. Building an ovary: Insights into establishment of somatic cell lineages in the mouse. Sexual Development. 2014;8(5):243-51.

125. Chassot AA, Gregoire EP, Lavery R, Taketo MM, de Rooij DG, Adams IR, et al. RSPO1/β-Catenin signaling pathway regulates oogonia differentiation and entry into meiosis in the mouse fetal ovary. PLoS One. 2011;6(10):e25641.

126. Wang Y, Teng Z, Li G, Mu X, Wang Z, Feng L, et al. Cyclic AMP in oocytes controls meiotic prophase I and primordial folliculogenesis in the perinatal mouse ovary. Development. 2015;142(2):343-51.

127. Schmidt D, Ovitt CE, Anlag K, Fehsenfeld S, Gredsted L, Treier AC, et al. The murine winged-helix transcription factor Foxl2 is required for granulosa cell differentiation and ovary maintenance. Development. 2004;131(4):933-42.

128. Uda M, Ottolenghi C, Crisponi L, Garcia JE, Deiana M, Kimber W, et al. Foxl2 disruption causes mouse ovarian failure by pervasive blockage of follicle development. Hum Mol Genet. 2004;13(11):1171-81.

129. Padua MB, Fox SC, Jiang T, Morse DA, Tevosian SG. Simultaneous gene deletion of Gata4 and Gata6 leads to early disruption of follicular development and germ cell loss in the murine ovary. Biol Reprod. 2014;91(1):24.

130. Pepling ME, Sundman EA, Patterson NL, Gephardt GW, Medico L, Wilson KI. Differences in oocyte development and estradiol sensitivity among mouse strains. Reproduction. 2010;139(2):349-57.

131. Chassot AA, Ranc F, Gregoire EP, Roepers-Gajadien HL, Taketo MM, Camerino G, et al. Activation of β-catenin signaling by Rspo1 controls differentiation of the mammalian ovary. Hum Mol Genet. 2008;17(9):1264-77.

132. Vainio S, Heikkilä M, Kispert A, Chin N, McMahon AP. Female development in mammals is regulated by Wnt-4 signalling. Nature. 1999;397(6718):405-9.

133. Soyal SM, Amleh A, Dean J. FIGα, a germ cell-specific transcription factor required for ovarian follicle formation. Development. 2000;127(21):4645-54.

134. Joshi S, Davies H, Sims LP, Levy SE, Dean J. Ovarian gene expression in the absence of FIGLA, an oocyte-specific transcription factor. BMC Dev Biol. 2007;7:67.

135. Rajkovic A, Pangas SA, Ballow D, Suzumori N, Matzuk MM. NOBOX deficiency disrupts early folliculogenesis and oocyte-specific gene expression. Science (1979). 2004;305(5687):1157-9.

136. Choi Y, Qin Y, Berger MF, Ballow DJ, Bulyk ML, Rajkovic A. Microarray analyses of newborn mouse ovaries lacking Nobox. Biol Reprod. 2007;77(2):312-9.

137. Hunt PA, Hassold TJ. Human female meiosis: what makes a good egg go bad? Trends in Genetics. 2008;24(2):86-93.

138. Skinner MK. Regulation of primordial follicle assembly and development. Human Reproduction Update. 2005;11(5):461-71.

139. Rajah R, Glaser EM, Hirshfield AN. The changing architecture of the neonatal rat ovary during histogenesis. Developmental Dynamics. 1992;194(3):177-92.

140. Li J, Kawamura K, Cheng Y, Liu S, Klein C, Liu S, et al. Activation of dormant ovarian follicles to generate mature eggs. Proc Natl Acad Sci U S A. 2010;107(22):10280-4.

141. Juengel JL, Sawyer HR, Smith PR, Quirke LD, Heath DA, Lun S, et al. Origins of follicular cells and ontogeny of steroidogenesis in ovine fetal ovaries. Molecular and Cellular Endocrinology. 2002;191(1):1-10.

142. Kenngott RAM, Vermehren M, Ebach K, Sinowatz F. The role of ovarian surface epithelium in folliculogenesis during fetal development of the bovine ovary: A histological and immunohistochemical study. Sexual Development. 2013;7(4):180-95.

143. Zheng W, Zhang H, Liu K. The two classes of primordial follicles in the mouse ovary: Their development, physiological functions and implications for future research. Molecular Human Reproduction. 2014;20(4):286-92.

144. Halpin DMG, Charlton HM. Effects of short-term injection of gonadotrophins on ovarian follicle development in hypogonadal (hpg) mice. J Reprod Fertil. 1988;82(1):393-400.

145. Peters H, Byskov AG, Lintern-Moore S, Faber M, Andersen M. The effect of gonadotrophin on follicle growth initiation in the neonatal mouse ovary. J Reprod Fertil. 1973;35(1):139-41.

146. Kumar TR, Wang Y, Lu N, Matzuk MM. Follicle stimulating hormone is required for ovarian follicle maturation but not male fertility. Nat Genet. 1997;15(2):201-4.

147. Dierich A, Sairam MR, Monaco L, Fimia GM, Gansmuller A, Lemeur M, et al. Impairing follicle-stimulating hormone (FSH) signaling in vivo: Targeted disruption of the FSH receptor leads to aberrant gametogenesis and hormonal imbalance. Proc Natl Acad Sci U S A. 1998;95(23):13612-7.

148. Lintern-Moore S, Moore GPM. The initiation of follicle and oocyte growth in the mouse ovary. Biol Reprod. 1979;20(4):773-8.

149. Braw-Tal R. The initiation of follicle growth: The oocyte or the somatic cells? Molecular and Cellular Endocrinology. 2002;187(1-2):11-8.

150. Cantley LC. The phosphoinositide 3-kinase pathway. Science. 2002;296(5573):1655-7.

151. Inoki K, Li Y, Zhu T, Wu J, Guan KL. TSC2 is phosphorylated and inhibited by Akt and suppresses mTOR signalling. Nat Cell Biol. 2002;4(9):648-57.

152. Maehama T, Dixon JE. The tumor suppressor, PTEN/MMAC1, dephosphorylates the lipid second messenger, phosphatidylinositol 3,4,5-trisphosphate. Journal of Biological Chemistry. 1998;273(22):13375-8.

153. Brunet A, Bonni A, Zigmond MJ, Lin MZ, Juo P, Hu LS, et al. Akt promotes cell survival by phosphorylating and inhibiting a forkhead transcription factor. Cell. 1999;96(6):857-68.

154. John GB, Gallardo TD, Shirley LJ, Castrillon DH. Foxo3 is a PI3K-dependent molecular switch controlling the initiation of oocyte growth. Dev Biol. 2008;321(1):197-204.

155. Castrillon DH, Miao L, Kollipara R, Horner JW, DePinho RA. Suppression of ovarian follicle activation in mice by the transcription factor Foxo3a. Science (1979). 2003;301(5630):215-8.

156. Liu K, Zhang H, Risal S, Gorre N, Busayavalasa K, Li X, et al. Somatic cells initiate primordial follicle activation and govern the development of dormant oocytes in mice. Current Biology. 2014;24(21):2501-8.

157. Thomas FH, Vanderhyden BC. Oocyte-granulosa cell interactions during mouse follicular development: Regulation of kit ligand expression and its role in oocyte growth. Reproductive Biology and Endocrinology. 2006;4:19.

158. Hutt KJ, McLaughlin EA, Holland MK. Kit ligand and c-Kit have diverse roles during mammalian oogenesis and folliculogenesis. Molecular Human Reproduction. 2006;12(2):61-9.

159. Manova K, Nocka K, Besmer P, Bachvarova RF. Gonadal expression of c-kit encoded at the W locus of the mouse. Development. 1990;110(4):1057-69.

160. Kidder GM, Vanderhyden BC. Bidirectional communication between oocytes and follicle cells: Ensuring oocyte developmental competence. Canadian Journal of Physiology and Pharmacology. 2010;88(4):399-413.

161. Saatcioglu HD, Cuevas I, Castrillon DH. Control of Oocyte Reawakening by Kit. PLoS Genet. 2016;12(8):e1006215.

162. Reddy P, Liu L, Adhikari D, Jagarlamudi K, Rajareddy S, Shen Y, et al. Oocyte-specific deletion of pten causes premature activation of the primordial follicle pool. Science. 2008;319(5863):611-3.

163. Adhikari D, Flohr G, Gorre N, Shen Y, Yang H, Lundin E, et al. Disruption of Tsc2 in oocytes leads to overactivation of the entire pool of primordial follicles. Mol Hum Reprod. 2009;15(12):765-70.

164. Adhikari D, Zheng W, Shen Y, Gorre N, Hämäläinen T, Cooney AJ, et al. Tsc/mTORC1 signaling in oocytes governs the quiescence and activation of primordial follicles. Hum Mol Genet. 2009;19(3):397-410.

165. Hirshfield AN. Development of Follicles in the Mammalian Ovary. Int Rev Cytol. 1991;124(C):43-101.

166. Da Silva-Buttkus P, Jayasooriya GS, Mora JM, Mobberley M, Ryder TA, Baithun M, et al. Effect of cell shape and packing density on granulosa cell proliferation and formation of multiple layers during early follicle development in the ovary. J Cell Sci. 2008;121(23):3890-900.

167. Magoffin DA. Ovarian theca cell. International Journal of Biochemistry and Cell Biology. 2005;37(7):1344-9.

168. Knight PG, Satchell L, Glister C. Intra-ovarian roles of activins and inhibins. Molecular and Cellular Endocrinology. 2012;359(1-2):53-65.

169. Abel MH, Wootton AN, Wilkins V, Huhtaniemi I, Knight PG, Charlton HM. The effect of a null mutation in the follicle-stimulating hormone receptor gene on mouse reproduction. Endocrinology. 2000;141(5):1795-803.

170. McGee EA, Perlas E, LaPolt PS, Tsafriri A, Hsueh AJW. Follicle-stimulating hormone enhances the development of preantral follicles in juvenile rats. Biol Reprod. 1997;57(5):990-8.

171. Wright CS, Hovatta O, Margara R, Trew G, Winslon RML, Franks, et al. Effects of follicle-stimulating hormone and serum substitution on the in-vitro growth of human ovarian follicles. Human Reproduction. 1999;14(6):1555-62.

172. Cortvrindt R, Smitz J, Van Steirteghem AC. Assessment of the need for follicle stimulating hormone in early preantral mouse follicle culture in vitro. Human Reproduction. 1997;12(4):759-68.

173. Xu M, West-Farrell ER, Stouffer RL, Shea LD, Woodruff TK, Zelinski MB. Encapsulated three-dimensional culture supports development of nonhuman primate secondary follicles. Biol Reprod. 2009;81(3):587-94.

174. Kreeger PK, Fernandes NN, Woodruff TK, Shea LD. Regulation of mouse follicle development by follicle-stimulating hormone in a three-dimensional in vitro culture system is dependent on follicle stage and dose. Biol Reprod. 2005;73(5):942-50.

175. Zeleznik AJ. Follicle selection in primates: 'Many are called but few are chosen'. Biology of Reproduction. 2001;65(3):655-9.

176. Reddy P, Zheng W, Liu K. Mechanisms maintaining the dormancy and survival of mammalian primordial follicles. Trends in Endocrinology and Metabolism. 2010;21(2):96-103.

177. Richards JS. Maturation of ovarian follicles: actions and interactions of pituitary and ovarian hormones on follicular cell differentiation. Physiological Reviews. 1980;60(1):51-89.

178. Hsueh AJW, Billig H, Tsafriri A. Ovarian Follicle Atresia: A Hormonally Controlled Apoptotic Process. Endocr Rev. 1994;15(6):707-24.

179. Goodman HM. Hormonal Control of Reproduction in the Female. Basic Medical Endocrinology. 2003.

180. Hunzicker-Dunn M, Mayo K. Gonadotropin Signaling in the Ovary. Knobil and Neill's Physiology of Reproduction: Two-Volume Set. 2015.

181. Casarini L, Simoni M. Recent advances in understanding gonadotropin signaling. Fac Rev. 2021;10:41.

182. Richards JAS, Pangas SA. New insights into ovarian function. Handbook of Experimental Pharmacology. 2010;(198):3-27.

183. Edson MA, Nagaraja AK, Matzuk MM. The mammalian ovary from genesis to revelation. Endocrine Reviews. 2009;30(6):624-712.

184. Piquette GN, Lapolt PS, Oikawa M, Hsueh AJW. Regulation of luteinizing hormone receptor messenger ribonucleic acid levels by gonadotropins, growth factors, and gonadotropin-releasing hormone in cultured rat granulosa cells. Endocrinology. 1991;128(5):2449-56.

185. Law NC, Weck J, Kyriss B, Nilson JH, Hunzicker-Dunn M. Lhcgr expression in granulosa cells: Roles for PKA-phosphorylated β-catenin, TCF3, and FOXO1. Molecular Endocrinology. 2013;27(8):1295-310.

186. Erickson GF, Wang C, Hsueh AJW. FSH induction of functional LH receptors in granulosa cells cultured in a chemically defined medium. Nature. 1979;279(5711):336-8.

187. El-Hayek S, Demeestere I, Clarke HJ. Follicle-stimulating hormone regulates expression and activity of epidermal growth factor receptor in the murine ovarian follicle. Proc Natl Acad Sci U S A. 2014;111(47):16778-83.

188. De Leon V, Johnson A, Bachvarova R. Half-lives and relative amounts of stored and polysomal ribosomes and poly(A)+ RNA in mouse oocytes. Dev Biol. 1983;98(2):400-8.

189. Eppig JJ, O'Brien MJ. Development in vitro of mouse oocytes from primordial follicles. Biol Reprod. 1996;54(1):197-207.

190. Picton H, Briggs D, Gosden R. The molecular basis of oocyte growth and development. Molecular and Cellular Endocrinology. 1998;145(1-2):27-37.

191. Sánchez F, Smitz J. Molecular control of oogenesis. Biochimica et Biophysica Acta - Molecular Basis of Disease. 2012;1822(12):1896-912.

192. Schultz RM, Letourneau GE, Wassarman PM. Program of early development in the mammal: Changes in patterns and absolute rates of tubulin and total protein synthesis during oogenesis and early embryogenesis in the mouse. Dev Biol. 1979;68(2):341-59.

193. Sternlicht AL, Schultz RM. Biochemical studies of mammalian oogenesis: Kinetics of accumulation of total and poly(A)-containing RNA during growth of the mouse oocyte. Journal of Experimental Zoology. 1981;215(2):191-200.

194. Collado-fernandez E, Picton HM, Dumollard R. Metabolism throughout follicle and oocyte development in mammals. 2013;808(10-12):799–808.

195. Svoboda P, Franke V, Schultz RM. Sculpting the Transcriptome During the Oocyte-to-Embryo Transition in Mouse. Current Topics in Developmental Biology. 2015;113:305-49.

196. Mahrous E, Yang Q, Clarke HJ. Regulation of mitochondrial DNA accumulation during oocyte growth and meiotic maturation in the mouse. Reproduction. 2012;144(2):177-85.

197. Eichenlaub-Ritter U, Peschke M. Expression in in-vivo and in-vitro growing and maturing oocytes: Focus on regulation of expression at the translational level. Hum Reprod Update. 2002;8(1):21-41.

198. Bachvarova R, De Leon V, Johnson A, Kaplan G, Paynton B V. Changes in total RNA, polyadenylated RNA, and actin mRNA during meiotic maturation of mouse oocytes. Dev Biol. 1985;108(2):325-31.

199. Moore GPM, Lintern Moore S. A correlation between growth and RNA synthesis in the mouse oocyte. J Reprod Fertil. 1974;39(1):163-6.

200. Eppig JJ. A comparison between oocyte growth in coculture with granulosa cells and oocytes with granulosa cell-oocyte junctional contact maintained in vitro. Journal of Experimental Zoology. 1979;209(2):345-53.

201. Winterhager E, Kidder GM. Gap junction connexins in female reproductive organs: Implications for women's reproductive health. Hum Reprod Update. 2015;21(3):340-52.

202. Su YQ, Sugiura K, Eppig JJ. Mouse oocyte control of granulosa cell development and function: Paracrine regulation of cumulus cell metabolism. Seminars in Reproductive Medicine. 2009;27(1):32-42.

203. Sugiura K, Pendola FL, Eppig JJ. Oocyte control of metabolic cooperativity between oocytes and companion granulosa cells: Energy metabolism. Dev Biol. 2005;279(1):20-30.

204. Eppig JJ, Pendola FL, Wigglesworth K, Pendola JK. Mouse oocytes regulate metabolic cooperativity between granulosa cells and oocytes: Amino acid transport. Biol Reprod. 2005;73(2):351-7.

205. Su YQ, Sugiura K, Wigglesworth K, O'Brien MJ, Affourtit JP, Pangas SA, et al. Oocyte regulation of metabolic cooperativity between mouse cumulus cells and oocytes: BMP15 and GDF9 control cholesterol biosynthesis in cumulus cells. Development. 2008;135(1):111-21.

206. Elvin JA, Clark AT, Wang P, Wolfman NM, Matzuk MM. Paracrine actions of growth differentiation factor-9 in the mammalian ovary. Molecular Endocrinology. 1999;13(6):1035-48.

207. Laitinen M, Vuojolainen K, Jaatinen R, Ketola I, Aaltonen J, Lehtonen E, et al. A novel growth differentiation factor-9 (GDF-9) related factor is co- expressed with GDF-9 in mouse oocytes during folliculogenesis. Mech Dev. 1998;78(1–2):135-40.

208. Peng J, Li Q, Wigglesworth K, Rangarajan A, Kattamuri C, Peterson RT, et al. Growth differentiation factor 9:bone morphogenetic protein 15 heterodimers are potent regulators of ovarian functions. Proc Natl Acad Sci U S A. 2013;110(8):E776-85.

209. Mottershead DG, Sugimura S, Al-Musawi SL, Li JJ, Richani D, White MA, et al. Cumulin, an oocyte-secreted heterodimer of the transforming growth factor-β family, is a potent activator of granulosa cells and improves oocyte quality. Journal of Biological Chemistry. 2015;290(39):24007-20.

210. Kaivo-Oja N, Jeffery LA, Ritvos O, Mottershead DG. Smad signalling in the ovary. Reproductive Biology and Endocrinology. 2006;4:21.

211. Dong J, Albertini DF, Nishimori K, Kumar TR, Lu N, Matzuk MM. Growth differentiation factor-9 is required during early ovarian folliculogenesis. Nature. 1996;383(6600):531-5.

212. Carabatsos MJ, Elvin J, Matzuk MM, Albertini DF. Characterization of oocyte and follicle development in growth differentiation factor-9-deficient mice. Dev Biol. 1998;204(2):373-84.

213. Elvin JA, Yan C, Wang P, Nishimori K, Matzuk MM. Molecular characterization of the follicle defects in the growth differentiation factor 9-deficient ovary. Molecular Endocrinology. 1999;13(6):1018-34.

214. Dube JL, Wang P, Elvin J, Lyons KM, Celeste AJ, Matzuk MM. The bone morphogenetic protein 15 gene is X-linked and expressed in oocytes. Molecular Endocrinology. 1998;12(12):1809-17.

215. Otsuka F, Yao Z, Lee TH, Yamamoto S, Erickson GF, Shimasaki S. Bone morphogenetic protein-15: Identification of target cells and biological functions. Journal of Biological Chemistry. 2000;275(50):39523-8.

216. Yan C, Wang P, Demayo J, Demayo FJ, Elvin JA, Carino C, et al. Synergistic roles of bone morphogenetic protein 15 and growth differentiation factor 9 in ovarian function. Molecular Endocrinology. 2001;15(6):854-66.

217. Galloway SM, McNatty KP, Cambridge LM, Laitinen MPE, Juengel JL, Jokiranta TS, et al. Mutations in an oocyte-derived growth factor gene (BMP15) cause increased ovulation rate and infertility in a dosage-sensitive manner. Nat Genet. 2000;25(3):279-83.

218. Shimasaki S, Moore RK, Erickson GF, Otsuka F. The role of bone morphogenetic proteins in ovarian function. Reproduction (Cambridge, England) Supplement. 2003;61:323-37.

219. Hanrahan JP, Gregan SM, Mulsant P, Mullen M, Davis GH, Powell R, et al. Mutations in the Genes for Oocyte-Derived Growth Factors GDF9 and BMP15 Are Associated with Both Increased Ovulation Rate and Sterility in Cambridge and Belclare Sheep (Ovis aries). Biol Reprod. 2004;70(4):900-9.

220. Bodin L, Di Pasquale E, Fabre S, Bontoux M, Monget P, Persani L, et al. A novel mutation in the bone morphogenetic protein 15 gene causing defective protein secretion is

associated with both increased ovulation rate and sterility in Lacaune sheep. Endocrinology. 2007;148(1):393-400.

221. Martinez-Royo A, Jurado JJ, Smulders JP, Martí JI, Alabart JL, Roche A, et al. A deletion in the bone morphogenetic protein 15 gene causes sterility and increased prolificacy in Rasa Aragonesa sheep. Anim Genet. 2008;39(3):294-7.

222. Monteagudo L V., Ponz R, Tejedor MT, Laviña A, Sierra I. A 17 bp deletion in the Bone Morphogenetic Protein 15 (BMP15) gene is associated to increased prolificacy in the Rasa Aragonesa sheep breed. Anim Reprod Sci. 2009;110(1–2):139-46.

223. Juengel JL, Hudson NL, Heath DA, Smith P, Reader KL, Lawrence SB, et al. Growth differentiation factor 9 and bone morphogenetic protein 15 are essential for ovarian follicular development in sheep. Biol Reprod. 2002;67(6):1777-89.

224. Juengel JL, Hudson NL, Whiting L, McNatty KP. Effects of Immunization Against Bone Morphogenetic Protein 15 and Growth Differentiation Factor 9 on Ovulation Rate, Fertilization, and Pregnancy in Ewes. Biol Reprod. 2004;70(3):557-61.

225. Shimasaki S, Moore RK, Otsuka F, Erickson GF. The Bone Morphogenetic Protein System in Mammalian Reproduction. Endocrine Reviews. 2004;25(1):72-101.

226. Wu X, Chen L, Brown CA, Yan C, Matzuk MM. Interrelationship of growth differentiation factor 9 and inhibin in early folliculogenesis and ovarian tumorigenesis in mice. Molecular Endocrinology. 2004;18(6):1509-19.

227. Sugiura K, Su YQ, Diaz FJ, Pangas SA, Sharma S, Wigglesworth K, et al. Oocyte-derived BMP15 and FGFs cooperate to promote glycolysis in cumulus cells. Development. 2007;134(14):2593-603.

228. Chesnel F, Eppig JJ. Synthesis and accumulation of p34cdc2 and cyclin B in mouse oocytes during acquisition of competence to resume meiosis. Mol Reprod Dev. 1995;40(4):503-8.

229. De Vantéry C, Stutz A, Vassalli JD, Schorderet-Slatkine S. Acquisition of meiotic competence in growing mouse oocytes is controlled at both translational and posttranslational levels. Dev Biol. 1997;187(1):43-54.

230. Nishimura T, Shimaoka T, Kano K, Naito K. Insufficient amount of Cdc2 and continuous activation of wee1 B are the cause of meiotic failure in porcine growing oocytes. Journal of Reproduction and Development. 2009;55(5):553-7.

231. Adhikari D, Zheng W, Shen Y, Gorre N, Ning Y, Halet G, et al. Cdk1, but not Cdk2, is the sole Cdk that is essential and sufficient to drive resumption of meiosis in mouse oocytes. Hum Mol Genet. 2012;21(11):2476-84.

232. Erickson GF, Sorensen RA. In vitro maturation of mouse oocytes isolated from late, middle, and pre-antral graafian follicles. Journal of Experimental Zoology. 1974;190(1):123-7.

233. Norris RP, Freudzon M, Mehlmann LM, Cowan AE, Simon AM, Paul DL, et al. Luteinizing hormone causes MAP kinase-dependent phosphorylation and closure of connexin 43 gap junctions in mouse ovarian follicles: One of two paths to meiotic resumption. Development. 2008;135(19):3229-38.

234. Piontkewitz Y, Dekel N. Heptanol, an alkanol that blocks gap junctions, induces oocyte maturation. Endocrine. 1993;1(5):189-98.

235. Sela-Abramovich S, Edry I, Galiani D, Nevo N, Dekel N. Disruption of gap junctional communication within the ovarian follicle induces oocyte maturation. Endocrinology. 2006;147(5):2280-6.

236. Richard S, Baltz JM. Prophase I arrest of mouse oocytes mediated by natriuretic peptide precursor C requires GJA1 (connexin-43) and GJA4 (connexin-37) gap junctions in the antral follicle and cumulus-oocyte complex. Biol Reprod. 2014;90(6):137.

237. Horner K, Livera G, Hinckley M, Trinh K, Storm D, Conti M. Rodent oocytes express an active adenylyl cyclase required for meiotic arrest. Dev Biol. 2003;258(2):385-96.

238. Bender AT, Beavo JA. Cyclic nucleotide phosphodiesterases: Molecular regulation to clinical use. Pharmacological Reviews. 2006;58(3):488-520.

239. Vaccari S, Weeks JL, Hsieh M, Menniti FS, Conti M. Cyclic GMP signaling is involved in the luteinizing hormone-dependent meiotic maturation of mouse oocytes. Biol Reprod. 2009;81(3):595-604.

240. Masciarelli S, Horner K, Liu C, Park SH, Hinckley M, Hockman S, et al. Cyclic nucleotide phosphodiesterase 3A-deficient mice as a model of female infertility. Journal of Clinical Investigation. 2004;114(2):196-205.

241. Tsafriri A, Chun SY, Zhang R, Hsueh AJW, Conti M. Oocyte maturation involves campartmentalization and opposing changes of cAMP levels in follicular somatic and germ cells: Studies using selective phosphodiesterase inhibitors. Dev Biol. 1996;178(2):393-402.

242. Zhang M, Su YQ, Sugiura K, Xia G, Eppig JJ. Granulosa cell ligand NPPC and its receptor NPR2 maintain meiotic arrest in mouse oocytes. Science. 2010;330(6002):366-9.

243. Mora JM, Fenwick MA, Castle L, Baithun M, Ryder TA, Mobberley M, et al. Characterization and significance of adhesion and junction-related proteins in mouse ovarian follicles. Biol Reprod. 2012;86(5):153.

244. Anderson E, Wilkinson RF, Lee G, Meller S. A correlative microscopical analysis of differentiating ovarian follicles of mammals. J Morphol. 1978;156(3):339-66.

245. Baena V, Terasaki M. Three-dimensional organization of transzonal projections and other cytoplasmic extensions in the mouse ovarian follicle. Sci Rep. 2019;9(1):1262.

246. Wassarman PM, Litscher ES. Biogenesis of the Mouse Egg's Extracellular Coat, the Zona Pellucida. Current Topics in Developmental Biology. 2013;102:243-66.

247. Wassarman PM, Litscher ES. Influence of the zona pellucida of the mouse egg on folliculogenesis and fertility. International Journal of Developmental Biology. 2012;56(10–12):833-9.

248. Chiquoine AD. The development of the zona pellucida of the mammalian ovum. American Journal of Anatomy. 1960;106(2):149-69.

249. Albertini DF, Rider V. Patterns of intercellular connectivity in the mammalian cumulus-oocyte complex. Microsc Res Tech. 1994;27(2):125-33.

250. Motta PM, Correr S, Makabe S, Naguro T. Oocyte Follicle Cells Association during Development of Human Ovarian Follicle. A Study by High Resolution Scanning and Transmission Electron Microscopy. Arch Histol Cytol. 1994;57(4):369-94.

251. De Lesegno CV, Reynaud K, Pechoux C, Thoumire S, Chastant-Maillard S. Ultrastructure of canine oocytes during in vivo maturation. Mol Reprod Dev. 2008;75(1):115-25.

252. De Smedt V, Szöllösi D. Cytochalasin D treatment induces meiotic resumption in follicular sheep oocytes. Mol Reprod Dev. 1991;29(2):163-71.

253. Makita M, Miyano T. Steroid hormones promote bovine oocyte growth and connection with granulosa cells. Theriogenology. 2014;82(4):605-12.

254. Yi YJ, Nagyova E, Manandhar G, Procházka R, Sutovsky M, Park CS, et al. Proteolytic activity of the 26S proteasome is required for the meiotic resumption, germinal vesicle breakdown, and cumulus expansion of porcine cumulus-oocyte complexes matured in vitro. Biol Reprod. 2008;78(1):115-26.

255. Browne CL, Werner W. Intercellular junctions between the follicle cells and oocytes of Xenopus laevis. Journal of Experimental Zoology. 1984;230(1):105-13.

256. Schroeder TE. Microfilament-mediated surface change in starfish oocytes in response to 1-methyladenine: Implications for identifying the pathway and receptor sites for maturation-inducing hormones. Journal of Cell Biology. 1981;90(2):362-71.

257. Li R, Albertini DF. The road to maturation: Somatic cell interaction and self-organization of the mammalian oocyte. Nature Reviews Molecular Cell Biology. 2013;14(3):141-52.

258. Chaigne A, Campillo C, Gov NS, Voituriez R, Sykes C, Verlhac MH, et al. A narrow window of cortical tension guides asymmetric spindle positioning in the mouse oocyte. Nat Commun. 2015;6:6027.

259. Macaulay AD, Gilbert I, Caballero J, Barreto R, Fournier E, Tossou P, et al. The gametic synapse: RNA transfer to the bovine oocyte. Biol Reprod. 2014;91(4):90.

260. Barrett SL, Shea LD, Woodruff TK. Noninvasive index of cryorecovery and growth potential for human follicles in vitro. Biol Reprod. 2010;82(6):1180-9.

261. Mcginnis LK, Kinsey WH. Role of focal adhesion kinase in oocyte-follicle communication. Mol Reprod Dev. 2015;82(2):90-102.

262. Albertini DF, Combelles CMH, Benecchi E, Carabatsos MJ. Cellular basis for paracrine regulation of ovarian follicle development. Reproduction. 2001;121(5):647-53.

263. El-Hayek S, Yang Q, Abbassi L, FitzHarris G, Clarke HJ. Mammalian Oocytes Locally Remodel Follicular Architecture to Provide the Foundation for Germline-Soma Communication. Current Biology. 2018;28(7):1124-1131.e3.

264. Eppig JJ. FSH stimulates hyaluronic acid synthesis by oocyte-cumulus cell complexes from mouse preovulatory follicles. Nature. 1979;281(5731):483-4.

265. Eppig JJ. Gonadotropin stimulation of the expansion of cumulus oophori isolated from mice: General condition for expansion in vitro. Journal of Experimental Zoology. 1979;208(1):111-20.

266. Wang XN, Greenwald GS. Hypophysectomy of the cyclic mouse. I. Effects on folliculogenesis, oocyte growth, and follicle-stimulating hormone and human chorionic gonadotropin receptors. Biol Reprod. 1993;48(3):585-94.

267. Marsh JM. The role of cyclic AMP in gonadal steroidogenesis. Biology of Reproduction. 1976;14(1):30-53.

268. Richards JS. Hormonal Control of Gene Expression in the Ovary. Endocr Rev. 1994;15(6):725-51.

269. Salvador LM, Maizels E, Hales DB, Miyamoto E, Yamamoto H, Hunzicker-Dunn M. Acute signaling by the LH receptor is independent of protein kinase C activation. Endocrinology. 2002;143(8):2986-94.

270. Russell DL, Doyle KMH, Gonzales-Robayna I, Pipaon C, Richards JS. Egr-1 induction in rat granulosa cells by follicle-stimulating hormone and luteinizing hormone: Combinatorial regulation by transcription factors cyclic adenosine 3′,5′-monophosphate regulatory element binding protein, serum response factor, Sp1, and early growth response factor-1. Molecular Endocrinology. 2003;17(4):520-33.

271. Maizels ET, Cottom J, Jones JCR, Hunzicker-dunn M. Follicle stimulating hormone (FSH) activates the p38 mitogen-activated protein kinase pathway, inducing small heat shock protein phosphorylation and cell rounding in immature rat ovarian granulosa cells. Endocrinology. 1998;139(7):3353-6.

272. Panigone S, Hsieh M, Fu M, Persani L, Conti M. Luteinizing hormone signaling in preovulatory follicles involves early activation of the epidermal growth factor receptor pathway. Molecular Endocrinology. 2008;22(4):924-36.

273. Fan HY, Shimada M, Liu Z, Cahill N, Noma N, Wu Y, et al. Selective expression of KrasG12D in granulosa cells of the mouse ovary causes defects in follicle development and ovulation. Development. 2008;135(12):2127-37.

274. Fan HY, Liu Z, Shimada M, Sterneck E, Johnson PF, Hedrick SM, et al. MAPK3/1 (ERK1/2) in ovarian granulosa cells are essential for female fertility. Science. 2009;324(5929):938-41

275. Espey LL, Richards JAS. Temporal and spatial patterns of ovarian gene transcription following an ovulatory dose of gonadotropin in the rat. Biology of Reproduction. 2002;67(6):1662-70.

276. Park JY, Su YQ, Ariga M, Law E, Jin SLC, Conti M. EGF-Like Growth Factors as Mediators of LH Action in the Ovulatory Follicle. Science. 2004;303(5658):682-4

277. Rimon E, Sasson R, Dantes A, Land-Bracha A, Amsterdam A. Gonadotropin-induced gene regulation in human granulosa cells obtained from IVF patients: modulation of genes coding for growth factors and their receptors and genes involved in cancer and other diseases. Int J Oncol. 2004;24(5):1325-38.

278. Kansra S, Stoll SW, Johnson JL, Elder JT. Autocrine extracellular signal-regulated kinase (ERK) activation in normal human keratinocytes: Metalloproteinase-mediated release of amphiregulin triggers signaling from ErbB1 to ERK. Mol Biol Cell. 2004;15(9):4299-309.

279. Edwards RG, Gates AH. Timing of the stages of the maturation divisions, ovulation, fertilization and the first cleavage of eggs of adult mice treated with gonadotrophins. J Endocrinol. 1959;18(3):292-304.

280. Hubbard CJ. Cyclic AMP changes in the component cells of Graafian follicles: Possible influences on maturation in the follicle-enclosed oocytes of hamsters. Dev Biol. 1986;118(2):343-51.

281. Norris RP, Ratzan WJ, Freudzon M, Mehlmann LM, Krall J, Movsesian MA, et al. Cyclic GMP from the surrounding somatic cells regulates cyclic AMP and meiosis in the mouse oocyte. Development. 2009;136(11):1869-78.

282. Schultz RM, Montgomery RR, Belanoff JR. Regulation of mouse oocyte meiotic maturation: Implication of a decrease in oocyte cAMP and protein dephosphorylation in commitment to resume meiosis. Dev Biol. 1983;97(2):264-73.

283. Shuhaibar LC, Egbert JR, Norris RP, Lampe PD, Nikolaev VO, Thunemann M, et al. Intercellular signaling via cyclic GMP diffusion through gap junctions restarts meiosis in mouse ovarian follicles. Proc Natl Acad Sci U S A. 2015;112(17):5527-32.

284. Robinson JW, Zhang M, Shuhaibar LC, Norris RP, Geerts A, Wunder F, et al. Luteinizing hormone reduces the activity of the NPR2 guanylyl cyclase in mouse ovarian follicles, contributing to the cyclic GMP decrease that promotes resumption of meiosis in oocytes. Dev Biol. 2012;366(2):308-16.

285. Egbert JR, Shuhaibar LC, Edmund AB, Van Helden DA, Robinson JW, Uliasz TF, et al. Dephosphorylation and inactivation of NPR2 guanylyl cyclase in granulosa cells contributes to the LH-induced decrease in cGMP that causes resumption of meiosis in rat oocytes. Development (Cambridge). 2014;141(18):3594-604.

286. Liu X, Xie F, Zamah AM, Cao B, Conti M. Multiple pathways mediate luteinizing hormone regulation of cGMP signaling in the mouse ovarian follicle. Biol Reprod. 2014;91(1):9.

287. Zhang M, Su YQ, Sugiura K, Wigglesworth K, Xia G, Eppig JJ. Estradiol promotes and maintains cumulus cell expression of natriuretic peptide receptor 2 (NPR2) and meiotic arrest in mouse oocytes in vitro. Endocrinology. 2011;152(11):4377-85.

288. Tsuji T, Kiyosu C, Akiyama K, Kunieda T. CNP/NPR2 signaling maintains oocyte meiotic arrest in early antral follicles and is suppressed by EGFR-mediated signaling in preovulatory follicles. Mol Reprod Dev. 2012;79(11):795-802.

289. Kawamura K, Cheng Y, Kawamura N, Takae S, Okada A, Kawagoe Y, et al. Pre-ovulatory LH/hCG surge decreases C-type natriuretic peptide secretion by ovarian granulosa cells to promote meiotic resumption of pre-ovulatory oocytes. Human Reproduction. 2011;26(11):3094-101.

290. Corbin JD, Turko I V., Beasley A, Francis SH. Phosphorylation of phosphodiesterase-5 by cyclic nucleotide-dependent protein kinase alters its catalytic and allosteric cGMP-binding activities. Eur J Biochem. 2000;267(9):2760-7.

291. Rybalkin SD, Rybalkina IG, Fei R, Hofmann F, Beavo JA. Regulation of cGMP-specific phosphodiesterase (PDE5) phosphorylation in smooth muscle cells. Journal of Biological Chemistry. 2002;277(5):3310-7.

292. Hunzicker-Dunn M. Selective activation of rabbit ovarian protein kinase isozymes in rabbit ovarian follicles and corpora lutea. Journal of Biological Chemistry. 1981;256(23):12185-93.

293. Egbert JR, Uliasz TF, Shuhaibar LC, Geerts A, Wunder F, Kleiman RJ, et al. Luteinizing hormone causes phosphorylation and activation of the cGMP phosphodiesterase PDE5 in rat ovarian follicles, contributing, together with PDE1 activity, to the resumption of meiosis. Biol Reprod. 2016;94(5):12185-93.

294. Holt JE, Lane SIR, Jones KT. The Control of Meiotic Maturation in Mammalian Oocytes. Current Topics in Developmental Biology. 2013;102:207-26.

295. Bortolussi M, Zanchetta R, Doliana R, Castellani I, Bressan GM, Lauria A. Changes in the organization of the extracellular matrix in ovarian follicles during the preovulatory phase and atresia. An immunofluorescence study. Basic Appl Histochem. 1989;33(1):31-8.

296. Palotie A, Peltonen L, Foidart JM, Rajaniemi H. Immunohistochemical Localization of Basement Membrane Components and Interstitial Collagen Types in Preovulatory Rat Ovarian Follicles. Top Catal. 1984;4(4):279-87.

297. Trau HA, Davis JS, Duffy DM. Angiogenesis in the primate ovulatory follicle is stimulated by luteinizing hormone via prostaglandin E2. Biol Reprod. 2015;92(1):15.

298. Trau HA, Brännström M, Curry TE, Duffy DM. Prostaglandin E2 and vascular endothelial growth factor A mediate angiogenesis of human ovarian follicular endothelial cells. Human Reproduction. 2016;31(2):436-44.

299. Espey LL. Current status of the hypothesis that mammalian ovulation is comparable to an inflammatory reaction. Biology of Reproduction. 1994;50(2):233-8.

300. Murdoch WJ, Wilken C, Young DA. Sequence of apoptosis and inflammatory necrosis within the formative ovulatory site of sheep follicles. J Reprod Fertil. 1999;117(2):325-9.

301. Espey LL. Ultrastructure of the apex of the rabbit graafian follicle during the ovulatory process. Endocrinology. 1967;81(2):267-76.

302. McClean D, Rowlands IW. Role of hyaluronidase in fertilization. Nature. 1942;150(3813) :118-9.

303. Weissmann B, Meyer K. The Structure of Hyalobiuronic Acid and of Hyaluronic Acid from Umbilical Cord. J Am Chem Soc. 1954;76(7).

304. Cell Biology of Extracellular Matrix. Cell Biology of Extracellular Matrix. 1988.

305. Weigel PH. Hyaluronan Synthase: The Mechanism of Initiation at the Reducing End and a Pendulum Model for Polysaccharide Translocation to the Cell Exterior. International Journal of Cell Biology. 2015;2015:367579.

306. Itano N, Sawai T, Yoshida M, Lenas P, Yamada Y, Imagawa M, et al. Three isoforms of mammalian hyaluronan synthases have distinct enzymatic properties. Journal of Biological Chemistry. 1999;274(35):25085-92.

307. Vigetti D, Karousou E, Viola M, Deleonibus S, De Luca G, Passi A. Hyaluronan: Biosynthesis and signaling. Biochimica et Biophysica Acta - General Subjects. 2014;840(8):2452-9.

308. Schulz T, Schumacher U, Prehm P. Hyaluronan export by the ABC transporter MRP5 and its modulation by intracellular cGMP. Journal of Biological Chemistry. 2007;282(29):20999-1004.

309. Csoka AB, Frost GI, Stern R. The six hyaluronidase-like genes in the human and mouse genomes. Matrix Biology. 2001;20(8):499-508.

310. Fülöp C, Salustri A, Hascall VC. Coding sequence of a hyaluronan synthase homologue expressed during expansion of the mouse cumulus-oocyte complex. Arch Biochem Biophys. 1997;337(2):261-6.

311. Salustri A, Yanagishita M, Underhill CB, Laurent TC, Hascall VC. Localization and synthesis of hyaluronic acid in the cumulus cells and mural granulosa cells of the preovulatory follicle. Dev Biol. 1992;151(2):541-51.

312. Eppig JJ. Regulation of cumulus oophorus expansion by gonadotropins in vivo and in vitro. Biol Reprod. 1980;23(3):545-52.

313. Salustri A, Yanagishita M, Hascall VC. Synthesis and accumulation of hyaluronic acid and proteoglycans in the mouse cumulus cell-oocyte complex during follicle-stimulating hormone-induced mucification. Journal of Biological Chemistry. 1989;264(23):13840-7.

314. Zuelke KA, Brackett BG. Effects of luteinizing hormone on glucose metabolism in cumulus-enclosed bovine oocytes matured in vitro. Endocrinology. 1992;131(6):2690-6.

315. Roy SK, Terada DM. Activities of glucose metabolic enzymes in human preantral follicles: In vitro modulation by follicle-stimulating hormone, luteinizing hormone,

epidermal growth factor, insulin-like growth factor I, and transforming growth factor β1. Biol Reprod. 1999;60(3):763-8.

316. Tsafriri A, Lieberman ME, Ahren K, Lindner HR. Dissociation between LH induced aerobic glycolysis and oocyte maturation in cultured Graafian follicles of the rat. Acta Endocrinol (Copenh). 1976;81(2):362-6.

317. Sutton ML, Gilchrist RB, Thompson JG. Effect of in-vivo and in-vitro environments on the metabolism of the cumulus-oocyte complex and its influence on oocyte developmental capacity. Human Reproduction Update. 2003;9(1):35-48.

318. Sutton-McDowall ML, Gilchrist RB, Thompson JG. Cumulus expansion and glucose utilisation by bovine cumulus-oocyte complexes during in vitro maturation: The influence of glucosamine and follicle-stimulating hormone. Reproduction. 2004;128(3):313-9.

319. Yudin AI, Cherr GN, Katz DF. Structure of the cumulus matrix and zona pellucida in the golden hamster: A new view of sperm interaction with oocyte-associated extracellular matrices. Cell Tissue Res. 1988;251(3):555-64.

320. Cherr GN, Yudin AI, Katz DF. Organization of the Hamster Cumulus Extracellular Matrix: A Hyaluronate-Glycoprotein Gel which Modulates Sperm Access to the Oocyte: Extracellular matrix/Hyaluronate/Oocyte-cumulus complex/Extracellular matrix glycoproteins/Sperm enzymes. Dev Growth Differ. 1990;32(4):353-365.

321. Chen L, Mao SJT, Larsen WJ. Identification of a factor in fetal bovine serum that stabilizes the cumulus extracellular matrix. A role for a member of the inter-α-trypsin inhibitor family. Journal of Biological Chemistry. 1992;267(17):12380-6.

322. Zhuo L, Salustri A, Kimata K. A physiological function of serum proteoglycan bikunin: The chondroitin sulfate moiety plays a central role. Glycoconjugate Journal. 2002; 19(4-5):241-7.

323. Mcclure N, Macpherson AM, Healy DL, Wreford N, Roger PAW. An immunohistochemical study of the vascularization of the human graafian follicle. Human Reproduction. 1994;9(8):1401-5.

324. Irving-Rodgers HF, Mussard ML, Kinder JE, Rodgers RJ. Composition and morphology of the follicular basal lamina during atresia of bovine antral follicles. Reproduction. 2002;123(1):97-106.

325. Nagyova E, Camaioni A, Prochazka R, Salustri A. Covalent transfer of heavy chains of inter-α-trypsin inhibitor family proteins to hyaluronan in in vivo and in vitro expanded porcine oocyte-cumulus complexes. Biol Reprod. 2004;71(6):1838-43.

326. Chen L, Zhang H, Powers RW, Russell PT, Larsen WJ. Covalent linkage between proteins of the inter-α-inhibitor family and hyaluronic acid is mediated by a factor produced by granulosa cells. Journal of Biological Chemistry. 1996;271(32):19409-14.

327. Zhuo L, Yoneda M, Zhao M, Yingsung W, Yoshida N, Kitagawa Y, et al. Defect in SHAP-hyaluronan complex causes severe female infertility. A study by inactivation of the bikunin gene in mice. Journal of Biological Chemistry. 2001;276(11):7693-6.

328. Sato H, Kajikawa S, Kuroda S, Horisawa Y, Nakamura N, Kaga N, et al. Impaired fertility in female mice lacking urinary trypsin inhibitor. Biochem Biophys Res Commun. 2001;281(5):1154-60.

329. Chen L, Mao SJT, McLean LR, Powers RW, Larsen WJ. Proteins of the inter-α-trypsin inhibitor family stabilize the cumulus extracellular matrix through their direct binding with hyaluronic acid. Journal of Biological Chemistry. 1994;269(45):28282-7.

330. Milner CM, Higman VA, Day AJ. TSG-6: A pluripotent inflammatory mediator? Biochemical Society Transactions. 2006;34(Pt 3):446-50.

331. Yoshioka S, Ochsner S, Russell DL, Ujioka T, Fujii S, Richards JS, et al. Expression of tumor necrosis factor-stimulated gene-6 in the rat ovary in response to an ovulatory dose of gonadotropin. Endocrinology. 2000;141(11):4114-9.

332. Carrette O, Nemade R V., Day AJ, Brickner A, Larsen WJ. TSG-6 is concentrated in the extracellular matrix of mouse cumulus oocyte complexes through hyaluronan and inter-alpha-inhibitor binding. Biol Reprod. 2001;65(1):301-8.

333. Mukhopadhyay D, Hascall VC, Day AJ, Salustri A, Fulop C. Two distinct populations of tumor necrosis factor-stimulated gene-6 protein in the extracellular matrix of expanded mouse cumulus cell-oocyte complexes. Arch Biochem Biophys. 2001;394(2):173-81.

334. Ochsner SA, Day AJ, Rugg MS, Breyer RM, Gomer RH, Richards JS. Disrupted function of tumor necrosis factor-α-stimulated gene 6 blocks cumulus cell-oocyte complex expansion. Endocrinology. 2003;144(10):4376-84.

335. Kahmann JD, O'Brien R, Werner JM, Heinegård D, Ladbury JE, Campbell ID, et al. Localization and characterization of the hyaluronan-binding site on the Link module from human TSG-6. Structure. 2000;8(7):763-74.

336. Fülöp C, Szántó S, Mukhopadhyay D, Bárdos T, Kamath R V., Rugg MS, et al. Impaired cumulus mucification and female sterility in tumor necrosis factor-induced protein-6 deficient mice. Development. 2003;130(10):2253-61.

337. Jessen TE, Ødum L. Role of tumour necrosis factor stimulated gene 6 (TSG-6) in the coupling of inter-α-trypsin inhibitor to hyaluronan in human follicular fluid. Reproduction. 2003;125(1):27-31.

338. Rugg MS, Willis AC, Mukhopadhyay D, Hascall VC, Fries E, Fülöp C, et al. Characterization of complexes formed between TSG-6 and inter-α- inhibitor that act as intermediates in the covalent transfer of heavy chains onto hyaluronan. Journal of Biological Chemistry. 2005;280(27):25674-86.

339. Sanggaard KW, Karring H, Valnickova Z, Thøgersen IB, Enghild JJ. The TSG-6 and IαI interaction promotes a transesterification cleaving the protein-glycosaminoglycan-protein (PGP) cross-link. Journal of Biological Chemistry. 2005;280(12):11936-42.

340. Doni A, Garlanda C, Mantovani A. Innate immunity, hemostasis and matrix remodeling: PTX3 as a link. Seminars in Immunology. 2016;8(6):570-577.

341. Varani S, Elvin JA, Yan C, Demayo J, Demayo FJ, Horton HF, et al. Knockout of pentraxin 3, a downstream target of growth differentiation factor-9, causes female subfertility. Molecular Endocrinology. 2002;16(6):1154-67.

342. Salustri A, Garlanda C, Hirsch E, De Acetis M, Maccagno A, Bottazi B, et al. PTX3 plays a key role in the organization of the cumulus oophorus extracellular matrix and in in vivo fertilization. Development. 2004;16(6):1154-67.

343. Inforzato A, Rivieccio V, Morreale AP, Bastone A, Salustri A, Scarchilli L, et al. Structural characterization of PTX3 disulfide bond network and its multimeric status in cumulus matrix organization. Journal of Biological Chemistry. 2008;283(15):10147-61.

344. Scarchilli L, Camaioni A, Bottazzi B, Negri V, Doni A, Deban L, et al. PTX3 interacts with inter-α-trypsin inhibitor: Implications for hyaluronan organization and cumulus oophorus expansion. Journal of Biological Chemistry. 2007;282(41):30161-70.

345. Ievoli E, Lindstedt R, Inforzato A, Camaioni A, Palone F, Day AJ, et al. Implication of the oligomeric state of the N-terminal PTX3 domain in cumulus matrix assembly. Matrix Biology. 2011;30(5–6):330-7.

346. Baranova NS, Inforzato A, Briggs DC, Tilakaratna V, Enghild JJ, Thakar D, et al. Incorporation of pentraxin 3 into hyaluronan matrices is tightly regulated and promotes matrix cross-linking. Journal of Biological Chemistry. 2014;289(44):30481-30498.

347. Briggs DC, Birchenough HL, Ali T, Rugg MS, Waltho JP, Ievoli E, et al. Metal Ion-dependent heavy chain transfer activity of TSG-6 mediates assembly of the cumulus-oocyte matrix. Journal of Biological Chemistry. 2015;290(48):28708-23.

348. Camaioni A, Salustri A, Yanagishita M, Hascall VC. Proteoglycans and proteins in the extracellular matrix of mouse cumulus cell-oocyte complexes. Arch Biochem Biophys. 1996;325(2):190-8.

349. Russell DL, Ochsner SA, Hsieh M, Mulders S, Richards JS. Hormone-regulated expression and localization of versican in the rodent ovary. Endocrinology. 2003;144(3):1020-31.

350. Familiari G, Verlengia C, Nottola SA, Renda T, Micara G, Aragona C, et al. Heterogeneous distribution of fibronectin, tenascin-C, and laminin immunoreactive material in the cumulus-corona cells surrounding mature human oocytes from IVF-ET protocols - Evidence that they are composed of different subpopulations: An immunohistochemical study using scanning confocal laser and fluorescence microscopy. Mol Reprod Dev. 1996;43(3):392-402.

351. Relucenti M, Heyn R, Correr S, Familiari G. Cumulus oophorus extracellular matrix in the human oocyte: A role for adhesive proteins. Italian Journal of Anatomy and Embryology. 2005;110(2 Suppl 1):219-24.

352. Richards JAS, Hernandez-Gonzalez I, Gonzalez-Robayna I, Teuling E, Lo Y, Boerboom D, et al. Regulated expression of ADAMTS family members in follicles and cumulus oocyte complexes: Evidence for specific and redundant patterns during ovulation. Biol Reprod. 2005;72(5):1241-55.

353. Yanagishita M, Hascall VC. Biosynthesis of proteoglycans by rat granulosa cells cultured in vitro. Journal of Biological Chemistry. 1979;254(24):12355-64.

354. Kobayashi H, Sun GW, Hirashima Y, Terao T. Identification of link protein during follicle development and cumulus cell cultures in rats. Endocrinology. 1999;140(8):3835-42.

355. Brown HM, Dunning KR, Robker RL, Boerboom D, Pritchard M, Lane M, et al. ADAMTS1 cleavage of versican mediates essential structural remodeling of the ovarian follicle and cumulus-oocyte matrix during ovulation in mice. Biol Reprod. 2010;83(4):549-57.

356. Liao HX, Lee DM, Levesque MC, Haynes BF. N-terminal and central regions of the human CD44 extracellular domain participate in cell surface hyaluronan binding. The Journal of Immunology. 1995;155(8):3938-45.

357. Prochazka L, Tesarik R, Turanek J. Regulation of alternative splicing of CD44 in cancer. Cellular Signalling. 2014;26(10):2234-9.

358. Knudson W, Chow G, Knudson CB. CD44-mediated uptake and degradation of hyaluronan. Matrix Biology. 2002;21(1):15-23.

359. Carvalho AM, Reis RL, Pashkuleva I. Hyaluronan Receptors as Mediators and Modulators of the Tumor Microenvironment. Advanced Healthcare Materials. 2023;12(5):e2202118.

360. Tolg C, McCarthy JB, Yazdani A, Turley EA. Hyaluronan and RHAMM in Wound Repair and the 'cancerization' of Stromal Tissues. BioMed Research International. 2014;2014:103923.

361. Day AJ, Prestwich GD. Hyaluronan-binding proteins: Tying up the giant. Journal of Biological Chemistry. 2002;277(7):4585-8.

362. Telmer PG, Tolg C, McCarthy JB, Turley EA. How does a protein with dual mitotic spindle and extracellular matrix receptor functions affect tumor susceptibility and progression? Commun Integr Biol. 2011;4(2):182-5.

363. Misra S, Hascall VC, Markwald RR, Ghatak S. Interactions between hyaluronan and its receptors (CD44, RHAMM) regulate the activities of inflammation and cancer. Frontiers in Immunology. 2015;6:201.

364. Crainie M, Belch AR, Mant MJ, Pilarski LM. Overexpression of the receptor for hyaluronan-mediated motility (RHAMM) characterizes the malignant clone in multiple myeloma: Identification of three distinct RHAMM variants. Blood. 1999;93(5):1684-96.

365. Assmann V, Marshall JF, Fieber C, Hofmann M, Hart IR. The human hyaluronan receptor RHAMM is expressed as an intracellular protein in breast cancer cells. J Cell Sci. 1998;111(Pt 12):1685-94.

366. Entwistle J, Hall CL, Turley EA. HA receptors: Regulators of signalling to the cytoskeleton. Journal of Cellular Biochemistry. 1996;61(4):569-77.

367. Tolg C, Hamilton SR, Nakrieko KA, Kooshesh F, Walton P, McCarthy JB, et al. Rhamm-/- fibroblasts are defective in CD44-mediated ERK1,2 motogenic signaling, leading to defective skin wound repair. Journal of Cell Biology. 2006;175(6):1017-28.

368. Hamilton SR, Fard SF, Paiwand FF, Tolg C, Veiseh M, Wang C, et al. The hyaluronan receptors CD44 and Rhamm (CD168) form complexes with ERK1,2 that sustain high basal motility in breast cancer cells. Journal of Biological Chemistry. 2007;282(22):16667-80.

369. Park D, Kim Y, Kim H, Kim K, Lee YS, Choe J, et al. Hyaluronic acid promotes angiogenesis by inducing RHAMM-TGFβ receptor interaction via CD44-PKCδ. Mol Cells. 2012;33(6):563-74.

370. Maxwell CA, Keats JJ, Belch AR, Pilarski LM, Reiman T. Receptor for hyaluronan-mediated motility correlates with centrosome abnormalities in multiple myeloma and maintains mitotic integrity. Cancer Res. 2005;65(3):850-60.

371. Assmann V, Jenkinson D, Marshall JF, Hart IR. The intracellular hyaluronan receptor RHAMM/IHABP interacts with microtubules and actin filaments. J Cell Sci. 1999;112(22):3943-54.

372. Ohta N, Saito H, Kuzumaki T, Takahashi T, Ito MM, Saito T, et al. Expression of CD44 in human cumulus and mural granulosa cells of individual patients in in-vitro fertilization programmes. Mol Hum Reprod. 1999;5(1):22-8.

373. Schoenfelder M, Einspanier R. Expression of hyaluronan synthases and corresponding hyaluronan receptors is differentially regulated during oocyte maturation in cattle. Biol Reprod. 2003;69(1):269-77.

374. Kimura N, Konno Y, Miyoshi K, Matsumoto H, Sato E. Expression of hyaluronan synthases and CD44 messenger RNAs in porcine cumulus-oocyte complexes during in vitro maturation. Biol Reprod. 2002;66(3):707-17.

375. Yokoo M, Kimura N, Sato E. Induction of oocyte maturation by hyaluronan-CD44 interaction in pigs. Journal of Reproduction and Development. 2010;56(1):15-9.

376. Dbouk HA, Mroue RM, El-Sabban ME, Talhouk RS. Connexins: A myriad of functions extending beyond assembly of gap junction channels. Cell Communication and Signaling. 2009;7:4.

377. Ackert CL, Gittens JEI, O'Brien MJ, Eppig JJ, Kidder GM. Intercellular communication via connexin43 gap junctions is required for ovarian folliculogenesis in the mouse. Dev Biol. 2001;233(2):258-70.

378. Filson AJ, Azarnia R, Beyer EC, Loewenstein WR, Brugge JS. Tyrosine phosphorylation of a gap junction protein correlates with inhibition of cell-to-cell communication. Cell Growth Differ. 1990;1(12):661-8.

379. Lin R, Warn-Cramer BJ, Kurata WE, Lau AF. v-Src phosphorylation of connexin 43 on Tyr247 and Tyr265 disrupts gap junctional communication. Journal of Cell Biology. 2001;154(4):815-27.

380. Dekel N, Hillensjo T, Kraicer PF. Maturational effects of gonadotropins on the cumulus-oocyte complex of the rat. Biol Reprod. 1979;20(2):191-7.

381. Motlik J, Fulka J, Flechon JE. Changes in intercellular coupling between pig oocytes and cumulus cells during maturation in vivo and in vitro. J Reprod Fertil. 1986;76(1):31-7.

382. Protin U, Schweighoffer T, Jochum W, Hilberg F. CD44-deficient mice develop normally with changes in subpopulations and recirculation of lymphocyte subsets. J Immunol. 1999; 163(9):4917-23.

383. Shen P, Xu J, Wang P, Zhao X, Huang B, Wu F, et al. A new three-dimensional glass scaffold increases the in vitro maturation efficiency of buffalo (Bubalus bubalis) oocyte via remodelling the extracellular matrix and cell connection of cumulus cells. Reproduction in Domestic Animals. 2020;55(2):170-180.

384. Li H, Moll J, Winkler A, Frappart L, Brunet S, Hamann J, et al. RHAMM deficiency disrupts folliculogenesis resulting in female hypofertility. Biol Open. 2015;4(4):562-71.

385. Conti M, Hsieh M, Musa Zamah A, Oh JS. Novel signaling mechanisms in the ovary during oocyte maturation and ovulation. Molecular and Cellular Endocrinology. 2012;356(1-2):65-73.

386. Eppig JJ, Wigglesworth K, Pendola F, Hirao Y. Murine oocytes suppress expression of luteinizing hormone receptor messenger ribonucleic acid by granulosa cells. Biol Reprod. 1997;56(4):976-84.

387. Richards JS. New Signaling Pathways for Hormones and Cyclic Adenosine 3′,5′-Monophosphate Action in Endocrine Cells. Molecular Endocrinology. 2001;15(2):209-18.

388. Conti M. Specificity of the cyclic adenosine 3′,5′-monophosphate signal in granulosa cell function. Biology of Reproduction. 2002;67(6):1653-61.

389. Downs SM, Hunzicker-Dunn M. Differential Regulation of Oocyte Maturation and Cumulus Expansion in the Mouse Oocyte- Cumulus Cell Complex by Site-Selective Analogs of Cyclic Adenosine Monophosphate. Dev Biol. 1995;172(1):72-85.

390. Eppig JJ. Prostaglandin E2 stimulates cumulus expansion and hyaluronic acid synthesis by cumuli oophori isolated from mice. Biol Reprod. 1981;25(1):191-5.

391. Sirois J, Richards JS. Purification and characterization of a novel, distinct isoform of prostaglandin endoperoxide synthase induced by human chorionic gonadotropin in granulosa cells of rat preovulatory follicles. Journal of Biological Chemistry. 1992;267(9):6382-8.

392. Lim H, Paria BC, Das SK, Dinchuk JE, Langenbach R, Trzaskos JM, et al. Multiple female reproductive failures in cyclooxygenase 2-deficient mice. Cell. 1997;91(2):197-208.

393. Davis BJ. Anovulation in Cyclooxygenase-2-Deficient Mice Is Restored by Prostaglandin E2 and Interleukin-1 . Endocrinology. 1999;140(6):2685-95.

394. Hizaki H, Segi E, Sugimoto Y, Hirose M, Saji T, Ushikubi F, et al. Abortive expansion of the cumulus and impaired fertility in mice lacking the prostaglandin E receptor subtype EP2. Proc Natl Acad Sci U S A. 1999;96(18):10501-6.

395. Kennedy CRJ, Zhang Y, Brandon S, Guan Y, Coffee K, Funk CD, et al. Salt-sensitive hypertension and reduced fertility in mice lacking the prostaglandin EP2 receptor. Nat Med. 1999;5(2):217-20.

396. Tilley SL, Audoly LP, Hicks EH, Kim HS, Flannery PJ, Coffman TM, et al. Reproductive failure and reduced blood pressure in mice lacking the EP2 prostaglandin E2 receptor. Journal of Clinical Investigation. 1999;103(11):1539-45.

397. Ochsner SA, Russell DL, Day AJ, Breyer RM, Richards JS. Decreased expression of tumor necrosis factor-α-stimulated gene 6 in cumulus cells of the cyclooxygenase-2 and EP2 null mice. Endocrinology. 2003;144(3):1008–19.

398. Downs SM. Specificity of epidermal growth factor action on maturation of the murine oocyte and cumulus oophorus in vitro. Biol Reprod. 1989;41(2):371-9.

399. Lorenzo PL, Illera MJ, Illera JC, Illera M. Enhancement of cumulus expansion and nuclear maturation during bovine oocyte maturation in vitro by the addition of epidermal growth factor and insulin-like growth factor I. J Reprod Fertil. 1994;101(3):697-701.

400. Boland NI, Gosden RG. Effects of epidermal growth factor on the growth and differentiation of cultured mouse ovarian follicles. J Reprod Fertil. 1994;101(2):369-74.

401. Inoue Y, Miyamoto S, Fukami T, Shirota K, Yotsumoto F, Kawarabayashi T. Amphiregulin is much more abundantly expressed than transforming growth factor-alpha and epidermal growth factor in human follicular fluid obtained from patients undergoing in vitro fertilization-embryo transfer. Fertil Steril. 2009;91(4):1035-41.

402. Harris RC, Chung E, Coffey RJ. EGF receptor ligands. The EGF Receptor Family: Biologic Mechanisms and Role in Cancer. 2003;284(1):2-13.

403. Ashkenazi H, Cao X, Motola S, Popliker M, Conti M, Tsafriri A. Epidermal growth factor family members: Endogenous mediators of the ovulatory response. Endocrinology. 2005;146(1):77-84.

404. Carletti MZ, Christenson LK. Rapid effects of LH on gene expression in the mural granulosa cells of mouse periovulatory follicles. Reproduction. 2009;137(5):843-55.

405. Yamashita Y, Shimada M. The release of EGF domain from EGF-like factors by a specific cleavage enzyme activates the EGFR-MAPK3/1 pathway in both granulosa cells and cumulus cells during the ovulation process. Journal of Reproduction and Development. 2012;58(5):510-4.

406. Shimada M, Hernandez-Gonzalez I, Gonzalez-Robayna I, Richards JAS. Paracrine and autocrine regulation of epidermal growth factor-like factors in cumulus oocyte complexes

and granulosa cells: Key roles for prostaglandin synthase 2 and progesterone receptor. Molecular Endocrinology. 2006;20(6):1352-65.

407. Hsieh M, Lee D, Panigone S, Horner K, Chen R, Theologis A, et al. Luteinizing Hormone-Dependent Activation of the Epidermal Growth Factor Network Is Essential for Ovulation. Mol Cell Biol. 2007;27(5):1914-24.

408. Prochazka R, Blaha M, Němcová L. Significance of epidermal growth factor receptor signaling for acquisition of meiotic and developmental competence in mammalian oocytes. Biology of Reproduction. 2017;97(4):537-549.

409. You-Qiang SU, Wigglesworth K, Pendola FL, O'Brien MJ, Eppig JJ. Mitogen-activated protein kinase activity in cumulus cells is essential for gonadotropin-induced oocyte meiotic resumption and cumulus expansion in the mouse. Endocrinology. 2002;143(6):2221-32.

410. Su YQ, Denegre JM, Wigglesworth K, Pendola FL, O'Brien MJ, Eppig JJ. Oocyte-dependent activation of mitogen-activated protein kinase (ERK1/2) in cumulus cells is required for the maturation of the mouse oocyte-cumulus cell complex. Dev Biol. 2003;263(1):126-38.

411. Buccione R, Vanderhyden BC, Caron PJ, Eppig JJ. FSH-induced expansion of the mouse cumulus oophorus in vitro is dependent upon a specific factor(s) secreted by the oocyte. Dev Biol. 1990;138(1):16-25.

412. Eppig JJ. Oocyte control of ovarian follicular development and function in mammals. Reproduction. 2001;122(6):829-38.

413. Gilchrist RB, Lane M, Thompson JG. Oocyte-secreted factors: Regulators of cumulus cell function and oocyte quality. Hum Reprod Update. 2008;14(2):159-77.

414. Chen L, Russell PT, Larsen WJ. Functional significance of cumulus expansion in the mouse: Roles for the preovulatory synthesis of hyaluronic acid within the cumulus mass. Mol Reprod Dev. 1993;34(1):87-93.

415. Talbot P. Videotape analysis of hamster ovulation in vitro. Journal of Experimental Zoology. 1983;225(1):141-8.

416. Suarez SS. Gamete and Zygote Transport. Knobil and Neill's Physiology of Reproduction: Two-Volume Set. 2015.

417. Norwood JT, Hein CE, Halbert SA, Anderson RGW. Polycationic macromolecules inhibit cilia-mediated ovum transport in the rabbit oviduct. Proc Natl Acad Sci U S A. 1978;75(9):4413-6.

418. Talbot P, Geiske C, Knoll M. Oocyte pickup by the mammalian oviduct. Mol Biol Cell. 1999;10(1):5-8.

419. Lam X, Gieseke C, Knoll M, Talbot P. Assay and importance of adhesive interaction between hamster (Mesocricetus auratus) oocyte-cumulus complexes and the oviductal epithelium. Biol Reprod. 2000;62(3):579-88.

420. Talbot P, Shur BD, Myles DG. Cell adhesion and fertilization: Steps in oocyte transport, sperm-zona pellucida interactions, and sperm-egg fusion. Biology of Reproduction. 2003;68(1):1-9.

421. Odor DL, Blandau RJ. Egg transport over the fimbrial surface of the rabbit oviduct under experimental conditions. Fertil Steril. 1973;24(4):292-300.

422. Mahi-Brown CA, Yanagimachi R. Parameters influencing ovum pickup by oviductal fimbria in the golden hamster. Gamete Res. 1983;8(1).

423. Chen L, Wert SE, Hendrix EM, Russell PT, Cannon M, Larsen WJ. Hyaluronic acid synthesis and gap junction endocytosis are necessary for normal expansion of the cumulus mass. Mol Reprod Dev. 1990;26(3):236-47.

424. Barratt CLR, Williams M, Warren MA. Gamete Transport and Fertilisation.

425. Mahé C, Zlotkowska AM, Reynaud K, Tsikis G, Mermillod P, Druart X, et al. Sperm migration, selection, survival, and fertilizing ability in the mammalian oviduct. Vol. 105, Biology of Reproduction. 2021;105(2):317-331.

426. Muro Y, Hasuwa H, Isotani A, Miyata H, Yamagata K, Ikawa M, et al. Behavior of mouse spermatozoa in the female reproductive tract from soon after mating to the beginning of fertilization. Biol Reprod. 2016;94(4):80.

427. Wang Z, Wei H, Wu Z, Zhang X, Sun Y, Gao L, et al. The oocyte cumulus complex regulates mouse sperm migration in the oviduct. Commun Biol. 2022;5(1):1327.

428. Mirczuk SM, Lessey AJ, Catterick AR, Perrett RM, Scudder CJ, Read JE, et al. Regulation and function of C-type natriuretic peptide (CNP) in gonadotrope-derived cell lines. Cells. 2019;8(9):1086.

429. Kong N, Xu X, Zhang Y, Wang Y, Hao X, Zhao Y, et al. Natriuretic peptide type C induces sperm attraction for fertilization in mouse. Sci Rep. 2017;7:39711.

430. Bedford JM, Kim HH. Cumulus oophorus as a sperm sequestering device, in vivo. Journal of Experimental Zoology. 1993;265(3):321-8.

431. Eisenbach M, Tur-Kaspa I. Do human eggs attract spermatozoa? BioEssays. 1999;21(3):203-10.

432. Hunter RHF. Sperm: Egg ratios and putative molecular signals to modulate gamete interactions in polytocous mammals. Molecular Reproduction and Development. 1993;35(3):324-7.

433. Shimada M, Yanai Y, Okazaki T, Noma N, Kawashima I, Mori T, et al. Hyaluronan fragments generated by sperm-secreted hyaluronidase stimulate cytokine/chemokine production via the TLR 2 and TLR4 pathway in cumulus cells of ovulated COCs, which may enhance fertilization. Development. 2008;135(11).

434. Sutovsky P, Flechon JE, Flechon B, Motlik J, Peynot N, Chesne P, et al. Dynamic changes of gap junctions and cytoskeleton during in vitro culture of cattle oocyte cumulus complexes. Biol Reprod. 1993;49(6):1277-87.

435. Sutovský P, Fléchon JE, Pavlok A. Microfilaments, microtubules and intermediate filaments fulfil differential roles during gonadotropin-induced expansion of bovine cumulus oophorus. Reprod Nutr Dev. 1994;34(5):415-25.

436. Šutovský P, Fléchon JE, Pavlok A. F-actin is involved in control of bovine cumulus expansion. Mol Reprod Dev. 1995;41(4):521-9.

437. Clarke HJ. Transzonal projections: Essential structures mediating intercellular communication in the mammalian ovarian follicle. Molecular Reproduction and Development. 2022;89(11):509-525.

438. Sela-Abramovich S, Chorev E, Galiani D, Dekel N. Mitogen-activated protein kinase mediates luteinizing hormone-induced breakdown of communication and oocyte maturation in rat ovarian follicles. Endocrinology. 2005;146(3):1236-44.

439. Yuan Y, Spate LD, Redel BK, Tian Y, Zhou J, Prather RS, et al. Quadrupling efficiency in production of genetically modified pigs through improved oocyte maturation. Proc Natl Acad Sci U S A. 2017;114(29):E5796-E5804.

440. Yokoo M, Miyahayashi Y, Naganuma T, Kimura N, Sasada H, Sato E. Identification of hyaluronic acid-binding proteins and their expressions in porcine cumulus-oocyte complexes during in vitro maturation. Biol Reprod. 2002;67(4):1165-71.

441. Dekel N, Phillips DM. Maturation of the rat cumulus oophorus. A scanning electron microscopic study. Biol Reprod. 1979;21(1):9-18.

442. Kawashima I, Liu Z, Mullany LK, Mihara T, Richards JAS, Shimada M. EGF-like factors induce expansion of the cumulus cell-oocyte complexes by activating calpain- mediated cell movement. Endocrinology. 2012;153(8):3949-59.

443. Goll DE, Thompson VF, Li H, Wei W, Cong J. The calpain system. Physiological Reviews. 2003;83(3):731-801.

444. Akison LK, Alvino ER, Dunning KR, Robker RL, Russell DL. Transient Invasive Migration in Mouse Cumulus Oocyte Complexes Induced at Ovulation by Luteinizing Hormone. Biol Reprod. 2012;86(4):125.

445. Justus CR, Marie MA, Sanderlin EJ, Yang L V. Transwell In Vitro Cell Migration and Invasion Assays. Methods in Molecular Biology. 2023;2644:349-359.

446. Webb DJ, Zhang H, Horwitz AF. Cell migration: an overview. Methods in molecular biology (Clifton, N.J.). 2005;294:3-11.

447. Franz CM, Jones GE, Ridley AJ. Cell migration in development and disease. Developmental Cell. 2002; 2(2):153-8.

448. Keller R. Cell migration during gastrulation. Current Opinion in Cell Biology. 2005; 17(5):533-41.

449. Sharma VP, Beaty BT, Patsialou A, Liu H, Clarke M, Cox D, et al. Reconstitution of in vivo macrophage-tumor cell pairing and streaming motility on one-dimensional micro-patterned substrates. Intravital. 2012;1(1):77-85.

450. Weigelin B, Bakker GJ, Friedl P. Intravital third harmonic generation microscopy of collective melanoma cell invasion: Principles of interface guidance and microvesicle dynamics. Intravital. 2012;1(1):32-43.

451. Esbona K, Yi Y, Saha S, Yu M, Van Doorn RR, Conklin MW, et al. The Presence of Cyclooxygenase 2, Tumor-Associated Macrophages, and Collagen Alignment as

Prognostic Markers for Invasive Breast Carcinoma Patients. American Journal of Pathology. 2018;188(3):559-573.

452. Provenzano PP, Eliceiri KW, Campbell JM, Inman DR, White JG, Keely PJ. Collagen reorganization at the tumor-stromal interface facilitates local invasion. BMC Med. 2006;4(1):38.

453. Boissonnas A, Fetler L, Zeelenberg IS, Hugues S, Amigorena S. In vivo imaging of cytotoxic T cell infiltration and elimination of a solid tumor. Journal of Experimental Medicine. 2007;204(2):345-56.

454. Estabridis HM, Jana A, Nain A, Odde DJ. Cell Migration in 1D and 2D Nanofiber Microenvironments. Ann Biomed Eng. 2018;46(3):392-403.

455. Ridley AJ, Schwartz MA, Burridge K, Firtel RA, Ginsberg MH, Borisy G, et al. Cell Migration: Integrating Signals from Front to Back. Science. 2003;302(5651):1704-9.

456. Parsons JT, Horwitz AR, Schwartz MA. Cell adhesion: Integrating cytoskeletal dynamics and cellular tension. Nature Reviews Molecular Cell Biology. 2010;11(9):633-43.

457. Case LB, Waterman CM. Integration of actin dynamics and cell adhesion by a three-dimensional, mechanosensitive molecular clutch. Nature Cell Biology. 2015;17(8):955-63.

458. Lehtimaki J, Hakala M, Lappalainen P. Actin filament structures in migrating cells. Handb Exp Pharmacol. 2017;235:123-152.

459. Krause M, Gautreau A. Steering cell migration: Lamellipodium dynamics and the regulation of directional persistence. Nature Reviews Molecular Cell Biology. 2014;15(9):577-90.

460. Abercrombie M, Heaysman JEM, Pegrum SM. The locomotion of fibroblasts in culture. III. Movements of particles on the dorsal surface of the leading lamella. Exp Cell Res. 1970;62(2–3):389-98.

461. Cramer LP. Molecular mechanism of actin-dependent retrograde flow in lamellipodia of motile cells. Frontiers in bioscience: a journal and virtual library. 1997;2:d260-70.

462. Paluch EK, Raz E. The role and regulation of blebs in cell migration. Current Opinion in Cell Biology. 2013;25(5):582-90.

463. Pepper I, Galkin VE. Actomyosin Complex. Subcellular Biochemistry. 2022;99:421-470.

464. Svitkina T. The actin cytoskeleton and actin-based motility. Cold Spring Harb Perspect Biol. 2018;10(1):a018267.

465. Pollard TD. Rate constants for the reactions of ATP- and ADP-actin with the ends of actin filaments. Journal of Cell Biology. 1986;103(6):2747-54.

466. Brenner SL, Korn ED. On the mechanism of actin monomer-polymer subunit exchange at steady state. Journal of Biological Chemistry. 1983;258(8):5013-20.

467. Skruber K, Read TA, Vitriol EA. Reconsidering an active role for G-actin in cytoskeletal regulation. Vol. 131, Journal of Cell Science. 2018;131(1):jcs203760.

468. Schaks M, Giannone G, Rottner K. Actin dynamics in cell migration. Essays Biochem. 2019;63(5):483–95.

469. Breitsprecher D, Goode BL. Formins at a glance. Journal of Cell Science. 2013;126(Pt 1):1-7.

470. Rotty JD, Wu C, Bear JE. New insights into the regulation and cellular functions of the ARP2/3 complex. Nat Rev Mol Cell Biol. 2013;14(1):7-12.

471. Campellone KG, Welch MD. A nucleator arms race: Cellular control of actin assembly. Nature Reviews Molecular Cell Biology. 2010;11(4):237-51.

472. Goley ED, Rodenbusch SE, Martin AC, Welch MD. Critical conformational changes in the Arp2/3 complex are induced by nucleotide and nucleation promoting factor. Mol Cell. 2004;16(2):269-79.

473. Small JV, Stradal T, Vignal E, Rottner K. The lamellipodium: Where motility begins. Trends in Cell Biology. 2002;12(3):112-20.

474. Sokolova OS, Chemeris A, Guo S, Alioto SL, Gandhi M, Padrick S, et al. Structural Basis of Arp2/3 Complex Inhibition by GMF, Coronin, and Arpin. J Mol Biol. 2017;429(2):237-248.

475. Chan C, Beltzner CC, Pollard TD. Cofilin Dissociates Arp2/3 Complex and Branches from Actin Filaments. Current Biology. 2009;19(7):537-45.

476. Suarez C, Roland J, Boujemaa-Paterski R, Kang H, McCullough BR, Reymann AC, et al. Cofilin tunes the nucleotide state of actin filaments and severs at bare and decorated segment boundaries. Current Biology. 2011;21(10):862-8.

477. Nadkarni A V., Brieher WM. Aip1 destabilizes cofilin-saturated actin filaments by severing and accelerating monomer dissociation from ends. Current Biology. 2014;24(23):2749-57.

478. Goldschmidt-Clermont PJ, Machesky LM, Doberstein SK, Pollard TD. Mechanism of the interaction of human platelet profilin with actin. Journal of Cell Biology. 1991;113(5):1081-9.

479. Mockrin SC, Korn ED. Acanthamoeba Profilin Interacts with G-Actin to Increase the Rate of Exchange of Actin-Bound Adenosine 5'-Triphosphate. Biochemistry. 1980;19(23):5359-62.

480. Nishida E. Opposite Effects of Cofilin and Profilin from Porcine Brain on Rate of Exchange of Actin-Bound Adenosine 5′-Triphosphate. Biochemistry. 1985;24(5):1160-4.

481. Kotila T, Kogan K, Enkavi G, Guo S, Vattulainen I, Goode BL, et al. Structural basis of actin monomer re-charging by cyclase-Associated protein. Nat Commun. 2018;9(1):1892.

482. Coluccio LM. Myosin- A Superfamily of Molecular Motors. Myosins. 2007.

483. Clark K, Langeslag M, Figdor CG, van Leeuwen FN. Myosin II and mechanotransduction: a balancing act. Trends in Cell Biology. 2007;17(4):178-86.

484. Conti MA, Adelstein RS. Nonmuscle myosin II moves in new directions. Journal of Cell Science. 2008;121(Pt 1):11-8.

485. Swailes NT, Colegrave M, Knight PJ, Peckham M. Non-muscle myosins 2A and 2B drive changes in cell morphology that occur as myoblasts align and fuse. J Cell Sci. 2006;119(17):3561-70.

486. Kim KY, Kovács M, Kawamoto S, Sellers JR, Adelstein RS. Disease-associated mutations and alternative splicing alter the enzymatic and motile activity of nonmuscle myosins II-B and II-C. Journal of Biological Chemistry. 2005;280(24):22769-75.

487. Kovács M, Wang F, Hu A, Zhang Y, Sellers JR. Functional divergence of human cytoplasmic myosin II. Kinetic characterization of the non-muscle IIA isoform. Journal of Biological Chemistry. 2003;278(40):22769-75.

488. Wang F, Kovács M, Hu A, Limouze J, Harvey E V., Sellers JR. Kinetic mechanism of non-muscle myosin IIB. Functional adaptations for tension generation and maintenance. Journal of Biological Chemistry. 2003;278(30):27439-48.

489. Vicente-Manzanares M, Zareno J, Whitmore L, Choi CK, Horwitz AF. Regulation of protrusion, adhesion dynamics, and polarity by myosins IIA and IIB in migrating cells. Journal of Cell Biology. 2007;176(5):573-80.

490. Bao J, Jana SS, Adelstein RS. Vertebrate nonmuscle myosin II isoforms rescue small interfering RNA-induced defects in COS-7 cell cytokinesis. Journal of Biological Chemistry. 2005;280(20):19594-9.

491. Nakasawa T, Takahashi M, Matsuzawa F, Aikawa S, Togashi Y, Saitoh T, et al. Critical regions for assembly of vertebrate nonmuscle myosin II. Biochemistry. 2005;44(1):174-83.

492. Bosgraaf L, van Haastert PJM. The regulation of myosin II in Dictyostelium. European Journal of Cell Biology. 2006;85(9-10):969-79.

493. Redowicz MJ. Regulation of nonmuscle myosins by heavy chain phosphorylation. J Muscle Res Cell Motil. 2001;22(2):163-73.

494. Even-Faitelson L, Ravid S. PAK1 and aPKCζ regulate myosin II-B phosphorylation: A novel signaling pathway regulating filament assembly. Mol Biol Cell. 2006;17(7):2869-81:2869-81.

495. Dulyaninova NG, Malashkevich VN, Almo SC, Bresnick AR. Regulation of myosin-IIA assembly and Mts1 binding by heavy chain phosphorylation. Biochemistry. 2005;44(18):6867-76.

496. Clark K, Middelbeek J, Lasonder E, Dulyaninova NG, Morrice NA, Ryazanov AG, et al. TRPM7 Regulates Myosin IIA Filament Stability and Protein Localization by Heavy Chain Phosphorylation. J Mol Biol. 2008;378(4):790-803.

497. Wendt T, Taylor D, Trybus KM, Taylor K. Three-dimensional image reconstruction of dephosphorylated smooth muscle heavy meromyosin reveals asymmetry in the interaction between myosin heads and placement of subfragment 2. Proc Natl Acad Sci U S A. 2001;98(8):4361-6.

498. Woodhead JL, Zhao FQ, Craig R, Egelman EH, Alamo L, Padrón R. Atomic model of a myosin filament in the relaxed state. Nature. 2005;436(7054):4361-6.

499. Hyun SJ, Komatsu S, Ikebe M, Craig R. Head-head and head-tail interaction: A general mechanism for switching off myosin II activity in cells. Mol Biol Cell. 2008;19(8):3234-42.

500. Craig R, Woodhead JL. Structure and function of myosin filaments. Current Opinion in Structural Biology. 2006;16(2):204-12.

501. Burgess SA, Yu S, Walker ML, Hawkins RJ, Chalovich JM, Knight PJ. Structures of Smooth Muscle Myosin and Heavy Meromyosin in the Folded, Shutdown State. J Mol Biol. 2007;372(5):1165-78.

502. Somlyo AP, Somlyo A V. Ca2+ sensitivity of smooth muscle and nonmuscle myosin II: Modulated by G proteins, kinases, and myosin phosphatase. Physiological Reviews. 2003;83(4):1325-58.

503. Sellers JR, Eisenberg E, Adelstein RS. The binding of smooth muscle heavy meromyosin to actin in the presence of ATP. Effect of phosphorylation. Journal of Biological Chemistry. 1982;257(23):13880-3.

504. Umemoto S, Bengur AR, Sellers JR. Effect of multiple phosphorylations of smooth muscle and cytoplasmic myosins on movement in an in vitro motility assay. Journal of Biological Chemistry. 1989;264(3):1431-6.

505. Ikebe M, Hartshorne DJ, Elzinga M. Identification, phosphorylation, and dephosphorylation of a second site for myosin light chain kinase on the 20,000-dalton light chain of smooth muscle myosin. Journal of Biological Chemistry. 1986;261(1):36-9.

506. Vicente-Manzanares M, Horwitz AR. Myosin light chain mono- and di-phosphorylation differentially regulate adhesion and polarity in migrating cells. Biochem Biophys Res Commun. 2010;402(3):537-42.

507. Livne A, Geiger B. The inner workings of stress fibers - From contractile machinery to focal adhesions and back. J Cell Sci. 2016;129(7):1293-304.

508. Verkhovsky AB, Svitkina TM, Borisy GG. Myosin II filament assemblies in the active lamella of fibroblasts: Their morphogenesis and role in the formation of actin filament bundles. Journal of Cell Biology. 1995;131(4):989-1002.

509. Verkhovsky AB, Svitkina TM, Borisy GG. Polarity sorting of actin filaments in cytochalasin-treated fibroblasts. J Cell Sci. 1997;110(15):1693-704.

510. Tojkander S, Gateva G, Lappalainen P. Actin stress fibers - Assembly, dynamics and biological roles. J Cell Sci. 2012;125(8):1855-64.

511. Yamada KM, Sixt M. Mechanisms of 3D cell migration. Nature Reviews Molecular Cell Biology. 2019;20(12):738-752.

512. Verkhovsky AB, Svitkina TM, Borisy GG. Network contraction model for cell translocation and retrograde flow. Biochem Soc Symp. 1999;65:207-22.

513. Chugh P, Paluch EK. The actin cortex at a glance. J Cell Sci. 2018;131(14):jcs186254.

514. Koenderink GH, Paluch EK. Architecture shapes contractility in actomyosin networks. Current Opinion in Cell Biology. 2018;50:79-85.

515. Clark AG, Wartlick O, Salbreux G, Paluch EK. Stresses at the cell surface during animal cell morphogenesis. Current Biology. 2014;24(10):R484-94.

516. Chugh P, Clark AG, Smith MB, Cassani DAD, Dierkes K, Ragab A, et al. Actin cortex architecture regulates cell surface tension. Nat Cell Biol. 2017;19(6):689-697.

517. Beach JR, Shao L, Remmert K, Li D, Betzig E, Hammer JA. Nonmuscle myosin II isoforms coassemble in living cells. Current Biology. 2014;24(10):402.

518. Matsumura F. Regulation of myosin II during cytokinesis in higher eukaryotes. Trends in Cell Biology. 2005;15(7):371-7.

519. Tan I, Yong J, Dong JM, Lim L, Leung T. A Tripartite Complex Containing MRCK Modulates Lamellar Actomyosin Retrograde Flow. Cell. 2008;135(1):123-36.

520. Driska SP, Aksoy MO, Murphy RA. Myosin light chain phosphorylation associated with contraction in arterial smooth muscle. Am J Physiol Cell Physiol. 1981;9(3):C222-33.

521. Alcala DB, Haldeman BD, Brizendine RK, Krenc AK, Baker JE, Rock RS, et al. Myosin light chain kinase steady-state kinetics: comparison of smooth muscle myosin II and nonmuscle myosin IIB as substrates. Cell Biochem Funct. 2016;34(7):469-474.

522. Beningo KA, Hamao K, Dembo M, Wang Y li, Hosoya H. Traction forces of fibroblasts are regulated by the Rho-dependent kinase but not by the myosin light chain kinase. Arch Biochem Biophys. 2006;456(2):224-31.

523. Di Cunto F, Calautti E, Hsiao J, Ong L, Topley G, Turco E, et al. Citron Rho-interacting kinase, a novel tissue-specific Ser/Thr kinase encompassing the Rho-Rac-binding protein citron. Journal of Biological Chemistry. 1998;273(45):29706-11.

524. Madaule P, Furuyashiki T, Reid T, Ishizaki T, Watanabe G, Morii N, et al. A novel partner for the GTP-bound forms of rho and rac. FEBS Lett. 1995;377(2):243-8.

525. Usui T, Okada M, Yamawaki H. Zipper interacting protein kinase (ZIPK): Function and signaling. Apoptosis. 2014;19(2):387-91.

526. Amano M, Ito M, Kimura K, Fukata Y, Chihara K, Nakano T, et al. Phosphorylation and activation of myosin by Rho-associated kinase (Rho- kinase). Journal of Biological Chemistry. 1996;271(34):387-91.

527. Kimura K, Ito M, Amano M, Chihara K, Fukata Y, Nakafuku M, et al. Regulation of myosin phosphatase by Rho and Rho-associated kinase (Rho- kinase). Science. 1996;273(5272):245-8.

528. Amano M, Chihara K, Nakamura N, Kaneko T, Matsuura Y, Kaibuchi K. The COOH terminus of Rho-kinase negatively regulates Rho-kinase activity. Journal of Biological Chemistry. 1999;274(45):32418-24.

529. Leung T, Chen XQ, Manser E, Lim L. The p160 RhoA-Binding Kinase ROKα Is a Member of a Kinase Family and Is Involved in the Reorganization of the Cytoskeleton. Mol Cell Biol. 1996;16(10):5313-27.

530. Ishizaki T, Naito M, Fujisawa K, Maekawa M, Watanabe N, Saito Y, et al. p160(ROCK), a Rho-associated coiled-coil forming protein kinase, works downstream of Rho and induces focal adhesions. FEBS Lett. 1997;404(2–3):118-24.

531. Riento K, Ridley AJ. Rocks: Multifunctional kinases in cell behaviour. Nature Reviews Molecular Cell Biology. 2003;4(6):446-56.

532. Newell-Litwa KA, Badoual M, Asmussen H, Patel H, Whitmore L, Horwitz AR. ROCK 1 and 2 differentially regulate actomyosin organization to drive cell and synaptic polarity. Journal of Cell Biology. 2015;210(2):225-42.

533. Zhao Z, Manser E. Myotonic dystrophy kinase-related Cdc42-binding kinases (MRCK), the ROCK-like effectors of Cdc42 and Rac1. Small GTPases. 2015;6(2):81-8.

534. Unbekandt M, Olson MF. The actin-myosin regulatory MRCK kinases: Regulation, biological functions and associations with human cancer. Journal of Molecular Medicine. 2014; 92(3):217-25.

535. Tan I, Seow KT, Lim L, Leung T. Intermolecular and Intramolecular Interactions Regulate Catalytic Activity of Myotonic Dystrophy Kinase-Related Cdc42-Binding Kinase α. Mol Cell Biol. 2001;21(8):2767-78.

536. Williams RL. Structural Principles of Lipid Second Messenger Recognition. Handbook of Cell Signaling, Second Edition. 2009;79(5):266.

537. Leung T, Chen XQ, Tan I, Manser E, Lim L. Myotonic Dystrophy Kinase-Related Cdc42-Binding Kinase Acts as a Cdc42 Effector in Promoting Cytoskeletal Reorganization. Mol Cell Biol. 1998;18(1):130-40.

538. Murányi A, Zhang R, Liu F, Hirano K, Ito M, Epstein HF, et al. Myotonic dystrophy protein kinase phosphorylates the myosin phosphatase targeting subunit and inhibits myosin phosphatase activity. FEBS Lett. 2001;493(2–3):80-4.

539. Giannone G, Dubin-Thaler BJ, Rossier O, Cai Y, Chaga O, Jiang G, et al. Lamellipodial Actin Mechanically Links Myosin Activity with Adhesion-Site Formation. Cell. 2007;128(3):561-75.

540. Steffen A, Ladwein M, Dimchev GA, Hein A, Schwenkmezger L, Arens S, et al. Rac function is crucial for cell migration but is not required for spreading and focal adhesion formation. J Cell Sci. 2013;126(20):4572-88.

541. Innocenti M. New insights into the formation and the function of lamellipodia and ruffles in mesenchymal cell migration. Cell Adh Migr. 2018;12(5):401-416.

542. Bryce NS, Clark ES, Leysath JL, Currie JD, Webb DJ, Weaver AM. Cortactin promotes cell motility by enhancing lamellipodial persistence. Current Biology. 2005;15(14):1276-85.

543. Watanabe N. Inside view of cell locomotion through single-molecule: Fast F-/G-actin cycle and G-actin regulation of polymer restoration. Proceedings of the Japan Academy Series B: Physical and Biological Sciences. 2010;86(1):62-83.

544. Mullins RD, Heuser JA, Pollard TD. The interaction of Arp2/3 complex with actin: Nucleation, high affinity pointed end capping, and formation of branching networks of filaments. Proc Natl Acad Sci U S A. 1998;95(11):6181-6.

545. Oakes PW, Bidone TC, Beckham Y, Skeeters A V., Ramirez-San Juan GR, Winter SP, et al. Lamellipodium is a myosin-independent mechanosensor. Proc Natl Acad Sci U S A. 2018;115(11):2646-2651.

546. Ferrero E, Fabbri M, Poggi A, Galati G, Bernasconi S, Zocchi MR. Tumor-driven matrix invasion by infiltrating lymphocytes: Involvement of the α1 integrin I-domain. Eur J Immunol. 1998;28(8):2530-6.

547. Kagami S, Kondo S, Löster K, Reutter W, Kuhara T, Yasutomo K, et al. α1β1 integrin-mediated collagen matrix remodeling by rat mesangial cells is differentially regulated by transforming growth factor-β and platelet-derived growth factor-BB. Journal of the American Society of Nephrology. 1999;10(4):779-89.

548. Batson J, Astin JW, Nobes CD. Regulation of contact inhibition of locomotion by Eph-ephrin signalling. J Microsc. 2013;251(3):232-41.

549. Davis JR, Luchici A, Mosis F, Thackery J, Salazar JA, Mao Y, et al. Inter-cellular forces orchestrate contact inhibition of locomotion. Cell. 2015;161(2):361-73.

550. Dimchev G, Steffen A, Kage F, Dimchev V, Pernier J, Carlier MF, et al. Efficiency of lamellipodia protrusion is determined by the extent of cytosolic actin assembly. Mol Biol Cell. 2017;28(10):1311-1325.

551. DeLisser HM. Modulators of endothelial cell filopodia: PECAM-1 joins the club. Vol. 5, Cell Adhesion and Migration. 2011;5(1):37-41.

552. Mattila PK, Lappalainen P. Filopodia: Molecular architecture and cellular functions. Nature Reviews Molecular Cell Biology. 2008;9(6):446-54.

553. Yang C, Svitkina T. Filopodia initiation: Focus on the Arp2/3 complex and formins. Cell Adhesion and Migration. 2011;5(5):402-8.

554. Alexandrova AY, Chikina AS, Svitkina TM. Actin cytoskeleton in mesenchymal-to-amoeboid transition of cancer cells. International Review of Cell and Molecular Biology. 2020;356:197-256.

555. Nobes CD, Hall A. Rho, Rac, and Cdc42 GTPases regulate the assembly of multimolecular focal complexes associated with actin stress fibers, lamellipodia, and filopodia. Cell. 1995;81(1):53-62.

556. Ahmed S, Goh WI, Bu W. I-BAR domains, IRSp53 and filopodium formation. Seminars in Cell and Developmental Biology. 2010;81(1):53-62.

557. Gallo G. RhoA-kinase coordinates F-actin organization and myosin II activity during semaphorin-3A-induced axon retraction. J Cell Sci. 2006;119(16):3413-23.

558. Ikenouchi J, Aoki K. Membrane bleb: A seesaw game of two small GTPases. Small GTPases. 2017;8(2):85-89.

559. Laster SM, Mackenzie JM. Bleb formation and F-actin distribution during mitosis and tumor necrosis factor-induced apoptosis. Microsc Res Tech. 1996;34(3):272-80.

560. Taneja N, Burnette DT. Myosin IIA drives membrane bleb retraction. Mol Biol Cell. 2019;30(9):1051-1059.

561. Charras G, Paluch E. Blebs lead the way: How to migrate without lamellipodia. Nature Reviews Molecular Cell Biology. 2008;9(9):730-6.

562. Fackler OT, Grosse R. Cell motility through plasma membrane blebbing. Journal of Cell Biology. 2008;181(6):879-84.

563. Cunningham CC. Actin polymerization and intracellular solvent flow in cell surface blebbing. Journal of Cell Biology. 1995;129(6):1589-99.

564. Goudarzi M, Tarbashevich K, Mildner K, Begemann I, Garcia J, Paksa A, et al. Bleb Expansion in Migrating Cells Depends on Supply of Membrane from Cell Surface Invaginations. Dev Cell. 2017;43(5):577-587.e5.

565. Charras GT, Coughlin M, Mitchison TJ, Mahadevan L. Life and times of a cellular bleb. Biophys J. 2008;94(5):1836-53.

566. Ikenouchi J, Aoki K. A Clockwork Bleb: cytoskeleton, calcium, and cytoplasmic fluidity. FEBS Journal. 2022;289(24):7907-7917.

567. Tinevez JY, Schulze U, Salbreux G, Roensch J, Joanny JF, Paluch E. Role of cortical tension in bleb growth. Proc Natl Acad Sci U S A. 2009;106(44):18581-6.

568. Maugis B, Brugués J, Nassoy P, Guillen N, Sens P, Amblard F. Dynamic instability of the intracellular pressure drives bleb-based motility. J Cell Sci. 2010;123(22).

569. Sanz-Moreno V, Gadea G, Ahn J, Paterson H, Marra P, Pinner S, et al. Rac Activation and Inactivation Control Plasticity of Tumor Cell Movement. Cell. 2008;135(3).

570. Ridley AJ. Rho GTPase signalling in cell migration. Current Opinion in Cell Biology. 2015;36:103-12.

571. Yoshida K, Inouye K. Myosin II-dependent cylindrical protrusions induced by quinine in Dictyostelium: Antagonizing effects of actin polymerization at the leading edge. J Cell Sci. 2001;114(11):2155-65.

572. Goudarzi M, Banisch TU, Mobin MB, Maghelli N, Tarbashevich K, Strate I, et al. Identification and Regulation of a Molecular Module for Bleb-Based Cell Motility. Dev Cell. 2012;23(1):210-8.

573. Blaser H, Reichman-Fried M, Castanon I, Dumstrei K, Marlow FLL, Kawakami K, et al. Migration of Zebrafish Primordial Germ Cells: A Role for Myosin Contraction and Cytoplasmic Flow. Dev Cell. 2006;11(5):613-27.

574. Sedzinski J, Biro M, Oswald A, Tinevez JY, Salbreux G, Paluch E. Polar actomyosin contractility destabilizes the position of the cytokinetic furrow. Nature. 2011;476(7361):462-6.

575. Paluch E, Piel M, Prost J, Bornens M, Sykes C. Cortical actomyosin breakage triggers shape oscillations in cells and cell fragments. Biophys J. 2005;89(1):724-33.

576. Fehon RG, McClatchey AI, Bretscher A. Organizing the cell cortex: The role of ERM proteins. Vol. 11, Nature Reviews Molecular Cell Biology. 2010;11(4):276-87.

577. Charras GT, Hu CK, Coughlin M, Mitchison TJ. Reassembly of contractile actin cortex in cell blebs. Journal of Cell Biology. 2006;175(3):477-90.

578. Dumstrei K, Mennecke R, Raz E. Signaling pathways controlling primordial germ cell migration in zebrafish. J Cell Sci. 2004;117(20):4787-95.

579. Diz-Muñoz A, Krieg M, Bergert M, Ibarlucea-Benitez I, Muller DJ, Paluch E, et al. Control of directed cell migration in vivo by membrane-to-cortex attachment. PLoS Biol. 2010;8(11):e1000544.

580. Stastna J, Pan X, Wang H, Kollmannsperger A, Kutscheidt S, Lohmann V, et al. Differing and isoform-specific roles for the formin DIAPH3 in plasma membrane blebbing and filopodia formation. Cell Res. 2012;22(4):728-45.

581. Bovellan M, Romeo Y, Biro M, Boden A, Chugh P, Yonis A, et al. Cellular control of cortical actin nucleation. Current Biology. 2014;24(14):1628-1635.

582. Chardin P. Function and regulation of Rnd proteins. Nature Reviews Molecular Cell Biology. 2006; 7(1):54-62.

583. Wennerberg K, Forget MA, Ellerbroek SM, Arthur WT, Burridge K, Settleman J, et al. Rnd proteins function as RhoA antagonists by activating p190 RhoGAP. Current Biology. 2003;13(13):1106-15.

584. Villalonga P, Guasch RM, Riento K, Ridley AJ. RhoE Inhibits Cell Cycle Progression and Ras-Induced Transformation. Mol Cell Biol. 2004;24(18):7829-40.

585. Riento K, Totty N, Villalonga P, Garg R, Guasch R, Ridley AJ. RhoE function is regulated by ROCK I-mediated phosphorylation. EMBO Journal. 2005;24(6):1170-80.

586. Haga RB, Ridley AJ. Rho GTPases: Regulation and roles in cancer cell biology. Small GTPases. 2016;7(4):207-221.

587. Smithers CC, Overduin M. Structural mechanisms and drug discovery prospects of rho GTpases. Cells. 2016;5(2):26.

588. Dovas A, Couchman JR. RhoGDI: Multiple functions in the regulation of Rho family GTPase activities. Biochemical Journal. 2005;390(1):1-9.

589. Boureux A, Vignal E, Faure S, Fort P. Evolution of the Rho family of Ras-like GTPases in eukaryotes. Mol Biol Evol. 2007;24(1):203-16.

590. Charras G, Sahai E. Physical influences of the extracellular environment on cell migration. Nat Rev Mol Cell Biol. 2014;15(12):813-24.

591. Graziano BR, Weiner OD. Self-organization of protrusions and polarity during eukaryotic chemotaxis. Current Opinion in Cell Biology. 2014;30:60-7.

592. Eden S, Rohatgi R, Podtelejnikov A V., Mann M, Kirschner MW. Mechanism of regulation of WAVE1-induced actin nucleation by Rac1 and Nck. Nature. 2002;418(6899):790-3.

593. Chen Z, Borek D, Padrick SB, Gomez TS, Metlagel Z, Ismail AM, et al. Structure and control of the actin regulatory WAVE complex. Nature. 2010;468(7323):533-8.

594. Nimnual AS, Taylor LJ, Bar-Sagi D. Redox-dependent downregulation of Rho by Rac. Nat Cell Biol. 2003;5(3):236-41.

595. Narumiya S, Tanji M, Ishizaki T. Rho signaling, ROCK and mDia1, in transformation, metastasis and invasion. Cancer and Metastasis Reviews. 2009;28(1-2):65-76.

596. Ehrlicher AJ, Nakamura F, Hartwig JH, Weitz DA, Stossel TP. Mechanical strain in actin networks regulates FilGAP and integrin binding to filamin A. Nature. 2011;478(7368):260-3.

597. Ohta Y, Hartwig JH, Stossel TP. FilGAP, a Rho- and ROCK-regulated GAP for Rac binds filamin A to control actin remodelling. Nat Cell Biol. 2006;8(8):803-14.

598. Shifrin Y, Arora PD, Ohta Y, Calderwood DA, McCulloch CA. The role of filGAP-filamin a interactions in mechanoprotection. Mol Biol Cell. 2009;20(5):1269-79.

599. Rohatgi R, Ma L, Miki H, Lopez M, Kirchhausen T, Takenawa T, et al. The interaction between N-WASP and the Arp2/3 complex links Cdc42-dependent signals to actin assembly. Cell. 1999;97(2):221-31.

600. Bear JE, Haugh JM. Directed migration of mesenchymal cells: Where signaling and the cytoskeleton meet. Current Opinion in Cell Biology. 2014;30:74-82.

601. Lauffenburger DA, Horwitz AF. Cell migration: A physically integrated molecular process. Cell. 1996;84(3):359-69.

602. Svitkina TM. Ultrastructure of protrusive actin filament arrays. Current Opinion in Cell Biology. 2013;25(5):574-81.

603. Shutova MS, Svitkina TM. Mammalian nonmuscle myosin II comes in three flavors. Biochem Biophys Res Commun. 2018;506(2):394-402.

604. Kechagia JZ, Ivaska J, Roca-Cusachs P. Integrins as biomechanical sensors of the microenvironment. Nature Reviews Molecular Cell Biology. 2019;20(8):457-473.

605. Seetharaman S, Etienne-Manneville S. Integrin diversity brings specificity in mechanotransduction. Biology of the Cell. 2018;110(3):49-64.

606. Bachir AI, Horwitz AR, Nelson WJ, Bianchini JM. Actin-based adhesion modules mediate cell interactions with the extracellular matrix and neighboring cells. Cold Spring Harb Perspect Biol. 2017;9(7):a023234.

607. Collins C, Nelson WJ. Running with neighbors: Coordinating cell migration and cell-cell adhesion. Current Opinion in Cell Biology. 2015;36:62-70.

608. Gauthier NC, Roca-Cusachs P. Mechanosensing at integrin-mediated cell–matrix adhesions: from molecular to integrated mechanisms. Current Opinion in Cell Biology. 2018;50:20-26.

609. Choma DP, Pumiglia K, DiPersio CM. Integrin αβ1 directs the stabilization of a polarized lamellipodium in epithelial cells through activation of Rac1. J Cell Sci. 2004;117(17):3947-59.

610. Nalbant P, Dehmelt L. Exploratory cell dynamics: A sense of touch for cells? Vol. 399, Biological Chemistry. 2018;399(8):809-819.

611. Roussos ET, Condeelis JS, Patsialou A. Chemotaxis in cancer. Nature Reviews Cancer. 2011;11(8):573-87.

612. King SJ, Asokan SB, Haynes EM, Zimmerman SP, Rotty JD, Alb JG, et al. Lamellipodia are crucial for haptotactic sensing and response. J Cell Sci. 2016;129(12):2329-42.

613. Lo CM, Wang HB, Dembo M, Wang YL. Cell movement is guided by the rigidity of the substrate. Biophys J. 2000;79(1):144-52.

614. Plotnikov S V., Waterman CM. Guiding cell migration by tugging. Current Opinion in Cell Biology. 2013;25(5):619-26.

615. Chen P, Parks WC. Role of matrix metalloproteinases in epithelial migration. Journal of Cellular Biochemistry. 2009; 108(6):1233-43.

616. Sahai E, Marshall CJ. Differing modes for tumour cell invasion have distinct requirements for Rho/ROCK signalling and extracellular proteolysis. Nat Cell Biol. 2003;5(8):711-9.

617. Petrie RJ, Yamada KM. At the leading edge of three-dimensional cell migration. Journal of Cell Science. 2012;125(24):5917-26.

618. Ruprecht V, Wieser S, Callan-Jones A, Smutny M, Morita H, Sako K, et al. Cortical contractility triggers a stochastic switch to fast amoeboid cell motility. Cell. 2015;160(4):673-685.

619. Murrell M, Oakes PW, Lenz M, Gardel ML. Forcing cells into shape: The mechanics of actomyosin contractility. Nature Reviews Molecular Cell Biology. 2015;16(8):486-98.

620. Shih W, Yamada S. Myosin IIA dependent retrograde flow drives 3D cell migration. Biophys J. 2010;98(8):L29-31.

621. Gadea G, Sanz-Moreno V, Self A, Godi A, Marshall CJ. DOCK10-Mediated Cdc42 Activation Is Necessary for Amoeboid Invasion of Melanoma Cells. Current Biology. 2008;18(19):1456-65.

622. Paluch EK, Aspalter IM, Sixt M. Focal Adhesion-Independent Cell Migration. Annu Rev Cell Dev Biol. 2016;32:469-490.

623. Friedl P, Borgmann S, Bröcker EB. Amoeboid leukocyte crawling through extracellular matrix: lessons from the Dictyostelium paradigm of cell movement. J Leukoc Biol. 2001;70(4):491-509.

624. Mandeville JTH, Lawson MA, Maxfield FR. Dynamic imaging of neutrophil migration in three dimensions: Mechanical interactions between cells and matrix. J Leukoc Biol. 1997;61(2):188-200.

625. Friedl P, Noble PB, Shields ED, Zänker KS. Locomotor phenotypes of unstimulated CD45RAhigh and CD45ROhigh CD4+ and CD8+ lymphocytes in three-dimensional collagen lattices. Immunology. 1994;82(4):617-24.

626. Friedl P, Zänker KS, Bröcker EB. Cell migration strategies in 3-D extracellular matrix: Differences in morphology, cell matrix interactions, and integrin function. Microscopy Research and Technique. 1998; 43(5):369-78.

627. Renkawitz J, Sixt M. Mechanisms of force generation and force transmission during interstitial leukocyte migration. EMBO Reports. 2010;11(10):744-50.

628. Tozluoğlu M, Tournier AL, Jenkins RP, Hooper S, Bates PA, Sahai E. Matrix geometry determines optimal cancer cell migration strategy and modulates response to interventions. Nat Cell Biol. 2013;15(7):751-62.

629. Petrie RJ, Doyle AD, Yamada KM. Random versus directionally persistent cell migration. Nature Reviews Molecular Cell Biology. 2009;10(8):538-49.

630. Keller HU, Bebie H. Protrusive activity quantitatively determines the rate and direction of cell locomotion. Cell Motil Cytoskeleton. 1996;33(4):241-51.

631. Collier S, Paschke P, Kay RR, Bretschneider T. Image based modeling of bleb site selection. Sci Rep. 2017;7(1):6692.

632. Olguin-Olguin A, Aalto A, Maugis B, Boquet-Pujadas A, Hoffmann D, Ermlich L, et al. Chemokine-biased robust self-organizing polarization of migrating cells in vivo. Proc Natl Acad Sci U S A. 2021;118(7):e2018480118.

633. Rossy J, Gutjahr MC, Blaser N, Schlicht D, Niggli V. Ezrin/moesin in motile Walker 256 carcinosarcoma cells: Signal-dependent relocalization and role in migration. Exp Cell Res. 2007;313(6):1106-20.

634. Lorentzen A, Bamber J, Sadok A, Elson-Schwab I, Marshall CJ. An ezrin-rich, rigid uropod-like structure directs movement of amoeboid blebbing cells. J Cell Sci. 2011;124(8):1256-67.

635. Lu W, Kang Y. Epithelial-Mesenchymal Plasticity in Cancer Progression and Metastasis. Developmental Cell. 2019;49(3):361-374.

636. Pastushenko I, Blanpain C. EMT Transition States during Tumor Progression and Metastasis. Trends in Cell Biology. 2019;29(3):212-226.

637. Scott LE, Weinberg SH, Lemmon CA. Mechanochemical Signaling of the Extracellular Matrix in Epithelial-Mesenchymal Transition. Frontiers in Cell and Developmental Biology. 2019;7:135.

638. Polyak K, Weinberg RA. Transitions between epithelial and mesenchymal states: Acquisition of malignant and stem cell traits. Nature Reviews Cancer. 2009;9(4):265-73.

639. Yang J, Antin P, Berx G, Blanpain C, Brabletz T, Bronner M, et al. Guidelines and definitions for research on epithelial–mesenchymal transition. Nature Reviews Molecular Cell Biology. 2020;21(6):341-352.

640. Mierke CT. Physical view on migration modes. Cell Adh Migr. 2015;9(5):367-79.

641. Paňková K, Rösel D, Novotný M, Brábek J. The molecular mechanisms of transition between mesenchymal and amoeboid invasiveness in tumor cells. Cellular and Molecular Life Sciences. 2010;67(1):63-71.

642. Ribatti D, Tamma R, Annese T. Epithelial-Mesenchymal Transition in Cancer: A Historical Overview. Translational Oncology. 2020;13(6):100773.

643. Yamamoto M, Sakane K, Tominaga K, Gotoh N, Niwa T, Kikuchi Y, et al. Intratumoral bidirectional transitions between epithelial and mesenchymal cells in triple-negative breast cancer. Cancer Sci. 2017;108(6):1210-1222.

644. Bergert M, Chandradoss SD, Desai RA, Paluch E. Cell mechanics control rapid transitions between blebs and lamellipodia during migration. Proc Natl Acad Sci U S A. 2012;109(36):14434-9.

645. Chikina AS, Rubtsova SN, Lomakina ME, Potashnikova DM, Vorobjev IA, Alexandrova AY. Transition from mesenchymal to bleb-based motility is predominantly exhibited by CD133-positive subpopulation of fibrosarcoma cells. Biol Cell. 2019;111(10):245-261.

646. Friedl P, Wolf K. Plasticity of cell migration: A multiscale tuning model. Journal of Cell Biology. 2010;188(1):11-9.

647. Pandya P, Orgaz JL, Sanz-Moreno V. Modes of invasion during tumour dissemination. Molecular Oncology. 2017;11(1):5-27.

648. Parri M, Chiarugi P. Rac and Rho GTPases in cancer cell motility control. Cell Communication and Signaling. 2010;8:23.

649. Wilkinson S, Paterson HF, Marshall CJ. Cdc42-MRCK and Rho-ROCK signalling cooperate in myosin phosphorylation and cell invasion. Nat Cell Biol. 2005;7(3):255-61.

650. Pinner S, Sahai E. Imaging amoeboid cancer cell motility in vivo. Journal of Microscopy. 2008;231(3):441-5.

651. Gandalovičová A, Rosel D, Fernandes M, Veselý P, Heneberg P, Čermák V, et al. Migrastatics—Anti-metastatic and Anti-invasion Drugs: Promises and Challenges. Trends in Cancer. 2017;3(6):391-406.

652. Livak KJ, Schmittgen TD. Livak KJ, Schmittgen TD. Analysis of relative gene expression data using real-time quantitative PCR and the 2(-Delta Delta C(T)) Method. Methods. Methods. 2001;25(4):402-8.

653. Rueden CT, Schindelin J, Hiner MC, DeZonia BE, Walter AE, Arena ET, et al. ImageJ2: ImageJ for the next generation of scientific image data. BMC Bioinformatics. 2017;18(1):529.

654. Petrachi T, Resca E, Piccinno MS, Biagi F, Strusi V, Dominici M, et al. An alternative approach to investigate biofilm in medical devices: A feasibility study. Int J Environ Res Public Health. 2017;14(12):1587.

655. Inman GJ, Nicolás FJ, Callahan JF, Harling JD, Gaster LM, Reith AD, et al. SB-431542 is a potent and specific inhibitor of transforming growth factor-β superfamily type I activin receptor-like kinase (ALK) receptors ALK4, ALK5, and ALK7. Mol Pharmacol. 2002;62(1):65-74.

656. Zhu XF, Liu ZC, Xie BF, Li ZM, Feng GK, Yang D, et al. EGFR tyrosine kinase inhibitor AG1478 inhibits cell proliferation and arrests cell cycle in nasopharyngeal carcinoma cells. Cancer Lett. 2001;169(1):27-32.

657. Campellone KG, Lebek NM, King VL. Branching out in different directions: Emerging cellular functions for the Arp2/3 complex and WASP-family actin nucleation factors. Eur J Cell Biol. 2023;102(2):151301.

658. Hetrick B, Han MS, Helgeson LA, Nolen BJ. Small molecules CK-666 and CK-869 inhibit actin-related protein 2/3 complex by blocking an activating conformational change. Chem Biol. 2013;20(5):701-12.

659. Van Zijl F, Krupitza G, Mikulits W. Initial steps of metastasis: Cell invasion and endothelial transmigration. Mutation Research - Reviews in Mutation Research. 2011;728(1-2):23-34.

660. Knights AJ, Funnell APW, Crossley M, Pearson RCM. Holding Tight: Cell Junctions and Cancer Spread. Trends Cancer Res. 2012;8:61-69.

661. Zaidel-Bar R, Cohen M, Addadi L, Geiger B. Hierarchical assembly of cell-matrix adhesion complexes. Biochemical Society Transactions. 2004;32(3):416-20.

662. Kerstein PC, Patel KM, Gomez TM. Calpain-mediated proteolysis of talin and FAK regulates adhesion dynamics necessary for axon guidance. Journal of Neuroscience. 2017;37(6):1568-1580.

663. Franco SJ, Huttenlocher A. Regulating cell migration: Calpains make the cut. Journal of Cell Science. 2005;118(17):3829-38.

664. Diaz FJ, Wigglesworth K, Eppig JJ. Oocytes determine cumulus cell lineage in mouse ovarian follicles. J Cell Sci. 2007;120(8):1330-40.

665. Piprek RP, Kloc M, Mizia P, Kubiak JZ. The central role of cadherins in gonad development, reproduction, and fertility. International Journal of Molecular Sciences. 2020;21(21):8264.

666. Agarwal P, Zaidel-Bar R. Diverse roles of non-muscle myosin II contractility in 3D cell migration. Essays in Biochemistry. 2019;63(5):497-508.

667. Várkuti BH, Képiró M, Horváth IÁ, Végner L, Ráti S, Zsigmond Á, et al. A highly soluble, non-phototoxic, non-fluorescent blebbistatin derivative. Sci Rep. 2016;6:26141.

668. Schick J, Raz E. Blebs—Formation, Regulation, Positioning, and Role in Amoeboid Cell Migration. Frontiers in Cell and Developmental Biology. 2022;10:926394.

669. Favata MF, Horiuchi KY, Manos EJ, Daulerio AJ, Stradley DA, Feeser WS, et al. Identification of a novel inhibitor of mitogen-activated protein kinase kinase. Journal of Biological Chemistry. 1998;273(29):18623-32.

670. Yamazaki D, Kurisu S, Takenawa T. Involvement of Rac and Rho signaling in cancer cell motility in 3D substrates. Oncogene. 2009;28(13):1570-83.

671. Soriano O, Alcón-Pérez M, Vicente-Manzanares M, Castellano E. The crossroads between ras and rho signaling pathways in cellular transformation, motility and contraction. Genes. 2021;2(6):819.

672. Mateus AR, Seruca R, Machado JC, Keller G, Oliveira MJ, Suriano G, et al. EGFR regulates RhoA-GTP dependent cell motility in E-cadherin mutant cells. Hum Mol Genet. 2007;16(13):1639-47.

673. Flatau G, Lemichez E, Gauthier M, Chardin P, Paris S, Fiorentini C, et al. Toxin-induced activation of the G protein p21 Rho by deamidation of glutamine. Nature. 1997;387(6634):729-33.

674. Shimizu T, Ihara K, Maesaki R, Amano M, Kaibuchi K, Hakoshima T. Parallel Coiled-coil Association of the RhoA-binding Domain in Rho-kinase. Journal of Biological Chemistry. 2003;278(46):46046-51.

675. Uehata M, Ishizaki T, Satoh H, Ono T, Kawahara T, Morishita T, et al. Calcium sensitization of smooth muscle mediated by a Rho-associated protein kinase in hypertension. Nature. 1997;389(6654):990-4.

676. Unbekandt M, Belshaw S, Bower J, Clarke M, Cordes J, Crighton D, et al. Discovery of potent and selective MRCK inhibitors with therapeutic effect on skin cancer. Cancer Res. 2018;78(8):2096-2114.

677. Sasseville M, Ritter LJ, Nguyen TM, Liu F, Mottershead DG, Russell DL, et al. Growth differentiation factor 9 signaling requires ERK1/2 activity in mouse granulosa and cumulus cells. J Cell Sci. 2010;123(18):3166-76.

678. Wrighton KH, Lin X, Feng XH. Phospho-control of TGF-β superfamily signaling. Cell Research. 2009;19(1):8-20.

679. Bootman MD, Bultynck G. Fundamentals of cellular calcium signaling: A primer. Cold Spring Harb Perspect Biol. 2020;12(1):a038802.

680. Rudini N, Felici A, Giampietro C, Lampugnani M, Corada M, Swirsding K, et al. VE-cadherin is a critical endothelial regulator of TGF-β signalling. EMBO Journal. 2008;27(7):993-1004.

681. Inoue Y, Tsuda S, Nakagawa K, Hojo M, Adachi T. Modeling myosin-dependent rearrangement and force generation in an actomyosin network. J Theor Biol. 2011;281(1):65-73.

682. Russell DL, Salustri A. Extracellular matrix of the cumulus-oocyte complex. Seminars in Reproductive Medicine. 2006;281(1):65-73.

683. Kale VP, Hengst JA, Desai DH, Dick TE, Choe KN, Colledge AL, et al. A novel selective multikinase inhibitor of ROCK and MRCK effectively blocks cancer cell migration and invasion. Cancer Lett. 2014;354(2):299-310.

684. Unbekandt M, Croft DR, Crighton D, Mezna M, McArthur D, McConnell P, et al. A novel small-molecule MRCK inhibitor blocks cancer cell invasion. Cell Communication and Signaling. 2014;12(1):54.

685. Baba D, Kashiwabara S ichi, Honda A, Yamagata K, Wu Q, Ikawa M, et al. Mouse sperm lacking cell surface hyaluronidase PH-20 can pass through the layer of cumulus cells and fertilize the egg. J Biol Chem. 2002;277(33):30310-4.

686. Kim E, Baba D, Kimura M, Yamashita M, Kashiwabara SI, Baba T. Identification of a hyaluronidase, Hyal5, involved in penetration of mouse sperm through cumulus mass. Proc Natl Acad Sci U S A. 2005;102(50):18028-33.

687. Robker RL, Russell DL, Espey LL, Lydon JP, O'Malley BW, Richards JS. Progesterone-regulated genes in the ovulation process: ADAMTS-1 and cathepsin L proteases. Proc Natl Acad Sci U S A. 2000;97(9):4689-94.

688. Dunning KR, Lane M, Brown HM, Yeo C, Robker RL, Russell DL. Altered composition of the cumulus-oocyte complex matrix during in vitro maturation of oocytes. Human Reproduction. 2007;22(11):2842-50.

689. Metzger D, Chambon P. Site- and time-specific gene targeting in the mouse. Methods. 2001;24(1):71-80.

690. Yanagida K, Shimizu T. Lysophosphatidic acid, a simple phospholipid with myriad functions. Pharmacology and Therapeutics. 2023;246:108421.

691. Tokumura A, Miyake M, Nishioka Y, Yamano S, Aono T, Fukuzawa K. Production of lysophosphatidic acids by lysophospholipase D in human follicular fluids of in vitro fertilization patients. Biol Reprod. 1999;61(1):195-9.

692. Jo JW, Jee BC, Suh CS, Kim SH. Addition of lysophosphatidic acid to mouse oocyte maturation media can enhance fertilization and developmental competence. Human Reproduction. 2014;29(2):234-41.

693. Kim JH, Adelstein RS. LPA 1-induced migration requires nonmuscle myosin II light chain phosphorylation in breast cancer cells. J Cell Physiol. 2011;226(11):2881-93.

694. Hinokio K, Yamano S, Nakagawa K, Irahara M, Kamada M, Tokumura A, et al. Lysophosphatidic acid stimulates nuclear and cytoplasmic maturation of golden hamster immature oocytes in vitro via cumulus cells. Life Sci. 2002;70(7):759-67.

695. Zihni C. MRCK: a master regulator of tissue remodeling or another 'ROCK' in the epithelial block? Tissue Barriers. 2021;9(3):1916380.